The glycine cleavage system in embryonic brain development

Yun Jin Pai

Thesis submitted to University College London for the degree of Doctor of Philosophy

2015

Developmental Biology of Birth Defects

Developmental Biology & Cancer Programme

UCL Institute of Child Health

Declaration of contribution

I, Yun Jin Pai, confirm that the work presented in this thesis is my own. The majority of experiments were performed by me and contributions by other members of the lab and our collaborators are declared here and indicated in the thesis where relevant.

Folate profiling was carried out by Dr Kit-Yi Leung (UCL Institute of Child Health), Gldc enzymatic assay by Dr Tim Hutchin (Birmingham Children's Hospital), amino acid profiling by Helen Prunty and Dr Simon Heales (UCL Institute of Child Health and Great Ormond Street Hospital for Children NHS Foundation Trust), and measurement of formate by Dr Margaret Brosnan and Dr John Brosnan (Memorial University of Newfoundland, Canada). I was aided by Maria-Chiara Autuori and Dawn Savery in sample collection. Where information has been derived from other sources, I confirm that this has been indicated in the thesis.

_____

Yun Jin Pai

Abstract

The glycine cleavage system (GCS) is a multi-enzyme complex localised in the mitochondria and serves as the main catabolic pathway for glycine. It contributes to supply of one-carbon units into folate one-carbon metabolism (FOCM) which utilises them for vital processes such as purines and thymidylate biosynthesis and methylation reactions. This thesis focuses on the role of glycine decarboxylase (Gldc), a member of the GCS, in embryonic development of the brain. It utilises two loss-of-function mouse models for *Gldc* which were found to exhibit two distinct disease phenotypes: non-ketotic hyperglycinemia (NKH) and neural tube defects (NTDs). The aims of this project are to investigate what effects GCS deficiency has on FOCM, the developmental mechanisms underlying NTDs caused by loss of *Gldc* expression, and suitability of the *Gldc* mice models as animal models for classical NKH.

NKH is a rare metabolic disease caused by mutations of GCS genes (mainly *GLDC*) and characterised by accumulation of glycine in body fluids, resulting in severe neurological dysfunction and poor survival. *Gldc*-deficient mice exhibited features of NKH including elevated glycine, early post-natal lethality, and hydrocephalus. Enlargement of the brain ventricles was found to already be present at late-foetal stage, while glycine levels in whole embryos were already elevated shortly after neurulation. *Gldc*-deficient embryos also displayed NTDs, a common birth defect of the central nervous system that result from failure of the neural tube to close. *Gldc*-deficient embryos displayed abnormal folate metabolism, growth retardation and reduced cell proliferation. Supplementation with one-carbon units through dietary means was able to normalise folate profiles, completely rescue the NTDs, and normalise proliferation and growth in *Gldc*-deficient embryos. Diet-induced folate deficiency and interactions with the *Mthfr* mutation (which results in a methylation defect) did not exacerbate the NTDs caused by the *Gldc* mutation.

This study provides the first mouse model for classical NKH and suggests that the pathology of NKH begins earlier in development than suspected. It also suggests that *Gldc* deficiency causes NTDs by reducing the supply of glycine-derived, mitochondrial one-carbon units for FOCM reactions.

Acknowledgements

I would like to thank my supervisor, Nick Greene, for giving me the chance to do my PhD under his supervision. Thank you for letting me work at my own pace but not leaving me to run astray, for always engaging in my inquiries no matter how trivial or tedious, and for the fun trips into crazy theoryland. I could not have asked for a more supportive and all-around awesome supervisor. I am also extremely grateful to Andy Copp for always being generous with his expertise, comments, and suggestions, for lending a critical eye, for making me think about future directions, and for being infectious in his love of science.

I am greatly indebted to all members of the Neural Tube Defects group, past and present, for being the most wonderful and supportive team I have ever had the pleasure of working with. Special thanks to Sandra Castro for her endless patience in guiding me through many techniques and for her wonderful friendship (and all the hot chocolates!), to Dawn Savery for all mouse and PCR-related things and for always willing to go out her way to help me, to Kit-Yi Leung for guiding me through a convoluted metabolic pathway and entertaining all my questions and rants, and to Ana Rolo for her beautiful friendship and endless support both inside and outside the lab.

I would like to acknowledge the Malaysian government for their financial support, without which this work would not be possible.

To my dearest friends Fauziah, Pandora, Chiara, Naho, Chia Mein, Alix, Alex, and Anna, thank you for making my life in London not just about the PhD. To Malcolm Billings, the loveliest landlord one could ask for, for helping make London feel like home. To my family and fossil friends half the world away- Shoba, Sabrina, Elaine, Chooi San, Yee Jenn, Atifi, Michelle, Lesley, and Parames- for proving that distance, time, and bad Wi-Fi make not a bit of difference. A special thanks to Ai Rene Ong, for keeping me sane on a regular basis and for being the most terrible enabler of guilty pleasures.

Finally, I owe a special debt of gratitude to Noraishah Abdul-Aziz, for inspiring me at a critical time of my life.

Table of Contents

Declaration of contribution **2**
Abstract **3**
Acknowledgements **4**
Table of Contents **5**
List of Figures **10**
List of Tables **12**
Abbreviations **13**
1. General Introduction **16**
1.1. Glycine cleavage system 16
1.1.1. Biochemistry of the GCS 16
1.1.2. Defects of the GCS 18
1.2. Non-ketotic hyperglycinemia 19
1.2.1. Clinical presentation 19
1.2.2. Diagnostic history 21
1.2.3. Current GCS mice models 22
1.3. Neural tube defects 23
1.3.1. Mammalian neurulation 24
1.3.2. Classification of NTDs 28
1.3.3. Differences between human and mouse primary neurulation 29
1.3.4. Aetiology of NTDs 30
1.3.4.1. Environmental factors 31
1.3.4.2. Genetic factors 34
1.3.4.2.1. Planar cell polarity genes 35
1.3.4.2.2. Sonic hedgehog and BMP genes 36
1.3.4.2.3. Proliferation, differentiation, and apoptosis genes 36
1.3.4.2.4. Genes in cytoskeletal regulation 37
1.3.4.2.5. Curly tail model 37
1.4. Folate metabolism and NTDs 38
1.4.1. History of folic acid treatment 38
1.4.2. Folate one-carbon metabolism 41
1.4.2.1. Folate transport mechanisms 41
1.4.2.2. Compartmentalisation of FOCM reactions 43
1.4.2.3. FOCM outputs 47
1.4.3. Association between genetic polymorphisms of FOCM genes with NTDs 48

1.4.4. FOCM-related mouse models 49
1.4.4.1. Genes encoding folate receptors and carriers 49
1.4.4.2. FOCM mutations conferring pre-neurulation lethality 50
1.4.4.3. FOCM mutations not presenting with NTDs 51
1.4.4.4. FOCM mutations that cause NTDs 52
1.5. Overview of thesis 53
2. Methodology 55
2.1. Mice colonies 55
2.1.1. Generation of *Gldc* mutant mice 55
2.1.2. Generation of *Gldc*^{GT2}*;Mthfr* mutant mice 55
2.1.3. Genotyping and sexing PCRs 56
2.1.4. Long-Range PCR and sequencing of gene-trap 59
2.1.5. Treatments and dietary interventions 61
2.1.6. Survival studies 61
2.2. Sample collection, fixation, and storage 61
2.2.1. Embryonic samples 61
2.2.2. Late-foetal and post-natal samples 62
2.2.3. Adult mice blood and urine samples 62
2.3. Investigating expression of *Gldc* mRNA 63
2.3.1. RNA isolation and cDNA synthesis 63
2.3.2. Cloning of *Gldc* cDNA into vector for *in situ* probe preparation 64
2.3.2.1. Gldc probe design 64
2.3.2.2. Ligation into vector system 64
2.3.2.3. Transformation into competent cells 65
2.3.2.4. Plasmid preparation 65
2.3.3. RNA probe preparation for *in situ* hybridisation 66
2.3.3.1. Plasmid DNA digestion 66
2.3.3.2. DIG probe transcription 67
2.3.4. Whole mount *in situ* hybridisation 68
2.3.4.1. Hybridisation of probe 68
2.3.4.2. DIG antibody detection 68
2.3.4.3. Colour development 69
2.3.4.4. Vibratome sectioning 69
2.4. Assessing efficiency of *Gldc* gene-traps 70
2.4.1. Quantitative, real-time PCR (qRT-PCR) 70
2.4.2. Whole mount X-gal staining 71

2.4.3. Glycine cleavage enzymatic assay 71
2.5. Histological studies 72
2.5.1. Paraffin processing and sectioning 72
2.5.2. Hematoxylin and eosin staining 72
2.5.3. Cresyl violet staining 73
2.5.4. Immunofluorescence staining of Phospho-Histone-H3 (PHH3) 73
2.6. Metabolic studies 74
2.6.1. Sample preparation 74
2.6.2. Protein assay 74
2.6.3. Amino acid analysis 75
2.6.4. Folate profiling 75
2.6.5. Assessment of formate levels 75
2.7. Gold chloride *en bloc* staining 76
2.8. Image capture and data analysis 76
3. Embryonic phenotypes in the *Gldc*-deficient mouse model 77
3.1. Introduction 77
3.1.1. Classical mutagenesis 77
3.1.2. Gene targeting and transgenesis 78
3.1.3. Gene-trapping 79
3.2. Results 80
3.2.1. Expression analysis of *Gldc* 80
3.2.1.1. Gldc mRNA expression in neurulation-stage mice embryos 80
3.2.2. *Gldc* gene-trap models 85
3.2.2.1. Defining the locus and trapping efficiency of the $Gldc^{GT1}$ allele 85
3.2.2.2. $Gldc^{GT2}$ gene-trap line 91
3.2.3. Developmental phenotypes of *Gldc* mutant embryos 93
3.2.3.1. NTD incidence in $Gldc^{GT}$ mutants 93
3.2.3.2. mRNA and protein expression levels during neurulation 97
3.2.3.3. Analysis of growth and development 99
3.2.3.4. Unusual cranial phenotypes in $Gldc^{GT1}$ mutants 103
3.2.3.5. Additional developmental phenotypes in $Gldc^{GT2}$ mutants 109
3.3. Discussion 111
3.3.1. *Gldc* is required for neural tube closure 111
3.3.2. Partial penetrance of NTDs in *Gldc* mutants 112
3.3.3. Forebrain defects in $Gldc^{GT2}$ mutants 113
3.3.4. Hypotheses for the unusual cranial phenotype 115

4. Investigating a possible role of abnormal folate metabolism in *Gldc*-deficient neural tube defects 117
4.1. Introduction 117
4.1.1. Mitochondrial-derived 1C units 117
4.1.2. Alternative sources of formate 122
4.2. Results 123
4.2.1. *Gldc* mutation increases glycine levels and disrupts FOCM 123
4.2.1.1. Glycine levels in Gldc mutant embryos 123
4.2.1.2. In silico modelling of the effects of defective GLDC on folate cycling . 125
4.2.1.3. Abnormal folate profiles in Gldc mutant embryos 128
4.2.2. Abnormal folate profiles in *Gldc* mutation are caused by lack of 1C units . 131
4.2.2.1. Formate treatment rescues NTDs and normalises folate profiles 131
4.2.2.2. $Gldc^{GT1}$ foetuses show signs of toxicity on prolonged formate supplementation 135
4.2.2.3. Folate deficiency does not exacerbate NTDs in Gldc mutants 137
4.2.2.4. Formate levels in Gldc mutant embryos 138
4.2.3. Effect of *Gldc* deficiency on cellular proliferation, growth, and development 139
4.2.3.1. Formate treatment normalises growth 140
4.2.3.2. Proliferation analysis of Gldc mutant embryos 141
4.2.3.3. Formate treatment normalises proliferation 147
4.2.3.4. SAM/SAH analysis of Gldc mutant embryos 148
4.2.3.5. Interaction between Gldc and Mthfr mutations 149
4.2.3.6. Effect of anti-helminthic treatment on $Gldc^{GT2}$ mutants 154
4.3. Discussion 157
4.3.1. Biochemical profiles of *Gldc* deficiency 157
4.3.2. Formate treatment and rescue 158
4.3.3. Formate toxicity 160
4.3.4. Interaction of the *Mthfr* mutation with *Gldc* deficiency 161
4.3.5. Effect of fenbendazole on phenotypes resulting from *Gldc* deficiency 162
5. *$Gldc^{GT1}$* mouse as a model for non-ketotic hyperglycinemia 164
5.1. Introduction 164
5.1.1. Pathology of NKH 164
5.1.2. Expression analysis of GCS genes in rat brains 165
5.1.3. Treatment options 166
5.1.4. Corpus callosum genesis and agenesis 167

5.1.5. The ventricular system and hydrocephalus 168
5.2. Results 170
5.2.1. Mendelian ratios of post-natal *Gldc*^{GT1} and *Gldc*^{GT2} mutant pups 170
5.2.2. Survival studies and hydrocephalus incidence 171
5.2.3. Elevated glycine in plasma and urine of *Gldc* mutant mice 174
5.2.4. Late-foetal ventriculomegaly in *Gldc* mutant mice 177
5.2.5. Analysis of the corpus callosum 183
5.2.6. Analysis of the cerebellum 183
5.3. Discussion 186
5.3.1. *Gldc* mutant mice exhibit characteristic features of NKH 186
5.3.2. Pathogenesis of hydrocephalus 187
5.3.3. Hydrocephalus in *Gldc*-deficient mice 191
6. General Discussion 194
6.1. Phenotypic spectrum of *Gldc* deficiency 194
6.1.1. Effect of background strain on disease severity in *Gldc*-deficient mice 194
6.1.2. Partial penetrance of NTDs in *Gldc* mutant mice and comparison with the spectrum of NKH severity 195
6.2. Abnormal FOCM in *Gldc* deficiency 196
6.2.1. Potential mechanisms for abnormal FOCM to result in NTDs 196
6.2.1.1. Effect of FOCM on proliferation 197
6.2.1.2. Increased genome instability 198
6.2.1.3. Abnormal FOCM and hypomethylation 199
6.2.1.4. Homocysteine toxicity 199
6.2.2. Proposed mechanism underlying NTDs in *Gldc*-deficient mutant embryos 200
6.2.3. Does a deficit of one-carbon units contribute to NKH-related phenotypes? 201
6.3. Glycine toxicity in *Gldc* deficiency 204
6.3.1. Over-activation of NMDARs in NKH-related phenotypes 204
6.3.2. Possibility of mitochondrial dysfunction in *Gldc* deficiency 205
6.3.3. Alternative pathways for glycine catabolism 206
References 208
Appendix: *Gldc*^{GT1} gene-trap sequence 236

List of Figures

Figure 1. Glycine cleavage system 17
Figure 2. Overview of mouse primary neurulation. 27
Figure 3. Structural representation of tetrahydrofolate. 42
Figure 4. Overview of folate one-carbon metabolism. 46
Figure 5. Primer walking strategy for sequencing of the *Gldc*^{GT1} construct. 60
Figure 6. Expression pattern of *Gldc* mRNA in E8.5 and E9.5 wild-type embryos. 82
Figure 7. Expression pattern of *Gldc* mRNA in E10.5 wild-type embryos. 84
Figure 8. *Gldc* gene-trap 1 (*Gldc*^{GT1}) design and genomic PCR genotyping strategy. 86
Figure 9. Whole mount X-gal staining of *Gldc*^{GT1} E10.5 embryos 87
Figure 10. Assessment of *Gldc* mRNA levels in *Gldc*^{GT1} adult mice liver and brain 90
Figure 11. Enzymatic activity of Gldc in *Gldc*^{GT1} adult mice livers 91
Figure 12. *Gldc* gene-trap2 (*Gldc*^{GT2}) design and genomic PCR genotyping strategy. 92
Figure 13. NTDs in *Gldc*^{GT1} mutant embryos. 93
Figure 14. NTDs and craniofacial defects in E10.5 *Gldc*^{GT2} mutant embryos. 94
Figure 15. Sex of *Gldc*$^{GT1/GT1}$ embryos and occurrence of NTDs 96
Figure 16. mRNA levels in E9.5 and E10.5 embryos of the *Gldc*^{GT1} and *Gldc*^{GT2} alleles. 98
Figure 17. Crown rump length and somite number of *Gldc*^{GT1} embryos. 100
Figure 18. Crown rump length and somite number of *Gldc*^{GT2} embryos. 101
Figure 19. Regression curve of crown rump length versus somite number of *Gldc*^{GT1} embryos 102
Figure 20. Transverse sections of *Gldc*^{GT1} embryos at E11.5. 105
Figure 21. Coronal sections of *Gldc*^{GT1} embryos at E10.5–E11.5 107
Figure 22. E10.5 *Gldc*^{GT1} embryo showing cranial haemorrhage 108
Figure 23. Eye defects and haemorrhage in *Gldc*^{GT2} mutant embryos. 110
Figure 24. *De novo* sources of one-carbon units for folate one-carbon metabolism. 121
Figure 25. One-Carbon Metabolism mathematical modelling software 126
Figure 26. *In silico* prediction of hepatic folate profiles in normal and GCS-deficient conditions. 127
Figure 27. *Gldc*^{GT1} mutant embryos show altered folate profiles 130
Figure 28. Effect of formate treatment on NTD incidence in *Gldc*$^{GT1/GT1}$ embryos 131
Figure 29. Glycine levels in untreated and formate-treated E11.5 *Gldc*^{GT1} embryos 132
Figure 30. Normalisation of folates of *Gldc*^{GT1} embryos after formate treatment. 134
Figure 31. Signs of non-genotype specific toxicity in *Gldc*^{GT1} foetuses after prolonged formate supplementation. 136
Figure 32. Effect of folate deficiency on *Gldc*$^{GT1/GT1}$ embryos. 137

Figure 33. Plasma formate levels in untreated and formate-treated *Gldc*^{GT1} mice.....139
Figure 34. Effect of formate treatment on growth of *Gldc*^{GT1} embryos. 140
Figure 35. Defining 5 regions of the E9.5 cranial neural tube for proliferation studies. 143
Figure 36. Positive PHH3 staining in the hindbrain of *Gldc*^{GT1} embryos. 144
Figure 37. Percentage of PHH3 labelled cells in *Gldc*^{GT1} embryos. 146
Figure 38. Percentage of PHH3 labelled cells in formate-treated *Gldc*^{GT1} embryos. 147
Figure 39. SAM/SAH ratios of E11.5 *Gldc*^{GT1} embryos.....148
Figure 40. Folate profiles of *Gldc*^{GT2}*;Mthfr* double mutants. 153
Figure 41. NTDs and craniofacial defects in E15.5 and E17.5 *Gldc*^{GT2} mutants collected after the period of fenbendazole treatment. 156
Figure 42. Survival curve of *Gldc*^{GT1} mice. 172
Figure 43. Hydrocephalus in *Gldc*$^{GT1/GT1}$ mice. 173
Figure 44. The ventricular system in an E18.5 mouse brain. 178
Figure 45. E18.5 *Gldc*$^{GT1/GT1}$ brains show dilation of lateral and third ventricles. 179
Figure 46. Aqueduct stenosis and obliteration of the subcommissural organ in E18.5 *Gldc*$^{GT1/GT1}$ brains. 181
Figure 47. Sections of E18.5 *Gldc*^{GT1} brains showing normal fourth ventricles. 182
Figure 48. Corpus callosum analysis. 184
Figure 49. Preliminary cerebellar folia analysis. 185
Figure 50. Schematic representation of possible mechanisms through which impaired FOCM may lead to NTDs (description in text) 197
Figure 51. Proposed mechanism for *Gldc* deficiency to result in NTDs. 201
Figure 52. Summary of possible mechanisms that could lead to hydrocephalus in *Gldc*-deficient mice. 203

List of Tables

Table 1. Notable environmental risk factors associated with NTDs. 32
Table 2. Primer sequences for genotyping and sexing *Gldc*^{GT1}, *Gldc*^{GT2}, and *Mthfr* samples. 57
Table 3. PCR reaction mixes for genotyping and sexing. 58
Table 4. PCR conditions for determination of genotype and sex. 58
Table 5. Long-Range PCR reaction mix. 59
Table 6. Primers used for *Gldc*^{GT1} construct sequencing. 60
Table 7. RT-PCR reaction mix for amplification of *Gldc* cDNA. 64
Table 8. Restriction enzymes and RNA polymerases for generation of *Gldc in situ* hybridisation probes. 67
Table 9. Primer sequences for quantification of *Gldc* mRNA by qRT-PCR. 70
Table 10. Litter information of *Gldc*$^{GT1/+}$ crosses on a C57BL/6 genetic background. 88
Table 11. Litter information of *Gldc*$^{GT2/+}$ crosses on a C57BL/6 genetic background. 92
Table 12. Incidence of NTDs in embryos with the *Gldc*^{GT1} allele. 95
Table 13. Incidence of NTDs in embryos with the *Gldc*^{GT2} allele. 95
Table 14. Incidence of unusual cranial phenotypes in *Gldc*^{GT1} embryos. 103
Table 15. Incidence of NTDs with and without inclusion of the unusual cranial phenotype in the *Gldc*^{GT1} allele. 109
Table 16. Incidence of eye defects and haemorrhage in *Gldc*^{GT2} mutant embryos. 109
Table 17. Percentage mRNA level and NTD incidence in *Gldc*^{GT1} and *Gldc*^{GT2} embryos. 113
Table 18. Concentration of amino acids in whole *Gldc*^{GT1} embryos. 124
Table 19. Incidence of toxic effects of prolonged formate supplementation in E15.5 and E18.5 *Gldc*^{GT1} foetuses. 135
Table 20. Incidence of NTDs in *Gldc*$^{GT2/+}$;*Mthfr*$^{+/-}$ double heterozygous crosses. 151
Table 21. Incidence of NTDs in fenbendazole-treated *Gldc*^{GT2} embryos. 155
Table 22. Incidence of NTDs in *Gldc*^{GT2} embryos after fenbendazole treatment. 155
Table 23. Incidence of craniofacial defects in exencephalic *Gldc*^{GT2} mutants during and after fenbendazole treatment. 155
Table 24. Ratio of genotypes of P10 *Gldc*^{GT1} mice from 15 litters. 170
Table 25. Ratio of genotypes of P10 *Gldc*^{GT2} mice from 7 litters. 170
Table 26. Number of hydrocephalus, non-hydrocephalic deaths before 6 weeks, and survivors up to 6 weeks in *Gldc*$^{GT1/GT1}$ mice. 174
Table 27. Concentration of amino acids in *Gldc* mice plasma. 175
Table 28. Concentrations of amino acids in *Gldc* mice urine. 176
Table 29. Hydrocephalic mouse mutants with NPC proliferation and/or ependymal defects. 190

Abbreviations

1C	One-carbon
ACC	Agenesis of the corpus callosum
ADHD	Attention deficit hyperactivity disorder
AICART	5-aminoimidazole-4-carboxamide ribonucleotide formyltransferase
AMT	Aminomethyltransferase
ANOVA	Analysis of variance
ATP	Adenosine triphosphate
BHMT	Betaine-homocysteine-methyltransferase
BMP	Bone morphogenetic protein
bp	base pair
BSA	Bovine serum albumin
cDNA	Complementary DNA
CRL	Crown rump length
CSF	Cerebrospinal fluid
DAPI	4',6-diamidino-2-phenylindole
DEPC	Diethylpyrocarbonate
DHF	Dihydrofolate
DIG	Digoxigenin
DLD	Dihydrolipoamide dehydrogenase
DLHP	Dorsolateral hinge point
DNA	Deoxyribonucleic acid
dNTP	Deoxynucleotide triphosphate
DPX	Dibutylphthalate polystyrene xylene
dTMP	Thymidine monophosphate/ thymidylate
dUMP	Deoxyuridine monophosphate
DW	Dandy-Walker
E	Embryonic day
ECM	Extracellular matrix
EEG	Electroencephalogram
EGL	External granular layer
ES	Embryonic stem (cells)
EUCOMM	European Conditional Mouse Mutagenesis
EX	Exencephaly
FGF	Fibroblast growth factor
FOCM	Folate one-carbon metabolism

Folbps	Folate-binding proteins
FPGS	folypoly-γ-glutamate synthetase
FR	Folate receptor
Gapdh	Glyceraldehyde-3-phosphate
GCPII	Glutamate carboxypeptidase II
GCS	Glycine cleavage system
GCSH	Glycine cleavage system H-protein
GFP	Green fluorescent protein
GLDC	Glycine decarboxylase
GlyR	Glycinergic receptor
GMP	Guanosine monophosphate
GPI	Glycosylphosphatidylinositol
H&E	Hematoxylin and eosin
HEK	Human embryonic kidney
HLF	Human lung fibroblasts
IRES	Internal ribosome entry site
kb	kilobase pair
LC/MS/MS	Liquid chromatography, tandem mass-spectrometry
LTR	Long Terminal Repeat
MHP	Median hinge point
mRNA	Messenger RNA
MS	Methionine synthase
MTHFD	Methylenetetrahydrofolate dehydrogenase
MTHFR	5,10-methylenetetrahydrofolate reductase
MTR	5-methyltetrahydrofolate-homocysteine-methyltransferase
MTRR	Methionine synthase reductase
NAD+	Nicotinamide adenine dinucleotide (oxidised)
NADH	Nicotinamide adenine dinucleotide (reduced)
NADP+	Nicotinamide adenine dinucleotide phosphate (oxidised)
NADPH	Nicotinamide adenine dinucleotide phosphate (reduced)
NCC	Neural crest cell
NE	Neuroepithelium
NKH	Non-ketotic hyperglycinemia
NMDAR	*N*-methyl-D-aspartate receptor
NorCOMM	North American Conditional Mouse Mutagenesis
NPC	Neural progenitor cell
NTD	Neural tube defect

OXPHOS	Oxidative phosphorylation
P	Post-natal day
PBS	Phosphate buffered saline
PBT	Phosphate buffered saline with Tween
PCD	Primary ciliary dyskinesia
PCFT	Proton-coupled folate transporter
PCP	Planar cell polarity
PCR	Polymerase chain reaction
PFA	Paraformaldehyde
PHH3	Phospho-Histone-H3
polyA/ pA	Polyadenylation
qRT-PCR	Quantitative RT-PCR
RBC	Red blood cell
RFC	Reduced folate carrier
RNA	Ribonucleic acid
RNAPII	RNA polymerase II
rpm	Revolutions per minute
RT-PCR	Reverse-transcriptase PCR
SA	Splice acceptor
SAH	S-adenosyl homocysteine
SAM	S-adenosyl methionine
SCO	Subcommissural organ
SD	Splice donor
SDS	Sodium dodecyl sulphate
SE	Surface ectoderm
SEM	Standard error of mean
Shh	Sonic hedgehog
SHMT	Serine hydroxymethyltransferase
SN	Somite number
TBS	Tris buffered saline
TBST	Tris buffered saline with Tween
TCA	Tricarboxylic acid
TGF	Transforming growth factor
THF	Tetrahydrofolate
TYMS	Thymidylate synthase
VEGF	Vascular endothelial growth factor

1. General Introduction

1.1. Glycine cleavage system

The glycine cleavage system (GCS) is the predominant pathway for glycine catabolism present in animals, plants, and bacteria. It is localized to the inner membrane of the mitochondria and contributes to a larger metabolic pathway: folate one-carbon metabolism (FOCM). It catalyses the cleavage of glycine in the presence of NAD+ to yield carbon dioxide, ammonia, NADH, and a one-carbon (1C) unit.

1.1.1. Biochemistry of the GCS

The GCS is a multi-enzyme complex comprising three enzymes: glycine decarboxylase (GLDC, or P-protein), aminomethyltransferase (AMT, or T-protein), and dihydrolipoamide dehydrogenase (DLD, or L-protein), and a carrier protein, glycine cleavage system H-protein (GCSH), which contains a bound lipoic acid group. They are encoded by the distinct genes *GLDC*, *AMT*, *DLD,* and *GCSH*, respectively (Kikuchi et al., 2008).

GLDC, AMT, and GCSH (at both mRNA and protein levels) were shown to be expressed in the liver, kidney, and astrocytes of the brain, with AMT and GCSH also showing low levels of expression in the heart and spleen (Kure et al., 1991, Sato et al., 1991). Unlike GLDC, AMT and GCSH, the DLD enzyme is not specific to the GCS and also participates in other 2-oxoacid dehydrogenase multi-enzyme complexes in the mitochondria.

Figure 1 illustrates the steps in the GCS. The first step involves the decarboxylation of glycine by GLDC, with GCSH as a co-substrate. The first of the two carbon units of glycine, 1C-glycine, is converted to carbon dioxide, while the other, 2C-glycine, is transferred to a sulfhydryl group of GCSH attached to its covalently bound lipoate group (Fujiwara and Motokawa, 1983, Ando et al., 1968). In the next reaction catalysed by AMT, the GCSH-bound carbon is then transferred to tetrahydrofolate (THF) to generate 5,10-methylene-THF and ammonia. The now-reduced form of GCSH is reoxidized by the action of DLD in an NAD^+-dependent manner, thus generating NADH and a hydrogen ion, and is then ready to participate in the next glycine cleavage reaction (Fujiwara et al., 1984, Fujiwara and Motokawa, 1983).

In the absence of THF, AMT converts the GCSH-bound intermediate into ammonia and formaldehyde, but at an extremely low velocity (2,400-fold lower turnover rate than when THF is present). All reactions in the GCS are reversible, though the conversion of 5,10-methylene THF back into glycine at the AMT-catalysed step is 6-fold slower than its forward reaction (Fujiwara et al., 1984, Okamura-Ikeda et al., 1987). 5,10-methylene-THF, formed after receiving the 1C unit from glycine, enters the one-carbon cycle in the mitochondria (see **Section 1.4.2.2** for details and **Figure 4** for a diagram of the full cycle).

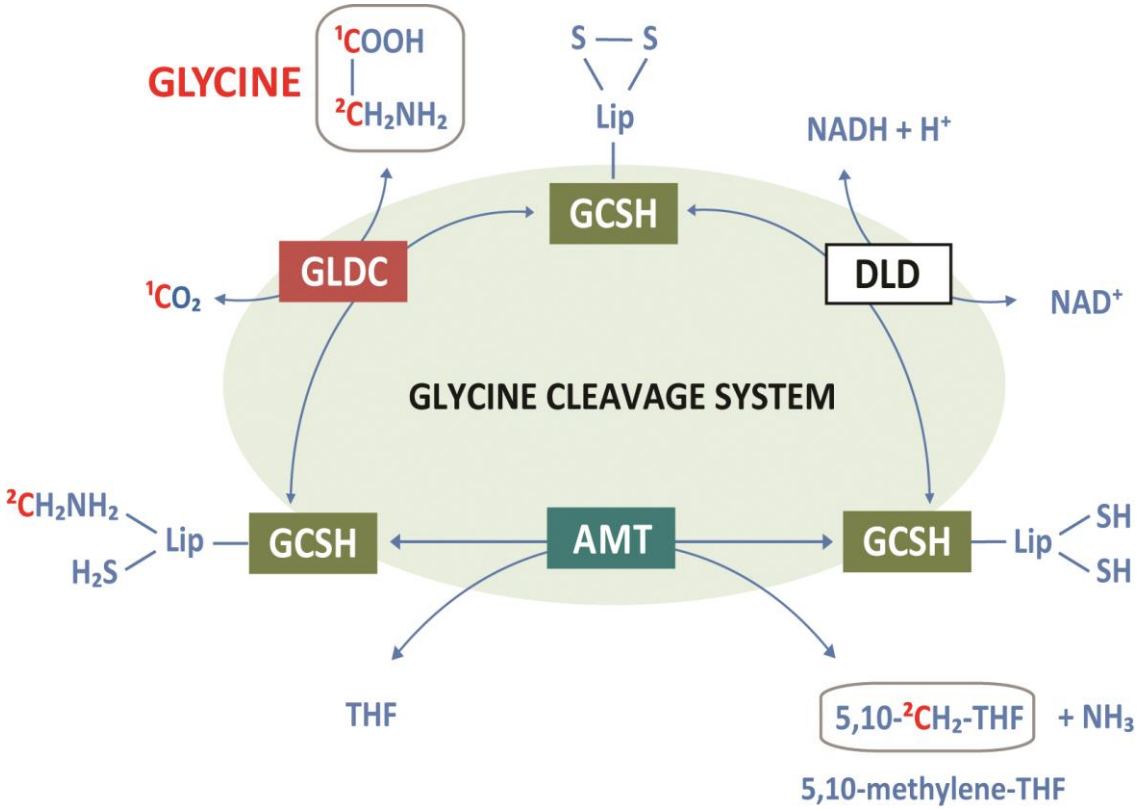

Figure 1. Glycine cleavage system

The glycine cleavage system (GCS) consists of four components: glycine decarboxylase (GLDC), aminomethyltransferase (AMT), GCS H-protein (GCSH), and dihydrolipoamide dehydrogenase (DLD), that collectively break down glycine, releasing one 1C unit as carbon dioxide (CO_2) and transferring the other to tetrahydrofolate (THF), converting it to 5,10-methylene-THF. All components of the GCS are localised within the inner mitochondrial membrane.

Reference: Kikuchi et al. (2008)

1.1.2. Defects of the GCS

Mutations in *GLDC* or *AMT* are typically known to cause non-ketotic hyperglycinemia (NKH, or glycine encephalopathy). NKH is an inborn error of metabolism characterised by abnormally high levels of glycine in body fluids, especially in the cerebrospinal fluid (CSF). It is an autosomal recessive condition that results in the complete or partial loss of GCS enzymatic activity, causing an accumulation of glycine to levels that are double to tenfold that of normal plasma and CSF ranges (Kure et al., 1997, Hoover-Fong et al., 2004, Hennermann et al., 2012). Details on NKH are provided in the next section, **1.2**.

In addition to causing NKH, impaired GCS activity also predispose to neural tube defects (NTDs) (Narisawa et al., 2012), which result from failure of the neural tube to close during early embryonic development. Sequencing of *GLDC*, *AMT*, and *GCSH* genes was carried out on control and NTD patients, revealing novel missense and splice acceptor site mutations in *GLDC* and *AMT* of NTD patients. Interestingly, missense variants identified in *GLDC* in the NTD patients exhibited significantly lowered enzymatic activity compared with controls. The findings from this study strongly indicate a link between GCS function and NTDs. Neural tube defects are described in **Section 1.3**.

When components of the GCS are over-expressed, however, this was found to produce a pro-oncogenic effect in various cancer cell lines. For example, *GLDC* was found to be upregulated in 158 out of 606 human cancer cell lines, and *GLDC* overexpression was shown to promote cell proliferation, glycolysis and tumorigenesis of lung cancer cells (Zhang et al., 2012). GCS involvement was also implicated alongside *de novo* serine biosynthesis and FOCM in a novel ATP production pathway hypothesised to be active in proliferating cancer cells (Vazquez et al., 2011, Tedeschi et al., 2013), with similar findings also observed in embryonic stem (ES) cells (Tedeschi et al., 2013). In support of this is the finding that rapidly proliferating cancer cell lines consume unusually high amounts of glycine and highly express glycine synthesis enzymes (Jain et al., 2012). While some studies report contradictory results on the pro-oncogenic role of the GCS or of glycine requirement (as opposed to serine) for cancer cell proliferation (Rose et al., 1999, Labuschagne et al., 2014), it remains clear that GCS enzyme activities, GCS-driven changes in glycine levels and its contribution to FOCM play an important role in cancer cell metabolism. A review of the contribution of serine, glycine, and one-carbon metabolism in cancer is provided by Locasale (2013) and Amelio et al. (2014).

1.2. Non-ketotic hyperglycinemia

NKH is a rare disorder with a prevalence of 1 in 63,000 in British Columbia (Applegarth et al., 2000) and 1 in 55,000 in Finland (von Wendt et al., 1979). Higher incidence can be found in certain geographical regions and ethnic groups, such as in north Finland with 1 in 12,000 (von Wendt et al., 1979) and in Israeli Arab families (Kure et al., 1998, Boneh et al., 2005, Flusser et al., 2005).

1.2.1. Clinical presentation

Disease presentation can be generally divided into three clinical sub-groups: the classical neonatal form, the atypical mild form, and the transient form.

Classical NKH is the most common and severe form of NKH, with a neonatal onset often within hours or days of birth. Patients present with a highly elevated CSF/plasma glycine ratio with negligible levels or complete absence of GCS activity in the liver. The initial symptom is hypotonia, followed by (though not always inclusive of) apnea in which intubation is often necessary, persistent and intractable seizures, coma, spasticity, a burst suppression pattern or hypsarrhythmia EEG reading, frequent hiccupping, feeding difficulties often requiring gastric tube feeding, and occasional microcephaly, choreiform movements, and severe hyperactivity (Hennermann et al., 2012).

Severe cases often present with brain malformations that can be detected by MRI scans, or were discovered upon autopsy. Common malformations include white matter atrophy, corpus callosum agenesis or hypoplasia, delayed or loss of myelination (Press et al., 1989, Viola et al., 2002), non-specific gyral malformations (Dobyns, 1989), and hydrocephalus often accompanied by presence of a posterior fossa cyst resembling the Dandy-Walker malformation (Van Hove et al., 2000, Hoover-Fong et al., 2004, Yis et al., 2009, Manel et al., 2012, Van Hove et al., 1998, Tsuyusaki et al., 2012). A rare case of pachygyria has also been reported in an NKH patient who also presented with agenesis of the corpus callosum (Fletcher et al., 1995).

Atypical NKH is much rarer and milder, with onset most commonly at the infantile age (although both neonatal and an older age of onset have been reported). Biochemical tests typically report modest elevation of glycine and CSF/plasma glycine ratios that do not reach the diagnostic threshold of the classical form, thus often complicating differential diagnoses of these patients. Hepatic GCS activity is also generally higher compared to classical NKH (Dinopoulos et al., 2005, Kure et al., 2004, Kure et al., 1997). The clinical

presentation of atypical NKH tends to be non-specific and heterogeneous with symptoms that include occasional seizures of any kind, febrile illness, episodes of ataxia, chorea, optic atrophy, vertical gaze palsy, delays in psychomotor and expressive language development, behavioural problems such as aggressiveness and outbursts of rage, autistic features, and intractable attention deficit hyperactivity disorder (ADHD).

While atypical NKH is not life-threatening, a majority of patients (about 61%) will suffer from severe mental retardation (Applegarth and Toone, 2001, Flusser et al., 2005). The modest elevations in glycine and non-specific nature of the symptoms sometimes overlap with other mental disorders such as ADHD and autism (Yu et al., 2013), and may cause atypical NKH to be underreported.

The transient, neonatal form of NKH is the rarest form, defined as a neonatal presentation of biochemical features and EEG burst-suppression patterns resembling classical NKH, but with symptoms that resolve completely or partially within days or months (Kure et al., 2002, Aliefendioglu et al., 2003). Diagnosis of transient NKH has often been debated. The seven cases of transient NKH reviewed by Applegarth and Toone (2001) did not have hepatic GCS activity tested, leading to the validity of their diagnoses being questioned. Kure et al. (2002) reported three cases of transient NKH with heterozygous mutations in *GLDC* in two of the patients, and a first report of a heterozygous *GCSH* mutation in the third. One of their patients with the *GLDC* mutation was followed up by Hamosh and Van Hove (2003), who reported that the patient's symptoms were not, in fact, "transient." They also raised the possibility that a second mutation may have been missed during the initial screen by Kure et al. (2002) and questioned the heterozygosity of those mutations.

Three cases of transient NKH were also reported by Korman et al. (2004), who found novel homozygous mutations in *GLDC* in those patients with high levels of residual GLDC activity (at 32%). Unlike previous cases of transient NKH in which biochemical features resolve within months along with symptoms, their patients' biochemical features persisted up to three and nine years of age despite resolution of symptoms within months. They suggested a new variant or form of NKH in these patients.

Gender differences in the clinical presentation of NKH have been suggested by Hoover-Fong et al. (2004). They reported significantly higher number of newborn deaths among girls compared with boys with NKH, and that boys reported better mental outcome. However, no gender differences were found with other parameters that were studied, such as total death and death in proportion to gender. In addition, no other survey of NKH patients has reported any gender differences (Hennermann et al., 2012).

1.2.2. Diagnostic history

The first diagnosis of NKH was made by Gerritsen et al. (1965) who described a hyperglycinemic patient who was non-ketotic. Early diagnoses of this condition were focused on differentiating it from the ketotic form of hyperglycinemia, which is not ascribed to single enzymatic defects and which can be seen in other metabolic conditions such as methylmalonic acidemia, proprionic acidemia, and isovaleric acidemia (Trijbels et al., 1974, Applegarth and Toone, 2001). Like NKH, ketotic hyperglycinemia presents with encephalopathy, hypotonia, and respiratory distress (Wajner and Goodman, 2011), but in addition to that patients also suffer from metabolic ketoacidosis which does not occur in NKH (Ando et al., 1972). Gerritsen et al.'s patient also had a defect in oxalic acid excretion, leading to an initial proposal that the disease was caused by a defect in the glycine oxidase system (Gerritsen et al., 1965).

Ando et al. (1968) then devised a method using labelled 1-^{14}C-glycine (carbon 1 of glycine which contributes to formation of CO_2) and 2-^{14}C-glycine (carbon 2 of glycine which gets incorporated into tetrahydrofolate, THF, or may alternatively become carbon 3 of serine) injected into NKH patients. They found a huge decrease in levels of exhaled $^{14}CO_2$ as well as virtually no incorporation of 2C-glycine to THF, as reflected by failure of 2-^{14}C-glycine to incorporate into serine.

Follow-up studies by the same group later found that the defect in conversion of 1C-glycine to CO_2 can occur in both the ketotic and non-ketotic form of hyperglycinemia, but that conversion of 2C-glycine to 5,10-methylene-THF resulted in defective conversion of 2C-glycine to 3C-serine in only the non-ketotic form (Ando et al., 1972). This led them to conclude that NKH patients have a defect in an enzyme that converts glycine to CO_2, NH_3, and THF, as opposed to other pathways of glycine catabolism such as the glycine oxidase system, and this condition was distinct from the ketotic form of hyperglycinemia. Their methods and findings were successfully replicated in subsequent studies (Tada et al., 1969, De Groot et al., 1970) and further supported by evidence that conversion of propionyl-CoA to methylmalonyl-CoA and methylmalonyl-CoA to succinyl-CoA (as would be expected in ketotic hyperglycinemia) in the liver of an NKH patient was, in fact, normal (Baumgartner et al., 1969, Tada and Arakawa, 1970).

Work done in the following decades was then able to characterise all four enzymatic components of the glycine cleavage system, which became recognized as the major pathway for glycine catabolism (Fujiwara and Motokawa, 1983, Fujiwara et al., 1984, Hiraga and Kikuchi, 1980, Kanno et al., 2007, Kure et al., 1997, Kure et al., 2006a). Mutations in genes that encode two of its components were found to be responsible for

nearly all cases of NKH. *GLDC* mutations account for approximately 80% of cases, while the rest were *AMT* mutations. Although no *GCSH* mutations have been found in NKH patients thus far, heterozygous mutations for *GCSH* have been reported in patients diagnosed with transient neonatal hyperglycinemia (Applegarth and Toone, 2001, Hennermann et al., 2012, Kure et al., 2002).

As the DLD enzyme is not specific to the GCS, mutations in *DLD* do not result in NKH. Due to its participation in three other alpha-ketoacid dehydrogenase multi-enzyme complexes in the mitochondria, *DLD* mutations result in L-protein deficiency with lactic acidosis, a variant of the maple syrup urine disease with none of the classical symptoms of NKH (Liu et al., 1993, Applegarth and Toone, 2001).

Currently, diagnosis of NKH begins with identification of the cardinal symptoms (e.g. hypotonia, apnea, and seizures) and biochemical studies showing elevated glycine in CSF and plasma, as well as increased CSF/plasma glycine ratio in which a threshold above 0.8 is considered diagnostic of classical NKH (Applegarth and Toone, 2001). The diagnosis is confirmed with enzymatic essays on liver biopsy or lymphoblast samples. The glycine exchange reaction between CO_2 and glycine using ^{14}C-bicarbonate ($NaH^{14}CO_3$) (i.e. decarboxylation assay) is used to assess activity of GLDC and GCSH, while the glycine synthesis reaction from methylene-THF, ammonium chloride (NH_4Cl), and $NaH^{14}CO_3$ is used for AMT (Hiraga et al., 1981, Kure et al., 1992). Kure et al. (2006b) also developed a rapid, non-invasive breath test by administering 1-^{13}C-glycine to NKH patients via gastric feeding and measuring amounts of $^{13}CO_2$ in breath samples. Mutation analysis is performed to identify the gene mutation. Brain imaging by itself is not diagnostic but is valuable for prediction of outcome of the severe form, as brain malformations seen in classical NKH tend to confer poor prognosis (Hoover-Fong et al., 2004).

1.2.3. Current GCS mice models

Two GCS mice models were created to assess the link between extracellular glycine concentration and ischemia via *N*-methyl-D-aspartate receptor (NMDAR) signalling (Oda et al., 2007). Both mice were generated by subcloning human GLDC cDNA (one normal and one carrying a dominant-negative mutation identified from an NKH-affected family) into pCAG vectors, injecting them into fertilised eggs of BDF1 mice, and backcrossing the mice into a C57BL/6 background. The mouse with wild-type human GLDC cDNA was designated high-GCS and expressed GCS activity that is 3.4X higher than in wild-type mice, while the mouse carrying the mutant cDNA, designated low-GCS, expressed 29% of GCS activity compared to wild-type mice. Both mice showed changes in cerebral glycine concentration

that corresponded to their respective levels of GCS activity. They showed that manipulating the level of GCS activity was able to alter infarct size produced by ischemic injury, and that the infarct volume could be ameliorated by administering an NMDAR antagonist.

In a second study by the same group, the high-GCS and low-GCS models were assessed for behavioural features resembling mild NKH. A third transgenic mouse was generated by injection of the same vector used in the making of the low-GCS mouse, and then backcrossing with C57BL/6 mice. This mouse was designated low-GCS-2 and had 33% GCS activity compared with wild-type mice (Kojima-ishii et al., 2008). Neither low-GCS mice exhibited brain malformations common in NKH patients (such as agenesis of the corpus callosum), but they did exhibit higher spontaneous locomotor activity, higher seizure susceptibility, elevated aggressiveness, and anxiety-like behaviour. All behavioural abnormalities were able to ameliorated using NMDAR antagonists.

In the Narisawa et al. (2012) study, a knockout mouse for *Amt* (*Amt*$^{-/-}$) was generated which exhibited undetectable levels of GCS enzymatic activity. The *Amt*$^{-/-}$ embryos developed NTDs (exencephaly at a frequency of 82% and craniorachischisis at 5%), and showed sensitivity to methionine and combined methionine plus thymidine monophosphate treatment but not to folic acid.

Unfortunately, none of the existing mice models are suitable as models for classical NKH. The low-GCS and high-GCS models were used for investigating the effect of glycine concentration on NMDAR signalling and certain behavioural features of mild NKH, but do not exhibit the hallmark features of the more common classical form, while the *Amt* knockout mouse with its very high incidence of NTDs would not have sufficient mutant survivors to be an effective working model for NKH.

1.3. Neural tube defects

Neural tube defects (NTDs) are a group of congenital defects that arise when the neural tube fails to close during development. They are amongst the most severe and second most common group of birth defects after heart defects, and affect approximately 0.5-2 per 1000 pregnancies worldwide (Mitchell, 2005). The aetiology of NTDs is complex and remains largely unknown due to their multifactorial nature. Despite having identified over 200 genes required for neural tube closure in mice (Harris and Juriloff, 2007, Harris and

Juriloff, 2010), no single genetic defect has been identified as the major cause of NTDs in humans, suggesting a contribution of multiple genetic and environmental factors.

1.3.1. Mammalian neurulation

As a vast majority of clinically classified NTDs are associated with neural tube development, an understanding of the embryological process of neural tube closure is important to investigate the pathology of these defects. The neural tube is the embryonic precursor of the central nervous system from which all neural precursor cells that later make up the brain and spinal cord derive. Neural tube closure, or neurulation, is evolutionarily conserved in amniotes like mammals, birds, and reptiles, and have been extensively studied in classical developmental biology animal models such as the fly, zebrafish, frog, chicken, and mouse. The description provided here is largely based on the mouse model, which has many parallels to human neurulation.

The process of neurulation occurs in two distinct phases: primary and secondary.

Primary neurulation involves the invagination of specialised, flat, ectoderm cells into the embryo body that then fold to form a closed tube along the midline axis of the embryo (**Figure 2B**). During gastrulation, a subset of cells on the dorsal surface ectoderm of the embryo, anterior to the primitive streak, acquire neural identity and thicken to form the flat neural plate in a process known as neural induction (Levine and Brivanlou, 2007). At the onset of primary neurulation, these cells and cells of the underlying axial mesoderm converge towards the midline and intercalate medio-laterally. This process of convergent-extension narrows the width while extending the length of the neural plate in concert with elongation of the embryo body's rostro-caudal axis (Copp et al., 2003, Keller et al., 2000, Keller, 2002, Ybot-Gonzalez et al., 2007b).

The neural plate then begins to bend in the midline with formation of the median hinge point (MHP) directly above the notochord. This forms a "groove" that runs along the length of the body axis, with the lateral neural folds elevating dorso-ventrally as the MHP gets more pronounced. A second bending event follows: the formation of dorsolateral hinge points (DLHPs), which directs the bilateral tips of the neural folds toward the midline.

Dorso-laterally bending is more dramatic in the cranial region, where the neural folds initially take on a convex curvature with its tips facing outwards after MHP formation (**Figure 2C**). The neural folds substantially thicken and bulge out into the lumen, accompanied by vast proliferation and expansion of the underlying mesenchyme. When

the DLHPs form, the folds take on a concave curvature instead and the tips flip towards the midline to form a keyhole-shaped lumen (Morriss-Kay, 1981).

The DLHPs bring the tips of the neural folds in apposition of one another for the final step of adhesion and fusion. The tips reach out and adhere to one another with the aid of cell surface protrusions (Geelen and Langman, 1979, Pyrgaki et al., 2010) and fuse to form a closed tube. The dorsal epithelia then undergo remodelling and the neural tube, consisting of a pseudostratified layer of neuroepithelial cells, is separated from the overlying surface ectoderm layer.

In primary neurulation, 3 distinct locations of closure initiation is known to occur in the mouse embryo (**Figure 2A**) (Golden and Chernoff, 1993). The first point of closure, known as closure 1, occurs at the future hindbrain-cervical boundary on embryonic day 8 (E8), at the third somite level of a 6-7 somite stage embryo (Copp et al., 2000). This is equivalent to days 22-23 in human embryos (Lew and Kothbauer, 2007). Closure proceeds bidirectionally from there: rostrally up the hindbrain, and caudally down the spine.

Closure 2 occurs at the forebrain-midbrain boundary at the 13-14 somite stage, also spreading bidirectionally and meeting the rostrally-moving closure front from closure 1 at the hindbrain neuropore (HNP). At the same time, closure 3 starts at the extreme rostral end of the forebrain. It proceeds up the forebrain towards the midbrain to meet the fusion front from the direction of closure 2 at the anterior neuropore (ANP). Cranial closure is complete at E9.5, at somite stage 17-18, or day 24 in human embryos.

Closure proceeds caudally down the spine from the closure 1 point in a zippering fashion and ends with the closure of the posterior neuropore (PNP) at the 29-30 somite stage on E10.5 (Copp et al., 2000), or days 26-28 in human embryos. Primary neurulation is complete after approximately 36 hours from time of onset.

Completion of primary neurulation is succeeded by secondary neurulation at E11 at the 32-34 somite level, and continues through gestation in mice (days 28-48 in human embryos). This forms the spinal cord at the lower sacral and caudal levels utilising a process known as “canalisation” (Copp and Greene, 2010 , Lew and Kothbauer, 2007, Schoenwolf, 1984). Directly caudal to the closed posterior neuropore, cells in the tail bud (known as the caudal cell mass in humans) acquire a neuroepithelial fate and begin to aggregate. They condense to form a medullary cord-like structure under the surface ectoderm, their apico-basal polarity leading to a radial orientation around the future lumen. A central cavity opens, becoming a tube that is directly continuous with that formed during primary neurulation (Harrington et al., 2009, Copp and Greene, 2010 , Schoenwolf, 1984).

Figure 2. Overview of mouse primary neurulation.

(A) (i) Closure 1 begins at the level of the 3rd somite of a 6-8 somite stage and occurs bidirectionally. The forebrain (FB), midbrain (MB), and hindbrain (HB) of the embryo is indicated. The future closure 2 site is located at the FB-MB boundary, closure 3 at the rostral end of the forebrain. **(ii)** At the 12-14 somite stage, closure 2 and closure 3 has initiated. Closure 1 and 2 meet at the hindbrain neuropore (HNP), closure 2 and 3at the anterior neuropore (ANP). Closure 1 proceeds caudally to close the posterior neuropore (PNP).

(B) (i) Primary neurulation begins with the induction of a group of flat epithelial cells during gastrulation to become neural ectoderm. **(ii)** Formation of the median hinge point (MHP) elevates the neural folds dorso-ventrally. **(iii)** Formation of the dorso-lateral hinge points (DLHPs) bring the tips of the neural folds toward the midline. **(iv)** Fusion of the neural folds and remodelling of the cells at the fusion point produces a closed neural tube (NT) with an overlying surface ectoderm (SE).

(C) (i) In the cranial region, formation of the MHP is succeeded by thickening of the neuroepithelium (NE), producing a convex curvature. **(ii)** Dorso-lateral bending flips the tips of the cranial neural folds toward the midline, obtaining a convex curvature (arrows). **(iii)** Fusion of the neural tips result in a keyhole-shaped lumen.

References: Greene and Copp (2009) and Copp (2005)

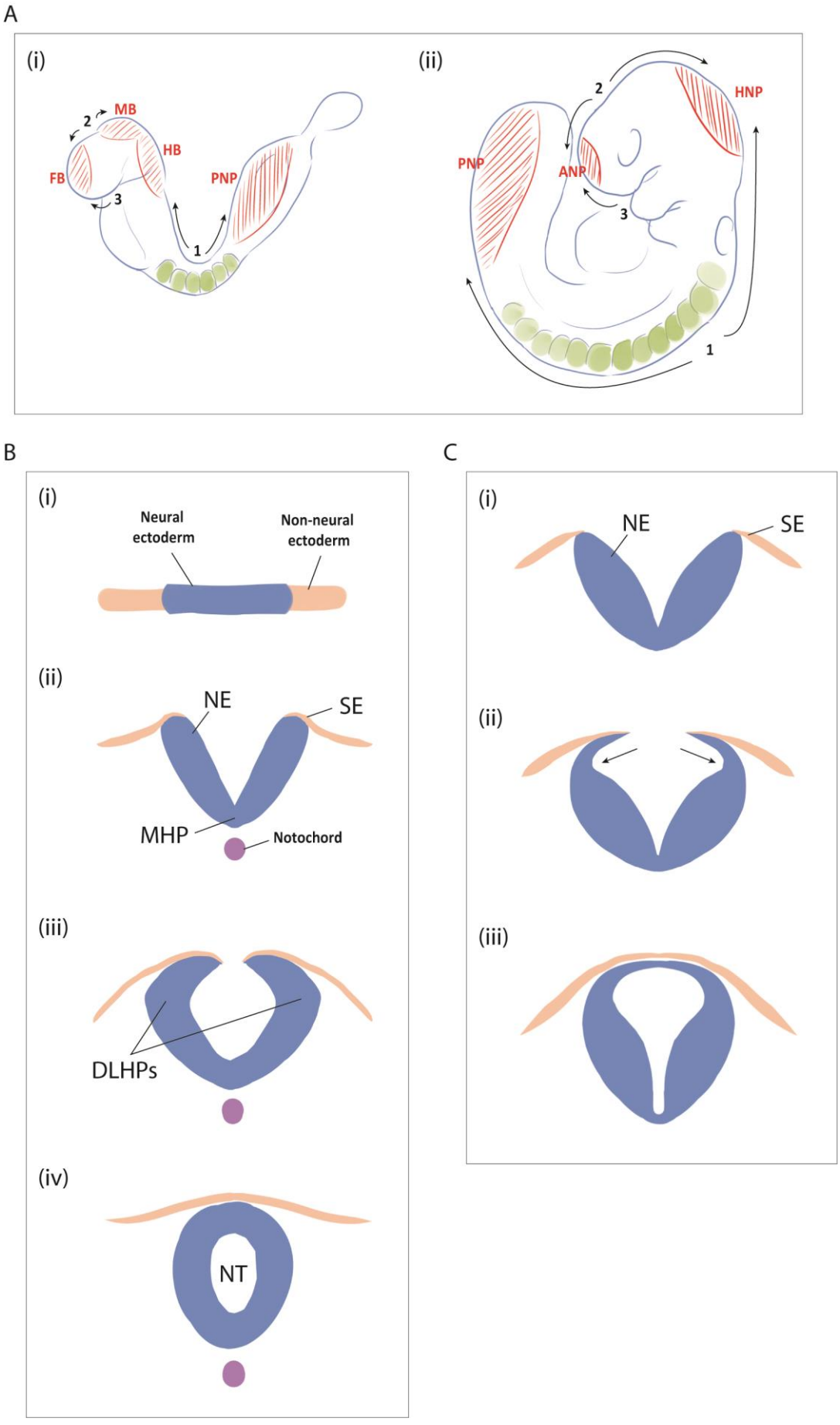

Figure 2. Overview of mouse primary neurulation.

In the final stages of secondary development, the medullary cord at the caudal end is sculpted by tissue degeneration and retrogressive differentiation. In mice and tailed mammals, the medullary cord and vertebrate column form the tail. In humans and tailless mammals, canalisation at the caudal-most terminal ends with the formation of the ventriculus terminalis. Throughout the rest of the human gestational period, this structure "ascends" relative to the elongation of the vertebral canal and forms the conus, cauda equina and fibrous strands of the filum terminale (Lew and Kothbauer, 2007, Pang et al., 2011, Tortori-Donati et al., 2000).

1.3.2. Classification of NTDs

Neural tube defects can be broadly classified as open and closed subtypes according to embryonic origin of the defect (Copp and Greene, 2013). Open NTDs occur when primary neurulation fails, leaving a part of the neural tube unfused. This exposes the brain tissue to the extra-embryonic environment, resulting in *in utero* degeneration and subsequent damage as embryonic development progresses. Closed NTDs have skin covering the lesion, and are attributed to failed secondary neurulation. The herniation subtype results from defective development of the overlying skeletal structure, causing the closed neural tube to herniate out with the meninges.

Craniorachischisis, exencephaly, and open spina bifida are open NTDs corresponding to the axial level at which the neural tube fails to close (Copp et al., 2003).

Failure of closure 1, the first and earliest closure event, results in craniorachischisis where the entire length of the neural tube caudal to the midbrain remains open. This condition is the rarest and severest form of NTD, and is combined with a shorter anterior-posterior embryo length due to a defect in convergent-extension (Copp and Greene, 2013).

When closure 2 is not completed, the hindbrain and/or anterior neuropore remain open. The cranial neural folds splay apart, get exposed to amniotic fluid, and gradually degenerate *in utero*, resulting in exencephaly. This condition then progresses to anencephaly (literally meaning "no brain"), where there is massive loss of brain tissue and failure of the skull vault to form (Copp, 2005). Failure of the anterior neuropore to close results in a condition known as "split face." Patients born with anencephaly die at or shortly after birth.

Open spina bifida (or spina bifida aperta) occurs when caudal progression from closure 1 down the spine arrests midway. The size of the spina bifida lesion depends on which axial level closure fails: the rest of the neural tube caudal to that point remains open. Similar to

the skull deformity accompanying exencephaly, the vertebrate arch fails to form around the open spinal folds, leaving an exposed lesion. Open spina bifida is divided to the rare myelocoele (or myeloschisis), in which the lesion is completely exposed, and the considerably more common myelomeningocoele (or spina bifida cystica), in which the lesion is covered by a meninges sac (Greene and Copp, 2014, Copp and Greene, 2013, Tortori-Donati et al., 2000). Unlike anencephaly and craniorachischisis, open spina bifida is not lethal but causes life-long disabilities and complications such as paralysis of the lower limbs, bladder incontinence and urinary tract infections, and bowel dysfunction. It is also frequently associated with other conditions such as hydrocephalus with Chiari type II malformations, in which the hindbrain herniates into the foramen magnum (Copp et al., 2003, Copp and Greene, 2010).

Defects in secondary neurulation result in closed defects (where neural tissue is unexposed under a skin covering) due to never having been "open" and exposed to extra-embryonic environment during development. They are often classified under a more diverse group of spinal malformations clinically known as occult spinal dysraphism (OSD, or spina bifida occulta) that vary in severity (Greene and Copp, 2014, Copp et al., 2015). They are also often accompanied by tethering of the spinal cord and lumbosacral cutaneous lesions that may serve as skin markers (Guggisberg et al., 2004, Drolet and Boudreau, 2004, Lew and Kothbauer, 2007). Examples of OSD subtypes include lipomyelomeningocoele in which neural and fatty tissue protrude through a defective vertebrate (Lew and Kothbauer, 2007), and dermal sinus tracts in which an epithelial tract joins the skin and dermal tissue to the spinal cord (Ackerman and Menezes, 2003).

Herniation-type NTDs can be divided to encephalocoele, where herniation of a region of the brain occurs through a skull defect, and spinal meningocoele, where meningeal tissue and spinal fluid herniate through an opening in the vertebrae and dura (Greene and Copp, 2009, Greene and Copp, 2014, Copp and Greene, 2013).

1.3.3. Differences between human and mouse primary neurulation

Anencephaly constitutes about half of human NTDs, but in mice models, it is the most common type of NTD observed (Copp et al., 2003, Copp et al., 2013). While the morphogenetic sequences of primary and secondary neurulation are mostly conserved between human and mouse embryos, some variation does exist. These variations may account for differences observed in the incidence of NTDs between the two. When comparing between stage-matched human and mouse embryos, one striking difference is that human embryos have noticeably smaller heads in proportion to the body (Copp,

2005). This suggests that cranial neurulation may be more easily achieved in human embryos than in mice for simple, mechanistic reasons.

Primary neurulation in human embryos was initially thought to begin with a single initial closure event at the brain-spinal cord junction, is followed by bidirectional zippering in a rostral and caudal direction, and end with the closure of rostral and caudal neuropores (O'Rahilly and Muller, 1994). However, the findings of multiple closure sites in mice embryos prompted a multi-site closure model in human embryos as well. This resulted in some studies describing 5 closure sites to account for the various types of human NTDs (Van Allen et al., 1993, Seller, 1995, Martinez-Frias et al., 1996). While the events of closure 1 and closure 3 in the human neural tube are generally agreed upon by most studies, the existence of closure 2 is debatable. Examination of human neurulating embryos and still-births with neural tube defects have led to some studies reporting a closure 2 event (Golden and Chernoff, 1995, Nakatsu et al., 2000, Seller, 1995) and others not (O'Rahilly and Muller, 2002).

The precise location of the closure 2 site also varies amongst various mice strains (Juriloff et al., 1991, Fleming and Copp, 2000). Closure 2 occurred consistently in the forebrain/midbrain boundary of some strains (such as randomly bred CD1 mice), while in others it consistently initiated further rostral into the forebrain region or caudal into the midbrain. This difference appears to affect the susceptibility of the strain to develop cranial NTDs, with a more rostrally located closure 2 conferring a higher, genetically-predetermined risk for cranial closure to fail (Fleming and Copp, 2000). Remarkably, mice on the SELH/Bc background strain do not undergo a closure 2 event (Macdonald et al., 1989). While 17% of these mice spontaneously develop exencephaly, the fact that the rest of them are able to successfully close their cranial neural tubes suggests that closure 2 is not essential for closure in mice embryos, but that its absence increases the risk of failure of closure to occur.

1.3.4. Aetiology of NTDs

The aetiology of NTDs is complex and involves both environmental and genetic factors. Maternal disease states, nutritional and socioeconomic statuses, intake of folic acid, and exposure to teratogens can all contribute to NTD risk. A genetic component to the aetiology of NTDs also exists. Variations in family inheritance patterns, degree of penetrance, and severity of disease manifestation all point to the involvement of multiple genes in a polygenic (i.e. combination of heterozygosity across multiple risk alleles), or oligogenic (i.e. presence of a second, or more, gene modifying the effect of a dominant

gene) inheritance pattern. Thus, NTDs appear to follow a multifactorial threshold model in which the additive effects of multiple genetic and non-genetic risk factors above a certain "threshold" is required to precipitate the phenotype (Harris and Juriloff, 2007, Copp and Greene, 2010 , Copp et al., 2013). Notable environmental and genetic factors gleaned from clinical and epidemiological findings as well as studies on mice models are outlined below.

1.3.4.1. Environmental factors

Due to the multifactorial nature of NTDs, identification of independent, definitive environmental factors is difficult and often complicated by the contribution of genetic factors and gene-environment interactions. **Table 1** provides an overview of notable non-genetic factors with established associations to NTDs (Copp and Greene, 2010). Many other factors such as maternal smoking, alcohol use, stress, and water chlorination have been proposed. While these are plausible factors, studies yield largely inconsistent findings, show weak association, or are relatively rare, and thus they would only contribute to a small proportion of all NTD cases (Wyszynski, 2006, Copp et al., 2015).

The link between poor nutrition and/ or lower socioeconomic status and birth defects has been observed since the Dutch winter famine of the mid-1900s. The biggest revelation to come out of pursuing this link is the finding that maternal folate status is an NTD risk factor, and that periconceptual folic acid supplementation is able to significantly reduce occurrence and recurrence of NTDs (see **Section 1.4**).

In addition to folate, low maternal blood vitamin B12 levels was also discovered to be an independent NTD risk factor (Kirke et al., 1993, Suarez et al., 2003), that women in the group with the lowest levels of both folate and B12 demonstrated the highest risk (Kirke et al., 1993), and that this finding remains true in populations with or without folic acid fortification (Ray et al., 2007, Molloy et al., 2009b).

Inositol deficiency was first shown to increase susceptibility to exencephaly of genetically predisposed, folate-resistant, *curly tail* mouse model in an embryo culture system (Cockroft et al., 1992). The spinal NTDs in *curly tail* embryos can be significantly rescued by *myo*-inositol and D-*chiro*-inositol through increased activation of specific isoforms of protein kinase C, which in turn increases proliferation in the hindgut of these embryos (Greene and Copp, 1997, Cogram et al., 2002, Cogram et al., 2004) (see **Section 1.3.4.2.5**). Studies of inositol deficiency in human NTDs is scarce, with just one study showing an association between low maternal inositol levels and a 2.6-fold increased risk of spina bifida (Groenen et al., 2003). This study also found an association between low maternal

zinc levels and increased spina bifida risk, zinc being another repeatedly cited micronutrient deficiency associated with NTDs with an unknown underlying mechanism (Milunsky et al., 1992).

Environmental risk factor	Proposed mechanism
Maternal nutrition	
Folate	Disturbance in folate metabolism
B12	Disturbance in folate metabolism
Inositol	Disturbance in downstream protein kinase C signalling
Maternal diabetes (hyperglycaemia)	Disturbance in glucose homeostasis, increased production of reactive oxygen species, increased apoptosis
Maternal obesity	Unknown
Maternal medication	
Carbamazepine	Folic acid antagonist
Trimethoprim	Folic acid antagonist
Valproic acid	Disturbance in histone deacetylase activity
Other exposures	
Fumonisin	Disturbance in sphingolipid synthesis
Maternal hyperthermia	Unknown

Table 1. Notable environmental risk factors associated with NTDs.

Maternal diabetes has long been recognised as a risk factor for various organ malformations, including the central nervous system, heart, eye, kidney, lower limbs and lower spine (Martinez-Frias, 1994, Correa et al., 2008). Maternal genes involved in glucose homeostasis, type-2 diabetes, and obesity have been associated with NTDs. These include glucose transporter (*GLUT1*), leptin (*LEP*), leptin receptor (*LEPR*), hexokinase (*HK1*), and transcription factor 7-like 2 (*TCF7L2*) (Davidson et al., 2008, Carter et al., 2011, Lupo et al., 2012). As pancreatic β cells do not develop until 7-8 weeks into gestation after most organogenesis processes have passed (Jovanovic-Peterson and Peterson, 1993), it has been suggested that teratogenicity is caused by the developing embryo being unable to cope with a hyperglycaemic *in utero* environment brought about by maternal diabetes.

The teratogenic effects of hyperglycaemia are hypothesised to occur through induction of changes in lipid peroxidation, resulting in increased production of reactive oxygen species which subsequently activates apoptotic pathways (Loeken, 2005, Reece, 2012). Induction of hyperglycaemia in mice was shown to inhibit *Pax3* expression and increase

neuroepithelial apoptosis and rate of NTDs (Fine et al., 1999). There is recent evidence that activation of the ASK1-FoxO3a-Caspase 8 pathway occurs in hyperglycaemic states through oxidative stress, resulting in increased apoptosis in the neuroepithelium of diabetic mice. Deletion of *Ask1*, *FoxO3a* or *Casp8* in these mice was able to reduce apoptosis and NTD incidence (Yang et al., 2013).

Many studies over the years have associated pregnancy weight, both underweight and overweight, to NTDs [reviewed in Wyszynski (2006) and Carmichael et al. (2010)] and other congenital malformations. Maternal obesity is often quoted as an NTD risk factor alongside diabetes, but it is not clear if obesity, without the effects of hyperglycaemia or other confounding factors (e.g. maternal nutrition or history of NTD-affected pregnancy), is in itself a risk factor. Studies have found association between overweightness and obesity with increased NTD risk when pre-existing diabetic mothers were excluded (Watkins et al., 2003). It should be noted, however, that some of the women may have undiagnosed diabetes or pre-diabetic glucose intolerance. Hyperinsulinaemia was found to be an NTD risk factor independent of diabetic history, and has been hypothesised to cause the increased risk in obese women (Hendricks et al., 2001).

In addition to nutritional risk factors, other substances and conditions have been identified as teratogenic and disruptive to neural tube closure. These include folate antagonists such as carbamazepine and trimethoprim, contaminants such as fumonisin, the anti-convulsant drug valproic acid, and maternal hyperthermia (Copp and Greene, 2010 , Copp and Greene, 2013).

The observation of low maternal folate being linked to increased NTD risk prompted research into folic acid antagonists (FAA) as potential risk factors. Hernandez-Diaz et al. (2001) looked into maternal exposure of FAAs in NTD-affected pregnancies and found increased risk upon exposure to the antiepileptic drug carbamazepine and antibiotic trimethoprim (taken in combination with a sulphonamide). This risk was further increased in mothers without folic acid supplementation. The effect of carbamazepine on NTD risk was also noted in other studies (Kaaja et al., 2003, Werler et al., 2011).

Antiepileptic drugs have long been linked to congenital malformations (Wlodarczyk et al., 2012). Where NTDs are concerned, the effects of valproic acid (VPA) was first noticed by Robert and Guibaud (1982) and later listed (alongside carbamazepine) to show association with increased risk of congenital malformations, notably NTDs, in mothers on antiepileptic medication (Kaaja et al., 2003, Werler et al., 2011). VPA is also capable of inducing NTDs in rodent models (Finnell et al., 1988, Ehlers et al., 1992, Menegola et al., 2005). VPA is proposed to cause its teratogenic effect by inhibiting histone deacetylase

(HDAC) activity and causing hyperacetylation in embryos, a hypothesis that is supported by similar findings with another HDAC inhibitor, Trichostatin A (Menegola et al., 2005).

Fumonisin is a corn mould mycotoxin that was shown to inhibit sphingolipid biosynthesis, leading to disruption of cellular uptake of 5-methyl-THF by glycosylphosphatidylinositol (GPI)-anchored folate receptors *in vitro* (Stevens and Tang, 1997). Fumonisin-induced disturbance in sphingolipid synthesis is also suggested to affect other cell signalling pathways that are important to neurulation. Increased maternal exposure to fumonisin from ingestion of contaminated corn products was found to be associated with increased risk of NTDs (Missmer et al., 2006). Fumonisin treatment also induced NTDs in a rodent embryo culture system which could be partially rescued by co-treatment with folinic acid (Sadler et al., 2002), as well as in a mouse *in vivo* model which could be partially rescued by folic acid (Gelineau-van Waes et al., 2005, Gelineau-van Waes et al., 2012).

Hyperthermia is commonly reported as an NTD-causing teratogen in many rodents (Edwards, 1986, Finnell et al., 1986). A meta-analysis of cases of maternal hyperthermia during the first trimester of pregnancy, caused by fever or external heat sources such as saunas, found an association between hyperthermia and increased risk of NTDs in humans as well (Moretti et al., 2005).

1.3.4.2. Genetic factors

A strong case can be made for the presence of a genetic predisposition to NTDs from family history of NTD-affected pregnancies. There exists a recurrence risk of 2 to 5% among siblings that cannot be accounted for by exposure to a similar environmental teratogen. In addition, twin studies revealed a higher penetrance in monozygotic compared to dizygotic twins, which would be expected if a genetic component is present (Detrait et al., 2005, Deak et al., 2008, Knox, 1974). Chromosomal aberrations such as trisomy 18 and trisomy 13 are often reported in NTDs, especially in encephalocoele and spina bifida (often accompanied by additional anomalies), and tend to result in spontaneous abortions (Coerdt et al., 1997, Kennedy et al., 1998, Sepulveda et al., 2004).

A striking gender bias exists in the occurrence of anencephaly, with consistently higher prevalence in females in both humans and mice (Juriloff and Harris, 2012b). Extreme examples of this gender bias, in which exencephaly occurs almost exclusively in females, is seen in some mice models such as the *Trp53* and *Nf1* mutants (Harris and Juriloff, 2007). The cause of this female preponderance is not known, and several hypotheses that have been proposed include inactivation of one X chromosome, death of affected males, and

developmental delay in females (Juriloff and Harris, 2012b). Data from Chen et al. (2008) suggested that incidence of NTDs in p53-null mice with transgene manipulation of the testis-determining gene *Sry* was higher when two copies of the X chromosome are present, independent of the presence or absence of the Y chromosome. However, the mechanism by which two X chromosomes can confer higher risk of NTDs is still unknown.

The search for NTD candidate genes tends to follow two main strategies: genes found to result in NTDs when mutated in mice, and genes related to known environmental factors such as maternal hyperglycaemia and folate metabolism (Greene and Copp, 2014). It must be noted that there are three times as many NTD mice models with exencephaly as there are spina bifida, which have to be taken into consideration when evaluating NTD mice models. In addition, many mice models with a single-gene knockout can result in NTDs, some with almost full penetrance in homozygotes, which is unlike the polygenic or oligogenic patterns of human NTDs. Nevertheless, mice models have been valuable in identifying pathways in which to look for candidate genes for human NTDs and have greatly contributed to the understanding of the cell biology of mammalian neurulation (Copp and Greene, 2010). A comprehensive list of over 200 NTD mice models was provided in Harris and Juriloff (2007) and Harris and Juriloff (2010), and a few pathways are noted as followed.

1.3.4.2.1. Planar cell polarity genes

The planar cell polarity (PCP) pathway is required for convergent-extension in the neural plate. A defect in PCP signalling results in the widening of the midline during gastrulation, such that the neural folds become spaced too far apart to close (Ybot-Gonzalez et al., 2007b). Mutations in many PCP pathway genes (e.g. *Scrb1, Vangl2*, *Celsr1*, and *Dvl* family) prevent closure 1 from happening and result predominantly in craniorachischisis when present in homozygosity (e.g. *Celsr1*$^{-/-}$ and *Vangl2*$^{Lp/Lp}$) or as digenic mutants in various combinations (e.g. *Vangl2*$^{Lp/+}$*;Celsr1*$^{Crsh/+}$, *Vangl2*$^{Lp/+}$*;Scrb1*$^{+/-}$, *Dvl1*$^{-/-}$*;Dvl2*$^{-/-}$, and *Vangl2*$^{Lp/+}$*;Dvl2*$^{-/-}$) (Murdoch et al., 2003, Murdoch et al., 2001a, Curtin et al., 2003, Hamblet et al., 2002, Etheridge et al., 2008, Murdoch et al., 2001b, Wang et al., 2006, Juriloff and Harris, 2012a).

In humans, putative mutations in core PCP (e.g. *VANGL1*, *VANGL2*, *CELSR1*, and *PRICKLE1*) and PCP-related genes (e.g. *SCRIB* and *LRP6*) have been found in patients with various NTD types including craniorachischisis, anencephaly and open and closed spina bifida (Kibar et al., 2007, Merello et al., 2015, Lei et al., 2010, Robinson et al., 2012, Lei et al., 2013, Allache et al., 2014). Putative mutations in *VANGL1*, *VANGL2*, and *CELSR1* were also

found in defects of secondary neurulation, especially involving the filum terminale (Juriloff and Harris, 2012a).

1.3.4.2.2. Sonic hedgehog and BMP genes

The sonic hedgehog (Shh) and bone morphogenetic protein (BMP) signalling pathways act in antagonism to one another in dorso-ventral patterning of the neural tube. They are both implicated in NTDs in mice. Ectopic expression of *Shh* and mutations in negative regulators of Shh signalling, e.g. *Ptch1*, *Sufu*, *Rab23*, and *Tulp3*, result in exencephaly and/or spina bifida (Echelard et al., 1993, Goodrich et al., 1997, Cooper et al., 2005, Gunther et al., 1994, Eggenschwiler et al., 2001, Ikeda et al., 2001, Patterson et al., 2009, Murdoch and Copp, 2010). This indicates that *increased* activation of Shh signalling, resulting in an expansion of ventral markers, prevents neural tube closure.

Various cellular mechanisms have been proposed for the action of Shh in the NTD phenotype, such as disruption in the balance of neuroepithelial cell proliferation, differentiation, and apoptosis. The most persuasive evidence is that of inhibition of DLHP formation by ventral Shh signalling (Ybot-Gonzalez et al., 2002). Shh and BMP signalling is able to inhibit the BMP antagonist, noggin, which is required for appropriate dorsolateral bending. *Zic2*$^{Ku/Ku}$ mutants (i.e. *Kumba* mutants where there is loss of function of *Zic2*) display downregulated noggin expression, lack DLHPs, and develop spina bifida (Ybot-Gonzalez et al., 2007a).

1.3.4.2.3. Proliferation, differentiation, and apoptosis genes

Mice with mutations in genes that regulate or alter cell-cycle progression and/or proliferation, e.g. *Jarid2* or *jumonji*, *Nf1*, and *Nup50* (Takeuchi et al., 1995, Lakkis et al., 1999, Smitherman et al., 2000), neuronal differentiation, e.g. *Pax3* and Notch pathway genes like *Hes1* and *Notch3* (Epstein et al., 1991, Ishibashi et al., 1995, Lardelli et al., 1996), and apoptosis, e.g. *Bcl10*, *Apaf1*, and *Casp3/9* (Ruland et al., 2001, Yoshida et al., 1998, Kuida et al., 1998) often exhibit exencephaly. This suggests that cranial neurulation is especially sensitive to perturbations in the balance between neuroepithelial cell proliferation, differentiation, and death. However, the precise morphological changes underlying the NTDs in these mutants and which step of neurulation is affected remain unclear. The role of apoptosis is further complicated by conflicting evidence: mutations that result in either excessive or insufficient cell death can result in NTDs, but embryos treated with apoptosis inhibitors showed no effect on neurulation (Massa et al., 2009).

1.3.4.2.4. Genes in cytoskeletal regulation

Exencephaly (and much less commonly, spina bifida) occurs in mutants of cytoskeletal components, e.g. vinculin, shroom and *n*-cofilin, as well as signal transduction proteins involved in cytoskeletal assembly, e.g. MARCKS, p190 RhoGAP, and Mena/VASP (Xu et al., 1998, Hildebrand and Soriano, 1999, Gurniak et al., 2005, Stumpo et al., 1995, Brouns et al., 2000, Menzies et al., 2004, Copp and Greene, 2010). In addition, earlier studies with embryos treated with cytoskeletal-disrupting teratogens also resulted in exencephaly but not spina bifida (Ybot-Gonzalez and Copp, 1999), revealing a higher sensitivity to cytoskeletal disruptions in cranial neurulation.

1.3.4.2.5. Curly tail model

The *curly tail* (*ct*) mouse is one of the most extensively studied NTD mouse model and demonstrates how a defect in adjacent, non-neural tissue can give rise to a failure of neural tube closure on mechanistic grounds. In the *ct* mouse, an increase in ventral curvature of the caudal region prevents the neural folds of the posterior neuropore from elevating and fusing, resulting in spina bifida (Brook et al., 1991). This increased curvature is brought about by an imbalance between decreased proliferation of hindgut endoderm, and normal proliferation of the neuroepithelium. The gene responsible for the *ct* phenotype remained elusive for many decades (van Straaten and Copp, 2001), and was finally discovered to be *grainyhead-like 3* (*Grhl3*) (Ting et al., 2003, Gustavsson et al., 2007). The effect of the *Grhl3* mutation is also influenced by modifier genes: the presence of a variant of the lamin B1 gene (*Lmnb1*) disrupts nuclear morphology, cell-cycle progression, and proliferative capacity of hindgut epithelium, and significantly increases NTD incidence in $Grhl3^{ct}$ mutants (De Castro et al., 2012).

Informative as mice models are, the search for associations between mutations in mice models and cases of human open NTDs have yielded largely insignificant results (Boyles et al., 2005, Greene et al., 2009). The only mutations that consistently show significant association, whether through NTD mice models or environmental risk factors, are those that encode maternal hyperglycaemia and/or obesity-related proteins, components of the PCP pathway and folate metabolism (see following section). It should be noted, however, that most studies have only focussed on specific polymorphisms. There is limited availability of whole exome data, and regulatory mutations have not been considered to a great extent. Identification of NTD risk alleles would likely require large-scale next generation sequencing with large patient cohorts.

1.4. Folate metabolism and NTDs

1.4.1. History of folic acid treatment

The association between folate status and NTDs first started with observations made on the Dutch famine or "Hunger Winter" of 1944, when poor nutrition was observed to precipitate developmental defects. Kalter and Warkany (1959) conducted animal studies and found that feeding pregnant mothers with vitamin-deficient diets or vitamin antagonists induced developmental defects in their foetuses. In the same period, a link was made between folic acid deficiency during pregnancy and megaloblastic anaemia in addition to defective foetal growth (Chanarin et al., 1959). The anaemia was found to respond to folic acid treatment (Gatenby and Lillie, 1960). Hibbard and Hibbard (1963) then found a relationship between maternal folic acid deficiency and abruptio placentae alongside a high incidence of megaloblastic anaemia. However, up until then, there was no clear evidence to link nutritional deficiency with foetal malformations in humans.

In 1964, a study conducted in Liverpool was published, suggesting a possible relationship between folic acid deficiency and foetal malformation (Hibbard, 1964). They presented evidence that a deficiency in folate *metabolism* causing a deficiency in folic acid (that may not be caused by insufficient dietary intake) could produce megaloblastic anaemia, abruptio placentae, and possible foetal malformations. They also observed that folic acid deficiency has a tendency to recur in successive pregnancies. The same group then found that women near delivery who had babies with severe (mostly CNS) malformations excreted abnormally high levels of formiminoglutamic acid (FIGLU), which indicated impaired folate absorption or metabolism (Hibbard and Smithells, 1965).

In the 1970s, Smithells et al. began scrutinising the link between maternal diet and NTDs. They found that women with NTD-affected pregnancies showed significantly lower red blood cell folate and white blood cell vitamin C compared with control groups, supporting the hypothesis that nutritional deficiencies can cause significant disturbances to CNS development (Smithells et al., 1976). They also reported that social class, maternal age, smoking, and vomiting during pregnancy can influence maternal diet during early pregnancy at the critical period for neural tube development (Smithells et al., 1977). These findings prompted them to investigate the prophylactic use of vitamin supplementation using a commercially available mixture of vitamins and folic acid to prevent NTDs, leading to a preliminary intervention study (Smithells et al., 1980) that then expanded into the Leeds Intervention Studies (Smithells et al., 1981). These intervention studies found highly significant, 7-fold decrease in NTD recurrence in the supplemented group

compared to unsupplemented, and they suggested repeating the study with a more selective mix of vitamins or with folic acid alone. Further evidence on a possible protective effect by folic acid then came in subsequent studies (Smithells et al., 1983, Schorah et al., 1983, Seller and Nevin, 1984, Sheppard et al., 1989, Smithells et al., 1989, Bower and Stanley, 1989, Milunsky et al., 1989, Mulinare et al., 1988). However, many of these findings were met with criticism due to the lack of randomised, double-blinded trial designs which had not been approved to them by research ethics committees (Oakley et al., 1983, Elwood, 1983, Wald and Polani, 1984). Most of these trials also used a multivitamin mix which did not single out folic acid as the main preventive element.

Finally, a randomised, double-blinded prevention trial was approved and carried out by the Medical Research Council (MRC). Experimental groups were given supplements of folic acid alone, other vitamins, both, or neither. Folic acid dose was at 4 mg/day, while that of other vitamins were relatively low. The folic acid-containing groups showed a 72% protective effect (calculated from a relative risk of 0.28, 95% confidence interval 0.12-0.71) while that of the other vitamins showed a decrease in relative risk that was not significant compared to controls (MRC, 1991). This provided conclusive evidence for the effectiveness of maternal folic acid supplementation during the periconception period in preventing recurrence of NTDs. Maternal folic acid supplementation was then shown to also reduce the first occurrence of NTDs in Hungary by about 70% (Czeizel and Dudas, 1992). Since then, further studies followed that linked folate metabolism with NTDs. Reduced maternal folate levels and elevated maternal homocysteine levels (an inverse marker of folate cycle production of 5-methyl-THF) are now well-established risk factors of NTDs (Kirke et al., 1993, Molloy et al., 1998, Steegers-Theunissen et al., 1994, Mills et al., 1995).

Soon after the results of the MRC and Hungarian trials, periconceptional folate supplementation was recommended by most governments to all women or women planning a pregnancy (Cornel and Erickson, 1997, Lee, 2013). However, the stages of neural tube closure are completed before many pregnancies are noticed, especially if unplanned, thus prevalence of NTDs was not significantly reduced by simply recommending supplementation (Botto et al., 2005, Blencowe et al., 2010). In the United Kingdom and Ireland, assessing the effectiveness of supplementation policies was complicated by the already declining rates of NTDs of 12-16 per 10,000 births in the 1990s compared with 49 per 10,000 births in 1980, though the decline might itself be a result of overall improved diet and folate status (Busby et al., 2005).

Several countries such as USA, Canada, South Africa, and most of Latin America introduced mandatory fortification of cereal grains with folic acid to ensure adequate folic acid

consumption by all women, which led to raised blood folate levels and a significant decrease in prevalence of NTDs (Honein et al., 2001, Lawrence et al., 1999, De Wals et al., 2007, Sayed et al., 2008, Hertrampf and Cortes, 2004, Rosenthal et al., 2014, Yoshida and Kikuchi, 1972). The preventive effect of folic acid appeared to be highest in countries, even regions within a country, with higher pre-existing "baseline" rates of NTDs (De Wals et al., 2007, Rosenthal et al., 2014), while countries that do not implement mandatory folic acid fortification of foods, i.e. Europe, did not show any significant decrease in NTD prevalence (Busby et al., 2005).

It is interesting to note that prevention of NTDs has never reached 100%, with a 70% estimated reduction in NTD recurrence and 62% in primary occurrence globally (Blencowe et al., 2010). In the United States, mandatory fortification of food with folic acid decreased the overall prevalence of NTDs by 19-32% (Crider et al., 2011), but taking additional folic acid supplements does not appear to confer any further protective effect (Mosley et al., 2009). In other countries where mandatory fortification is carried out, e.g. Canada and Latin America, the decline in NTD prevalence still leaves a baseline prevalence of 5-6 per 10,000 pregnancies (Crider et al., 2011). This strongly indicates that folic acid fortification is highly effective in reducing prevalence of folic acid-sensitive NTDs especially in high-risk populations. However, a proportion of remaining NTD cases appear to be resistant to folic acid and increasing the dosage of folic acid is not likely to be effective (Heseker et al., 2009).

Despite the link between folate metabolism and NTDs provided by the intervention studies, and the success of folic acid supplementation and fortification, a direct causal relationship between defective FOCM and NTDs remains unclear. While there is evidence noting that risk of an NTD pregnancy is inversely proportional to red blood cell folate concentration (Daly et al., 1995, Arakawa et al., 1972), it should be noted that most women with NTD-affected pregnancies had folate levels within the 'normal' range (Kirke et al., 1993). This indicates that while blood folate levels can serve as a predictor of NTD risk, having a normal folate status does not eliminate the risk of having an affected pregnancy. It also suggests that folic acid supplementation may be producing its protective effect in ways other than simply correcting a nutritional deficiency. Metabolic studies carried out on cell lines derived from NTD patients indicated that genetically-determined abnormalities in foetal folate metabolism may be contributing to the development of *some* NTDs (Dunlevy et al., 2007).

The evidence for a genetic predisposition to NTDs and the protective effect of folic acid make genes encoding folate-metabolising enzymes good candidates as NTD risk genes and targets for exploring gene-environment interactions.

1.4.2. Folate one-carbon metabolism

Folate one-carbon metabolism (FOCM) comprises a large network of enzymatic reactions that convert one folate species to another by shuttling one-carbon (1C) units in the form of methyl groups between them. Folates are obtained through dietary sources such as green leafy vegetables (e.g. spinach, broccoli, and Brussels sprouts), dried beans and peas, citrus fruits, and liver (Brouwer et al., 1999, Matherly and Hou, 2008), with folic acid being a synthetic form that is converted to tetrahydrofolate (THF) upon entry into the folate cycle. 1C units are derived from various donors such as serine, glycine and methionine, which in turn can be obtained through dietary means or *in vivo* biosynthesis pathways. Through FOCM reactions, 1C units are directed to *de novo* synthesis of thymidylate and purines, the methylation cycle, and polyamine synthesis (Beaudin and Stover, 2009).

1.4.2.1. Folate transport mechanisms

The basic structure of a folate compound is a 2-amino-4-hydroxy-pteridine double ring connected to a *p*-aminobenzoic acid ring which is linked to glutamic acid (**Figure 3**). In its various oxidation states, 1C units are added to the N-5 and/or N-10 positions. Folates can exist in polyglutamated, i.e. containing a chain of five to eight glutamate peptides (longer in mitochondrial folates), or monoglutamated form (Blom et al., 2006, Tibbetts and Appling, 2010). Polyglutamated folates are the form that dietary folates mostly comprise of, and that is used for storage or retention within cells. On the other hand, folates have to be transported through cell membranes in monoglutamated forms due to the high affinity binding of folate transport proteins to the monoglutamates. As such, transport of folates first begins with conversion of dietary folates to their monoglutamated forms to allow intestinal absorption (Zhao et al., 2009, Visentin et al., 2014).

Cleaving of the glutamate moieties is carried out by the intestinal glutamate carboxypeptidase II (GCPII, or folate hydrolase) enzyme. Another enzyme that does this is γ-glutamyl hydrolase (γ-GH), an intracellular hydrolase localised in the lysosome of enterocytes and hepatocytes. γ-GH removes glutamate residues of stored folates to allow release of their monoglutamated forms (primarily as 5-methyl-THF) into systemic circulation and to be taken up by target tissue (Visentin et al., 2014). In rodents, intestinal cleavage is achieved by γ-GH and not GCPII (Shafizadeh and Halsted, 2007). Within cells, folypoly-γ-glutamate synthetase (FPGS) reattaches the glutamate residues, converting the monoglutamates back to their polyglutamated forms so that they can be retained for storage or participation in FOCM reactions (Tibbetts and Appling, 2010).

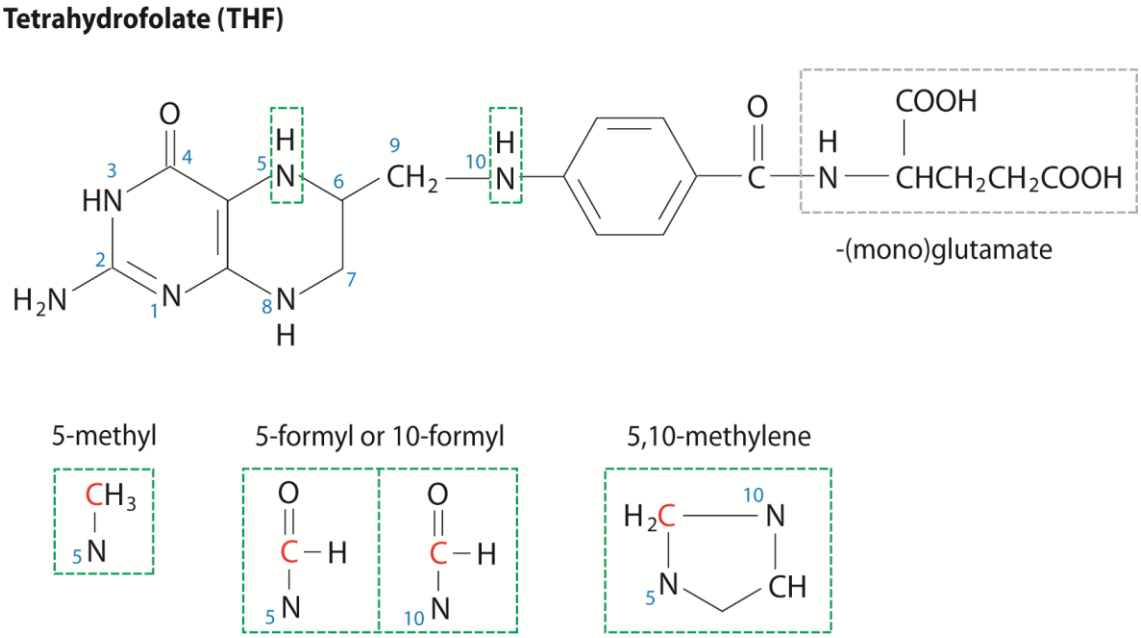

Figure 3. Structural representation of tetrahydrofolate.

Tetrahydrofolate (THF) consists of a double ring structure connected to *p*-aminobenzoic acid capped with a glutamate tail (grey dotted box). 1C units (red) are added to THF at the N-5 and/or N-10 positions (green dotted boxes) in the form of methyl (N-5 only), formyl (N-5 or N-10), or methylene (N-5, N-10 bridge) moieties. Glutamate molecules are added at the terminal γ-carboxyl residue ($-COO^-$) to form polyglutamated chains.

Adapted from: Blom et al. (2006), Zhao et al. (2009) and Tibbetts and Appling (2010)

The passage of folates through cell membranes is facilitated by various membrane transport proteins [reviewed by Zhao et al. (2011) and Visentin et al. (2014)]. A major transporter of folate in mammalian cells is the transmembrane protein, reduced folate carrier (RFC, or SLC19A1). RFC is expressed in all tissue and cell types and is the main route of entry for folates into cells. It also aids in intestinal absorption, transport across the blood-brain barrier, renal tubular secretion and reabsorption, and transplacental transfer of folates (Matherly and Hou, 2008).

Another route through which uptake of cellular folate is achieved is via folate receptors (FRs) in humans, or their murine homologues, the folate-binding proteins (Folbps, or Folrs). FRs are GPI-anchored, high-affinity receptors that, unlike the ubiquitous RFC, show tissue-specific expression. The FRα and FRβ isoforms are expressed in foetal, placental and adult tissue, with FRα localising in epithelial tissue and FRβ in hematopoietic tissue (Zhao et al., 2011). The isoforms also have varying folate-binding affinities, FRβ being the weaker of the two (Ross et al., 1994).

The proton-coupled folate transporter (PCFT, or SLC46A1, previously known as pH-independent heme carrier protein, HCP1) is a relatively new addition to the folate transport mechanism. It was first implicated as the optimal means of folate transport at more acidic pH (Qiu et al., 2006), when RFC, which has optimal activity at neutral pH, was still considered the prime route through which folates are absorbed in the gut and received in cells from circulation. It is now known that while RFC is still largely responsible for the latter, PCFT holds a critical role in intestinal absorption of folate (Zhao et al., 2011), and mutations in human *PCFT* were found in patients with hereditary folate malabsorption syndrome (Qiu et al., 2006, Zhao et al., 2007).

The mitochondrial folate transporter (MFT) is a specific carrier with which folates transverse mitochondrial membranes (Titus and Moran, 2000, McCarthy et al., 2004, Lawrence et al., 2011). In both the cytoplasm and mitochondria, the monoglutamated folates are converted back to their polyglutamated forms to participate in one-carbon metabolism. The FPGS enzyme is also present in the mitochondria to help maintain mitochondrial folate pools, as polyglutamated folates are unable to cross the mitochondrial membrane (Lawrence et al., 2014).

1.4.2.2. Compartmentalisation of FOCM reactions

In the cytoplasm (**Figure 4** - unshaded area), dietary folates enter the one-carbon cycle primarily as 5-methyltetrahydrofolate (5-methyl-THF) and is a substrate for methionine synthase (MS) (also known as 5-methyltetrahydrofolate-homocysteine-methyltransferase, MTR). The 1C/methyl group from 5-methyl-THF is transferred by MTR to homocysteine generating methionine and THF. Methionine then enters the methylation cycle while THF is utilised in the folate cycle. MTR requires the presence of vitamin B12 as a cofactor, and is dependent on methionine synthase reductase (MTRR) for activation.

THF can receive a 1C unit and be converted to 5,10-methylene-THF, either in a 3-step reaction catalysed by a cytoplasmic member of the methylenetetrahydrofolate dehydrogenase (MTHFD) family, the trifunctional MTHFD1, or by the action of serine hydroxymethyltransferase 1 (SHMT1).

MTHFD1 has three domains which mediate different activities that act in sequential order. First, the 10-formyl-THF synthetase domain combines THF with available formate (the 1C source) and generates 10-formyl-THF, followed by 5,10-methenyl-THF cyclohydrolase which converts that to 5,10-methenyl-THF, and lastly 5,10-methylene-THF dehydrogenase

which finally yields 5,10-methylene-THF (Momb et al., 2013). 10-formyl-THF is also a purine precursor, and may be shuttled towards *de novo* purine biosynthesis.

SHMT1, or cytoplasmic SHMT, breaks down serine to obtain 1C units in the presence of THF, thus generating glycine and 5,10-methylene-THF. SHMT can also catalyse conversion of 5,10-methenyl-THF to 5-formyl-THF, which does not participate in FOCM reactions but may be a stable storage form. The reverse reaction is catalysed by 5,10-methenyltetrahydrofolate synthetase (MTHFS) (Field et al., 2011).

5,10-methylene-THF, the product of MTHFD1 or SHMT1-catalysed reactions, has two fates. Thymidylate synthase (TYMS) may transfer its 1C unit to deoxyuridine monophosphate (dUMP) to generate thymidine monophosphate or thymidylate (dTMP), as part of the *de novo* thymidylate synthesis pathway. This reaction also produces dihydrofolate (DHF), which is subsequently reduced to THF by dihydrofolate reductase (DHFR) (Tibbetts and Appling, 2010). Folic acid enters FOCM at this point, being reduced to DHF. 5,10-methylene-THF may alternatively serve as a substrate for 5,10-methylenetetrahydrofolate reductase (MTHFR) which irreversibly converts it to 5-methyl-THF and shunts the 1C unit towards the methylation cycle.

In more recent studies, there is increasing emphasis on the importance of the highly compartmentalized nature of FOCM reactions, with particular interest in mitochondrial reactions (Tibbetts and Appling, 2010, Christensen et al., 2014). Stable isotope labelling in cell culture revealed that the mitochondria supplies greater than 75% of one-carbon units that are used in methylation reactions in the cytoplasm (Pike et al., 2010).

In the mitochondria (**Figure 4** – pink shaded area), conversion of THF to 5,10-methylene-THF is achieved either through the AMT-catalysed step of the GCS (**Figure 1**, **Section 1.1.1**), or through the reaction of mitochondrial SHMT (SHMT2) (Anderson and Stover, 2009). Either route serves to attach a 1C unit, donated from glycine (AMT) or serine (SHMT2), to THF.

Another member of the MTHFD family, the mitochondrial MTHFD2 in embryonic tissue (or its isozyme MTHFD2L in adult tissue), is a bifunctional enzyme that carries out the dehydrogenase and cyclohydrolase steps to yield 10-formyl-THF (Bolusani et al., 2011). The synthetase step to convert 10-formyl-THF to THF is carried out by MTHFD1L, which unlike its cytoplasmic, trifunctional counterpart MTHFD1, only shows 10-formyl-THF synthetase activity (Walkup and Appling, 2005). This step releases formate from 10-formyl-THF, which regenerates THF, thus restarting the cycle. Most mitochondrial-derived formate enters the cytoplasm to participate in cytosolic FOCM reactions (Pike et al., 2010).

Figure 4. Overview of folate one-carbon metabolism.

Folate one-carbon metabolism (FOCM) is compartmentalised to cytoplasmic, mitochondrial, and nuclear (not shown) reactions. Dietary folates enter the cycle primarily as 5-methyl-THF. The methylation cycle (**purple-shaded area**) is closely linked to the one-carbon cycle through the action of MTR, which transfers the 1C unit from 5-methyl-THF to homocysteine to generate methionine and THF. Methionine is converted to S-adenosyl methionine (SAM) and used in the methylation cycle as a 1C donor for methyltransferases or as substrate for polyamine synthesis.

THF in the cytoplasmic one-carbon cycle (**unshaded area**) combines with formate (majority of which is generated by the mitochondrial cycle) to form 10-formyl-THF (which may enter the purine synthesis pathway) and subsequently converted to 5,10-methylene-THF by MTHFD1. THF may also receive 1C units from serine to generate 5,10-methylene-THF through the action of SHMT1. 5,10-methylene-THF then either donates its 1C unit to dUMP for pyrimidine synthesis and regenerates THF in the process, or reduced by MTHFR to regenerate 5-methyl-THF.

In the mitochondria (**pink-shaded area**), THF combines with 1C units generated primarily from serine and glycine sources (through SHMT2 and the glycine cleavage system). The action of MTHFD2/2L and MTHFD1L produces formate and regenerates THF.

Adapted from: Copp et al. (2013) and Tibbetts and Appling (2010)

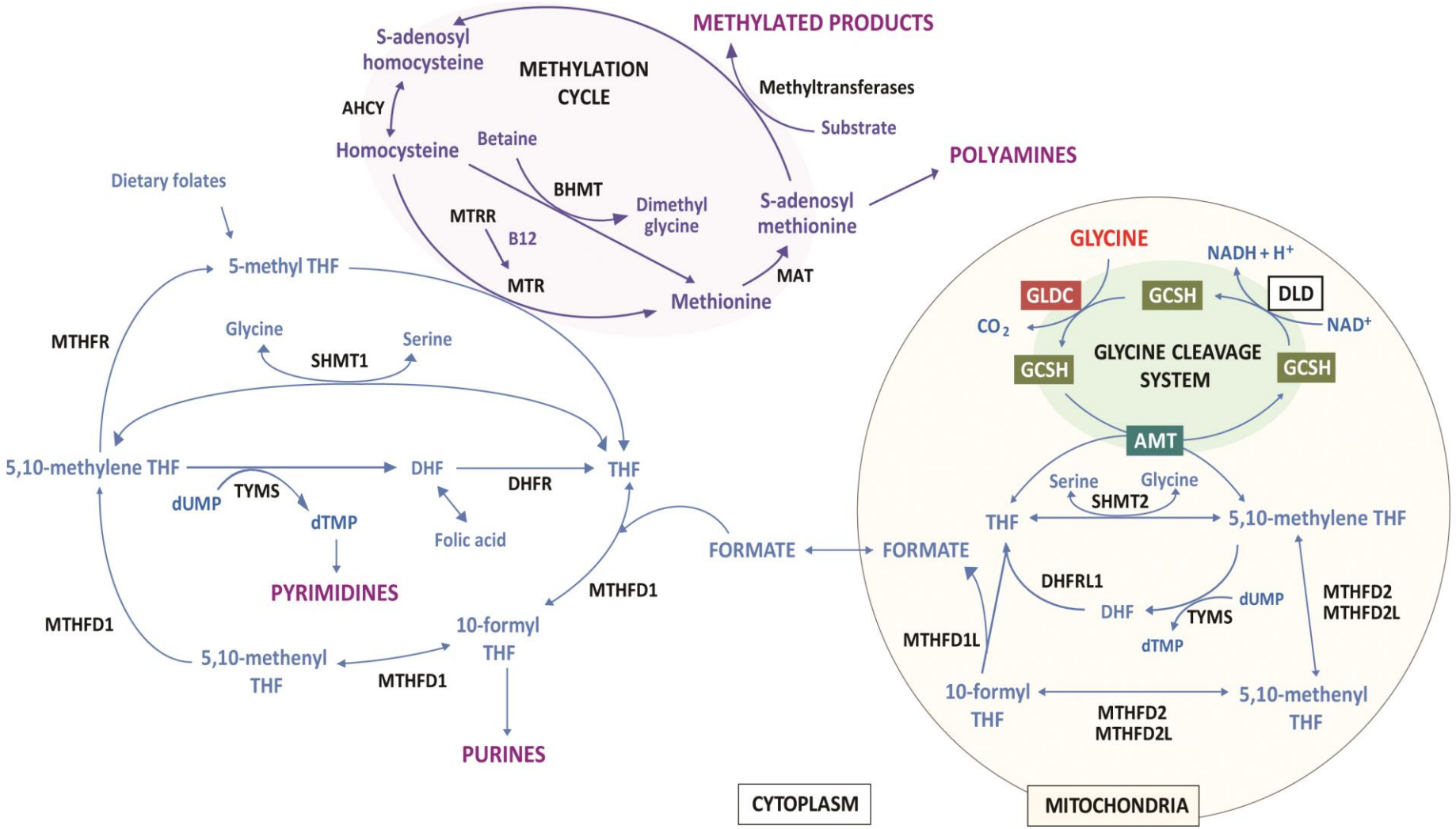

Figure 4. Overview of folate one-carbon metabolism.

1.4.2.3. FOCM outputs

The main outputs of FOCM are *de novo* biosynthesis of purines, thymidylate, and transferable methyl groups for which methylation processes are the biggest use.

De novo purine synthesis in mammals is a 10-step pathway catalysed by six enzymes to produce inosine monophosphate (IMP), the precursor to the adenine and guanine bases. The two folate-dependent enzymes of this pathway are the trifunctional GART[1] and bifunctional ATIC[2], which incorporate 1C units from 10-formyl-THF into the purine ring (Knox et al., 2009, Zhao et al., 2014, Field et al., 2011). The salvage pathway converts an already-produced precursor, hypoxanthine, back to IMP by action of the enzyme HPRT[3] (Zhao et al., 2014).

Synthesis of the thymine pyrimidine also occurs through *de novo* synthesis or a salvage pathway. In the *de novo* pathway, 5,10-methylene-THF supplies the 1C for methylation of dUMP to dTMP by TYMS. dTMP is then further phosphorylated to form the triphosphate, dTTP, the precursor to the thymine base. The salvage pathway converts thymidine to thymidylate through the action of thymidine kinase 1 (TK1). Both pathways also exist within the mitochondria for regulation of mitochondrial dTTP pools (Anderson et al., 2011).

In the methylation cycle, methionine is converted to S-adenosyl methionine (SAM) through action of methionine adenosyltransferase (MAT). SAM serves as a 1C donor to methylate DNA, RNA, proteins and lipids. Methyltransferases such as DNA methyltransferase (DNMT), RNA methyltransferase (RNMT), protein arginine methyltransferase (PRMT), and isoprenylcysteine carboxyl methyltransferase (ICMT), utilise 1C units from SAM converting it to S-adenosyl homocysteine (SAH). SAH is hydrolysed to homocysteine by adenosylhomocysteine hydrolase (AHCY). Remethylation of homocysteine to methionine can be catalysed by MTR or betaine-homocysteine-methyltransferase (BHMT) (Locasale, 2013, Greene et al., 2011).

Another fate of SAM is as substrate for SAM decarboxylase (SAMDC) in polyamine synthesis, for conversion of putrescine to spermidine and spermidine to spermine. Polyamines are implicated in multiple processes such as DNA conformational changes, cancer cell proliferation, glutamate receptor potentiation, and free-radical scavenging (Casero and Marton, 2007, Pegg, 2009).

---

[1] Phosphoribosylglycinamide formyltransferase (GARFT)/ phosphoribosylglycinamide synthetase (GARS)/ phosphoribosylaminoimidazole synthetase (AIRS)
[2] 5-aminoimidazole-4-carboxamide ribonucleotide formyltransferase (AICART)/ IMP cyclohydrolase
[3] Hypoxanthine phosphoribosyltransferase

1.4.3. Association between genetic polymorphisms of FOCM genes with NTDs

MTHFR was the first folate enzyme-encoding gene in which a polymorphism was found that was significantly associated with human NTDs. Severe deficiency in MTHFR is an inborn error of metabolism characterised by hyperhomocysteinemia and homocystinuria and, in severe cases, can result in postnatal lethality within the first year.

van der Put et al. (1995)'s study was among the earliest to report a higher incidence of the 677C>T (A222V) variant of the *MTHFR* gene in Dutch NTD triads compared to controls. In a large genetic study of the variant in the Irish population, significant association with NTDs was found with patient TT genotype (i.e. homozygous for the 677C>T variant), but not with mothers (i.e. maternal TT genotype) (Shields et al., 1999). A meta-analysis performed by Botto and Yang (2000) reported increased spina bifida risk with a TT genotype (as well as a combination of the 677C>T and 1298A>C variants) in the infant *or* mother. Both variants have since been screened in many populations and the 677C>T is now an established NTD risk factor. However, this association is not found in all populations and most TT individuals are apparently healthy [reviewed by Boyles et al. (2005), Molloy et al. (2009a) and Greene et al. (2009)].

The significant findings in *MTHFR* spurred a search for variants in other FOCM-related genes, but these studies have generated largely negative, inconsistent or conflicting results. These include genes for enzymes within the one-carbon cycle (e.g. *MTHFD2*, *SHMT1* and *DHFR*), homocysteine remethylation (e.g. *MTR*, *MTRR* and *BHMT*), methylation reactions (e.g. *PRMT1* and *PRMT2*), purine or pyrimidine synthesis (e.g. *GART* and *TYMS*), and folate carriers (e.g. *RFC1*, *GCPII*, *FRα* and *FRβ*) (Boyles et al., 2005, Molloy et al., 2009a, Greene et al., 2009). The limitation of most of these studies is that only specific polymorphisms were studied. Results from large scale sequencing studies, which may reveal causative mutations, are awaited. Nevertheless, several genes conferring significant risk have been successfully identified.

The 1958G>A (R653Q) mutation in *MTHFD1* was first suspected to be a risk factor in a Dutch population (Hol et al., 1998) and later found to be associated with spina bifida in an Irish population (Brody et al., 2002), especially when present as a maternal homozygous AA genotype (Parle-McDermott et al., 2006). However, another study in the Dutch population a decade after the 1998 study did not find any association with spina bifida risk (van der Linden et al., 2007). A polymorphism in the *MTHFD1L* gene encoding the mitochondrial isozyme of MTHFD1 was also found to be strongly associated with NTDs in the Irish population (Parle-McDermott et al., 2009). A larger study looking at common variants in 82 candidate NTD genes in the Irish population picked up variants in 9 genes

that showed the most significant associations (Pangilinan et al., 2012). These included genes that have previously been looked at, such as *MTHFD1*, *GART* (purine synthesis), and *DNMT3A* (methylation reactions). They also identified significant association with a new gene, *MFTC*, which encodes the mitochondrial folate transporter.

Of the FOCM-related genes found to show strong association with NTDs so far (i.e. *MTHFR*, *MTHFD1*, *MTHFD1L*, and *MFTC*), two pertain to mitochondrial FOCM reactions. This finding is noteworthy in itself, considering the much larger number of genes encoding cytoplasmic FOCM that showed no (or conflicting) association.

1.4.4. FOCM-related mouse models

In normal mice, severe, diet-induced folate deficiency results in high resorption rates and failure of implantation, but surviving embryos do not have NTDs (Heid et al., 1992). However, diet-induced folate deficiency can exacerbate or induce NTDs in mouse models with a genetic predisposition. This genetic predisposition can be a mutation in an FOCM enzyme-encoding gene such as *Shmt1* (Beaudin et al., 2011) or in mutations where a genetic link to FOCM is not recognised, such as the *Pax3* mutant, *Splotch* (*Sp^{2H}*) (Burren et al., 2008), and the *Grhl3* hypomorph, *curly tail* (Burren et al., 2010). In addition, folic acid supplementation has a preventive effect in some NTD mice models, such as *Splotch* (*Sp^{2H}*) (Fleming and Copp, 1998, Wlodarczyk et al., 2006), and *Cited2* (Barbera et al., 2002).

Mouse models carrying mutations in genes encoding FOCM-related enzymes have been made in attempts to probe FOCM function and investigate NTDs, congenital heart defects, folate deficiency syndromes, hyperhomocysteinemia, and hypomethylation. The models described below are summarised in the context of NTDs.

1.4.4.1. Genes encoding folate receptors and carriers

Deletions of folate receptor and carrier genes in mouse models result in early embryonic lethality and very severe developmental anomalies, thus demonstrating the importance of adequate supply of folates in general embryonic development. This partially recapitulates the finding in the diet-induced folate deficiency model.

Homozygous deletion of the mouse reduced folate carrier gene, *Rfc1*, results in embryonic lethality by E9.5. Maternal folic acid supplementation was able to support survival in some embryos to E18.5 and birth, but neonatal animals develop multi-organ malformations and die within 12 days due to failure of erythropoiesis (Zhao et al., 2001, Gelineau-van Waes et

al., 2008). The *Rfc1* mouse model showed that folic acid was important in pre-neurulation stages of development, erythropoiesis, and development of various organs including the neural tube, heart, lungs, eyes and limbs.

Knockout mice for folate-binding protein, Folbp1 (murine homologue of human FRα) displayed similarly severe phenotypes and also resulted in NTDs. Homozygous mutants for the *Folbp1* gene were severely growth retarded and exhibited aberrant morphology of the neural tube, craniofacial region, limbs, and cardiovascular system by E8.5. They were embryonically lethal by E10, but had only developed to pre-neurulation somite stages. Maternal supplementation with folinic acid was able to rescue a significant proportion of embryonic lethality and malformations in a dose-dependent manner, and improved survival *in utero*, but a proportion of the survivors exhibited NTDs (Piedrahita et al., 1999, Spiegelstein et al., 2004). On the other hand, null mice for Folbp2 are phenotypically normal but showed increased sensitivity towards arsenic-induced exencephaly compared with wild-types (Piedrahita et al., 1999, Wlodarczyk et al., 2001).

Pcft-deficient mice were generated as a model for hereditary folate malabsorption syndrome. Homozygous mice survived to birth but failed to thrive, showed impaired erythropoiesis and megaloblastic anaemia, and responded to folinic and folic acid treatment. There were no reports of malformations (Salojin et al., 2011).

1.4.4.2. FOCM mutations conferring pre-neurulation lethality

Mouse models with FOCM gene mutations that are lethal before or by neurulation include *Mtr* (or *MS*), *Mtrr*, cytoplasmic *Mthfd1*, and *Mthfs*.

No *MS* null embryos were successfully recovered, and the loss of mutants through early resorptions (prior to E9.5) was unable to be rescued by dietary treatment with 5-formyl-THF, 1C donors (methionine, choline, and betaine), purines and thymidine, threonine, or inositol, although the authors speculated that insufficient dosage may have been the reason for this (Swanson et al., 2001).

A hypomorphic gene-trap mutant of *Mtrr* was generated, in which homozygotes displayed mild hyperhomocysteinemia and heart defects (Elmore et al., 2007, Deng et al., 2008). The authors also reported unpublished preliminary results of a true *Mtrr* knockout conferring embryonic lethality (R. Gravel, unpublished), which is consistent with the role of Mtrr in activating MS.

Homozygous *Mthfd1* gene-trap mice exhibited embryonic lethality, while heterozygotes showed reduced hepatic adenosylmethionine levels. They reported a surprising decrease in uracil misincorporation into DNA which they interpreted as an indication of increased thymidylate synthesis (MacFarlane et al., 2009). An *Mthfd1S* mutant was also generated, in which only the 10-formyl-THF synthetase activity of the MTHFD1 enzyme was disrupted. Homozygous mutants were also embryonically lethal. *Mthfd1S*$^{-/-}$ embryos at E10.5 were severely delayed with abnormalities in the neural tube (but were not NTDs), somites, and heart, while *Mthfd1S*$^{+/-}$ pregnant females showed reduced white blood cell counts (Christensen et al., 2013).

A null mutation of *Mthfs*, whose enzyme substrate is non-cofactor 5-formyl-THF, is also not viable. Embryonic lethality occured pre-neurulation and was not rescued by hypoxanthine supplementation (Field et al., 2011).

1.4.4.3. FOCM mutations not presenting with NTDs

FOCM mouse models that survived past neurulation but did not display NTDs include mitochondrial *Mthfd2*, *Mthfr* and *Shmt1*.

Mthfd2 (or *nmdmc*) homozygous mutants died after E12.5, potentially from defects in erythropoiesis, but did not display any severe malformations or neural tube abnormalities before that. Embryonic lethality was not rescued by formate treatment or a glycine-rich diet (Di Pietro et al., 2002, Patel et al., 2003).

The *Mthfr* knockout mouse presented with early postnatal loss and homocystinuria, which mimics some of the human phenotypes for *MTHFR* deficiency. The SAM/SAH ratio was severely decreased, and correspondingly, global DNA methylation was decreased as well at post-natal stages (Chen et al., 2001, Schwahn et al., 2004). The *MTHFR* mutation is of particular interest as it is the first genetic risk factor to be associated with human NTDs. However, this knockout mouse did not exhibit NTDs and showed Mendelian genotype ratios at birth. Postnatal mutants displayed facial abnormalities, cerebellar defects, and aortic lipid deposition (Chen et al., 2001).

Cytoplasmic *Shmt1* null mice were viable and fertile, but displayed increased levels of SAM combined with decreased levels of SAH, i.e. elevated SAM/SAH ratio (MacFarlane et al., 2008). An isoform of *Shmt2* which localises to the cytoplasm and nucleus was hypothesised to provide redundancy to *Shmt1* function, which may explain the viability of *Shmt1* null mice (Anderson and Stover, 2009). However, *Shmt1*$^{+/-}$ and *Shmt1*$^{-/-}$ embryos did exhibit exencephaly when challenged with induced folate deficiency, indicating that

the *Shmt1* mutation confers a genetic predisposition to higher NTD risk (Beaudin et al., 2011, Beaudin et al., 2012). Interestingly, treatment of *Shmt1*$^{-/-}$ with uridine nucleosides also increased NTD incidence, while deoxyuridine supplementation showed a rescue effect in NTDs induced by folate deficiency (Martiniova et al., 2015).

1.4.4.4. FOCM mutations that cause NTDs

FOCM mouse models that do display NTDs without treatment of any kind include *Mthfd1L*, *Amt*, and *Gldc*.

Mthfd1L null mice were embryonically lethal. No homozygous mutants were recovered after E12.5, and some did not survive to neurulation stages. All mutants that survived to neurulation stages (and up to E12.5) showed complete penetrance of exencephaly (one embryo had craniorachischisis), with E12.5 embryos also showing immature mandibular processes. Supplementation with sodium formate conferred partial rescue of the NTD phenotype and allowed some mutants to be retrieved at E15.5 (Momb et al., 2013).

The *Amt* gene-trap mouse (briefly mentioned in **Section 1.2.3**) generated a null allele which was also embryonically lethal in a homozygous state. At E17.5, 87% of homozygous mutants exhibited NTDs (82% exencephaly and 5% crahiorachischisis). No post-natal survivors were retrieved. Treatment with folic acid or TMP alone was non-responsive, but treatment with methionine or methionine and TMP combined produced significant rescue effect and reduced the rate of NTDs from 87% in untreated mutants to about 60% (Narisawa et al., 2012).

The *Gldc* mouse model is described in this thesis.

Hence, consistent with studies of FOCM-encoding genes in human NTDs, FOCM mouse models that survive past gastrulation but fail neurulation without requiring additional insult (i.e. *Mthfd1L*, *Amt*, and *Gldc*) are mitochondrial FOCM models.

1.5. Overview of thesis

Despite the historical link between folate one-carbon metabolism (FOCM) and neural tube defects (NTDs), the precise mechanism by which defective FOCM may lead to the development of NTDs is still poorly understood, as is the mechanism behind folate-resistant NTDs. Recent studies of FOCM enzyme-encoding genes in human NTDs and FOCM-related NTD mice models hint at the importance of the mitochondrial component of FOCM in the pathogenicity of NTDs. The mitochondria-specific glycine cleavage system (GCS) is thus an attractive and relatively unexplored candidate for probing the contribution of mitochondrial FOCM. In addition, GCS mutations are known to result in non-ketotic hyperglycinemia (NKH), the pathogenicity of which is also not well understood and which lacks a working animal model.

This thesis investigates the effect of loss of function of a member of the GCS, glycine decarboxylase (GLDC), during mouse embryonic and post-natal development. *Gldc* was chosen for this study because *Amt*, another GCS component, has been demonstrated to result in NTDs when mutated in the mouse but the developmental mechanisms were not investigated and it is not known if *Gldc* is also essential for neural tube closure. In addition, the NTD phenotype in the *Amt* model was too severe and post-natal mutant survivors too few to allow for observations of possible NKH-like phenotypes. This study introduces two novel gene-trap models ($Gldc^{GT1}$ and $Gldc^{GT2}$), which are found to exhibit both NTDs and NKH-like phenotypes, with the purpose of addressing the following specific questions:

- What are the biochemical and cellular mechanisms underlying the NTDs in *Gldc* loss-of-function mice models, and do they result from an FOCM disturbance?
- How does a *Gldc* mutation alter FOCM and its downstream pathways?
- Are NTDs caused by a *Gldc* mutation rescued by folate-related metabolites?
- Can effects of the *Gldc* mutation be influenced by environmental factors (e.g. folate deficiency) and mutations in other folate enzyme-encoding genes (e.g. *Mthfr*)?
- Are *Gldc* mutants suitable as animal models for studying the pathogenesis and treatment options for classical NKH?

Chapter 3 begins with an analysis of the spatial expression pattern of *Gldc* in wild-type neurulating embryos. Characterisation of the loss-of-function gene-traps used and the NTD phenotype of neurulation-staged mutant embryos are then provided. The correlation between level of gene knockdown and NTD incidence is investigated to account for the observed partial penetrance. Additional developmental phenotypes and unusual cranial abnormalities are also described.

Chapter 4 attempts to elucidate how GCS deficiency affects FOCM which may subsequently result in NTDs. Changes in folate profiles and amino acid levels in mutant conditions are presented. This is then followed by rescue and exacerbation experiments (via dietary supplementation) to further probe how this model responds to environmental interventions as well as to provide information for potential therapeutic strategies. The effect of GCS deficiency on cellular proliferation is explored in an attempt to understand how defective FOCM can lead to NTDs. Genetic interactions between *Gldc* and *Mthfr* is also investigated by crossing the two loss of function models together.

The moderately low penetrance of NTDs in the $Gldc^{GT1}$ model allowed sufficient numbers of homozygous mutants to survive to post-natal stages where NKH manifests. Thus, **Chapter 5** focuses on the evaluation of late-foetal and post-natal mutant phenotypes to assess their suitability as models for classical NKH. Emphasis is given on post-natal survival, biochemical parameters, and brain malformations commonly associated with NKH, i.e. corpus callosum defects and hydrocephalus.

2. Methodology

2.1. Mice colonies

2.1.1. Generation of *Gldc* mutant mice

An embryonic stem cell line carrying a gene-trap allele of *Gldc* (clone EUCG0001_D02; denoted as $Gldc^{GT1}$) was obtained from the European Conditional Mouse Mutagenesis (EUCOMM) project. Chimeric mice were generated by blastocyst injection of ES cells (carried out the Embryonic Stem Cell Facility, UCL Institute of Child Health). These mice were crossed with wild-type 129/Sv mice to confirm germ-line transmission. Due to high levels of embryonic lethality in the 129/Sv background, the chimeras were then outcrossed to wild-type mice on a C57BL/6 background for 5 generations and a heterozygous colony was established. Experimental litters were generated by mating heterozygous mice from this cross.

A second *Gldc* gene-trap mouse (clone CMHD-GT_519C8; denoted $Gldc^{GT2}$) was similarly generated from a cell line provided by the North American Conditional Mouse Mutagenesis (NorCOMM) project, bred onto a C57BL/6 background and a heterozygous colony established. Experimental litters were generated by mating heterozygous mice.

2.1.2. Generation of $Gldc^{GT2}$;*Mthfr* mutant mice

Targeted *Mthfr* null mice were obtained from the Rozen lab (Chen et al., 2001) and maintained as a colony by backcrossing to BALB/c mice, the genetic background of the *Mthfr* mutant strain. $Mthfr^{+/-}$ heterozygous mice were crossed to $Gldc^{GT2/+}$ heterozygous mice to obtain double heterozygous mutants ($Gldc^{GT2/+}$;$Mthfr^{+/-}$) on a mixed C56BL/6 and BALB/c background. Experimental litters were generated by mating double heterozygous mice together.

Generation and maintenance of all mice colonies was performed by Dawn Savery.

2.1.3. Genotyping and sexing PCRs

A lysis buffer solution was prepared containing 1M Tris at pH 8, 0.5M of EDTA, 5M of sodium chloride (NaCl), and 10% sodium dodecyl sulphate (SDS). Ear clips, tail tips, or yolk sacs collected for genotyping purposes were lysed in 180 µL of lysis buffer with 20 µL of 10 mg/mL proteinase K overnight at 55 °C. 80 µL of saturated NaCl was added to each tube, vortexed briefly, and placed on ice for 20 min. The tubes were then centrifuged at 14,000g for 20 min at 4 °C to pellet cell debris. The supernatants were transferred to fresh tubes and 1 mL of 100% ethanol added. The tubes were inverted several times and then spun at 14,000g for 20 min in 4 °C. The supernatants were discarded and 70% ethanol added to wash the DNA pellets. The tubes were spun again and the supernatants discarded. The remaining pellets were allowed to air dry for several hours. When dry, the DNA pellets were re-suspended in 50 µL of deionized, distilled water and stored at -20 °C.

A second, quicker alternative to salt extraction was used later for genotyping large batches of samples. This method involved incubation of samples in 50 µL of DirectPCR®-Tail Lysis Reagent (Peqlab), and 1 µL of 10 mg/mL proteinase K for 3 hrs at 55 °C followed by a 45 min enzyme inactivation step at 85 °C. The sample was then ready to be added to a PCR reaction mix.

All primer sequences with band sizes, reaction mixes, and PCR conditions mentioned below are provided in **Table 2**, **Table 3**, and **Table 4** respectively.

For genomic DNA genotyping of *Gldc*^{GT1} mice and embryos, 3 PCRs were used. The first reaction consisted of primers that amplify the *neo* reporter sequence (primers **F3** and **R2** in **Table 2**, reaction **mix 1** in **Table 3**, PCR **condition 1** in **Table 4**). The second reaction consisted of a forward primer which binds to a region in intron 3-4 of the *Gldc* gene, and a reverse primer in the Long Terminal Repeat (LTR) region of the gene-trap (primers **F2** and **R1**, reaction **mix 2**, PCR **condition 2**). The third reaction, for detecting the wild-type allele, targets a region in intron 3-4 that flanks the gene-trap insertion site and will only amplify the wild-type locus in the absence of the gene-trap (primers **F1** and **R3**, reaction **mix 3**, PCR **condition 2**). The gene-trap design, location of all genotyping primers, and genotyping strategy are illustrated in **Chapter 4**, **Figure 4**.

For genotyping of the *Gldc*^{GT2} allele, primers binding to the *EGFP* reporter sequence of the *Gldc*^{GT2} gene-trap was used to detect the mutant allele (primers **F5** and **R4**, reaction **mix 1**, PCR **condition 2**), while a forward primer in exon 19 and reverse in intron 19-20, located 3' to the gene-trap, were used to amplify the wild-type allele (primers **F4** and **R5**, reaction **mix 1**, PCR **condition 2**). In the *Gldc*^{GT2}*;Mthfr* cross, the *Mthfr* allele was genotyped by 3

primers in one reaction as reported by (Chen et al., 2001) (primers **M1**, **M2** and **M3**, reaction **mix 1**, PCR **condition 1**).

The sex of embryos and P1 pups was determined by PCR using sex-specific primers to the *Smcx* and *Smcy* genes (primers **SMCX1** and **SMC4-1**, reaction **mix 1**, PCR **condition 2**).

Allele	Primers	Sequences (5' – 3')	Band size (bp)
Gldc^{GT1} mutant 1 (*neo*)	F3	CTGTGCTCGACGTTGTCACTG	567
	R2	GATCCCCTCAGAAGAACTCGT	
Gldc^{GT1} mutant 2	F2	GTGAACGGAGTCCCTCTCTCTCCC	602
	R1	GTCCTCCGATTGACTGAGTCG	
Gldc^{GT1} wild-type	F1	TACAGTCTGTGAACGGAGTCC	644
	R3	TCACTTTCTGAAGGGTTGGAGAGG	
Gldc^{GT2} mutant (*EGFP*)	F5	GCGAGGAGCTGTTCACCGGG	325
	R4	ACCTCGGCGCGGGTCTTGTA	
Gldc^{GT2} wild-type	F4	TCTGCCGCCCTGGGGACTTT	658
	R5	GCTGTCTGCCTTCCAACTA	
Mthfr	M1	GAAGCAGAGGGAAGGAGGCTTCAG	216 (KO allele) 145 (WT allele)
	M2	AGCCTGAAGAACGAGATCAGCAGC	
	M3	GACTAGCTGGCTATCCTCTCATCC	
Smcx and *Smcy*	SMCX1	CCGCTGCCAAATTCTTTGG	~330 (both)
	SMC4-1	TGAAGCTTTTGGCTTTGAG	~300 (male only)

Table 2. Primer sequences for genotyping and sexing *Gldc*^{GT1}, *Gldc*^{GT2}, and *Mthfr* samples.

PCR reagent	Volume per reaction (µL)		
	Mix 1	**Mix 2**	**Mix 3**
10X PCR buffer	5	5	5
dNTP mix (2 mM)	5	5	5
$MgCl_2$ (50 mM)	1.5	2	1.5
Forward primer (40 µM)	0.3	0.3	0.3
Reverse primer (40 µM)	0.3	0.3	0.3
Taq DNA polymerase (5 U/µL)	0.25	0.25	0.25
Betaine	-	-	5
Distilled, deionized water	35.65	35.15	30.65
Template DNA	2	2	2
Total	**50**	**50**	**50**

Table 3. PCR reaction mixes for genotyping and sexing.

PCR step	PCR conditions			No. of cycles
	1	**2**	**3**	
Initial denaturation	2 min, 94 °C	5 min, 94 °C	5 min, 94 °C	1
Denaturation	30 sec, 94 °C	1 min, 94 °C	1 min, 94 °C	
Annealing	30 sec, 60 °C	1 min, 58 °C	1 min, 60 °C	30-32
Extension	45 sec, 72 °C	1 min, 72 °C	1 min, 72 °C	
Final extension	5 min, 72 °C	5 min, 72 °C	5 min, 72 °C	1

Table 4. PCR conditions for determination of genotype and sex.

2.1.4. Long-Range PCR and sequencing of gene-trap

Long-Range PCR was carried out on *Gldc*^{GT1} samples using the SequalPrep™ Long PCR kit (Invitrogen) to amplify the entire *Gldc*^{GT1} construct. The PCR reaction mix used is detailed in **Table 5** and amplification was performed using the following conditions: initial denaturation for 3 min at 93 °C, followed by 35 cycles of 15 sec denaturation at 93 °C, 30 sec annealing at 62 °C, and 4 min extension at 68°C (1 min/kb), and a final extension step for 5 min at 68 °C. Fragments of the construct obtained from Long-Range PCR reactions were sequenced using a primer walking strategy from both 5' and 3' ends to confirm the presence of all loxP and Frt sites **Figure 5**. All primers used for the primer walking and sequencing of the gene-trap are listed in **Table 6**. All sequencing was carried out by the UCL Wolfson Centre for Biomedical Science genomics services.

Long-Range PCR reagent	Volume per reaction (µL)
10X Reaction buffer with $MgCl_2$	5
dNTP mix (10 mM)	2.5
Forward primer (40 µM)	0.3
Reverse primer (40 µM)	0.3
Long Polymerase (5 U/µL)	0.4
Distilled, deionized water	40.5
Template DNA	1
Total	**50**

Table 5. Long-Range PCR reaction mix.

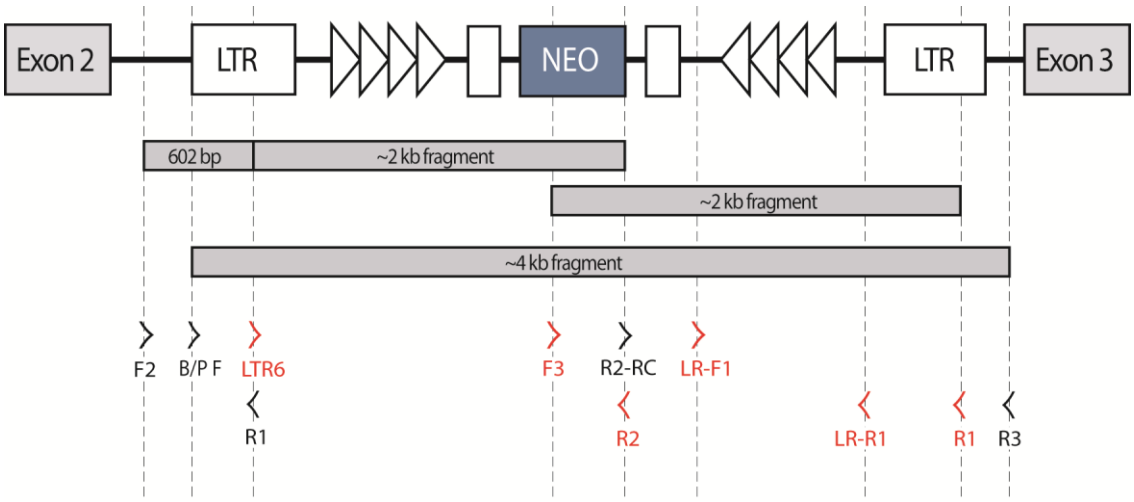

Figure 5. Primer walking strategy for sequencing of the *Gldc*^{GT1} construct.

Approximately 2 and 4 kb fragments of the *Gldc*^{GT1} construct were successfully amplified using Long-Range PCR with the [LTR6 x R2], [F3 x R1], and [B/P F x R3] primer pairs. Sequencing of both 2 kb fragments were carried out using the primers indicated in red to confirm the sites and sequences of all loxP and Frt regions (triangles).

Primer orientation	Primer	Sequences (5' – 3')
Forward	F2	GTGAACGGAGTCCCTCTCTCTCCC *
	B/P F	TTCTCAGGCCCACCACTGAAAGA
	LTR6	GCGACTCAGTCAATCGGAGGAC
	F3	CTGTGCTCGACGTTGTCACTG *
	R2-RC	ACGAGTTCTTCTGAGGGGATC
	LR-F1	ATTGCATCGCATTGTCTGAG
Reverse	R1	GTCCTCCGATTGACTGAGTCG *
	R2	GATCCCCTCAGAAGAACTCGT *
	LR-R1	CGTTGGGTTACCTTCTGCTC
	R3	TCACTTTCTGAAGGGTTGGAGAGG *

Table 6. Primers used for *Gldc*^{GT1} construct sequencing.

* The F2, F3, R1, R2, and R3 primers are the same genotyping primers listed in **Table 2**. Primers indicated in red were used for sequencing reactions.

2.1.5. Treatments and dietary interventions

Formate treatment was performed by addition of 30 mg/mL sodium formate (Sigma-Aldrich) to drinking water of females on the day a vaginal plug was found (E0.5), and maintained until the litters were collected.

For diet-induced folate deficiency experiments, female mice were kept on an *ad libitum* folic acid-deficient diet containing 1% succinylsulfathiazole (10 g/kg) (Harlan Teklad; TD.02490) for at least 3 weeks before mating (Burren et al., 2008). This diet was maintained throughout pregnancy until collection of litters.

All mice were placed on an 18% sterilisable rodent diet with fenbendazole (8 mg/kg) (Harlan Teklad; TD.01432) for treatment of pinworm infection over a period of 3 months. Litters collected during this treatment period were analysed separately and are indicated in the appropriate results chapters.

2.1.6. Survival studies

Litters from *Gldc*^{GT1} heterozygous mice crosses were allowed to litter down and monitored from birth until 1 year of age. A cohort of homozygous mutant mice (*Gldc*$^{GT1/GT1}$) that were viable and healthy past 6 weeks of age were inter-crossed to establish a homozygous colony and expedite collection of mutants. The numbers of surviving pups were followed throughout, with any ill or dead mice collected for genotyping and sexing. Mice that developed acute hydrocephalus were culled within 48 hours due to rapidly deteriorating health.

2.2. Sample collection, fixation, and storage

2.2.1. Embryonic samples

E9.5 and E10.5 embryos were dissected out of the uterus in Dulbecco's Modified Eagle's Medium (DMEM) with high glucose and HEPES formulation (Invitrogen; 42430), with 10% fetal bovine serum (Sigma-Aldrich), and rinsed briefly in cold phosphate buffered saline (PBS). Embryos at E11.5 and older were dissected out in cold PBS.

Embryos to be used for mRNA extraction and metabolic studies were immediately frozen on dry ice and stored at -80 °C.

Embryos for *in situ* hybridisation and antibody detection studies were fixed in 4% paraformaldehyde (PFA) overnight at 4 °C, while those to be used only for morphological studies were fixed in Bouin's solution (Sigma-Aldrich). They were then washed briefly in PBS, dehydrated in ascending concentrations of methanol (25%, 50%, 75%, 100%), and stored in absolute methanol at -20 °C. For X-gal staining, embryos were fixed in 0.2% gluteraldehyde for an hour at 4 °C and processed immediately (see **Section 2.4.2**).

2.2.2. Late-foetal and post-natal samples

For analysis of E18.5 foetal brains, the foetuses were dissected out of the mother's uterus in cold PBS and decapitated. The heads were then skinned with forceps to allow better penetration of the fixative and solutions in subsequent processing steps. They were fixed in 4% PFA (for antibody detection) or Bouin's solution (for morphological studies) for 48 hours on a roller at 4 °C. Samples fixed with 4% PFA were given a fresh solution change after the first 24 hours. For 5-week old mice brains, the brain was carefully removed from the skull, rinsed briefly in cold PBS, and similarly fixed. The E18.5 foetal heads and 5-week brains were then dehydrated with ethanol (25%, 50%, 70%) and stored at 70% ethanol at 4 °C. Brains to be used for corpus callosum studies were processed immediately after fixation without dehydrating (see **Section 2.7**).

Gldc adult liver and brain samples at 8–12 weeks of age were harvested for mRNA extraction and measurements of Gldc enzymatic activity. The samples were rinsed briefly in cold PBS, immediately frozen on dry ice, and stored on -80 °C.

2.2.3. Adult mice blood and urine samples

Blood from *Gldc* mutant mice was collected by cardiac puncture, transferred to lithium-heparin tubes (BD Microtainer), and spun at 3,500 rpm for 5 min. The plasma layer was carefully transferred to 1.5 mL tubes, immediately frozen on dry ice, and stored at -80 °C.

For the collection of urine, *Gldc* mice were placed in metabolic cages designed for urine and faeces collection, one mouse to a cage, overnight. Urine collected from this method was then centrifuged briefly to remove any debris in the sample, frozen on dry ice, and stored at -80 °C.

2.3. Investigating expression of *Gldc* mRNA

2.3.1. RNA isolation and cDNA synthesis

500 mL of TRIzol® Reagent (Ambion® RNA) was added to the tube containing E9.5/E10.5 embryo sample or a sliver of liver/ brain sample (at a similar wet weight as an E10.5 embryo). The tissue was homogenized by pipetting in Trizol several times, then incubated in room temperature for 5 min. 100 mL of chloroform (BDH, UK) was added and the tube shaken vigorously. The tube was incubated at room temperature for 2 to 3 min, and then spun at 12,000 g for 15 min at 4 °C. The upper, aqueous phase was transferred to a new tube and 250 mL of isopropyl alcohol added to it. It was then incubated on ice for 10 min, and then spun at 18,800 g for 10 min at 4 °C. The supernatant was decanted and the RNA pellet washed with 500 mL of 75% ethanol. The sample was vortexed briefly and spun again at 14,000 rpm (18,800 g) for 5 min at 4 °C. The pellet was air dried for 5 to 10 min and re-suspended in 20 µL of DEPC-treated water.

The RNA sample was then DNase-treated to remove DNA contamination using a DNA-free™ DNase Treatment and Removal kit (Ambion® RNA). 0.5 µL of RNAse Inhibitor (Roche), 2.5 µL of 10X DNase 1 buffer, and 0.5 µL rDNase-1 enzyme were added to the re-suspended RNA. The mix was then incubated at 37 °C for 30 min. 2.5 µL of DNase Inactivation Reagent was added, further incubated for 2 min and spun at 10,000 rpm (9,600 g) for 2 min. The supernatant was transferred to a fresh tube and stored at -80 °C.

The purity of the RNA sample was assessed by its absorbance ratio at 260/280 nm and 260/230 nm wavelengths using the Nanodrop Spectrophotometer ND-1000 (Thermo Scientific). Ideally, this ratio would be in the 2.0-2.2 range; ratios appreciably lower than that indicates the presence of phenol or DNA contamination. As the same nucleic acid sample may give a ±0.4 difference in 260/280 ratio on any 2 similar spectrophotometers, samples that differed by more than ±0.5 from the ideal range were discarded. The concentration of the sample in ng/µL was also ascertained with the Nanodrop machine.

RNA samples were used to generate cDNA using the SuperScript® VILO™ cDNA Synthesis Kit (Invitrogen). 4 µL of 5X VILO™ Reaction Mix and 2 µL of 10X SuperScript® Enzyme Mix were added to 2 µg of RNA. The mix was topped up to 20 µL total volume using DEPC-treated water. It was than incubated at 25 °C for 10 min, followed by 42 °C for an hour, and lastly 85 °C for 5 min. The resultant cDNA was stored at -20 °C and diluted 1:5 to a concentration of 400 ng/µL for use in quantitative, real-time, reverse-transriptase PCR (qRT-PCR; see **Section 2.4.1**)

The quality of the cDNA was assessed by RT-PCR using primers that amplify an endogenous control, i.e. the gene for the housekeeping enzyme glyceraldehyde-3-phosphate dehydrogenase (*Gapdh*). The reaction mix was set up as outlined in **Table 7** below. The mix was vortexed briefly and the RT-PCR reaction was carried out with 35 cycles of 1 min at 94 °C, 1 min at 60 °C, and 1 min at 72 °C.

Reagent	Volume per reaction (µL)
10X PCR buffer	2.5
dNTP mix (2 mM)	2.5
$MgCl_2$ (50 mM)	0.75
Forward primer (10 µM)	1.5
Reverse primer (10 µM)	1.5
Taq DNA polymerase (5 U/µL)	0.2
Distilled, de-ionized water	15.05
cDNA sample	1
Total	**25**

Table 7. RT-PCR reaction mix for amplification of *Gldc* cDNA.

2.3.2. Cloning of *Gldc* cDNA into vector for *in situ* probe preparation

2.3.2.1. *Gldc* probe design

A 587 bp probe complimentary to nucleotide 30,151,484–30,139,376 of the *Gldc* transcript coding sequence (ENSMUST00000025778) was designed and amplified by RT-PCR using cDNA prepared from wild-type embryos. Primer sequences were: 5'-GCCAACGCTTCCCTGCTGGA-3' forward in exon 4, and 5'-AGGGCCTGAGCCGTGCAGAT-3' reverse in exon 8/9 (crosses exon-intron boundaries), carried out in the reaction mix used in **Table 7** with 35 cycles of 1 min at 94 °C, 1 min at 58 °C, and 1 min at 72 °C. The PCR had been optimised to produce a single band.

2.3.2.2. Ligation into vector system

The PCR product containing the probe sequence was ligated into pGEM®-T Easy Vector System (Promega) which contains T7 and Sp6 polymerase recognition sites. This was done

by incubating a ligation mixture containing 5 µL of 2X Ligation Buffer, 1 µL of pGEM-T Easy Vector, 3 µL of the PCR product, and 1 µL of T4 Ligase for an hour at room temperature. The amount of PCR product added to the mix was calculated for optimal ligation efficiency with a 3:1 product/insert to vector ratio as followed:

$$\frac{ng\ vector\ \times kb\ size\ of\ insert}{kb\ size\ vector} \times \frac{product\ or\ insert}{vector}\ molar\ ratio\ = ng\ PCR\ product$$

$$\frac{50\ ng\ \times 0.6\ kb\ [Gldc\ probe]}{3.0\ kb} \times \frac{3}{1} = 30\ ng\ PCR\ product$$

2.3.2.3. Transformation into competent cells

After ligation, 50 µL of DH5α™ competent cells was added to 2 µL of ligation reaction. The tube was flicked gently to mix and incubated on ice for 20 min. The cells were then heat-shocked for 45–50 sec at 42 °C, and incubated on ice for a further 2 min. 950 µL of Luria Bertani (LB) broth was then added to the tube and the mix was incubated at 37 °C, shaking, for 90 min. 100 µL of this mix was then plated onto an LB plate containing 100 µg/mL of Ampicillin, 100 µM of isopropyl β-D-1-thiogalactopyranoside (IPTG), and 0.3% of X-gal (Sigma-Aldrich; prepared in dimethyl formamide), and incubated overnight (16–18 hrs) at 37 °C. White colonies (carrying the vector insert) were picked out, plated onto fresh LB plates containing 100 µg/mL of Ampicillin (LB-Amp), and incubated at 37 °C overnight. The following day, the colonies were inoculated into 10 mL of LB-Amp broth. After incubation at 37 °C overnight on a shaker, the broth was ready for plasmid preparation.

2.3.2.4. Plasmid preparation

Plasmid preparation was performed using the QIAprep Spin Miniprep Kit (Qiagen). First, the broth was centrifuged at 4,600 rpm for 15-30 min at room temperature. The supernatant was discarded and the pelleted cells resuspended in 250 µL of chilled Buffer P1 (Resuspension Buffer). 250 µL of Buffer P2 (Lysis Buffer) was then added and mixed, followed by addition of 350 µL of Buffer N3 (Neutralization Buffer). This solution was then spun for 10 min at 13,000 rpm. The resultant supernatant was added to the QIAprep spin column and spun for 1 min at 13,000 rpm. The flow-through was discarded and the column spun dry for an additional minute to remove residual wash buffer. 50 µL of

deionized, distilled water was added to the column, let stand for 1 min, and spun for 1 min at 13,000 rpm to elute DNA from the column. The concentration of the DNA was determined using the Nanodrop spectrophotometer.

The 5'-3' directionality of the insert within the vector was determined by PCR with probe primers combined with Sp6 and T7 primers. Using this method, the *Gldc* probe sequence was determined to be 5' at the T7 end and 3' at the Sp6 end, thus an antisense probe would be generating by a digestion at the T7 promoter end, followed by RNA synthesis using the Sp6 RNA polymerase, and a sense probe by digestion at the Sp6 promoter end followed by RNA synthesis using the T7 polymerase. For further confirmation of the probe sequence, a sample of the DNA extracted from the plasmids was sent for sequencing at the UCL Wolfson Centre for Biomedical Science. The DNA could then be used for preparation of an RNA probe, or further amplified by repeating the transformation (with 50–100 ng of plasmid) and plasmid preparation steps.

2.3.3. RNA probe preparation for *in situ* hybridisation

2.3.3.1. Plasmid DNA digestion

Test digests of the plasmids were first carried out using 200–500 ng of plasmid DNA (approximately 1 µL from a QIAprep Spin Mini preparation) and 5–10 U of the appropriate restriction enzyme (see **Table 8**), and ran on an agarose gel to confirm the presence of a single, linearized plasmid DNA band at approximately 4kb. This was followed by a large-scale digest using 3–5 µg of plasmid DNA and 20–50 U of restriction enzyme in 1X restriction enzyme buffer, made up to a 50 µL total reaction volume. The reaction mix was left to incubate for 2 hrs at 37 °C.

After digestion was complete, the linearized DNA was purified using the QIAquick PCR Purification Kit (QIAGEN) protocol. 5 volumes of Buffer PBI (Binding Buffer) was added to 1 volume of DNA and inverted several times. The DNA was bound to a QIAquick membrane by pipetting it into a QIAquick spin column and centrifuging for 1 min at 17,900 g. The flow-through was discarded. 750 µL of Buffer PE (Wash Buffer) was applied to the column and spun for 1 min at 17,900 g to wash the column. The resultant flow-through was discarded again and the column re-spun for a further 1 min to remove residual wash buffer. 30 µL of DEPC-treated water was carefully applied to the centre of the membrane to elute the DNA. The column was left to stand for 1 min, and then spun for 1 min at 17,900 g. The concentration of resultant DNA was ascertained using Nanodrop.

2.3.3.2. DIG probe transcription

A digoxigenin(DIG)-labelled, single-stranded RNA probe was prepared by transcribing the purified digest in the following mixture: 1 µg of digested plasmid DNA, 2 µL of DIG RNA labelling mix (Roche), 2 µL of transcription buffer (Roche), 0.5 µL of RNAse Inhibitor (Roche), and 2 µL of the appropriate RNA polymerases (see **Table 8**), made up to a 20 µL reaction mix with DEPC-treated water. The mix was incubated for 2 hrs at 37 °C, and 1 µL of this mix was then run on an agarose gel to assess transcription efficiency by the presence of two clean bands.

The DIG-labelled probe was purified using CHROMA SPIN-1000 DEPC-H_2O Columns (ClonTech). An empty spin was first performed by centrifuging the columns at 700 g for 5 min at 4 °C to dry the columns. The probe was then applied to the centre of the column and spun at 700 g for 5 min at 4 °C into a clean, RNAse-free tube. 1 µL of RNAse Inhibitor (Roche) was added to the purified probe, and the probe was stored at -20 °C until use.

Probe	Restriction enzyme, RE (Promega)	Catalogue number	RE Buffer (Promega)	RNA Polymerase (Roche)
Gldc antisense	Apa1	R6361	A	Sp6
	Nco1	R6513	D	Sp6
Gldc sense	Sal1	R6051	D	T7

Table 8. Restriction enzymes and RNA polymerases for generation of *Gldc in situ* hybridisation probes.

2.3.4. Whole mount *in situ* hybridisation

2.3.4.1. Hybridisation of probe

The embryos were first rehydrated from storage with a series of methanol washes (100%, 75%, 50%, 25%) in PBS containing 0.1% Tween-20 (PBT), followed by brief PBT washes. They were then bleached with 6% hydrogen peroxide in PBT for 1 hr on ice, treated with 5 µg/ mL of proteinase K in PBT at room temperature for 2 min (for E9.5 embryos) or 7 min (for E10.5 embryos), and briefly incubated in 2 mg/mL of glycine in PBT for 5 min at room temperature. The embryos were then re-fixed in 0.2% gluteraldehyde prepared in 4% PFA for 20 min at room temperature. After fixation, the embryos were washed in PBT, transferred to 1 mL of pre-warmed pre-hybridisation buffer containing 50% formamide, 5X saline sodium citrate (SSC) at pH 4.5, 50 ug/mL yeast RNA, 1% SDS, and 50 µg/mL heparin in DEPC-treated water, and incubated at 70 °C for 2 hours. 10 µL of each *Gldc* RNA probe was added per 1 mL of pre-hybridisation buffer and left to incubate overnight at 70 °C.

2.3.4.2. DIG antibody detection

Following hybridisation, the embryos were washed in pre-warmed formamide solutions: twice in Solution 1 (50% formamide, 5X SSC, and 1% SDS in DEPC-treated water) for 30 min each at 70 °C, and then twice in Solution 2 (50% formamide, 2X SSC, and 1% SDS in DEPC-treated water) for 30 min each at 65 °C. A TBST wash solution was prepared with 1% Tween-20 in tris-buffered saline (TBS; made with 50 mM of Tris-Cl at pH 7.6 and 150 mM of NaCl) and approximately 0.2 g (per 500 mL of TBST solution) of tetramisole hydrochloride (Sigma-Aldrich). The embryos were washed in TBST and blocked with 10% heat-inactivated sheep serum (Invitrogen) in TBST for at least an hour at room temperature. The blocking solution was replaced with anti-DIG-AP antibody (Roche; 11 093 274 910) at 1:2,000 dilution prepared in TBST containing 1% sheep serum. The embryos were left to incubate on a shaker at 4°C overnight.

The following day, the embryos were washed with five, 1 hr washes in TBST. After the last wash, the embryos were left washing in TBST on a shaker at 4°C overnight.

2.3.4.3. Colour development

An NTMT wash solution was prepared consisting of 100 mM NaCl, 100 mM Tris at pH 9.5, 50 mM magnesium chloride ($MgCl_2$), 1% Tween-20, and approximately 25 mg (per 50 mL of NTMT solution) of tetramisole hydrochloride, in distilled water. The colour developing solution was prepared with 4.5 µL/mL 4-nitroblue tetrazolium chloride, NBT (Roche) and 3.5 µL/mL 5-bromo-4-chloro-3-indoylphosphate, BCIP (Roche) in NTMT solution. The embryos were washed thrice in NTMT for 10 min each and then incubated with the developing solution at room temperature in the dark. Signal development was stopped after sufficient staining was achieved (about 7.5 hr) by making brief PBT washes. The embryos were photographed at this point and then re-fixed in 4% PFA overnight at 4°C.

2.3.4.4. Vibratome sectioning

Embryos labelled by whole mount *in situ* hybridisation were embedded in a gelatin/albumin mix (0.45% gelatin, 27% albumin, and 18% sucrose in PBS) for vibratome sectioning, which allows 50 µm sections (or thicker) to be obtained. Following fixation, the embryos were washed in PBS and incubated in 1 mL of the gelatin/albumin embedding medium overnight at 4°C. Approximately 200 µL of embedding medium was pipetted into plastic embedding moulds. 20 µL of gluteraldehyde (0.2%) was added to the medium in each mould and mixed in quickly. The embryos was transferred into the moulds and orientated as quickly as possible. The blocks were left to set completely for 30 min, then cut out of the mould and incubated in PBS for at least 1 hr in 4°C. Vibratome sectioning was then performed on the blocks to obtain sections at a thickness of 50 µm. The sections were mounted in 50% glycerol and coverslips sealed with clear nail varnish.

2.4. Assessing efficiency of *Gldc* gene-traps

2.4.1. Quantitative, real-time PCR (qRT-PCR)

The *Gldc*^{GT1} and *Gldc*^{GT2} gene-trap vectors contain splice acceptor sites. Transcription of *Gldc* from the endogenous promoter splices the mRNA to the gene-trap construct, resulting in early termination and a truncated mRNA. To assess the efficiency of the trapping, qRT-PCR was used to measure the levels of wild-type *Gldc* transcripts produced by the gene-trapped alleles.

For the *Gldc*^{GT1} allele which was inserted in intron 2, primers were designed to bind to exon 2 and exon 4 of the *Gldc* transcript which would not amplify a product if alternative splicing occurred. For *Gldc*^{GT2} inserted in intron 19, primers in exon 19 and 21 were used. A range of annealing temperatures and several primer designs were tested to ensure amplification of a single band and avoid non-specific amplification. Primer sequences are provided in **Table 9**. The *Gapdh* gene was used as an endogenous control to which all target samples were normalised.

Allele	Primer	Sequence (5'-3')
Gldc^{GT1}	Exon 2 forward	AGCATTGATGAGCTCATCGAG
	Exon 4 reverse	TCCAGCAGGGAAGCGTTGGC
Gldc^{GT2}	Exon 19 forward	TTCTGCATTCCCCACGGA
	Exon 21 reverse	AGGCCCTTTCCACCCATCAT
Gapdh	Forward	ATGACATCAAGAAGGTGGTG
	Reverse	CATACCAGGAAATGAGCTTG

Table 9. Primer sequences for quantification of *Gldc* mRNA by qRT-PCR

RNA and subsequent cDNA samples of all genotypes of *Gldc*^{GT1} and *Gldc*^{GT2} E9.5 and E10.5 embryos were prepared as outlined in **Section 2.3.1**. The cDNA samples were loaded onto Optical 96-Well Fast Thermal Cycling Plates (Applied Biosystems) in triplicates, 1 µL per well. A master mix of MESA Blue qPCR MasterMix Plus for SYBR® Assay Low ROX (Eurogentec) was prepared, containing 12.5 µL Mesa Blue reaction buffer, 2 µL of 10 µM forward primer, 2 µL of 10 µM reverse primer, and 7.5 µL of DEPC-treated water (per reaction). 24 µL of this mix was pipetted into each well. The plate was sealed with a clear adhesive, vortexed, centrifuged, and loaded into a 7500 Fast Real-Time PCR System machine (Applied Biosystems).

A standard qPCR cycle run was used: 2 min at 50 °C, 5 min at 95 °C, and 40 cycles of 95 °C for 15 sec (denaturation) and 60 °C for 1 min (annealing and extension). A dissociation curve was run after every successfully completed qPCR run to check for presence of primer dimers, genomic DNA, or non-specific products.

Analysis of results was carried out using the 7500 Software v2.0.6. For every primer pair used, the baseline value was set to above background fluorescence (prior to target amplification) and threshold value set above the baseline and at the point when the exponential region of the amplification curve begins. Any samples flagged by the software as containing outlier values or not producing a clean, single peak on the dissociation curve (thus indicating presence of contaminants) was discarded. A wild-type sample was set as the reference value with a Relative Quantification value of 1 (RQ = 1). All other samples were quantitated relative to this reference value.

2.4.2. Whole mount X-gal staining

The *Gldc*^{GT1} construct was reported by EUCOMM to contain a *β-Geo* reporter cassette which produces β-galactosidase in tissue where *Gldc* is expressed and can be stained for with an X-gal solution. The X-gal reaction buffer was prepared containing 2 mM of $MgCl_2$, 20 mM of Tris-HCl in pH 7, 0.2% of Nonidet P-40, 10 mM of potassium ferricyanide ($K_3Fe(CN)_6$), and 10 mM of potassium ferrocyanide ($K_4Fe(CN)_6.3H_2O$) in PBS. A 100 mg/mL dilution of X-gal was made in dimethyl sulfoxide (DMSO), added to 10 mL of reaction buffer, filtered through a 0.2 μm filter (Millipore), and warmed to 37 °C. Embryos were fixed as described in **Section 2.2.1** and washed several times in PBT. They were then incubated in X-gal staining solution overnight in the dark at 37 °C. The next day, the embryos were washed in PBS and photographed.

2.4.3. Glycine cleavage enzymatic assay

Gldc enzymatic activity was determined by a decarboxylation assay on *Gldc* adult mice liver samples. The liver samples were homogenised in cofactor solution containing THF, pyridoxal phosphate, and NAD, and incubated with [1-^{14}C]glycine. The amount of $^{14}CO_2$ released from the reaction was trapped in filter paper, measured with a scintillation counter, and normalised to protein content. The assay was carried out by Dr Tim Hutchins (Birmingham Children's Hospital).

2.5. Histological studies

2.5.1. Paraffin processing and sectioning

E9.5, E10.5 and E11.5 embryos (stored in absolute methanol) were first incubated in two changes of absolute ethanol for 30 min at room temperature each. The embryos were then cleared with Histo-Clear® solution (Agar Scientific) for 20 min for E9.5 embryos and 30 min for E10.5 and E11.5 embryos in room temperature. They were then given a fresh change of Histo-Clear solution and placed in a 60 °C oven to incubate for a further 20 or 30 min for E9.5 and E10.5/E11.5 embryos respectively. This was followed by four changes of paraffin wax at 30 min each. The samples were then given a fresh change of paraffin wax, placed on the stage of a stereomicroscope (Leica), and quickly orientated for transverse or coronal sections to be made. Once the wax has set overnight, the embryos were cut with a microtome (Leica) to obtain serial sections at a thickness of 7 µm or 4 µm (the latter for immunofluorescence staining using anti-Phospho-Histone-H3 antibody, see **Section 2.5.4**).

For E18.5 foetal heads and 5-week brains (stored in 70% ethanol), samples were brought to 100% ethanol with 1hr incubations of 85% and 95% ethanol each, followed by two 1 hr incubations with 100% ethanol. Samples were subsequently cleared with Histo-Clear for 1 hr at room temperature and a further 1 hr (with fresh solution change) in a 60 °C oven. The samples were then incubated in a pre-warmed mix of Histo-Clear and paraffin wax at a 50:50 ratio for 1hr 30 min in the oven. This is followed by four 100% paraffin wax changes for 1 hr each. The samples were then transferred to plastic moulds and similarly orientated and sectioned.

2.5.2. Hematoxylin and eosin staining

Paraffin wax sections of E9.5–E18.5 embryos were stained with Mayer's hematoxylin solution (Sigma-Aldrich) and a 1% solution of Eosin Y (ACROS Organics), a routinely used cytoplasmic and nucleic histology stain for morphological studies.

Sections were first deparaffinised with Histo-Clear, rehydrated with two 100% ethanol solutions followed by 95% and 70% ethanol solutions, and brought to water. They were then stained in hematoxylin for 1-3 min, and then submerged in gently running water for 2-3 min until the water ran clear. The purplish staining of hematoxylin on the sections was assessed under a stereomicroscope. As Mayer's hematoxylin is a progressive stain, slides

were returned to the staining solution at this point and left to stain until a satisfactory level of staining was achieved. Sections were then stained with eosin for 1-3 min, and then briefly submerged in water. The pinkish orange staining of eosin was similarly assessed and the sections returned to eosin solution if needed. Sections were then quickly dehydrated with ethanol (70%, 95%, 100%) and cleared in Histo-Clear. The slides were mounted in DPX mounting media with coverslips and left to dry in the fume hood overnight.

2.5.3. Cresyl violet staining

5-week brain sections were stained for morphological studies using cresyl violet, a routine stain for Nissl substances (rough endoplasmic reticulum) in the cell bodies of neurons. The staining solution was prepared with 0.1% cresyl violet acetate (Alfa Aesar) and 1% glacial acetic acid. Deparaffinized and rehydrated slides were stained for 15 min, dipped quickly in water, and differentiated in 95% ethanol to remove background and improve staining contrast. The violet staining was assessed under a stereomicroscope and further stained and differentiated if required. Slides were dehydrated to absolute ethanol, cleared, and mounted with DPX.

2.5.4. Immunofluorescence staining of Phospho-Histone-H3 (PHH3)

Slides were deparaffinised, rehydrated, placed in a 1:20 dilution (with distilled water) of Declere (Cell Marque), and steamed for 40 minutes. They were left to cool to room temperature. The slides were then washed three times in TBST solution. Blocking was performed using a solution containing 2 mg/mL bovine serum albumin (BSA; Sigma-Aldrich), 0.15% glycine, 0.1% Triton X-100, and 5% heat-inactivated sheep serum prepared in TBST. The sections were blocked for at least 30 min at room temperature. The blocking solution was then replaced with rabbit, anti-PHH3 primary antibody (Millipore; 06-570) at a 1:250 dilution (in blocking solution) and the slides were left to incubate overnight in a humidified chamber at 4 °C.

The next day, the slides were washed in three changes of TBST solution. Next, they were incubated in goat, anti-rabbit, Alexa Fluor® 488-conjugated, secondary antibody (Life Technologies; A11070) at a 1:500 dilution (in blocking solution) for 1 hr at room temperature in a humidified chamber and in the dark. Slides were then washed once in TBST solution, and then twice in TBS solution.

DAPI (Invitrogen) nucleic acid staining was then performed using a 1:10,000 dilution (in TBS) for 5 min. The slides were mounted with Mowiol® 4-88 (Sigma-Aldrich) mounting medium (prepared in a pH 6.8 solution containing 12% Mowiol, 0.2 M Tris Base, 0.2 M Tris HCl, and 30% glycerol) and coverslips were secured with clear nail varnish.

Mitotic cells were scored by visual inspection, counted, and normalised against DAPI-stained cell counts to obtain a percentage of PHH3-stained cells.

2.6. Metabolic studies

2.6.1. Sample preparation

E11.5 embryo extracts for glycine measurements were prepared by first sonicating them in PBS containing 1X cOmplete, Mini Protease Inhibitor Cocktail (Roche) to homogenise them. For samples to be used in folate metabolite analysis, sonication was performed in folate buffer (20 mM ammonium acetate, 0.1% ascorbic acid, 0.1% citric acid, 15 mg/mL dithiothreitol, adjusted to pH 7.0 with ammonia) containing 0.2 µM methotrexate. 10 µL of the homogenised samples were kept for protein assay (see **Section 2.6.2**). Two volumes of acetonitrile were then added to the samples to precipitate protein. The precipitate was removed by centrifugation at 14,000 g for 15 min at 4 °C. Supernatants were transferred into fresh tubes, lyophilised, and stored at -80 °C. Prior to mass spectrometry analysis, the samples were re-suspended in deionized, distilled water.

2.6.2. Protein assay

Total protein quantitation was carried out on E11.5 embryos with the Pierce™ BCA™ Protein Assay (Thermo Scientific). A set of diluted BSA standards was prepared with a working range of 20–2,000 µg/mL using the 2 mg/mL albumin standard ampules provided. A working reagent mix of Reagent A and Reagent B was made to a 50:1 ratio, for 1 mL per sample of total volume. 1 mL of this working reagent was added to 50 µL of each standard and 50 µL of diluted sample. A dilution factor of X50 was generally used and increased when necessary. All standard/sample tubes were prepared in duplicates.

The tubes were incubated for 30 min at 37 °C, then transferred to cuvettes and their absorbance read at 562 nm, beginning first with the standards (from blank to highest concentration) in order for a calibration curve to be plotted, quickly followed by the

samples. Protein concentration of each sample in µg/mL was read from the curve and total protein content in mg was determined by multiplying back to the sample dilution factor.

2.6.3. Amino acid analysis

Amino acid analysis was carried out on blood, urine, and E11.5 embryo samples (prepared as outlined in **Section 2.6.1**) by ion-exchange chromatography (Biochrom 30 Amino Acid Analyser). Protein was first precipitated with 5-sulphosalicylic acid and removed by centrifugation. The supernatant was then filtered, injected on a Lithium High Performance Physiological (cation-exchange) Column, and measured at 570 nm using post-column ninhydrin derivatisation. Embryo samples were normalised to total protein content (as determined in **Section 2.6.2**), while urine samples were normalised to creatinine levels. Amino acid analysis was performed by Helen Prunty and Dr Simon Heales (Great Ormond Street Hospital for Children NHS Foundation Trust). Measurement of creatinine levels was carried out by Dr Kit-Yi Leung (UCL Institute of Child Health).

2.6.4. Folate profiling

Folate profiling was carried out on E11.5 embryo samples (prepared as described in **Section 2.6.1**) by ultra-performance liquid chromatography tandem mass spectrometry (UPLC/MS/MS). Samples were injected on an ACQUITY UPLC BEH C18 column and resolved by reserved-phase UPLC (Waters Corporation) coupled to a XEVO TQ-S tandem quadrupole mass spectrometer (Waters Corporation) in negative-ion mode. The relative abundance of mono- and polyglutamated forms of six folate species were quantified by multiple reaction monitoring (MRM) of precursor and product ions, normalised to DNA concentration (Leung et al., 2013, Pai et al., 2015). Analysis of folate metabolites was performed by Dr Kit-Yi Leung.

2.6.5. Assessment of formate levels

Formate levels in blood and urine samples were measured by gas chromatography mass spectrometry (GC-MS). Formate was derivatised by incubating with pentafluorobenzyl bromide in acetone (alkylating reagent) and the organic phase extracted by addition of n-hexane. The organic phase was then injected on an Agilent DB-225 J&W GC column and resolved with a Thermo Fisher TRACE ULTRA Gas Chromatograph coupled to an ISQ mass selective detector and AS3000 Autosampler in electron-impact ionisation mode. Formate

was quantified with reference to a standard curve (Lamarre et al., 2014). Formate levels were analysed by Dr John Brosnan and Dr Margaret Brosnan (Memorial University of Newfoundland, Canada).

2.7. Gold chloride *en bloc* staining

Gold chloride stains for myelinated axons and was used for studies on the corpus callosum. The protocol used was simplified from an *en bloc* staining technique outlined by (Wahlsten et al., 2003). After a 48 hr fixation in 4% PFA, the 5-week brains were rinsed briefly in distilled water. They were then carefully sliced mid-sagitally into left and right halves with a scalpel and incubated in 0.1% gold chloride solution (Sigma-Aldrich) at 37 °C. Incubation was stopped after approximately 1 hr 30 min, when staining of the corpus callosum became visible to the naked eye. The staining was then fixed by immersing in 2.5% sodium thiosulfate (Sigma-Aldrich) for 5 min. The half brains were transferred to PBS for measurement of the corpus callosum under a stereo microscope using an eyepiece graticule.

2.8. Image capture and data analysis

All images of whole embryos and brains were captured with a DFC490 camera (Leica) mounted on a Stemi SV11 stereomicroscope (Zeiss). For sections, bright-field micrographs were captured on an Axioplan 2 microscope (Zeiss) using the AxioVision v4.8.2 software, while fluorescence images were taken with an Axiophot microscope (Zeiss) mounted with a Leica DC500 camera using the Leica FireCam software.

Brightness and contrast adjustments, image cropping, and composite image assemblies were done with Adobe Photoshop CS3 or the ImageJ 1.47v software (National Institutes of Health, USA). Cell counting for proliferation studies using anti-phospho-histone H3 staining was performed using the Cell Counter plugin in ImageJ. All graphs were plotted with SigmaPlot 2001 or Microsoft Excel 2010. All statistical analyses were carried out with SigmaStat 3.5.

3. Embryonic phenotypes in the *Gldc*-deficient mouse model

3.1. Introduction

Much of the pathogenicity of non-ketotic hyperglycinemia (NKH) and GCS-associated neural tube defects (NTDs) is unknown. The complications of studying NKH, like many metabolic disorders, stem largely from its heterogeneous presentation and the lack of a suitable *in vivo* system to model its most common form. On the other hand, NTDs are far from lacking in animal models but their multifactorial aetiology remains notoriously difficult to unpick. The success of folic acid treatment is undeniable, but its mechanism of rescue is poorly understood and the phenomenon of folic acid resistance is largely unexplained.

The first step in this project is to obtain a suitable mouse model for *Gldc* that would allow investigation of its requirement during embryonic development, involvement in folate metabolism and NTDs, modelling of the classical form of NKH, and testing of treatment options for its associated disease phenotypes. The various strategies for mouse mutagenesis and transgenesis are thus explored below.

3.1.1. Classical mutagenesis

Large-scale, classical mutagenesis projects in the mouse were originally performed to assess effects of germ-line mutations as a consequence of nuclear and chemical weapons, and were carried out in centres that were historically established as nuclear physics laboratories such as Oak Ridge and MRC Harwell (Silver, 1995). Whole body exposure to ionising radiation such as X-rays or injections with alkylating agents like *N*-ethyl-*N*-nitrosourea (ENU) and chlorambucil (CHL) into differentiating germ cells were used to randomly target multiple regions of the genome. Ionising radiation produced large deletions, translocations and chromosomal aberrations, while ENU and CHL injections resulted in point mutations and large-scale, multi-locus deletions respectively (Russell et al., 1979, Russell et al., 1989).

The nature of classical mutagenesis techniques was such that target sites in the genome were entirely random and required positional cloning with sufficient molecular resolution to identify them. Where large lesions were produced, such as with ionizing radiation and CHL injections, multiple disease phenotypes may occur which complicates the task of discerning the specific genes responsible. On the other hand, the single nucleotide hits produced by ENU may at times be difficult to identify. As technology for generating genetically modified mice progressed, a more directed approach to mutagenesis was introduced with gene targeting.

3.1.2. Gene targeting and transgenesis

The most direct method for generating genetically modified mice begins with cloning of the desired gene with a ubiquitous or tissue-specific promoter, a positive selection marker and/ or reporter gene, and a 3' polyadenylation (polyA) transcription termination site, into a plasmid, viral, or artificial chromosome backbone. The construct is then microinjected into the pronucleus of a fertilised oocyte, integrates randomly, and replicates along with the host genome (Jackson and Abbott, 2000).

Gene targeting techniques were developed to create gene-specific mutations in ES cells and are based on the principle of homologous recombination between sequences in the construct and its precise endogenous counterpart for integration. ES cells with successfully integrated vectors can then be injected into blastocyst-staged embryos, and the resultant chimeric mice would be able to produce transgenic offspring if germ-line transmission from the ES cells is successful. Pioneering work on gene targeting was carried out in the labs of Oliver Smithies, Mario Capecchi, and Martin Evans, who jointly won the 2007 Nobel Prize in Medicine or Physiology (Evans and Kaufman, 1981, Smithies et al., 1985, Thomas and Capecchi, 1987).

The classical "knock-out" model involves replacing or interrupting the endogenous coding sequence of a gene with a selection marker gene, resulting in a null allele. Vector constructs may be designed to cause a frameshift mutation or to remove the entire gene (if possible) to ablate gene function. The vector DNA is introduced into ES cells in culture. Successfully transfected clones are then used to produce chimeric mice by blastocyst or morula injection (Joyner, 2000). A "knock-in" strategy was later devised, whereby a transgene is inserted into the target region and placed under endogenous transcriptional control. While the knock-out technique was limited to studying the effects of losing the gene, knock-ins allowed for more specific or subtle mutations to be examined (Joyner, 2000).

3.1.3. Gene-trapping

Gene-trap strategies were developed next, which reverted back to random integration of reporter genes, but in a way that allowed for successful transcription of the reporter gene only when the endogenous splicing mechanism is active. A gene-trap vector design contains a splice acceptor site at the 5' end, a promoterless reporter gene such as *lacZ* or *gfp* with a polyA tail, and a selector marker gene such as *neomycin* (or a combined reporter/selector fusion gene such as *β-geo*). In-frame integration of the vector into an intronic sequence (or, alternatively, inclusion of an IRES sequence 5' to the reporter) allows for splicing of fusion transcripts containing a truncated endogenous sequence followed by the vector reporter sequence and ending at the vector's polyA tail (Joyner, 2000). Usually, this also results in the disruption of the gene. Successful transription and translation of the reporter gene produces a signal (i.e. positive staining of β-galactosidase or green fluorescent protein, GFP) wherever and whenever the endogenous gene is *actively* expressed, allowing for visualisation of the spatiotemporal pattern of gene expression (Skarnes et al., 1992, Chalfie, 1995).

The completion of the human genome project and, subsequently, the mouse genome project, made available a wealth of genetic information. That, combined with gene-trapping techniques, provided a strategy for high-throughput generation of new mutations, as ES cell lines containing gene-traps can be mass-produced and stored in liquid nitrogen with relative ease. As the integration sites (i.e. the random targets of the gene-traps) of all these ES clones can be sequenced and identified, selected target genes can then be introduced into mice to produce transgenic animals ready for functional studies. Tens of thousands of ES cell lines are now made available through large-scale mouse mutagenesis projects such as the International Gene Trap Consortium (IGTC; http://www.genetrap.org/info/overview.html), whose members and affiliates include the European Conditional Mouse Mutagenesis Program (EUCOMM) and the North American Conditional Mouse Mutagenesis project (NorCOMM).

This project utilises two *Gldc* gene-trap models available as ES cells from EUCOMM and NorCOMM. This chapter focuses on characterisation of the gene-traps and the embryonic phenotypes obtained.

3.2. Results

3.2.1. Expression analysis of *Gldc*

3.2.1.1. *Gldc* mRNA expression in neurulation-stage mice embryos

The mRNA and protein expressions of GCS genes have been explored at late-developmental and post-natal stages (Sakata et al., 2001, Ichinohe et al., 2004), but their expression patterns in early development are not known. As NTDs occur in the *Amt* knockout mouse, the question arises as to whether GCS genes are expressed at neurulation stages. An mRNA probe spanning exons 4 to 9 of the *Gldc* transcript was generated and whole mount *in situ* hybridisation was carried out on E8.5 to E10.5 wild-type embryos.

Figure 6 shows the expression pattern of *Gldc* mRNA at E8.5 when neural tube closure has initiated and at E9.5 when cranial closure was complete but spinal closure still ongoing. At E8.5 (**Figure 6A-E**), *Gldc* mRNA was intensely expressed in the neural folds throughout the entire anterior-posterior length of the neural tube at all stages of neural tube closure (open neural folds, elevated but unfused folds, and fused folds) and in the branchial arches and foregut. At E9.5 (**Figure 6F-J**), strong expression of *Gldc* in the entire neural tube persisted. Intense staining was also found in the periphery of the branchial arches, optic vesicles, otic vesicles, hindgut, and limb buds.

At E10.5 (**Figure 7**) when spinal neurulation is complete, *Gldc* mRNA was still present throughout the neural tube, branchial arches, optic vesicles, hindgut and limb buds but the staining was fainter and more ubiquitous than earlier stages.

Thus, *Gldc* is present in the appropriate tissue (i.e. neural folds) at the appropriate stages for loss of function to have an effect on neural tube closure. *Gldc* expression also closely matched areas with high proliferation during those stages of embryonic development.

Figure 6. Expression pattern of *Gldc* mRNA in E8.5 and E9.5 wild-type embryos.

(A) Whole mount *in situ* hybridisation for *Gldc* on an E8.5 embryo. **(B-E)** Sections through **(A)**, where *Gldc* mRNA was expressed in open cranial folds **(B)**, elevated but unfused folds **(C)**, closed neural tube (NT) **(D)**, and open posterior neuropore **(E)**. **(F)** Whole mount *in situ* hybridisation for *Gldc* on an E9.5 embryo. **(G)** Dorsal view of **(A)**. **(H-J)** Sections through **(F, G)**, in which expression of *Gldc* persisted through the entire neural tube. *Gldc* expression was also seen in the branchial arch pouches (BA), optic vesicles (OP), otic vesicles (OV), foregut (FG) and hindgut (HG), and limb buds (LB).

Other abbreviations: hindbrain (HB), forebrain (FB). Scale bars: 1 mm.

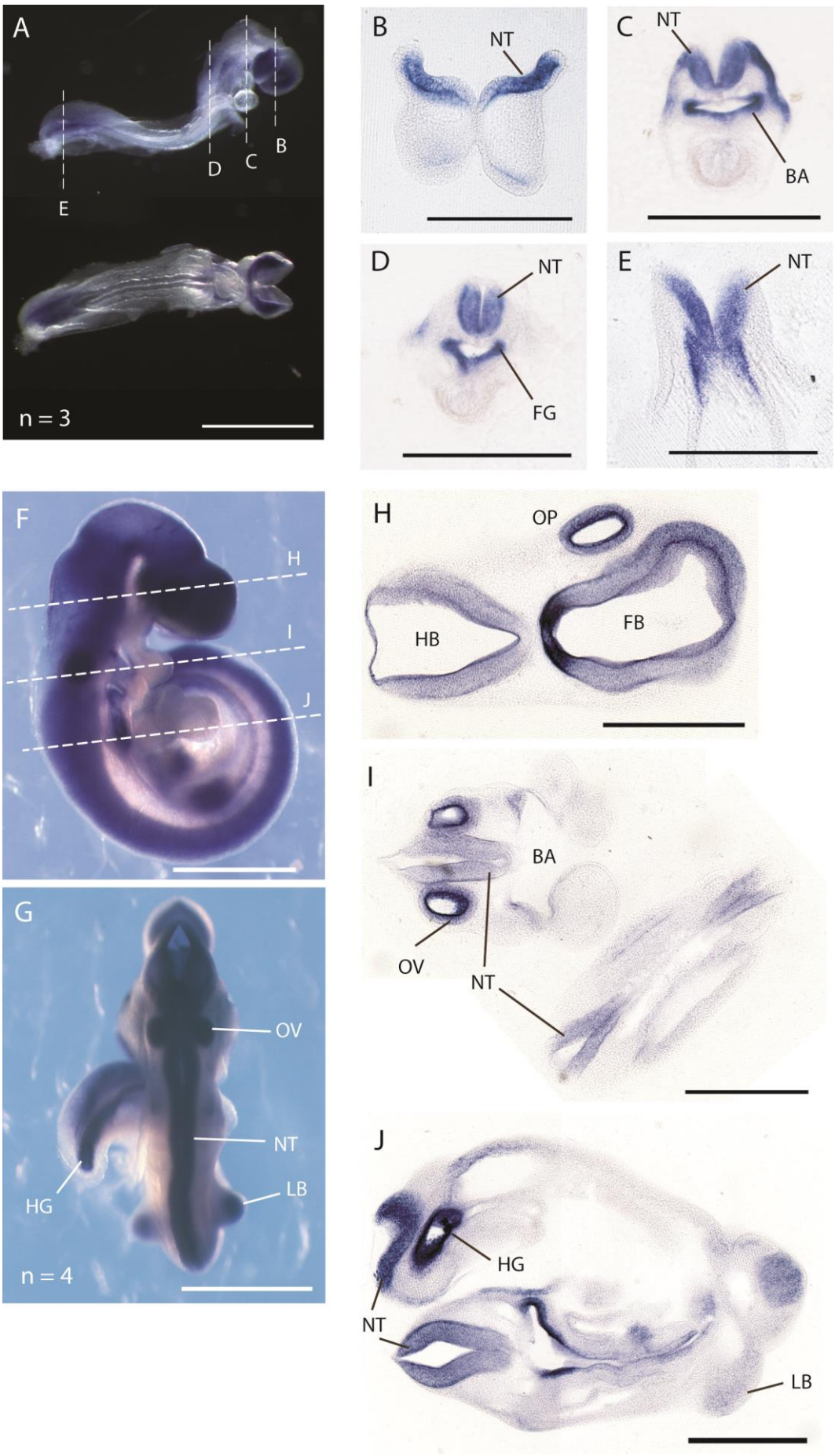

Figure 6. Expression pattern of *Gldc* mRNA in E8.5 and E9.5 wild-type embryos.

Figure 7. Expression pattern of *Gldc* mRNA in E10.5 wild-type embryos.

(A) Whole mount *in situ* hybridisation for *Gldc* on an E10.5 embryo. **(B-D)** Sections through **(A)**, where *Gldc* mRNA expression was overall less intense than at E8.5 and E9.5 (as shown in **Figure 6**), but was nonetheless still specific to the neural tube, optic vesicles (OP), hindgut (HG), and limb bud (LB). **(E, G)** represent sense control embryos, with vibratome sections through them **(F, H)**.

Other abbreviations: hindbrain (HB), forebrain (FB). Scale bars: 1 mm.

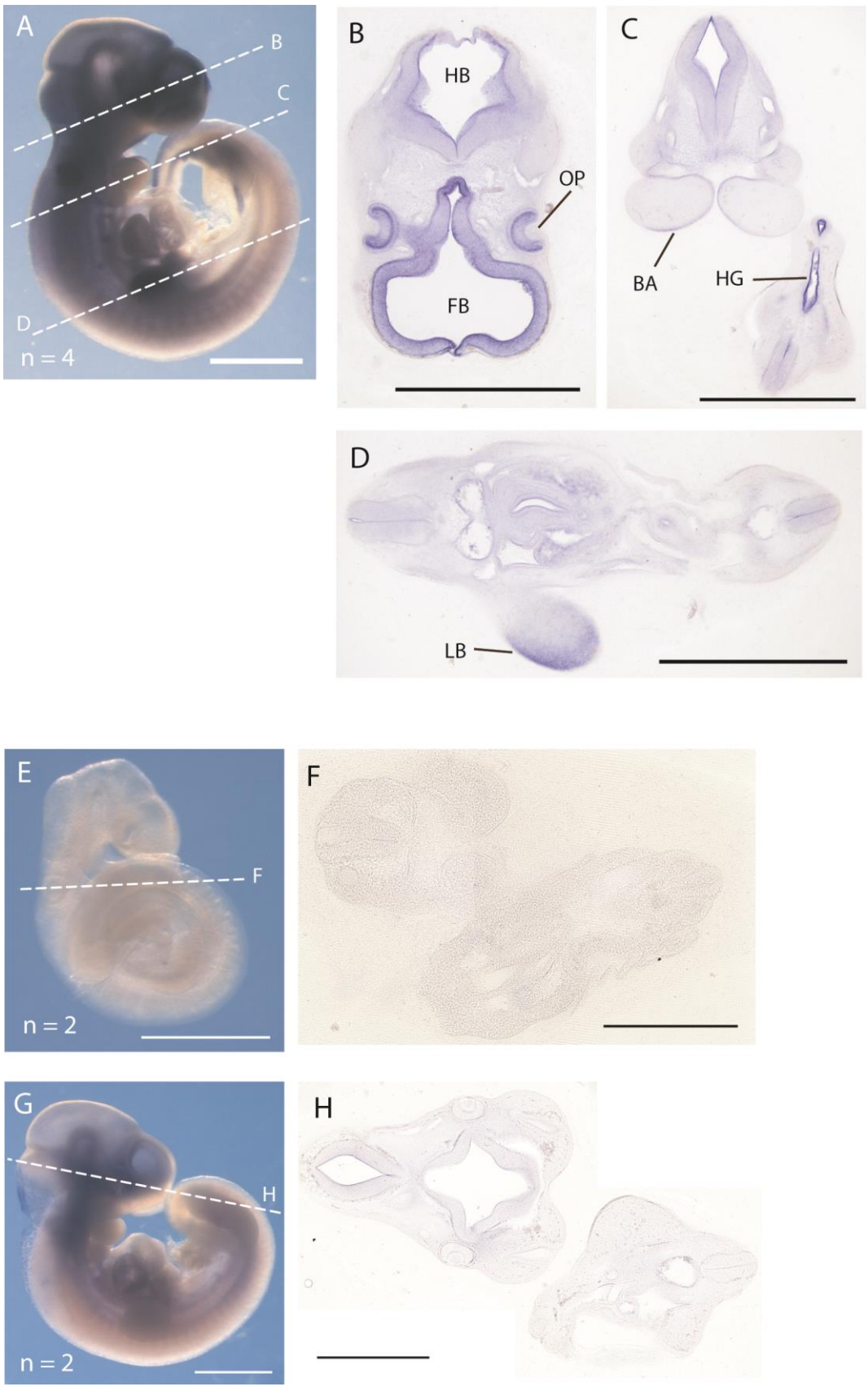

Figure 7. Expression pattern of *Gldc* mRNA in E10.5 wild-type embryos.

3.2.2. *Gldc* gene-trap models

3.2.2.1. Defining the locus and trapping efficiency of the *Gldc^{GT1}* allele

The *Gldc* mouse model is a novel model and is used in this project to determine whether loss of Gldc function is sufficient to cause NTDs. *Gldc^{GT1}* gene-trap mice were generated from ES cells obtained from EUCOMM (*Gldc* clone EUCG0001_DO2) and crossed into a 129/Sv wild-type background as described in **Chapter 2**. The *Gldc^{GT1}* allele carries a conditional gene-trap construct that was reportedly inserted into intron 2-3 of the *Gldc* gene, and should contain a *β-geo* reporter which would stain for *lacZ* expression in ES cells and embryos (information provided by EUCOMM).

To detect the gene-trap allele, PCR primers were designed to bind to the intronic sequence at the immediate 5' end of the construct and to the LTR sequence (F2R1 primer pair in **Figure 8A**). A pair of *neo* primers also produced a PCR product in the presence of the gene-trap allele (F3R2 primer pair in **Figure 8A**). The wild-type allele is detected by a pair of PCR primers that bind to intronic sequences on either ends of the construct and only amplify in the absence of the construct (F1R3 primer pair in **Figure 8A, B**). This genotyping strategy, as illustrated in **Figure 8C**, was tested on genomic DNA from the *Gldc^{GT1}* ES cell line as well as offspring of chimeric mice crossed with wild-type 129/Sv mice which, with successful germline transmission, would produce heterozygous *Gldc$^{GT1/+}$* mice.

When whole mount X-gal staining was carried out on mutant embryos from this initial cross to detect for *Gldc-lacZ* staining, none was observed (**Figure 9**). To investigate the lack of X-gal staining and initial problems with optimizing the genomic DNA PCR genotyping, the entire gene-trap was amplified and sequenced. Sequencing of the F2R1 PCR product confirmed that the site of gene-trap insertion (i.e. the breakpoint) was between nucleotides 30,171,315 and 30,171,314 of intron 2-3 of the *Gldc* gene (ENSMUSG00000024827). Long-Range PCR was then carried out to amplify the construct from this breakpoint site and across the entire gene-trap to the intronic region at the 3' end of the construct, producing a 4 kb-sized fragment.

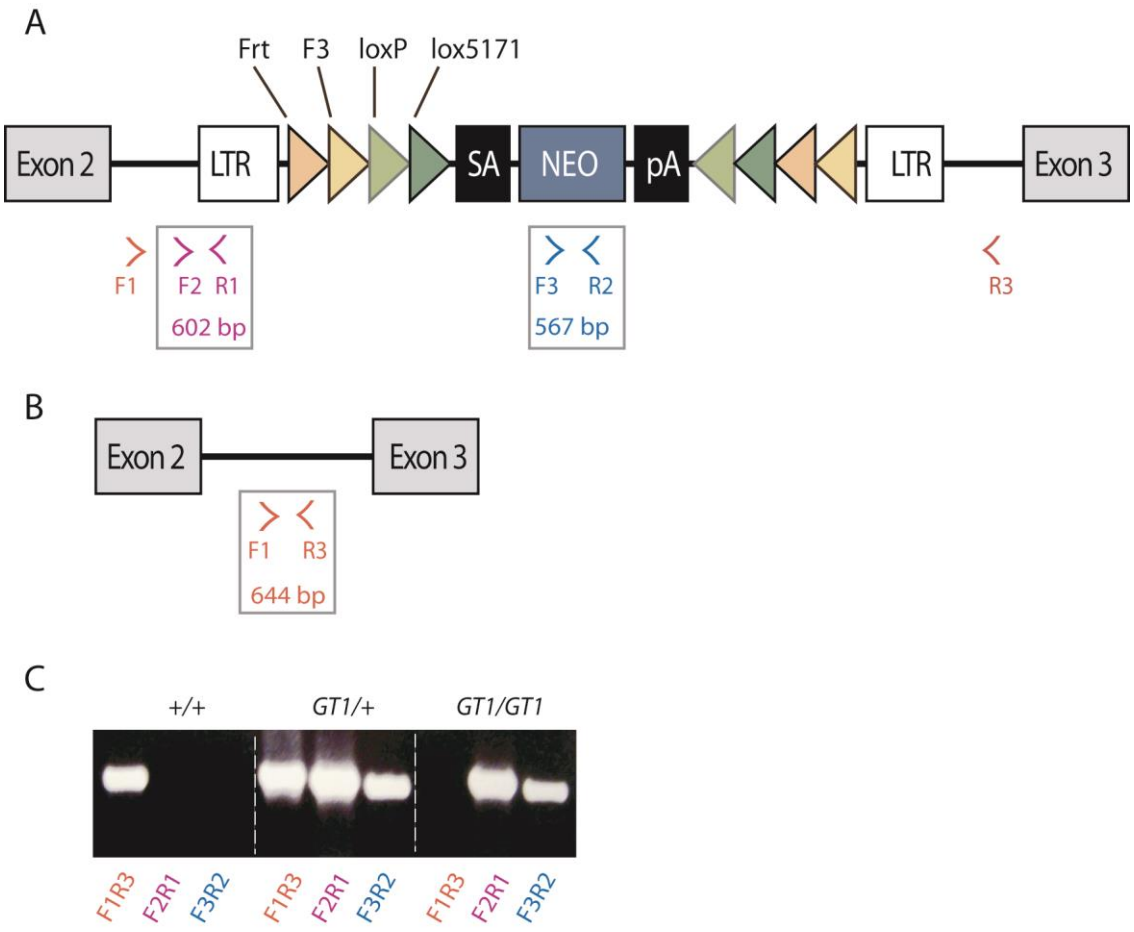

Figure 8. *Gldc* gene-trap 1 (*Gldc*^{GT1}) design and genomic PCR genotyping strategy.

(A) The *Gldc*^{GT1} gene-trap allele showing the construct inserted between exons 2 and 3 of the *Gldc* gene. The F2R1 and F3R2 primer pairs were designed to amplify only in the presence of the construct. **(B)** The wild-type allele of the *Gldc* gene, showing the F1R3 primer pair which is only able to amplify when the 4 kb construct in between them is absent. **(C)** The genomic PCR genotyping strategy for *Gldc*^{GT1} mice, in which presence of only the F1R3 band denotes a wild-type (*Gldc*$^{+/+}$), all 3 bands denote a heterozygote (*Gldc*$^{GT1/+}$), and only the F2R1 and F3R2 bands denote a homozygote (*Gldc*$^{GT1/GT1}$).

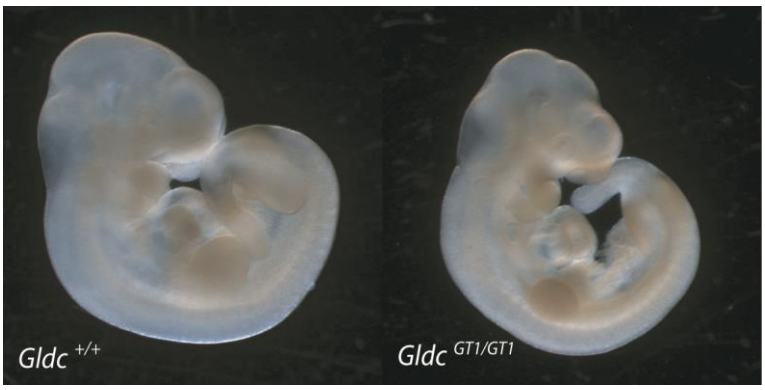

Figure 9. Whole mount X-gal staining of *Gldc*^{GT1} E10.5 embryos.

Gldc^{GT1} embryos did not stain positive for *Gldc-lacZ* expression as predicted from the initial gene-trap design provided.

Sequencing of various parts of this 4 kb fragment using a primer walking strategy (outlined in **Chapter 2**) led to the identification of the Frt, F3, loxP, and lox5171 sites on the 5' end of the construct up to the *neo* reporter sequence by comparing to reference sequences found online at http://www.ncbi.nlm.nih.gov/nuccore/ (accession numbers: CS436287.1 for Frt, CS436288.1 for F3, 116807196 for loxP, and CS436285.1 for lox5171). However, the reporter sequence contained only a *neomycin* cassette and not the full *β-geo* sequence that was indicated in the original gene-trap design. This would explain the successful amplification of a *neo* PCR band but the lack of *lacZ* staining in the embryos. The full sequencing results (with annotation) are provided in **Appendix 1**.

When initial matings to generate experimental litters were carried out with *Gldc*$^{GT1/+}$ pairs on the 129/Sv background, a large number of resorption and embryonic lethality was observed at E10.5. Very few *Gldc*$^{GT1/GT1}$ were successfully collected, and the few that survived to E10.5 exhibited severe growth retardation and occasional cranial NTDs. The number of viable mutants was insufficient to carry out experiments. To circumvent this problem, the chimeras were crossed to wild-type mice on a C57BL/6 genetic background to generate heterozygous mice. These mice were viable and fertile, and were inter-crossed to produce experimental litters. This cross was able to produce all 3 genotypes that survived to birth, with an average litter size of 7 and resorption rates of no more than 1 per litter. The proportion of embryo genotypes collected followed a 1:2:1 Mendelian ratio (**Table 10**), indicating that no embryonic lethality had occurred in homozygous embryos. All experiments hereon in using the *Gldc*^{GT1} allele was generated with this cross.

Stage (E-)	No. of litters	Average litter size	Average no. of resorptions per litter	No. of embryos		
				Gldc$^{+/+}$	*Gldc*$^{GT1/+}$	*Gldc*$^{GT1/GT1}$
10.5	16	7.9	0.69	35	64	28
11.5	23	7.6	1.04	30	94	51
12.5	1	-	-	1	5	3
13.5	1	-	-	1	0	3
15.5	12	7.1	0.33	28	31	26
16.5	1	-	-	0	4	3
18.5	9	6	0	12	27	15
TOTAL	-	-	-	**107**	**225**	**129**
Proportion	-	-	-	**0.23**	**0.49**	**0.28**

Table 10. Litter information of *Gldc*$^{GT1/+}$ crosses on a C57BL/6 genetic background.

To test the trapping efficiency of the *Gldc*^{GT1} gene-trap, *Gldc* mRNA levels in adult mice were assessed. A quantitative RT-PCR (qRT-PCR) strategy was used on cDNA generated from liver and brain samples (where *Gldc* is known to be highly expressed). The qRT-PCR primers were designed to amplify a 338 bp product corresponding to exons 2 to 4 of the wild-type *Gldc* transcript (ENSMUST00000025778). In the gene-trap allele, alternative splicing from exon 2 to the splice acceptor site of the construct would result in a truncated mRNA missing exons 3 to 25 (illustrated in **Figure 10A, B**) which would fail to be detected by the wild-type primers (i.e. no wild-type *Gldc* mRNA is produced).

As shown in **Figure 10C**, heterozygous mutants (*Gldc*$^{GT1/+}$) only produced 30-40% of wild-type *Gldc* mRNA, while homozygous mutants (*Gldc*$^{GT1/GT1}$) showed 0–10% mRNA levels. The residual qRT-PCR product from homozygous mutants was run on an agarose gel, and demonstrated the same band size as the wild-type band. This would correspond to low-level expression of *Gldc* (as opposed to a non-specific product) and indicates that the *Gldc*^{GT1} gene-trap confers a strongly hypomorphic allele.

Measurement of actual Gldc enzymatic activity was performed on liver samples using the [1-^{14}C]glycine decarboxylation reaction which is based on release of labelled CO_2 from glycine (carried out by Dr Tim Hutchin, Birmingham Children's Hospital). Despite the 60% reduction in abundance of mRNA in *Gldc*$^{GT1/+}$ mice, enzymatic activity was still comparable to wild-type levels. However, enzymatic activity in *Gldc*$^{GT1/GT1}$ mice was almost completely undetectable (**Figure 11**).

Figure 10. Assessment of *Gldc* mRNA levels in *Gldc*^{GT1} adult mice liver and brain.

(A) Splicing of wild-type *Gldc* mRNA produces a transcript corresponding to the 25 exons of the *Gldc* gene. Primers for qRT-PCR were designed to amplify the region corresponding to exons 2 to 4. **(B)** Alternative splicing to the *Gldc*^{GT1} gene-trap results in a truncated mRNA containing only exons 1 and 2, and the primers would fail to amplify a product. **(C)** qRT-PCR results showing levels of *Gldc* mRNA in *Gldc*^{GT1} mutant liver and brain samples, normalised to their respective wild-types. In *Gldc*$^{GT1/+}$ mutants, 30–40% of mRNA was produced. In *Gldc*$^{GT1/GT1}$ mutants, only 0–10% of mRNA could be detected. Error bars represent mean ± SEM (ANOVA, $p<0.001$).

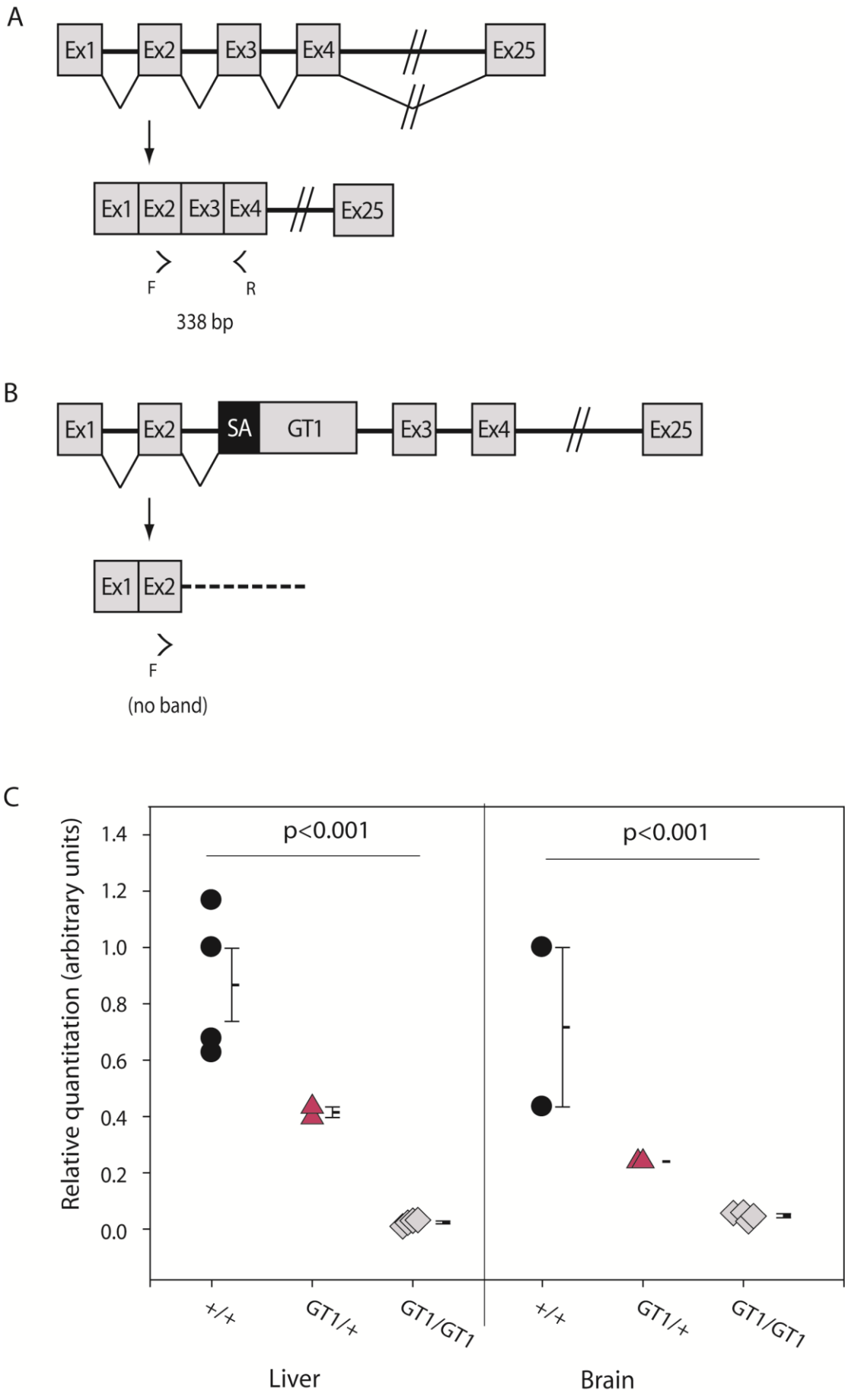

Figure 10. Assessment of *Gldc* mRNA levels in *Gldc*^{GT1} adult mice liver and brain.

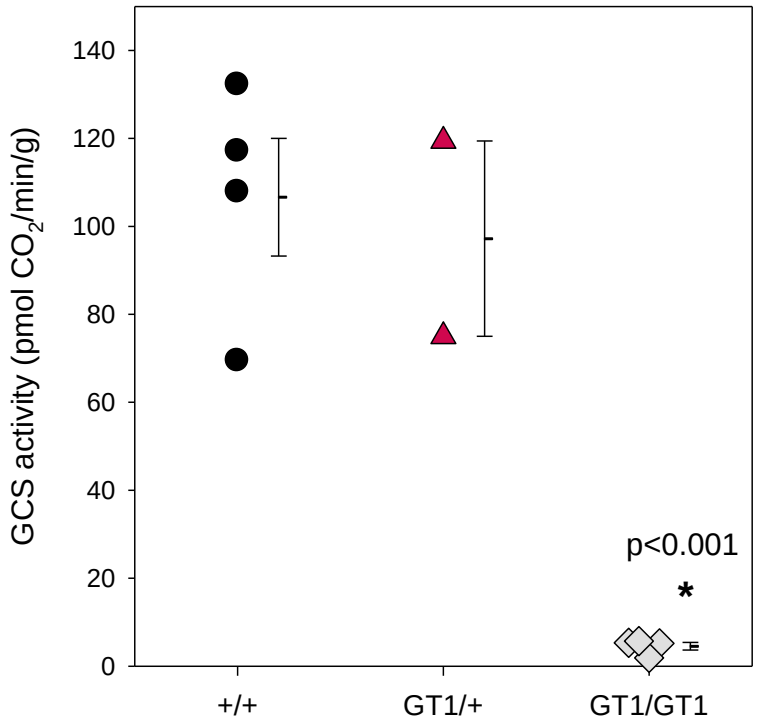

Figure 11. Enzymatic activity of Gldc in *Gldc^{GT1}* adult mice livers.

Gldc$^{GT1/+}$ mice livers show Gldc enzymatic activity comparable with wild-types at average 106.6 and 97.2 pmol CO_2/min/g respectively, while *Gldc$^{GT1/GT1}$* livers showed a significant decrease in enzymatic activity, at average 4.5 pmol CO_2/min/g. Error bars represent mean ± SEM (*ANOVA, p<0.001).

3.2.2.2. *Gldc^{GT2}* gene-trap line

Owing to the initial difficulties in genotyping and confirming efficiency of the *Gldc^{GT1}* gene-trap, an ES cell line containing a different *Gldc* gene-trap was ordered from NorCOMM (clone CMHD-GT_519C8). This cell line was similarly used to generate a second *Gldc* gene-trap mouse model, designated *Gldc^{GT2}*, on C57BL/6 background.

The *Gldc^{GT2}* gene-trap construct was inserted into intron 19-20 of the *Gldc* gene. Alternative splicing to the construct's splice acceptor site should result in truncated *Gldc* mRNA lacking exons 20 to 25. Genomic PCR genotyping was carried out using primers that bind to the *EGFP* reporter sequence for detection of the gene-trap allele, and intronic primers that bind to either ends of the construct for detection of the wild-type allele (**Figure 12**). The genotypes of litters generated by crosses of heterozygous *Gldc$^{GT2/+}$* mice did not differ significantly from a 1:2:1 Mendelian genotype ratio (Z-test) (**Table 11**).

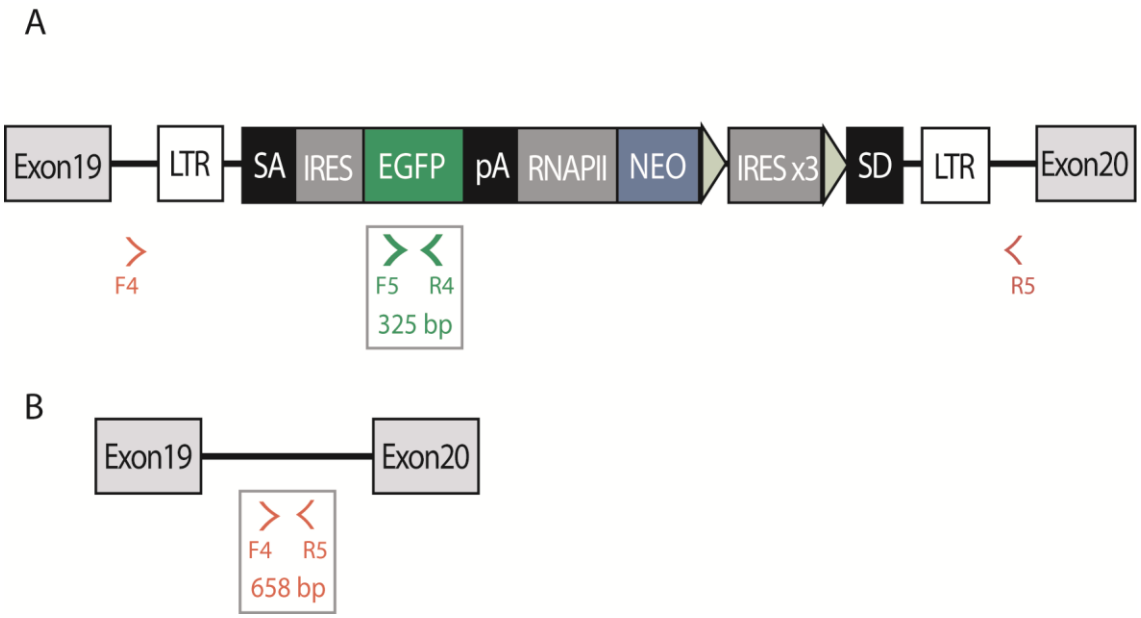

Figure 12. *Gldc* gene-trap2 (*Gldc*^{GT2}) design and genomic PCR genotyping strategy.

(A) The *Gldc*^{GT2} gene-trap is inserted between exons 19 and 20 of *Gldc*, where alternative splicing to the splice acceptor (SA) results in a truncated mRNA missing exon 20 onwards. F5R4 primers bind to the *EGFP* reporter sequence of the gene-trap allele. **(B)** The F4R5 primer pair binds to a region in intron 19-20 and would only amplify in the absence of the gene-trap.

Stage (E-)	No. of litters	Average litter size	Average no. of resorptions per litter	No. of embryos		
				Gldc$^{+/+}$	*Gldc*$^{GT2/+}$	*Gldc*$^{GT2/GT2}$
10.5	12*	8	0.1	23	59	14
11.5	6*	8.7	0	14	32	6
13.5	5*	7.4	0	4	25	8
14.5	2	9.5	0.5	3	9	7
15.5	4	8.8	1	5	17	13
16.5	1	8	0	2	3	3
TOTAL	-	-	-	**51**	**145**	**51**
Proportion	-	-	-	**0.21**	**0.59**	**0.21**

Table 11. Litter information of *Gldc*$^{GT2/+}$ crosses on a C57BL/6 genetic background.

*7 out of 23 litters at E10.5, E11.5, and E13.5 stages collected by Maria-Chiara Autuori

3.2.3. Developmental phenotypes of *Gldc* mutant embryos

3.2.3.1. NTD incidence in *Gldc*^{GT} mutants

Examination of experimental litters generated by heterozygous crosses of both *Gldc*^{GT1} and *Gldc*^{GT2} mice revealed that at E9.5 and E10.5, cranial neural folds remained open at the midbrain-hindbrain region of some homozygous mutants. This failure of closure resulted in exencephaly, which is characterised by the exposed brain tissue at E15.5 (**Figure 13**).

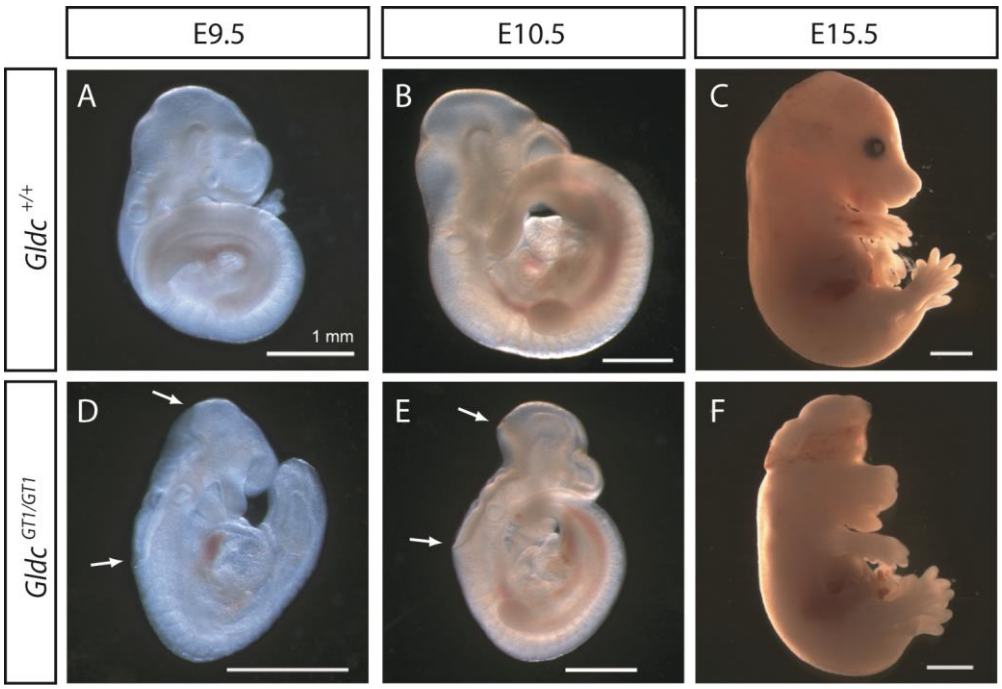

Figure 13. NTDs in *Gldc*^{GT1} mutant embryos.

(A-C) *Gldc*$^{+/+}$ embryos appeared normal at all stages of development. Cranial NTDs were observed in *Gldc*$^{GT1/GT1}$ embryos where neural folds were open in the midbrain-hindbrain region at E9.5 **(D)** and E10.5 **(E)** and resulted in exposed brain tissue at E15.5 **(F)**. Arrows denote regions where the neural tube remained open. Scale bars: 1mm.

More severe cranial phenotypes were observed in *Gldc*^{GT2} mutants (**Figure 14**). Hindbrain exencephaly tended to extend further rostrally into the midbrain as well as to a more caudal somite level. In some mutants, the cranial neural tube was open throughout the midbrain and forebrain, resulting in a characteristic split face phenotype. This was often accompanied by what appears to be moderate to severe truncation of the forebrain, resulting in shortening of the rostro-caudal length of the cranial region. Craniorachischisis was also observed at very low frequencies.

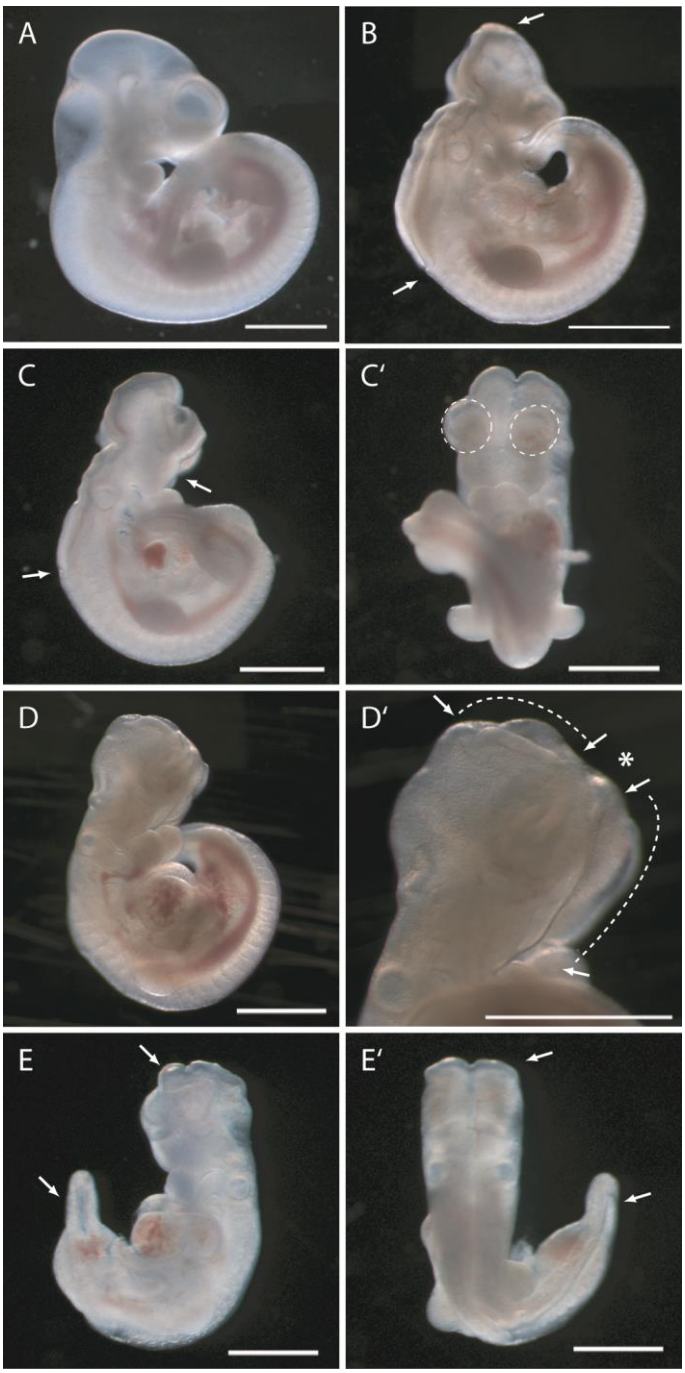

Figure 14. NTDs and craniofacial defects in E10.5 *Gldc^{GT2}* mutant embryos.

(A) *Gldc$^{+/+}$* embryos from a *Gldc$^{GT2/+}$* inter-cross appeared normal. The cranial NTDs in *Gldc$^{GT2/GT2}$* **(B, C, C')** and *Gldc$^{GT2/+}$* **(D, D', E, E')** embryos showed varying severity. In **(B)** the midbrain-hindbrain region was unfused. In (**C)** the entire cranial region was open, resulting in split face with underdeveloped maxillary processes (dashed-line circles) and truncated forebrain as observed in a frontal view **(C')**. Hindbrain fusion occurred in **(D)** but at higher magnification **(D')** the midbrain and anterior neuropore (dashed lines) were open on either sides of the closure 2 point (*). **(E)** Frontal view of a *Gldc$^{GT2/+}$* embryo displaying craniorachischisis, with a dorsal view of the same embryo shown in **(E')**. Arrows denote regions where the neural tube remained open. Scale bars: 1mm.

The incidence of NTDs in *Gldc*^{GT1} and *Gldc*^{GT2} mutants are reported in **Table 12** and **Table 13**, respectively. The specific stage of cranial neural tube closure may vary between mouse strains and mutations may also delay closure to a later somite stage. To account for possible delayed closure, NTDs in *Gldc*^{GT} mutants were defined as an open neural tube in embryos with 18 or more somites, as all wild-type littermates had completed cranial closure by the 17-somite stage.

Stage (E-)	No. of NTDs/ Total no. of embryos (% NTD)		
	Gldc$^{+/+}$	*Gldc*$^{GT1/+}$	*Gldc*$^{GT1/GT1}$
9.5 (≥18 somites)	0/45	0/76	11/38 (29%)
10.5	0/35	0/64	2/28 (7%)
11.5	0/30	2/94 (2.4%)	7/51 (13.7%)
12.5	0/1	0/5	0/3
13.5	0/1	0	0/3
15.5	0/28	0/31	6/26 (23%)
16.5	0	0/4	1/3 (33%)
18.5	0/12	0/27	4/15 (27%)
TOTAL	**0/152**	**2/301 (0.7%)**	**31/167 (18.6%)**

Table 12. Incidence of NTDs in embryos with the *Gldc*^{GT1} allele.

Stage (E-)	No. of NTDs/ Total no. of embryos (% NTD)		
	Gldc$^{+/+}$	*Gldc*$^{GT2/+}$	*Gldc*$^{GT2/GT2}$
9.5 (≥18 somites)	0/18	0/32	9/11 (82%)
10.5*	0/23	5[a]/59 (8.5%)	8[b]/14 (57%)
11.5*	0/14	2/32 (6.25%)	6/6 (100%)
13.5*	0/4	3/25 (12%)	3/8 (37.5)
14.5	0/3	0/9	3/7 (43%)
15.5	0/5	0/17	4/13 (31%)
16.5	0/2	0/3	2/3 (67%)
TOTAL	**0/69**	**10/177 (5.6%)**	**35/62 (56.5%)**

Table 13. Incidence of NTDs in embryos with the *Gldc*^{GT2} allele.

[a]3 exencephaly (EX) only, 1 EX with forebrain truncation, 1 craniorachischisis

[b]5 EX only, 3 EX with split face and/or forebrain truncation

*7 litters (56 embryos) at E10.5, E11.5, and E13.5 stages collected by Maria-Chiara Autuori

On average, NTDs occurred in 18.6% of *Gldc*$^{GT1/GT1}$ and 0.7% of *Gldc*$^{GT1/+}$ embryos (**Table 12**). There was a curious reduction in incidence of NTDs at E10.5 and E11.5 (7% and 13.7%, respectively) compared with other developmental stages, in which the lowest proportion of NTDs was 23%. This discrepancy is investigated in **Section 3.2.3.4.**

In the presence of the *Gldc*^{GT2} allele, NTD incidence was an average of 57% in *Gldc*$^{GT2/GT2}$ and 5.6% in *Gldc*$^{GT2/+}$ (**Table 13**). Craniorachischisis was also observed in two embryos, one E10.5 *Gldc*$^{GT2/+}$ embryo, and a 15-somite staged *Gldc*$^{GT2/GT2}$ embryo (not included in **Table 13** as the somite count is below 18). Out of the total number of exencephalic embryos in both heterozygous and homozygous embryos (n = 44), 4 embryos (9.1%) displayed split face and/or forebrain truncation. Also not represented in this table are two more occurrences of craniorachischisis and higher numbers of exencephaly coupled with split face and/or forebrain truncation which occurred during and after the period of fenbendazole exposure (see **Chapter 4** for details).

In humans, cranial NTDs are known to occur at a higher incidence in females (Juriloff and Harris, 2012b). This finding is also true in several NTD mice models, e.g. *Splotch*^{2H} (Burren et al., 2008). However, the NTDs in *Gldc*$^{GT1/GT1}$ embryos occurred in roughly the same proportion of males and females; no gender bias was observed (**Figure 15**).

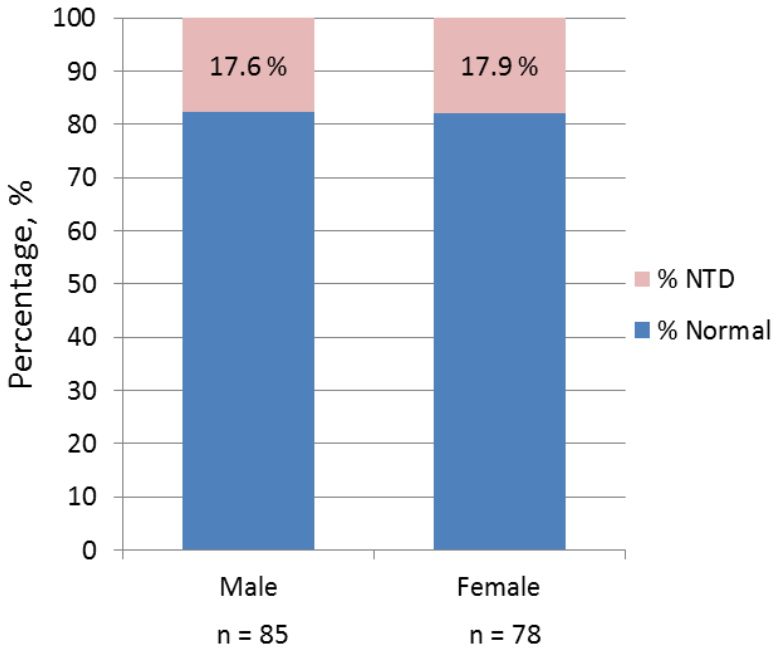

Figure 15. Sex of *Gldc*$^{GT1/GT1}$ embryos and occurrence of NTDs.

The incidence of NTDs in *Gldc*$^{GT1/GT1}$ embryos appeared the same in both males (17.6%) and females (17.9%) (Z-test, P = 0.877).

3.2.3.2. mRNA and protein expression levels during neurulation

To investigate the partial penetrance of NTDs in *Gldc*^{GT} embryos as well the difference in NTD incidence between the *Gldc*^{GT1} and *Gldc*^{GT2} alleles, mRNA expression levels were measured and assessed. *Gldc* mRNA levels in E9.5 and E10.5 embryos of both alleles were first quantified by qRT-PCR. For each experimental group (E9.5 and E10.5 of *Gldc*^{GT1} and *Gldc*^{GT2}), one wild-type was chosen as the reference sample, set to a Relative Quantitation value of "1" (corresponding to an expression level at 100%) to which other samples were normalised.

For the *Gldc*^{GT1} allele (**Figure 16A**), heterozygous embryos showed about 40-50% of wild-type *Gldc* mRNA levels. In homozygous embryos, this level was reduced to 10-30%. Homozygous embryos with NTDs showed 10–20% of wild-type levels.

For the *Gldc*^{GT2} allele (**Figure 16B**), a greater reduction in expression of wild-type mRNA was observed. With the exception of a few embryos, most heterozygotes showed 30% of wild-type mRNA levels, while most homozygotes showed no detectable *Gldc* mRNA at all. Most strikingly, *Gldc* mRNA was not detectable in heterozygous and homozygous embryos with NTDs for the *Gldc*^{GT2} allele; they were apparently nulls.

These findings suggest that the level of *Gldc* mRNA could partly explain the partial penetrance of NTDs in these embryos. A lower level of *Gldc* expression appeared to produce higher NTD incidence, as seen in the *Gldc*^{GT2} allele where all embryos displaying NTDs were nulls. Hence, all embryos with NTDs showed very little to no detectable *Gldc* mRNA (this is especially true for the *Gldc*^{GT2} allele), and there appears to be a correlation between mRNA levels and rate of NTDs. Heterozygotes had a larger spread of mRNA levels that typically fell between wild-type and homozygote values, and one heterozygous *Gldc*$^{GT2/+}$ mutant that presented with an NTD showed no detectable levels of mRNA.

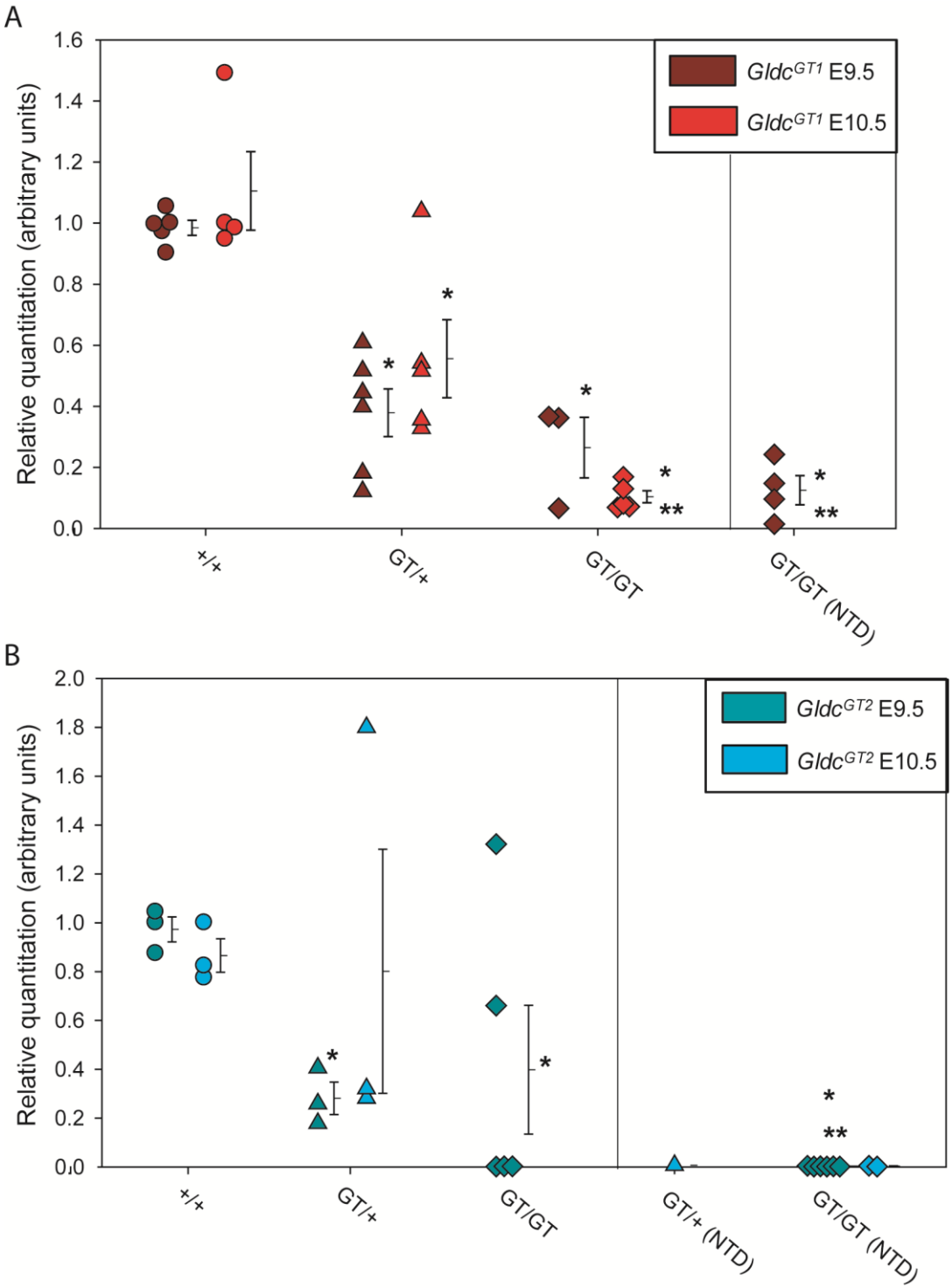

Figure 16. mRNA levels in E9.5 and E10.5 embryos of the *Gldc^{GT1}* and *Gldc^{GT2}* alleles.

(A) *Gldc$^{GT1/+}$* embryos showed 40–50% of wild-type mRNA levels, while *Gldc$^{GT1/GT1}$* embryos showed 20–30% expression. In homozygous mutants with NTDs, the level of expression was about 10–20%. **(B)** Most *Gldc$^{GT2/+}$* embryos showed 20–30% of wild-type mRNA levels, while most *Gldc$^{GT2/GT2}$* embryos showed no mRNA. *Gldc$^{GT2/+}$* and *Gldc$^{GT2/GT2}$* embryos with NTDs were complete nulls. (*) and (**) denote significant difference when compared with wild-type and heterozygotes, respectively. Error bars represent mean ± SEM (ANOVA, P<0.001).

3.2.3.3. Analysis of growth and development

Perturbation of the FOCM in other mouse models (e.g. *Splotch* and *curly tail*) via diet-induced folate deficiency has resulted in retardation of growth and development (Burren et al., 2008). As Gldc is an FOCM enzyme, $Gldc^{GT}$ mutant embryos were predicted to also show similar defects. The rate of growth and development of $Gldc^{GT}$ embryos were thus assessed by measuring crown rump length (CRL) and somite number (SN), respectively.

$Gldc^{GT1/+}$ embryos did not show any difference in CRL and SN from wild-type embryos (**Figure 17**). However, $Gldc^{GT1/GT1}$ embryos had significantly reduced CRL and SN at E9.5 and E10.5, indicating that they were growth and developmentally delayed. The same significant reduction in CRL and SN was seen in homozygous $Gldc^{GT2/GT2}$ embryos compared with wild-type and heterozygous embryos (**Figure 18**). In $Gldc^{GT2/GT2}$ embryos at E10.5, CRL values were reduced compared with wild-types and heterozygotes, but this difference was not significant (**Figure 18A**). The difference in SN values, however, was significant (**Figure 18B**). The CRL and SN of $Gldc^{GT2/+}$ embryos also showed non-significant reductions compared with wild-types.

To investigate whether there was a correlation between the extent of growth and developmental retardation and occurrence of NTDs, a second CRL graph was plotted that divided the E9.5 homozygous mutant groups into those with NTDs (affected) and without NTDs (normal) (**Figure 17A'** and **Figure 18A'**). All embryos with somite number below 18 were excluded as embryos at an earlier stage than that could not be reliably scored for an NTD. This plot demonstrates that normal mutants did have decreased CRL, thus growth retardation occurs in homozygous mutants but is not necessarily accompanied by an NTD. Interestingly, NTD-affected mutants carrying the $Gldc^{GT1}$ allele were more severely growth-retarded compared to unaffected $Gldc^{GT1}$ mutants (**Figure 17A'**). It must be noted, however, that this analysis risks introducing selection bias by excluding embryos that may be developmentally retarded to below 18 somites when compared with a wild-type littermate, thus possibly underestimating their rate of NTD.

When CRL values of $Gldc^{GT1}$ embryos were plotted against their respective SN values, no dissociation between rate of growth and rate of development was seen between different genotypes, as indicated by the overlapping regression lines in **Figure 19**. Thus, while homozygous embryos were smaller and less developed compared with wild-types, their sizes were appropriate to their developmental stages. Nonetheless, the mutants that exhibit NTDs tend to be growth and developmentally delayed, suggesting that developmental retardation may contribute to failure of closure.

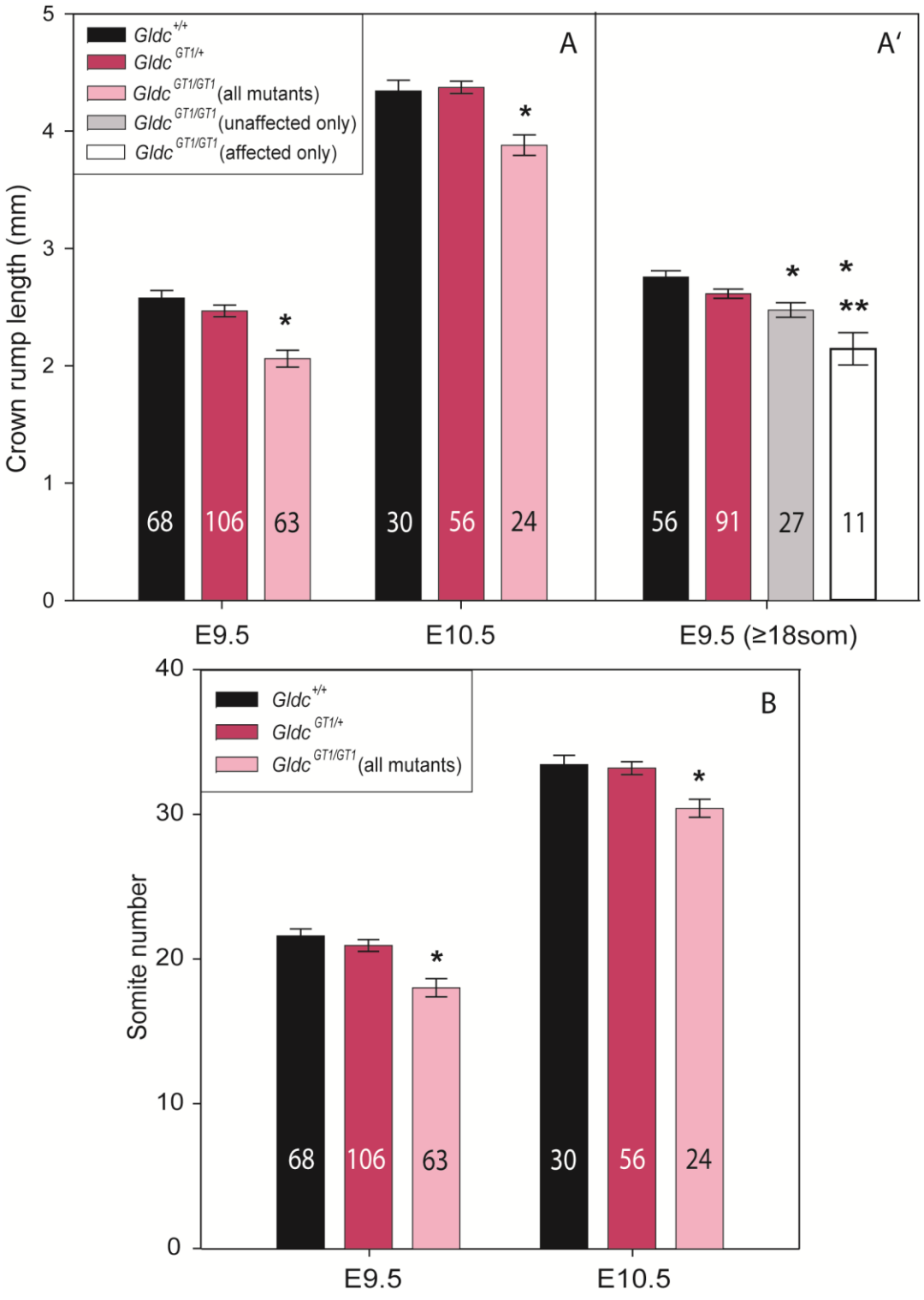

Figure 17. Crown rump length and somite number of *Gldc^{GT1}* embryos.

Gldc$^{GT1/GT1}$ embryos have significantly reduced crown rump length, CRL **(A)** and somite numbers **(B)** at E9.5 and E10.5, when compared with *Gldc$^{+/+}$* and *Gldc$^{GT1/+}$* (*). When E9.5 normal and affected *Gldc$^{GT1/GT1}$* embryos were analysed as separate groups **(A')**, the CRL of both groups showed significant reduction from *Gldc$^{+/+}$* (*), with the affected group showing further significant reductions compared with the unaffected mutant group (**). ANOVA, $P<0.001$. Sample sizes indicated in each bar, error bars represent mean ± SEM.

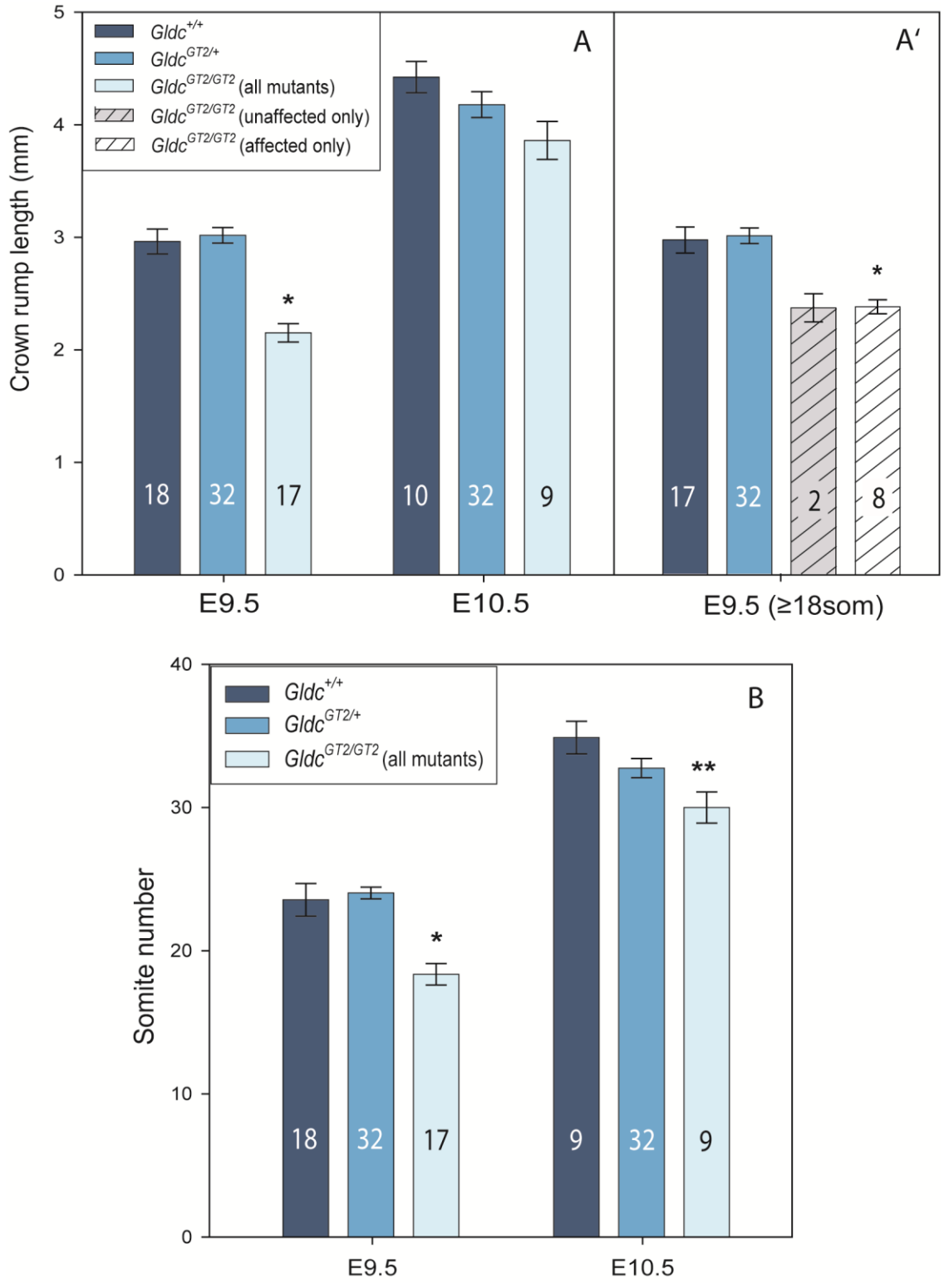

Figure 18. Crown rump length and somite number of *Gldc^{GT2}* embryos.

Gldc$^{GT2/GT2}$ embryos have significantly reduced crown rump length **(A)** and somite number **(B)** at E9.5 and E10.5, when compared with *Gldc$^{+/+}$*. When E9.5 unaffected and affected embryos were analysed separately, both showed similar reductions in CRL but the reduction was only significant in the affected group. ANOVA, *P<0.001, **P<0.05. Sample sizes indicated in each bar, error bars represent mean ± SEM.

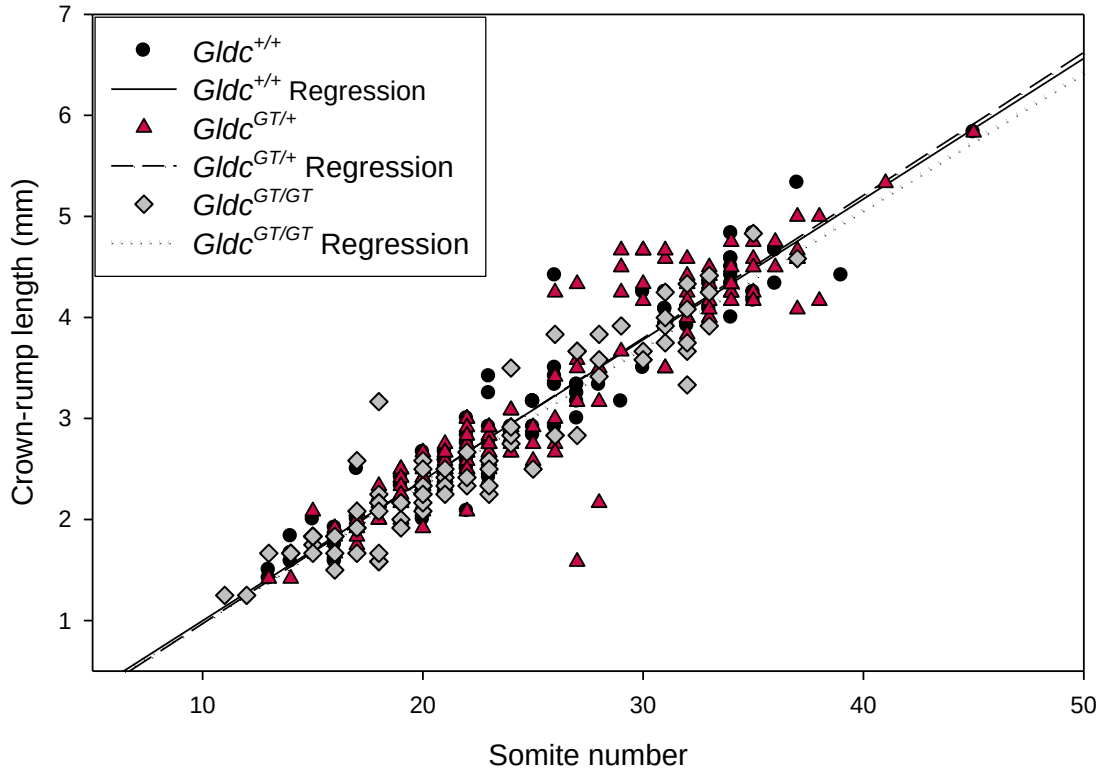

Figure 19. Regression curve of crown rump length versus somite number of *Gldc^{GT1}* embryos.

When crown rump length of E9.5 and E10.5 embryos with more than 12 somites (after axial rotation has occurred) was plotted against somite number, with the exception of a few outliers, no overall dissociation between rate of growth and rate of development was observed.

3.2.3.4. Unusual cranial phenotypes in *Gldc^{GT1}* mutants

Amongst E10.5 and E11.5 *Gldc^{GT1}* mutant embryos that did not show an open NTD, a small subset presented with a distorted cranial region and spots of haemorrhage (**Table 14**).

Stage (E-)	No. with unusual cranial phenotype/ Total no. of embryos		
	Gldc$^{+/+}$	*Gldc$^{GT1/+}$*	*Gldc$^{GT1/GT1}$*
9.5 (≥18 somites)	1/45 (2.2%)	2/76 (2.6%)	1/38 (2.6%)
10.5	1/35 (2.9%)	6/64 (9.4%)	6/28 (21.4%)
11.5	0/30	8/94 (8.5%)	3/51 (5.9%)
TOTAL	**2/110 (1.8%)**	**16/234 (6.8%)**	**10/117 (8.5%)**

Table 14. Incidence of unusual cranial phenotypes in *Gldc^{GT1}* embryos.

To examine this phenotype in more detail, 10 of these embryos were sectioned in the transverse (**Figure 20**) or coronal (**Figure 21**) planes and compared with respective wild-types.

Among embryos with abnormal cranial phenotypes that were sectioned, 9 had neuroepithelial layers that successfully elevated and apposed but had a small region that remained unfused (shown in **Figure 20E**, and **Figure 21E**, **K**, **R**). The hindbrain and forebrain cavities appeared "collapsed in" and the neuroepithelial layers were severely distorted (seen in **Figure 20E**, **H**, and **Figure 21E**, **F**, **H**, **I**, **K**, **L**, **N**, **O**, **Q**, **R**). In sections through the exencephalic embryo shown in **Figure 20C**, the neural folds in the hindbrain region were splayed open (**Figure 20F**, **I**, **L**). Interestingly, in 2 of these embryos with abnormal cranial region, the overlying surface ectoderm layer was found to be intact over the unfused neuroepithelial layer (shown in **Figure 21F**, **H**, **I**, **N**, **O**).

Another common finding in these embryos was the presence of haemorrhagic spots in the cranial region (7 out of 10). Curiously, clumps of nucleated cells that often stained intensely red with eosin, resembling juvenile red blood cells (RBCs), were present in the extracellular matrix between the surface ectoderm and neuroepithelium and in the adjacent mesoderm (seen in **Figure 20E**, **K**, and **Figure 21H**, **I**, **L**, **O**, **R**). In 1 out of the 10 embryos, the neuroepithelial layer appeared fused throughout but a thick layer of juvenile RBCs was found in between the surface ectoderm and neuroepithelium (**Figure 22**).

Figure 20. Transverse sections of *GldcGT1* embryos at E11.5.

A wild-type embryo **(A)**, a mutant with an abnormal cranial region **(B)**, and a mutant with an overt, visible NTD **(C)** were sectioned in the transverse plane as indicated by the dotted lines. **(D, G, J)** Sections through embryo **(A)** with the hindbrain (HB) and forebrain (FB) labelled. Regions boxed with dotted lines are shown in higher magnification in **(D', G', J')** and indicate the fused neuroepithelium (NE) and surface ectoderm (SE) layers. **(E, E', H, H', K, K')** Sections through embryo **(B)** show distorted hindbrain and forebrain, a region of unfused NE **(E'),** and clumps of cells that may be juvenile RBCs between the SE and NE layers (black arrows in **E'** and **K'**). **(F, I, L)** Sections through embryo **(C)** with hindbrain exencephaly (white arrow), showing neural folds splayed open (*) and distorted forebrain.

Scale bars: 1 mm for A-C; 0.5 mm for D-L. Sections were stained with H&E.

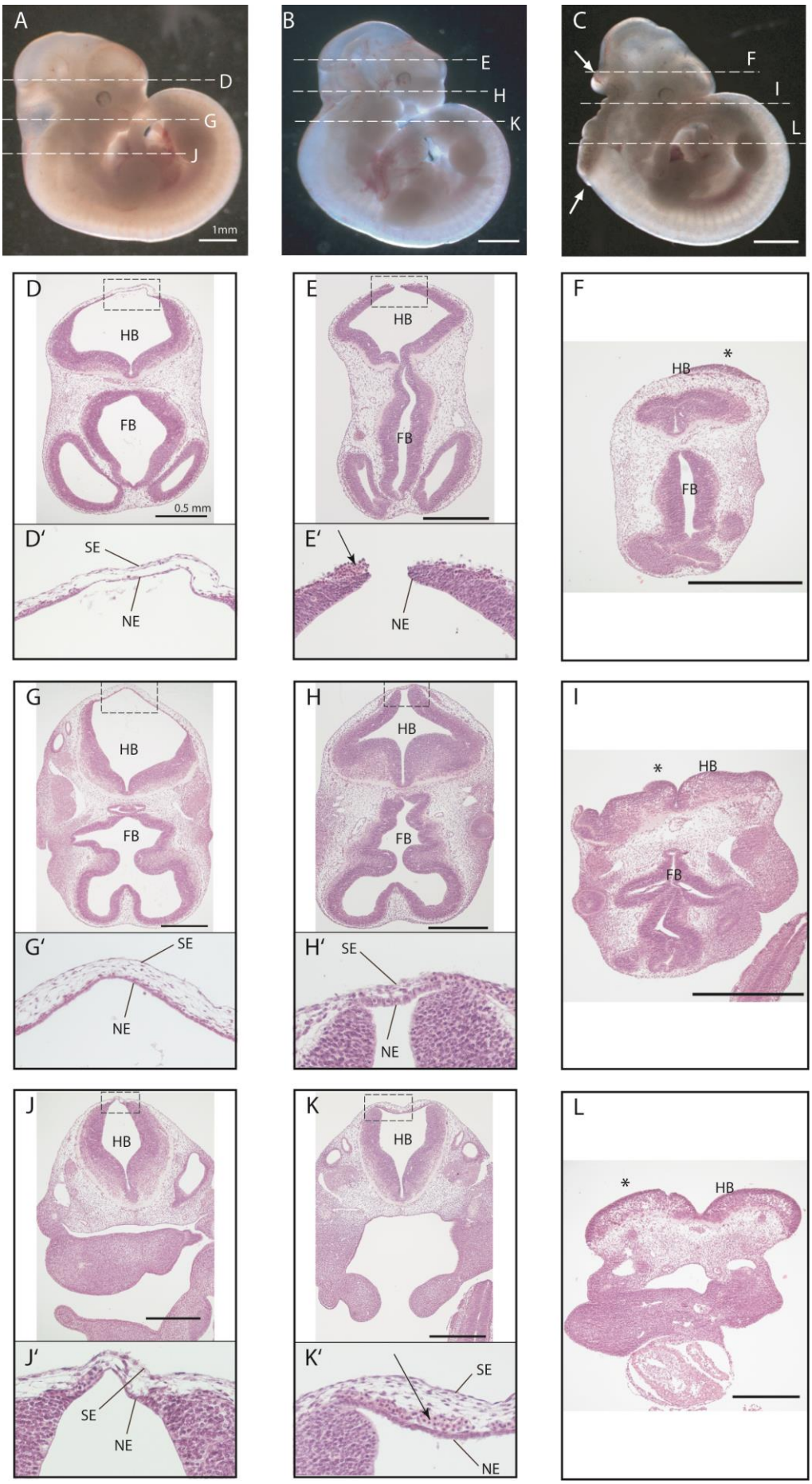

Figure 20. Transverse sections of *Gldc*^{GT1} embryos at E11.5.

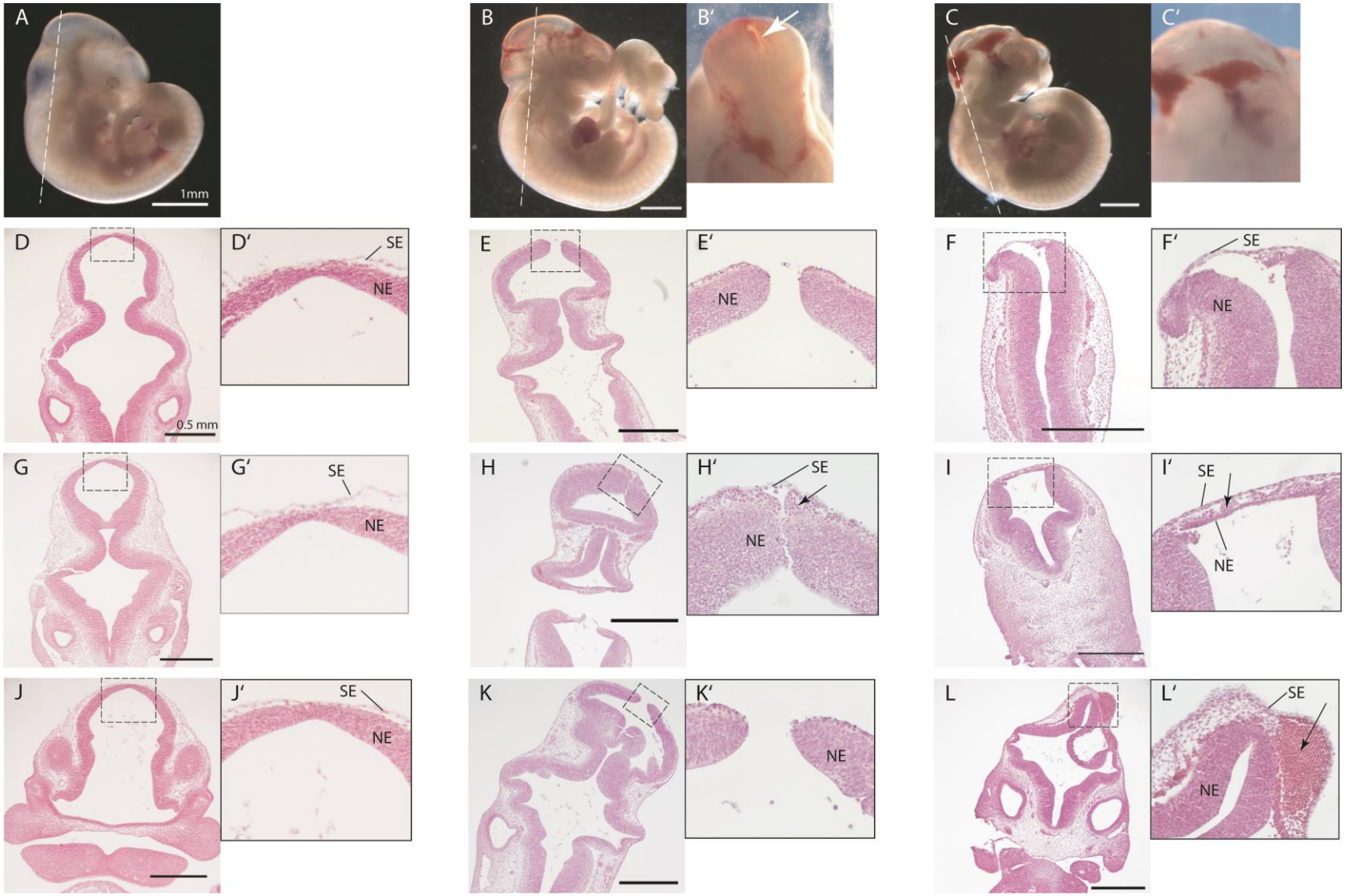
A
1mm
B
B′
C
C′
D
D′
SE
NE
0.5 mm
E
E′
NE
F
F′
SE
NE
G
G′
SE
NE
H
H′
SE
NE
I
I′
SE
NE
J
J′
SE
NE
K
K′
NE
L
L′
SE
NE

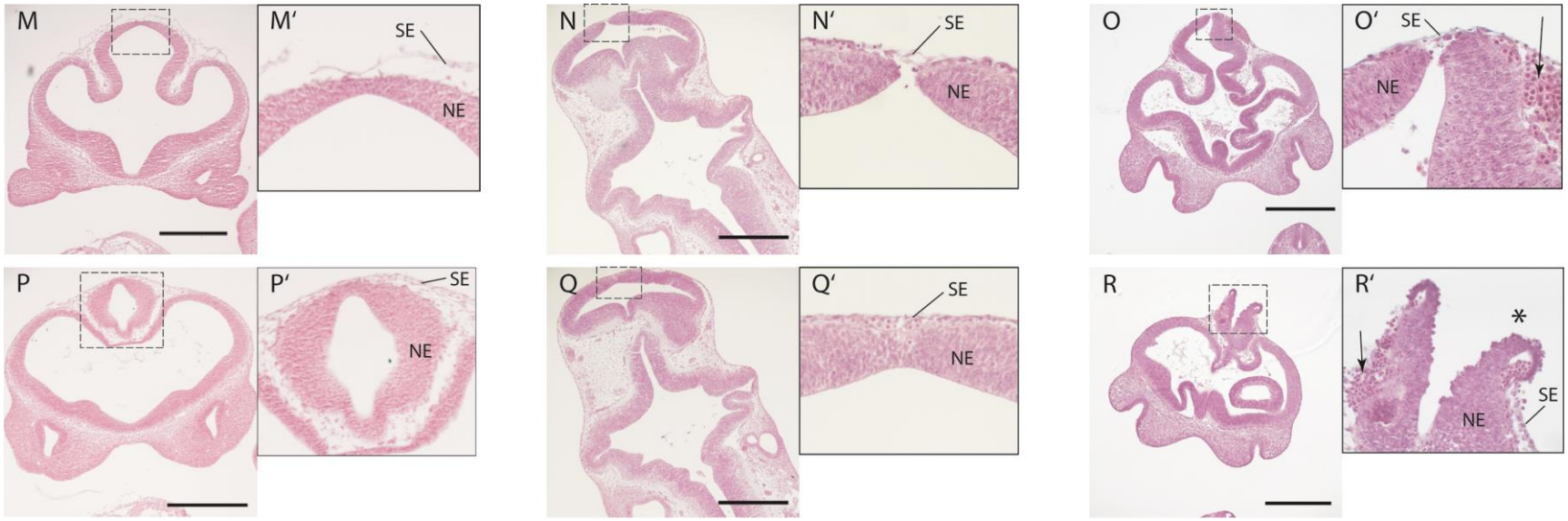

Figure 21. Coronal sections of *Gldc*^{GT1} embryos at E10.5–E11.5.

A wild-type embryo **(A)** and mutants with abnormal cranial phenotype **(B, C)** sectioned in the coronal plane as indicated by the dotted lines. White arrow indicates a visible opening in the midbrain of embryo **(B')**. **(D, G, J, M, P)** Sections through embryo **(A)**, showing normal neural tube morphology with boxed regions shown in higher magnification on the right **(D', G', J', M', P')**. **(E, E', H, H', K, K', N, N', Q, Q')** Sections through embryo **(B)**, showing unfused neuroepithelium (NE) with the overlying surface ectoderm (SE) intact in some regions (**H', N'**) and not in others (**E', K'**). **(F, F', I, I', L, L', O, O', R, R')** Sections through embryo **(C)**, showing unfused NE underneath an intact SE (**F', I', O'**). Cells resembling juvenile RBCs (black arrows in **H'**, **I'**, **L'**, **O'**, **R'**) were found in regions corresponding to the haemorrhage, frequently between the NE and SE layers and surrounding mesoderm.

Scale bars: 1 mm for A-C; 0.5 mm for D-R. Sections were stained with H&E.

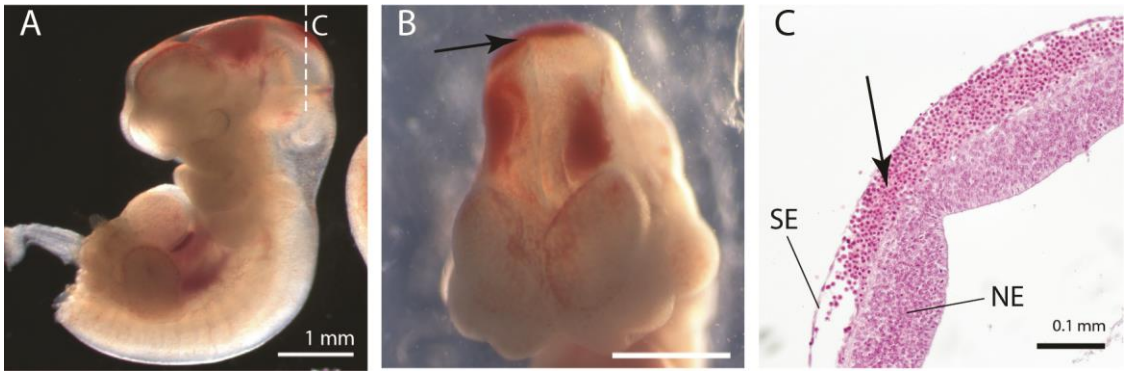

Figure 22. E10.5 *Gldc*^{GT1} embryo showing cranial haemorrhage.

A homozygous mutant embryo showing distorted cranial region viewed from the left **(A)** and dorsally **(B)**. **(C)** Coronal section through the region indicated by the dotted line in **(A)**, showing presence of juvenile RBCs in the extracellular matrix between the surface ectoderm (SE) and neuroepithelium (NE) that corresponds to the spots of haemorrhage (black arrows).

The distorted cranial phenotype appeared in both heterozygous and homozygous *Gldc* mutants carrying either the *Gldc*^{GT1} or *Gldc*^{GT2} alleles. To investigate whether the unfused neuroepithelium of these embryos ultimately fuses or if they fail in closure and become persistent exencephaly, the incidence of NTDs was compared with and without the addition of these embryos with the *Gldc*^{GT1} allele. The developmental stages were grouped into three groups to allow comparison and statistical analysis: at E9.5 (before onset of the distorted cranial phenotype), E10.5–E11.5 (when the phenotype is present), and E15.5–E18.5 (when any exencephaly present would be obvious and unambiguous).

The incidence of NTDs in *Gldc*$^{GT1/GT1}$ embryos at E10.5–E11.5 was significantly lower than at E9.5, while the incidence at E15.5–E18.5 is comparable to E9.5 (**Table 15**). When embryos with the cranial phenotype were added to the numbers of NTDs, the incidence at E10.5–E11.5 increased to levels that are not significantly different from E9.5 or E15.5–E18.5.

Stage (E-)	No. of NTDs/ Total no. of embryos (%)			No. of NTDs and cranial phenotype/ Total no. of embryos (%)		
	Gldc$^{+/+}$	*Gldc*$^{GT1/+}$	*Gldc*$^{GT1/GT1}$	*Gldc*$^{+/+}$	*Gldc*$^{GT1/+}$	*Gldc*$^{GT1/GT1}$
9.5 (≥18 somites)	0/45	0/76	11/38 (29%)	1/45 (2.2%)	2/76 (2.6%)	12/38 (31.6%)
10.5–11.5	0/65	2/158 (1.3%)	9/79 **(11.4%)***	1/65 (1.3%)	16/158 (10.1%)	18/79 (22.8%)
15.5–18.5	0/40	0/62	11/44 (25%)	0/40	0/62	13/44 (29.5%)

Table 15. Incidence of NTDs with and without inclusion of the unusual cranial phenotype in the *Gldc*^{GT1} allele.

Asterisk (*) denotes significant difference in NTD incidence compared with E9.5 embryos within the same genotype group (Z-test, $p<0.05$).

3.2.3.5. Additional developmental phenotypes in *Gldc*^{GT2} mutants

In addition to NTDs, a proportion of *Gldc*^{GT2} mutant embryos collected at stages E14.5–E16.5 also exhibited eye defects and non-cranial haemorrhage (**Table 16**).

Defect	No. with defects/ Total no. of embryos (E14.5–E16.5)		
	Gldc$^{+/+}$	*Gldc*$^{GT2/+}$	*Gldc*$^{GT2/GT2}$
Eye	0/10	1/29 (3.4%)	7/23 (30.4%)
Haemorrhage	0/10	2/29 (6.9%)	2/23 (8.7%)

Table 16. Incidence of eye defects and haemorrhage in *Gldc*^{GT2} mutant embryos.

The eye defects tended to be unilateral and resembled anophthalmia/ microphthalmia (**Figure 23B**, **B'**, **C**, **C'**), although this was not confirmed by histological examination. They were present in 3.4% of *Gldc*$^{GT2/+}$ and 30.4% of *Gldc*$^{GT2/GT2}$ embryos collected at E14.5 to E16.5. The microphthalmia-like eye defect was also observed in *Gldc*$^{GT1/+}$;*Gldc*$^{GT2/+}$ compound heterozygotes collected by Maria-Chiara Autuori. Non-cranial haemorrhage was present in very small numbers: 2 out of 29 of *Gldc*$^{GT2/+}$ and 2 out of 23 of *Gldc*$^{GT2/GT2}$ embryos collected at E14.5 to E16.5 (**Figure 23D**, **D'**, **E**, **E'**). In 2 of the 4 embryos reported here, it appeared in one or both of the fore or hind limb buds. Eye defects and non-cranial haemorrhage at these stages of development have not been observed in embryos carrying the *Gldc*^{GT1} allele.

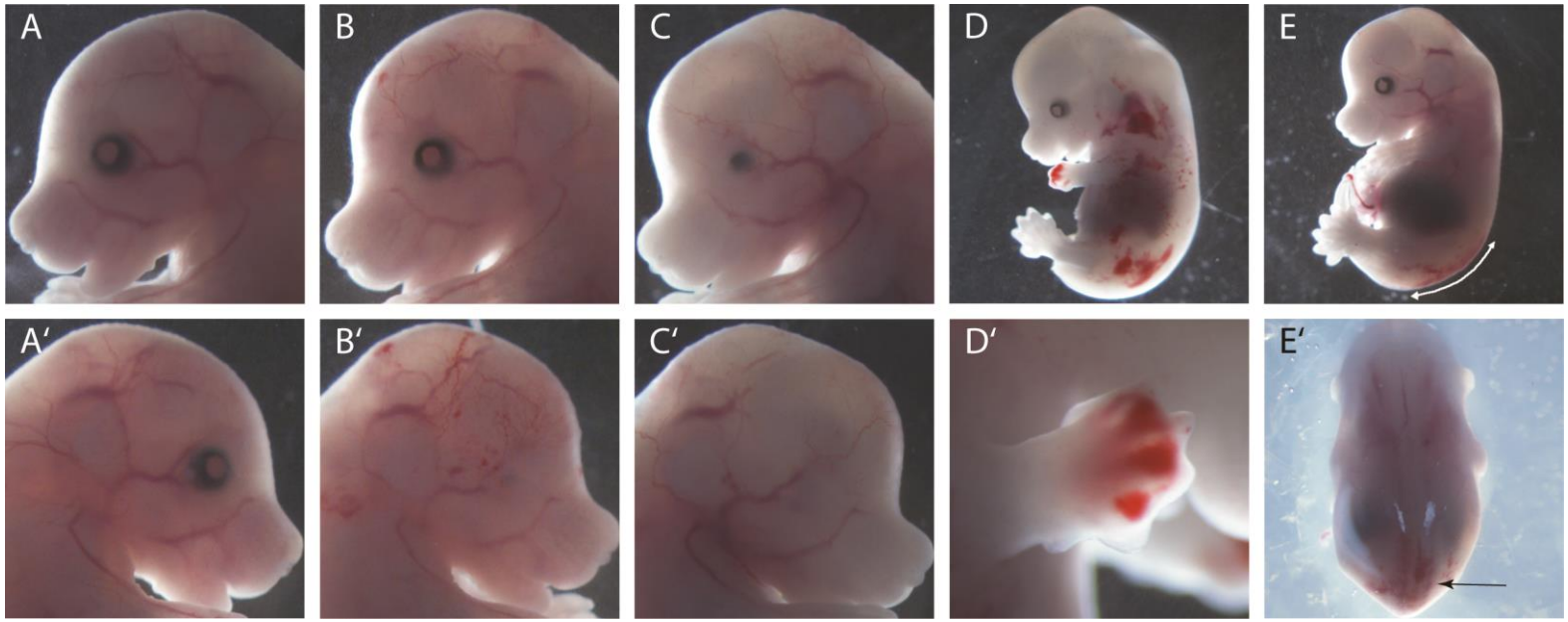

Figure 23. Eye defects and haemorrhage in *Gldc*^{GT2} mutant embryos.

(A, A') Normal left and right eye of a wild-type littermate. **(B, B')** Unilateral eye defect in a *Gldc*$^{GT2/GT2}$ embryo showing a normal left eye and a degenerated right eye. **(C, C')** *Gldc*$^{GT2/GT2}$ embryo with a degenerated left eye and no apparent right eye. **(D)** *Gldc*$^{GT2/+}$ embryo showing superficial haemorrhage on the trunk. **(D')** Close-up of right forelimb bud of embryo **(D)**, showing underdeveloped digits and haemorrhage. **(E)** Sagittal and **(E')** dorsal view of a *Gldc*$^{GT2/GT2}$ embryo with mild haemorrhage in the lower trunk along the spine (white and black arrows point to same region).

3.3. Discussion

3.3.1. *Gldc* is required for neural tube closure

The severe *Amt* null mouse (Narisawa et al., 2012) and mild GCS models (Oda et al., 2007, Kojima-ishii et al., 2008) from previous studies appear to represent two extremes of phenotypic severity in GCS deficiency. This thesis describes the $Gldc^{GT1}$ and $Gldc^{GT2}$ models with a more "intermediate" severity.

As evident from *in situ* studies, the spatial and temporal pattern of *Gldc* mRNA expression in early embryonic development corresponds to the most commonly observed phenotype in $Gldc^{GT1}$ and $Gldc^{GT2}$ mutants, i.e. NTDs. While expression of *Gldc* is strong along the entire length of the neural tube at E8.5 and E9.5 and at all steps of neurulation (open neural folds, the recently closed neural tube, and intact neural tube), the type of NTD displayed is predominantly exencephaly with craniorachischisis only occurring in the presence of the more deleterious $Gldc^{GT2}$ allele. This corresponds to observations made in the *Amt* knockout, suggesting that cranial neural folds are more sensitive to the cellular consequences that result from a loss of GCS activity.

Among other NTD mouse models, the cranial neural tube also appears especially sensitive to mutations in genes involved in, or influencing, neuroepithelial cell proliferation e.g. *Nup50* (Smitherman et al., 2000), apoptosis e.g. *Casp9* (Kuida et al., 1998), and actin cytoskeletal regulation e.g. *n-cofilin* (Gurniak et al., 2005). From the expression studies, *Gldc* mRNA is also strongly expressed in other highly proliferative (and apoptotic) tissue during neurulation-stages of development, such as the gut endoderm, branchial arches, optic and otic vesicles, and limb buds. The growth and developmental delay observed at E9.5 and E10.5 in both $Gldc^{GT1}$ and $Gldc^{GT2}$ homozygous mutants are also indicative of an overall proliferation defect. Eye defects were also observed in $Gldc^{GT2}$ mutants, correlating with the presence of *Gldc* mRNA in the optic vesicles, but eye development appears to be less sensitive to perturbations in *Gldc* function as defects were only precipitated by the stronger knockdown conferred by the $Gldc^{GT2}$ allele. It is possible that subtle defects in other tissue are also present but have not yet been characterised.

The next chapter, **Chapter 4,** investigates FOCM disturbances and the possibility of a proliferation defect in *Gldc* mutants leading to NTDs in this model.

3.3.2. Partial penetrance of NTDs in *Gldc* mutants

Unlike the 87% NTD rate reported in *Amt* null embryos (Narisawa et al., 2012), the *Gldc* mutants in this study showed considerably lower penetrance of NTDs despite both genes encoding for an enzyme in the GCS. Furthermore, despite carrying a mutation in the same gene, the penetrance of NTDs in $Gldc^{GT1}$ and $Gldc^{GT2}$ mutants are also different.

The $Gldc^{GT1}$ allele in homozygosity still retains low levels of *Gldc* mRNA transcription, owing to splicing around the gene-trap vector. This results in residual levels of enzymatic activity only just above the detection limit of the assay (as measured in adult mutant mice, **Figure 10C**), which indicates that very low levels of enzymatic activity is still capable of allowing normal neurulation to proceed in about 80% of homozygous mutants (post-natal phenotype evaluation of $Gldc^{GT1}$ mutants is described in **Chapter 5**). The significantly lower levels of mRNA in NTD-affected compared with apparently normal homozygous $Gldc^{GT1/GT1}$ mutants support this hypothesis.

In heterozygous adult mice liver, a 50% loss of *Gldc* mRNA still confers the same functional capacity for cleaving glycine as wild-type mice, as evident from their comparable levels of Gldc enzymatic activity. This corresponds to the mostly normal phenotype of heterozygous $Gldc^{GT1/+}$ embryos and mice, and the fact that non-ketotic hyperglycinemia (NKH) does not manifest in human heterozygous carriers of a mutated *GLDC* allele. When level of mRNA knockdown is higher, as produced by the $Gldc^{GT2}$ allele, the incidence of NTDs also increased in homozygous as well as heterozygous mutants, but not to the degree of the *Amt* null model.

Viewed collectively, this suggests that mRNA expression levels could go some ways in accounting for the partial penetrance of a particular GCS model, with decreasing levels of *Gldc* mRNA conferring higher risk of NTDs (**Table 17** below). Although not detected by qRT-PCR, it is possible that a very low level of *Gldc* mRNA is produced in $Gldc^{GT2/GT2}$ embryos due to incomplete gene-trap activity, whereas the *Amt* allele may be truly null. Alternatively, there may be an effect of variation in genetic background or environmental conditions in the *Amt* mice (generated in a different laboratory) compared with *Gldc*-deficient mice.

However, mRNA expression alone does not predict which individual embryo will fail neural tube closure as there are homozygous $Gldc^{GT1/GT1}$ mutant embryos with comparable levels of mRNA as NTD-affected mutants, but which appeared to complete neural tube closure normally. In addition, some null $Gldc^{GT2/GT2}$ mutants also successfully completed closure. As enzymatic activity was not measured in neurulation-staged embryos, it would be interesting to determine whether NTD incidence also correlates with enzymatic activity

of the GCS. If enzymatic activity does not distinguish between normal and NTD-affected mutants, then other factors, possibly cellular or tissue morphogenetic changes affected by the *Gldc* mutation, might introduce a certain degree of "randomness" to influence the final phenotype. Partial penetrance of NTDs within mouse strains that are congenic occurs with many gene mutants.

Allele and genotype	Percentage mRNA level (%)	NTD incidence (%)
+/+	100	0
$Gldc^{GT1/+}$	40 – 50	1
$Gldc^{GT2/+}$	20 – 30	6
$Gldc^{GT1/GT1}$	10 – 20	20
$Gldc^{GT2/GT2}$	0	> 56

Table 17. Percentage mRNA level and NTD incidence in $Gldc^{GT1}$ and $Gldc^{GT2}$ embryos. mRNA levels were normalised to their respective wild-types.

Chapter 6 will further discuss a similar relationship between the level of GCS enzymatic activity and the NKH disease spectrum based on case reports from the literature.

3.3.3. Forebrain defects in $Gldc^{GT2}$ mutants

In addition to failure of hindbrain neural tube closure, $Gldc^{GT2}$ mutants also present with additional and more severe cranial phenotypes. Exencephaly in $Gldc^{GT2}$ was sometimes accompanied by split face and/or forebrain truncation, with more frequent occurrences during and after treatment with the anti-helminthic drug, fenbendazole (see **Chapter 4**).

The forebrain truncation seen in some exencephalic $Gldc^{GT2}$ mutants are reminiscent of mouse mutants for genes required in forebrain patterning, such as *Six3* null embryos which lack a rostral forebrain (Lagutin et al., 2003). Forebrain patterning begins very early in development from the stage of neural induction, requiring signals from the anterior visceral endoderm (AVE), gastrula organizers, and axial mesendoderm coupled with inhibition of the Wnt/β-catenin, BMP and TGFβ signalling pathways. Graded levels of Wnt activity are required for posterior-to-anterior specification, while rostral forebrain specification requires inhibition of caudalising signals. Mutations in genes involved in AVE development and BMP or Wnt antagonism often result in forebrain truncations (Andoniadou and Martinez-Barbera, 2013, Lagutin et al., 2003, Lavado et al., 2008).

Craniofacial defects can also result from neural crest cell (NCC) defects. NCCs are a transient population of cells that are induced in the dorsal neural tube, undergo epithelial to mesenchymal transition, delaminate, and migrate away around a similar developmental temporal window as neurulation. They differentiate to give rise to a wide variety of cell types including bone and cartilage, melanocytes, smooth muscle cells, and neurons and glia of the peripheral and enteric nervous system (Sauka-Spengler and Bronner-Fraser, 2008). Much of the cartilage, bone, and connective tissue that develop from the frontonasal, maxilla, and mandibular processes of the vertebrate head derive from cranial (mid- and hindbrain) NCC populations. Cranial NCCs originating from the mid-diencephalon and anterior mesencephalon give rise to the frontal and premaxillary bones of the upper jaw, while posterior mesencephalic NCCs contribute to the maxillary bone of the upper jaw, dentary bone of the lower jaw, and the first branchial arch (Santagati and Rijli, 2003, Le Douarin et al., 2007). Unlike the spinal region where migration occurs after completion of closure, cranial NCC migration occurs prior to neural tube closure and has been proposed to play an important role in cranial neurulation from observations in several exencephalic mice models that also exhibit cranial NCC defects, such as *Cited2* and *Pax3* (Copp, 2005).

Gldc is not known to be involved in any signalling pathways that affect embryonic patterning or suspected of neural crest cell involvement. However, this cannot yet be excluded. Alternatively, its involvement in folate metabolism may influence proliferation or apoptosis of cell populations in the forebrain and midbrain that effect head development. Further investigation with forebrain markers such as *Hesx1*, *Six3*, *Bf1*, and *Fgf8* and NCC markers such as *Sox9*, *Twist1*, and *Foxd3*, are required to better define the forebrain defect and presence/absence of the telencephalon and NCC populations in $Gldc^{GT2}$ mutants.

It can be argued that the forebrain truncation in $Gldc^{GT2}$ mutants are often accompanied by split face resulting from failure of forebrain and midbrain neural tube closure, and that is responsible for an apparent forebrain truncation. In the chick, ablation of cranial NCCs result in exencephaly and missing forebrain, midbrain, and facial structures (Creuzet et al., 2006), but the abundance of exencephalic mouse mutants not accompanied by NCC defects is evidence that neural tube closure in mice is not needed for NCC migration and function. Fore- and midbrain exencephaly resulting in a split face phenotype also occurs in the *Grhl2* loss-of-function model but without truncation of the forebrain and a clearly distinguishable telencephalon (Brouns et al., 2011), suggesting that forebrain truncation is not a consequence of a split face phenotype.

3.3.4. Hypotheses for the unusual cranial phenotype

The non-NTD, unusual cranial phenotypes characterised in E10.5 and E11.5 *Gldc*^{GT1} mutants (**Figure 20**, **Figure 21**, **Figure 22**) are a novel finding in NTD mouse models. They are not likely due to a reopening of an initially closed neural tube as NTD rates at E9.5 are comparable to the rates recorded at E15.5-E18.5. The histological appearance of these embryos indicates that neural tube closure progressed to median hinge point formation at the hindbrain neuropore. The neural folds were able to appose each other at the midline but ultimately do not adhere and fuse. This persistent opening could result in a loss of pressure from the fluid which normally fills a closed neural tube cavity pushing against the neuroepithelial walls. Thus, the hindbrain cavity appears "collapsed" and the neuroepithelium become severely distorted. Continuous distortion and degeneration from exposure to amniotic fluid might cause the lesion size to increase and result in a more typical exencephalic appearance in later stages. The appearance of an intact surface ectoderm overlying the small openings in the neural folds suggests that the surface ectoderm does not play a passive role in the normal closure process and may functionally contribute to closure, at least in the hindbrain region, and/or that a "wound healing" like process may occur over small open lesions in the neural tube. Nevertheless, the apparent transition of these "closed" lesions to exencephaly at later stages suggests that the surface ectoderm alone is insufficient to maintain closure.

A recurring feature of this phenotype is the presence of clumps of cells resembling juvenile RBCs in between the neuroepithelium and overlying surface ectoderm layer (**Figure 21** and **Figure 22**). This could hint at a potential vascular defect and/or abnormal assembly of the extracellular matrix (ECM) between the two epithelial layers. In addition, localised haemorrhage was also present in some *Gldc*^{GT2} mutant embryos, observed at E14.5-E16.5 (**Figure 23**).

During vasculogenesis at E7.5, signals from the visceral endoderm induce the mesoderm to form blood islands, consisting of primitive endothelial cells and erythroblasts, in the yolk sac. As angiogenesis progresses through embryonic development, many signalling pathways such as the VEGF, TGF, Notch, and Wnt interact with ECM proteins such as angiopoietin 1, fibronectin, and integrins, and axon guidance signals such as Eph-ephrins, semaphorins, and Roundabout (ROBO) receptors to regulate endothelial cell proliferation and remodelling (Bohnsack and Hirschi, 2004, Herbert and Stainier, 2011).

Defects in vascular development can result in localised haemorrhaging and oedema in the mouse. For example, some mouse models with vascular defects such as *Vezf1* nulls, *Sox18/Vegfd* double knockouts, and p120-catenin nulls are hypervascularised or have

disorganised vasculature and display subcutaneous haemorrhaging. In *Vezf1* nulls, lesions are present in the endothelial vessel walls that cause RBCs to leak into surrounding mesenchyme and connective tissue, producing localised spots of haemorrhage in the cranial and jugular region (Kuhnert et al., 2005). The superficial appearance of this haemorrhagic phenotype is not unlike the cranial haemorrhage observed in $Gldc^{GT1}$ mutant embryos and the haemorrhage in $Gldc^{GT2}$ mutants at E14.5-16.5. Further investigation is needed to determine if a vascular defect is present in *Gldc* mice or if the cranial haemorrhage is secondary to neural tube distortion. There is also insufficient data to suggest whether the blood cells near the tips of the neural folds are a cause or consequence of failure of closure.

4. Investigating a possible role of abnormal folate metabolism in *Gldc*-deficient neural tube defects

4.1. Introduction

The glycine cleavage system (GCS), in its role as predominant pathway for glycine catabolism, is intrinsically linked to glycine synthesis and other uses of glycine. One would assume that under healthy physiological conditions glycine cleavage would be closely balanced with synthesis and metabolic demand. In addition, the action of cleaving glycine plays a major role in providing one-carbon (1C) units for folate one-carbon metabolism (FOCM). However, glycine through GCS is by no means the only 1C donor available. Serine, for example, is another major 1C donor and could theoretically compensate for the lack of glycine-derived 1C units. The GCS contributes to the mitochondrial 1C pool and while mitochondrial FOCM has a key function in producing formate to be utilised in cytoplasmic FOCM reactions, formate can also be made elsewhere.

Thus, the lack of GCS activity could potentially disrupt the balance of each of the synthetic and catabolic pathways alluded to above. This chapter investigates the biochemical consequences of the loss-of-function of *Gldc* and examines its contribution to NTDs, beginning with a description of the various sources of mitochondrial-derived 1C units and extra-mitochondrial formate.

4.1.1. Mitochondrial-derived 1C units

Mitochondrial-derived 1C units exit the mitochondria as formate and can be derived from a variety of sources, including glycine, serine, choline/ betaine/ dimethylglycine/ sarcosine, threonine and hydroxyproline/ glyoxylate (**Figure 24**).

Glycine is the smallest amino acid consisting of two carbon units. Isotope tracer studies of glycine revealed that the C4, C5 and N7 atoms of purines are contributed by glycine. In fact, glycine can contribute to *de novo* synthesis of purines in two ways; by providing the C4, C5, and N7 backbone in the initial step, and by contributing to the 10-formyl-THF-derived C2 and C8 atoms of the purine double-ring via GCS (Kikuchi et al., 2008, Fan et al., 2014). In addition to use in protein synthesis and providing 1-carbon units for folate

metabolism and nucleotide synthesis, another major physiological role of glycine is as an inhibitory neurotransmitter in the brain stem, spinal cord and retina, and as an excitatory co-agonist of the NMDA receptor alongside glutamate (Johnson and Ascher, 1987). Glycine is primarily synthesized from serine, another major 1C donor, through SHMT (Stover, 2004, Fan et al., 2014). It can also be synthesized from choline, threonine, or hydroxyproline (Wang et al., 2013).

While choline, betaine, and sarcosine can be obtained through dietary means, the latter two are also synthesised *de novo* from choline catabolism which occurs primarily in the mitochondria of hepatic cells and produces glycine as an end product (Hoffmann et al., 2013, Craig, 2004). Conversion of choline to glycine occurs through the actions of four demethylating enzymes. First, choline dehydrogenase (CHDH) converts choline to betaine (also known as trimethylglycine and glycine betaine). This is followed by betaine-homocysteine-methyltransferase (BHMT) converting betaine to dimethylglycine, which is then converted to sarcosine (also known as *N*-methylglycine) by dimethylglycine dehydrogenase (DMGDH). Finally, sarcosine dehydrogenase (SARDH) produces glycine, which is cleaved by the GCS. The action of DMGDH and SARDH also releases 1C units which can combine with THF in the mitochondria (Tibbetts and Appling, 2010). Betaine, through the action of BHMT, also serves as an alternative 1C donor to the methylation cycle (in place of 5-methyl-THF) through remethylation of homocysteine to methionine (Christensen et al., 2015).

Glycine can be synthesised from threonine through threonine dehydrogenase (TDH) and glycine C-acetyltransferase (GCAT; also known as aminoacetone synthase) (Wang et al., 2011, Aoyama and Motokawa, 1981, Tressel et al., 1986). Mouse ES cells uniquely utilise threonine as their major 1C source through the action of TDH, and are able to proliferate faster than cancer cell lines. TDH is localized in the mitochondria, and threonine-derived glycine then feeds into the similarly mitochondria-localized GCS (Wang et al., 2011). *GCAT* along with *GLDC*, *SHMT1*, and serine synthesis genes (*PSPH* and *PSAT1*) were found to be upregulated in human lung cancer cells and were hypothesised to be fuelling tumourigenesis (Zhang et al., 2012).

Wang et al. (2013) also highlighted another pathway for glycine synthesis from glyoxylate through the irreversible action of alanine:glyoxylate aminotransferase (AGT), which comprises the final step of hydroxyproline catabolism in the mitochondria of kidney cells. This pathway has been suggested as a potentially significant source of glycine, leading also to increased serine production in rat kidneys (Lowry et al., 1985a, Lowry et al., 1985b).

Serine is a significant 1C donor that is catabolised to glycine by SHMT or to pyruvate by serine dehydratase. It is assumed that in most vertebrates the former reaction (via SHMT) is the predominant pathway, especially in uricotelic animals such as chickens which do not have serine dehydratase (Kikuchi et al., 2008). Through SHMT, serine donates one of its carbon atoms to THF to form methyl-THF, producing glycine in the process. The SHMT enzyme has two isozymes: cytoplasmic (SHMT1) and mitochondrial (SHMT2) (Garrow et al., 1993, Anderson and Stover, 2009). Serine-to-glycine conversion via SHMT occurs readily, accounting for 40% of glycine flux in the whole body, while glycine-to-serine conversion accounts for about 46% of serine synthesis rate in healthy men and women (Lamers et al., 2007).

The *de novo* L-serine biosynthesis pathway involves 3-phosphoglycerate dehydrogenase (PHGDH) which converts 3-phosphoglycerate (3PG), an intermediate in glycolysis, into phospho-hydroxypyruvate, followed by conversion to serine by phosphoserine aminotransferase 1 (PSAT1) and phosphoserine phosphatase (PSPH) (Possemato et al., 2011). Tracer studies showed that in cancer cells serine is preferentially shunted by increased PHGDH activity into the FOCM, away from glycolysis and other serine metabolic pathways (such as serine hydratase) (Snell et al., 1987, Possemato et al., 2011, Locasale, 2013). Like glycine, D-serine is also a strong agonist of the glycine-binding site of NMDA receptors (Henneberger et al., 2013).

The action of the MTHFD1L enzyme converting 10-formyl-THF to THF produces formate in the mitochondria, which goes into the cytosol.

Figure 24. *De novo* sources of one-carbon units for folate one-carbon metabolism.

Sources of 1C units through *de novo* synthesis of glycine and/or serine that occur primarily in the mitochondria are grouped within the **beige-shaded area**. Glycine can be derived from serine-glycine interconversion, hydroxyproline (through glyoxylate), threonine, and choline catabolism. Serine is biosynthesised from 3PG (intermediate of glycolysis), and releases 1C units when converted to glycine by SHMT1 or SHMT2. Catabolism of dimethylglycine and sarcosine by DMGDH and SARDH also releases 1C units.

The pathway in the **grey-shaded area** illustrates breakdown of methanol, producing formate which enters the one-carbon cycle to be further metabolised.

Reactions in the **yellow-shaded area** illustrate various other non-mitochondrial, non-folate-dependant, metabolic pathways that yield formate which may potentially enter the one-carbon cycle (dotted-line arrow). This includes tryptophan degradation via the kynurenine pathway, alpha-oxidation of phytanic acid, conversion of lanosterol to cholesterol, and of androstenedione to oestrogen. Formate is alternatively converted to water and carbon dioxide through the action of catalase.

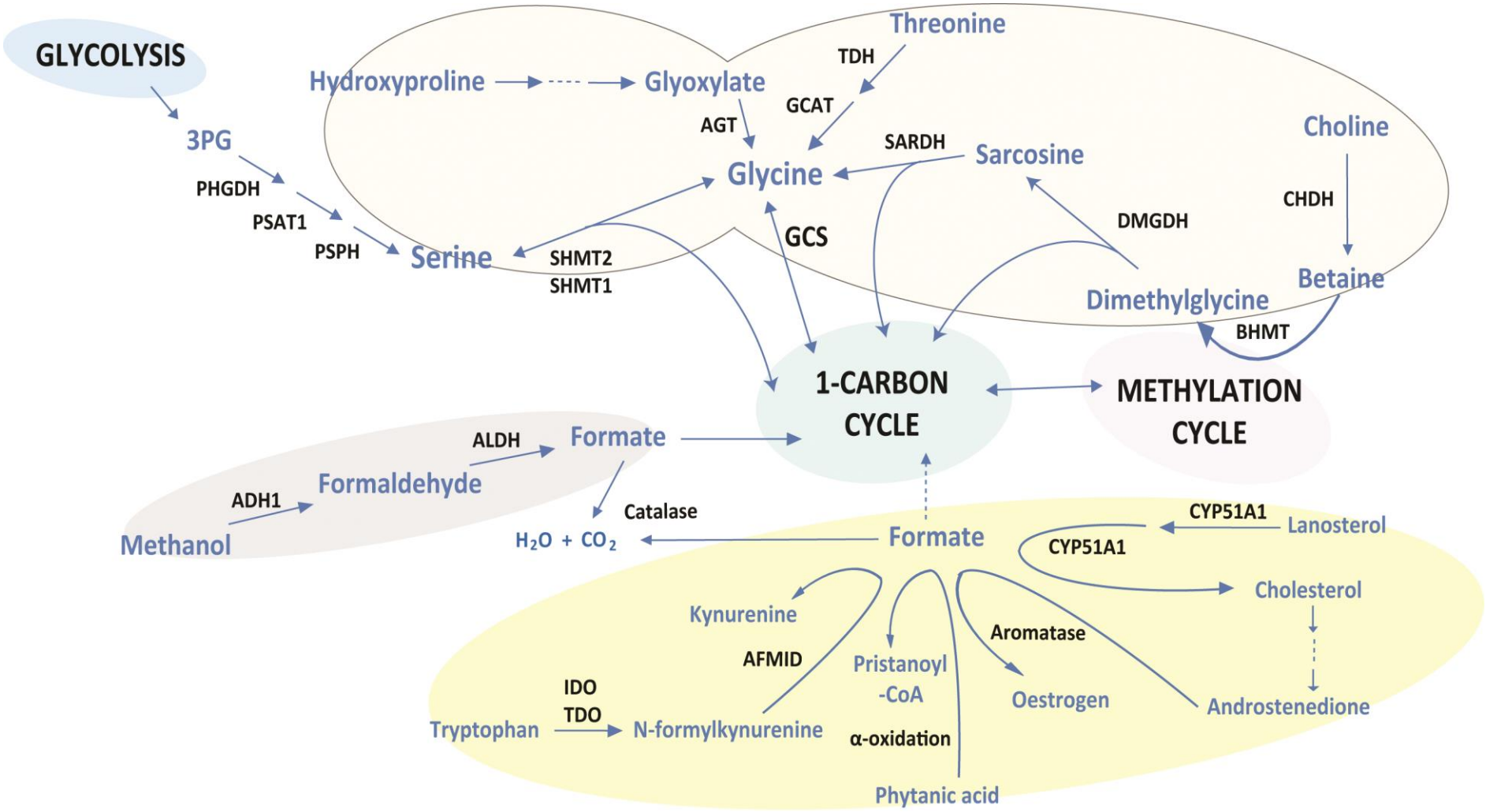

Figure 24. ***De novo*** **sources of one-carbon units for folate one-carbon metabolism.**

4.1.2. Alternative sources of formate

In addition to mitochondrial sources, formate can also be produced via several non-mitochondrial, non-folate-dependant pathways (**Figure 24**) (Lamarre et al., 2013).

In the cytosol, breakdown of methanol comprise two steps, the first of which converts methanol to formaldehyde. This step requires the action of alcohol dehydrogenase 1 (ADH1) in humans and peroxisomal catalase in rodents, or may act though action of catalase and hydroxyl radicals in microsomes (Cederbaum and Qureshi, 1982). The second step involves aldehyde dehydrogenase (ALDH), which yields formic acid as an end product. Methanol metabolism is extensively studied in the context of methanol poisoning, in which the occurrence of acute metabolic acidosis is attributed to accumulation of formic acid (Tephly, 1991, Hansen et al., 2005).

Tryptophan degradation through the kynurenine pathway in the cytosol involves conversion of tryptophan to *N*-formylkynurenine through the action of indoleamine 2,3-dioxygenase (IDO) and tryptophan 2,3-dioxygenase (TDO). *N*-formylkynurenine is then converted by kynurenine formamidase (also known as arylformamidase, AFMID) to kynurenine, a reaction which also yields formic acid (Schwarcz et al., 2012, Han et al., 2012).

Alpha-oxidation of phytanic acid, a branched-chain fatty acid, occurs in peroxisomes and involves a carbon-carbon cleavage, producing pristanoyl-CoA. Another yield of this cleavage is formate (Poulos et al., 1993, Croes et al., 1996, Verhoeven and Jakobs, 2001).

In the cholesterol synthesis pathway, lanosterol is converted to cholesterol through three cytochrome mono-oxygenation steps by lanosterol 14α-demethylase (CYP51A1), a member of the cytochrome P450 family, in endoplasmic reticulum (ER). The first reaction yields an alcohol product, the second reaction an aldehyde, and the final step releases formic acid (Debeljak et al., 2003, Lepesheva and Waterman, 2007). Cholesterol then enters synthesis pathways of steroid molecules, in which conversion of androstenedione to oestrogen by the aromatase complex (another cytochrome P450 family member) in smooth ER of placental cells also yields formate (Akhtar et al., 1982).

Formate gets metabolised either by combining with THF and entering FOCM, or by being oxidised by catalase into water and carbon dioxide in the presence of hydrogen peroxide (Siu et al., 2013). What the contributions of non-mitochondrial derived formate are to total body formate, or as 1C donors to FOCM reactions (as opposed to being metabolised by catalase), is not well defined.

4.2. Results

4.2.1. *Gldc* mutation increases glycine levels and disrupts FOCM

4.2.1.1. Glycine levels in *Gldc* mutant embryos

A biochemical hallmark of mutations in the GCS, as evident in NKH patients, is highly elevated glycine in body fluids. High glycine is often quoted as the cause of the pathology of NKH. As homozygous mutations in GCS genes have not been picked up in NTD patients (as anencephalic cases are fatal, NKH would not manifest and thus any possible GCS mutations would not be suspected), it remains unknown if high glycine by itself can cause NTDs. To what magnitude the increase in glycine levels is at early embryonic development is also unknown.

The $Gldc^{GT1}$ mouse provides a model with which to investigate these questions. Embryos from heterozygous crosses were collected at E11.5, a day after neurulation is complete, and whole embryo preparations done for measurement of glycine as well as other amino acids using ion-exchange chromatography (carried out by Helen Prunty and Dr Simon Heales, Great Ormond Street Hospital for Children NHS Foundation Trust).

Table 18 lists the levels of all detectable amino acids. At such early embryonic stages, $Gldc^{GT1/GT1}$ embryos showed a highly significant, 3-fold increase ($P<0.001$) in glycine levels compared with $Gldc^{+/+}$ embryos. The increase in glycine levels of $Gldc^{GT1/+}$ embryos compared with wild-types was also highly significant. The only other amino acid to show a significant increase (with $P<0.05$) in mutants compared with wild-types is taurine. This is the earliest stage of development where significant elevation of glycine due to a GCS mutation is demonstrated, suggesting that whatever pathological effects glycine may have on brain development may already be in effect from just after neurulation.

Amino acid	Concentration (nmol/mg protein)		
	Gldc$^{+/+}$ (n=6)	*Gldc*$^{GT1/+}$ (n=6)	*Gldc*$^{GT1/GT1}$(n=7)
Alanine (ALA)	54.0 ± 5.54	68.2 ± 3.55	63.3 ± 7.29
Asparagine (ASN)	8.78 ± 0.99	10.2 ± 0.43	8.96 ± 1.01
Aspartic acid (ASP)	8.63 ± 0.85	11.2 ± 1.44	11.8 ± 2.12
Glutamine (GLN)	22.2 ± 1.85	26.0 ± 2.54	21.2 ± 2.77
L-glutamate (GLT)	63.1 ± 5.83	75.5 ± 4.32	71.3 ± 7.30
Glycine (GLY)	22.6 ± 2.33	**38.8 ± 2.73***	**66.7 ± 7.00***
Histidine (HIS)	4.03 ± 0.49	4.49 ± 0.22	4.06 ± 0.33
Leucine (LEU)	8.00 ± 0.97	10.2 ± 0.59	9.39 ± 0.98
Isoleucine (ILEU)	2.50 ± 0.33	3.43 ± 0.35	2.95 ± 0.39
Lysine (LYS)	14.5 ± 1.31	17.5 ± 0.57	16.5 ± 1.66
Methionine (MET)	2.69 ± 0.21	3.51 ± 0.29	3.05 ± 0.34
Ornithine (ORN)	2.72 ± 0.39	3.13 ± 0.29	2.80 ± 0.35
Phenylalanine (PHE)	3.61 ± 0.44	4.57 ± 0.22	3.91 ± 0.38
Serine (SER)	16.1 ± 1.61	21.5 ± 1.72	17.0 ± 2.18
Taurine (TAU)	66.1 ± 4.57	75.8 ± 3.71	**90.6 ± 6.75****
Threonine (THR)	8.45 ± 1.23	11.6 ± 1.01	10.6 ± 1.31
Tryptophan (TRY)	1.13 ± 0.25	1.17 ± 0.11	1.11 ± 0.12
Tyrosine (TYR)	3.16 ± 0.34	3.94 ± 0.21	3.75 ± 0.37
Valine (VAL)	7.98 ± 0.81	9.54 ± 0.53	8.80 ± 0.88

Table 18. Concentration of amino acids in whole *Gldc*^{GT1} embryos.

Values quoted are mean ± SEM, */** denotes significant difference compared with wild-types (ANOVA, *P<0.001, **P<0.05).

4.2.1.2. *In silico* modelling of the effects of defective GLDC on folate cycling

The second metabolic defect that may occur when glycine is not catabolised is disruption of FOCM due to glycine's role as a 1C donor. The effects of not having glycine contribution on folate cycling and downstream pathways have been implicated but not characterised by experiments prior to this study.

A mathematical model of intracellular hepatic folate metabolism (One-Carbon Metabolism Version 2.1), developed by Nijhout et al. (2006), was first used to make an *in silico* prediction of how the balance of folates might shift in response to defective glycine cleavage. This model is an extension of a previous model (Reed et al., 2006) to include mitochondrial components of FOCM, which was itself a combined model of previously published folate and methionine cycles (Nijhout et al., 2004, Reed et al., 2004, Prudova et al., 2005). The software utilises kinetic formulae and rate constants of cytosolic and mitochondrial folate enzymes to model levels of folate metabolites, utilising published experimentally observed values from a variety of human and rodent hepatic tissue and cell lines. The model was then tested by simulating specific mutations and disease conditions with known changes in FOCM parameters, for example the *MTHFR* 677C>T polymorphism, B12 deficiency, folate deficiency, combined B12 deficiency with folate deficiency or elevated folate levels, methionine loading, and effect of betaine on homocysteine. Changes predicted by the model were reported to be comparable to those observed in human populations and experimental rodents (Reed et al., 2006, Nijhout et al., 2006).

When a perturbation is introduced to the model's "normal" steady-state values, it computes the resulting changes in concentrations (μM) and velocities (μM/hr) of folate metabolites and enzymes as well as total cellular and blood concentrations of several amino acids. When the velocity of GLDC (abbreviated as mitochondrial GDC in the model) was changed from the model's steady-state value of 1,664 μM/hr to 0 μM/hr (from 0 to -100% change) to mimic the loss of GLDC enzymatic activity (shown as screenshots of the software in **Figure 25**), the model predicts a 150-fold increase in total cellular glycine from 1,203 to 179,215 μM, and a more modest 20-fold increase in blood glycine concentration from 221 to 4,092 μM. The increase in glycine levels matches observational evidence in NKH patients where GLDC activity is completely null, albeit to much exaggerated levels in the model.

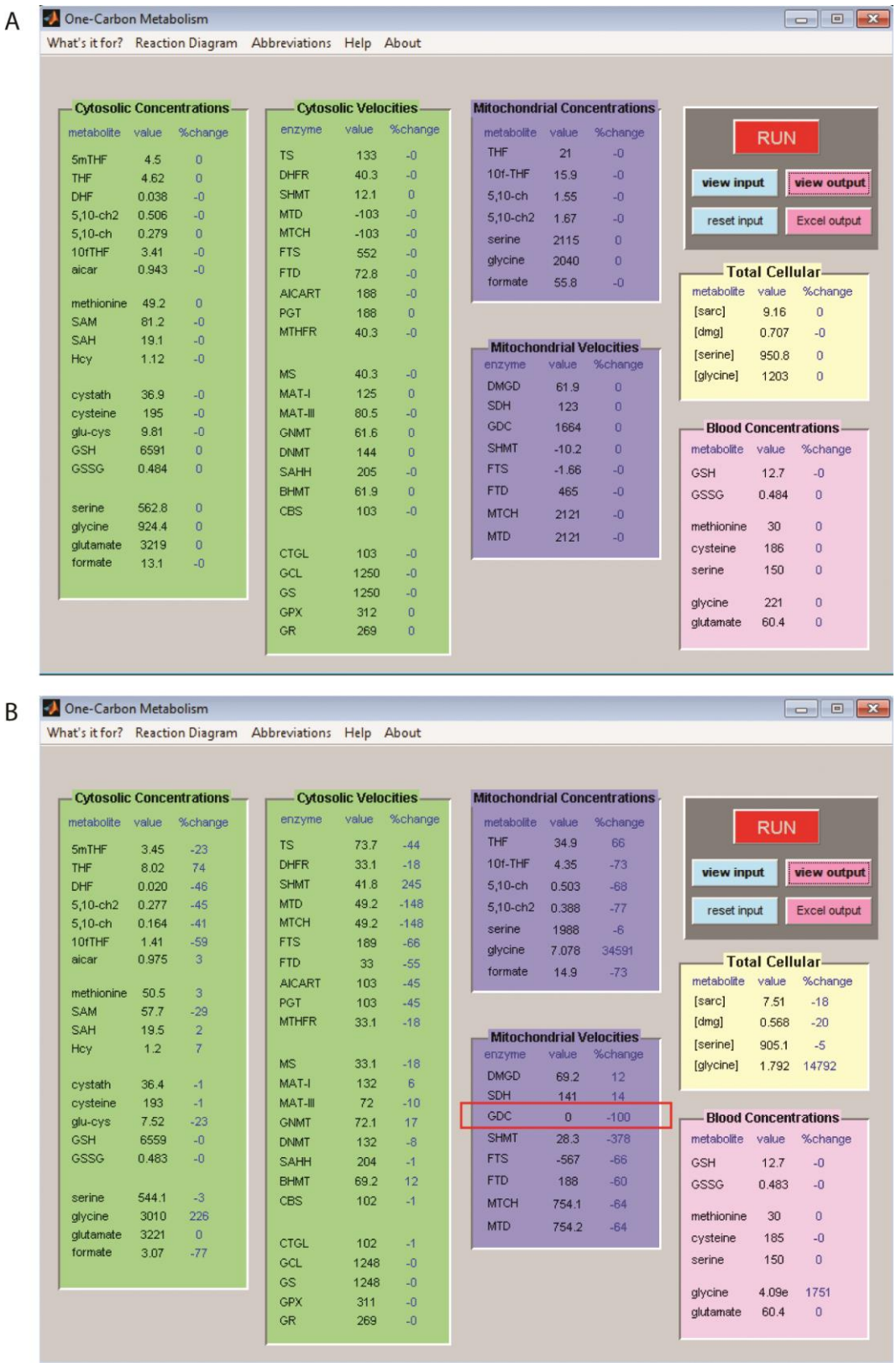

Figure 25. One-Carbon Metabolism mathematical modelling software

(A) Normal, steady-state values of substrate concentrations and enzyme velocities, with GDC at a default velocity of 1,664 μM/hr. **(B)** Changes in concentrations and velocities when GDC is set to 0%, i.e. enzyme velocity of 0 μM/hr (indicated in red box).

Figure 26 illustrates changes in folate metabolites of a 50% and 100% deficiency in GCS compared with normal values, plotted as percentage total folate (values combined cytosolic and mitochondrial fractions). In the 100%-GCS deficient profile, there was an increase in proportion of THF and corresponding decrease in 5-methyl-THF, 5,10-methenyl-THF, 5,10-methylene-THF, and 10-formyl-THF. The predicted changes are that of decrease in 1C-carrying folates and increase in a non-1C-carrying folate. The 50%-GCS deficient profile showed intermediate levels between normal and 100% deficiency, though appeared to more closely resemble 100% deficiency values.

Thus, the key comparisons to experimentally observe for would be the relative changes in proportion of 1C and non-IC carrying folates between wild-type and mutant embryos, and whether addressing this change is sufficient to correct the overall folate profiles and consequently rescue the phenotype. This is addressed in the following sections by using a mass spectrometry technique (**Section 4.2.1.3**) and dietary supplementation with a 1C source (**Section 4.2.2.1**), respectively.

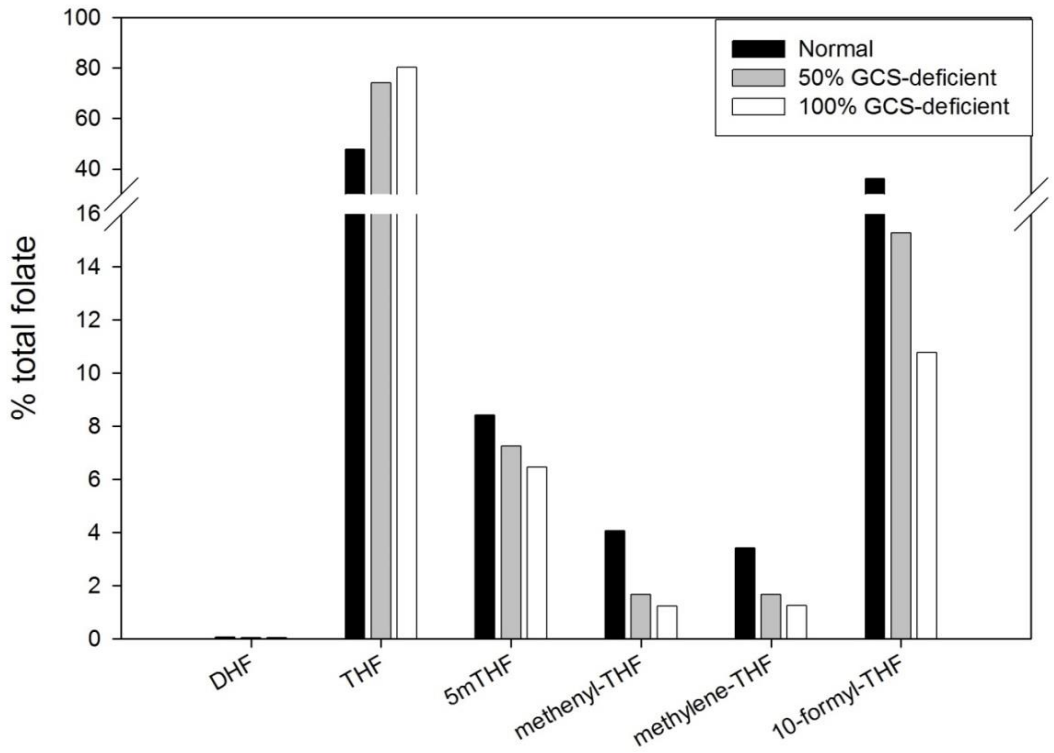

Figure 26. *In silico* prediction of hepatic folate profiles in normal and GCS-deficient conditions.

In 100%-GCS deficient conditions (GDC activity set to 0%), the relative abundance of hepatic folates was predicted to show an increase in THF and decrease in 5-methyl-THF, 5,10-methenyl-THF, 5,10-methylene-THF, and 10-formyl-THF. 50%-GCS deficient conditions was predicted to show intermediary levels between normal and 100%-GCS deficient.

4.2.1.3. Abnormal folate profiles in *Gldc* mutant embryos

To test the predictions of the *in silico* experiment, E11.5 $Gldc^{GT1}$ embryos were collected and prepared for folate profiling using a liquid chromatography, tandem mass-spectrometry (LC/MS/MS) method developed in the Copp and Greene lab (performed by Dr Kit-Yi Leung). This developmental stage was chosen as it is the earliest post-neurulation stage at which the LC/MS/MS technique is able to reproducibly quantify seven glutamated forms of six folate metabolites in single embryos (Pai et al., 2015). The levels of individual polyglutamated forms were summated as one measurement for each folate.

Figure 27 illustrates changes in the folate profiles of the three genotypes of $Gldc^{GT1}$ embryos, expressed as percentage total folate. Unlike the *in silico* model in which the highest proportion of total folates consist of THF followed by 10-formyl-THF, 5-methyl-THF, 5,10-methenyl-THF, 5,10-methylene-THF, and barely detectable levels of DHF, results from the LC/MS/MS measurements showed that the highest proportion of total folates consist of 5-methyl-THF, followed by THF and DHF, and levels of 5,10-methenyl-THF, 5,10-methylene-THF and 10-formyl-THF that are only just above detection limit. The discrepancy could partly be due to a biological difference in proportion of folate metabolites between adult liver (on which the *in silico* model is based) and whole embryo samples.

Nevertheless, when comparing $Gldc^{GT1/GT1}$ with $Gldc^{+/+}$ samples, the changes observed agreed with that of the *in silico* modelling: significant increase was found in relative abundance of the non-1C-carriers DHF and THF, and significant decrease in 1C-carrier 5-methyl-THF. The folate profiles in $Gldc^{GT1/+}$ were comparable with that of the wild-types, indicating that one allele of functioning *Gldc* is sufficient to produce a normal balance of folates. This finding is in agreement with results in **Chapter 3** showing that $Gldc^{GT1/+}$ adult mice showed levels of enzymatic activity that did not differ significantly from $Gldc^{+/+}$ mice.

In wild-type conditions, mitochondrial-derived 1C units enter the cytoplasm as formate and combine with THF to make 10-formyl-THF. 5,10-methylene-THF then loses a 1C unit by conversion to 5-methyl-THF or to dTMP synthesis (thus making DHF, a non-1C-carrying folate, in the process). The abnormal folate profiles displayed by $Gldc^{GT1/GT1}$ embryos indicate that defective glycine cleavage is causing a decrease in 1C units to enter the folate cycle, resulting in a build-up of THF (and consequently DHF) as well as decrease in 1C-carrying folates, of which only changes in 5-methyl-THF levels were detectable by the assay.

Figure 27. *Gldc*^{GT1} mutant embryos show altered folate profiles.

Folate profiling by LC/MS/MS revealed significant increases in relative abundance of **(A)** dihydrofolate (DHF) and **(B)** tetrahydrofolate (THF) and significant decrease in **(C)** 5-methyl-THF of E11.5 *Gldc*$^{GT1/GT1}$ mutants (n = 10) compared with wild-types (n = 7), while *Gldc*$^{GT1/+}$ embryos (n = 8) showed levels comparable to wild-types, which matches the changes predicted in the *in silico* modelling. In addition, there was a significant increase in levels of **(D)** 5,10-methenyl-THF in *Gldc*$^{GT1/+}$ embryos compared with wild-types. No significant changes were found in the relative abundance of **(E)** 5,10-methylene-THF or **(F)** 10-formyl-THF in the mutants compared with wild-types (*ANOVA, $p<0.001$). Error bars represent mean ± SEM.

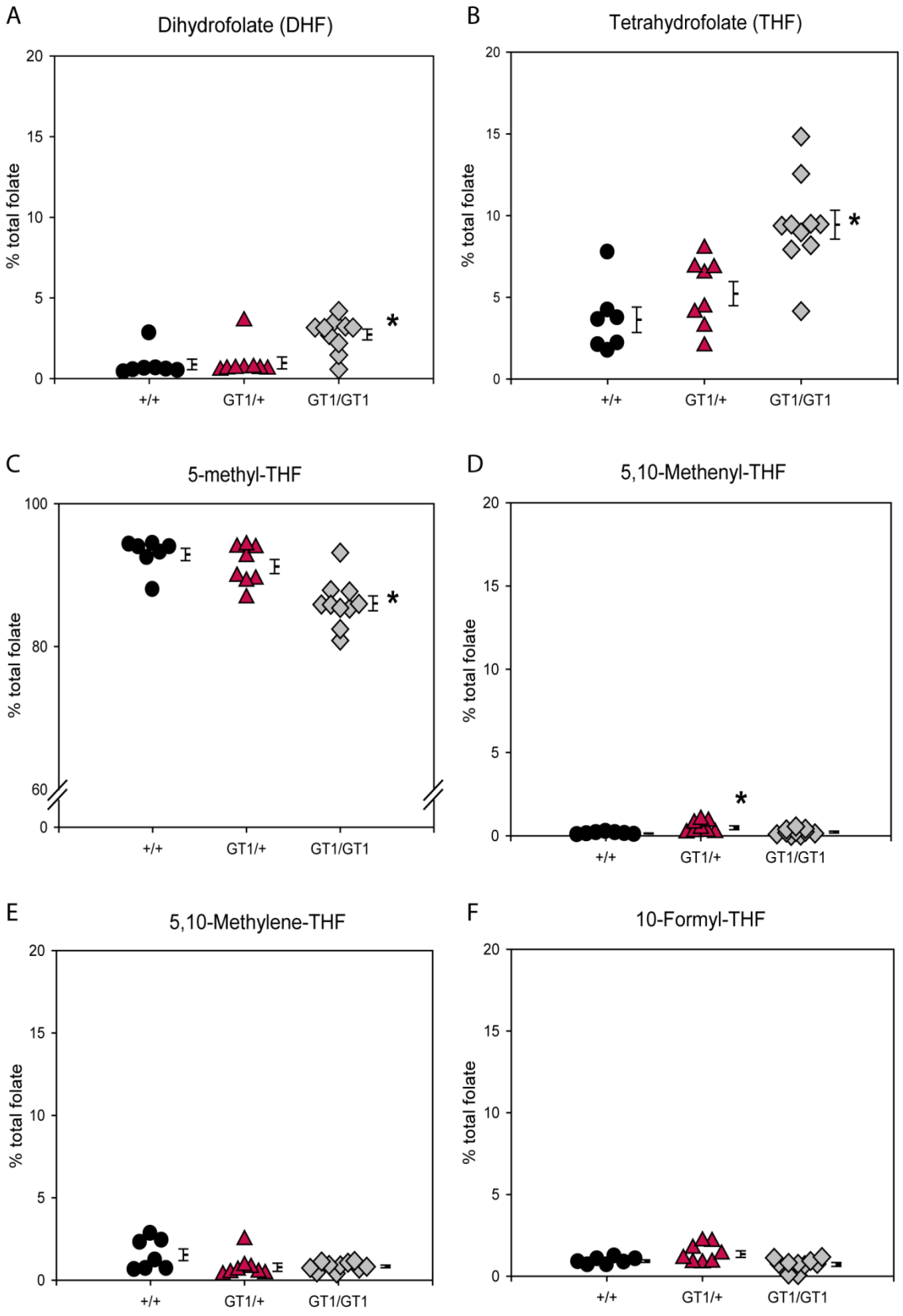

Figure 27. *Gldc*^{GT1} mutant embryos show altered folate profiles.

4.2.2. Abnormal folate profiles in *Gldc* mutation are caused by lack of 1C units

To test the hypothesis of insufficient 1C units causing the changes in relative abundance of folate metabolites in $Gldc^{GT1}$ mutants, $Gldc^{GT1/+}$ mice were inter-crossed and pregnant females supplemented with 30 mg/mL of sodium formate in their drinking water to potentially restore 1C pools in homozygous mutant embryos. The concentration of 30 mg/mL of sodium formate delivers 7,500 mg per kg body weight per day, and was chosen based on a previous study that achieved significant phenotypic improvement with that dose on *Mthfd1L* mutant mice, another mitochondrial FOCM model (Momb et al., 2013).

4.2.2.1. Formate treatment rescues NTDs and normalises folate profiles

Formate treatment was found to significantly reduce the frequency of NTDs in $Gldc^{GT1/GT1}$ embryos analysed at E11.5, with an incidence of just 2% (1 out of 45 treated embryos), compared with 22% in a contemporaneous untreated cohort (**Figure 28**).

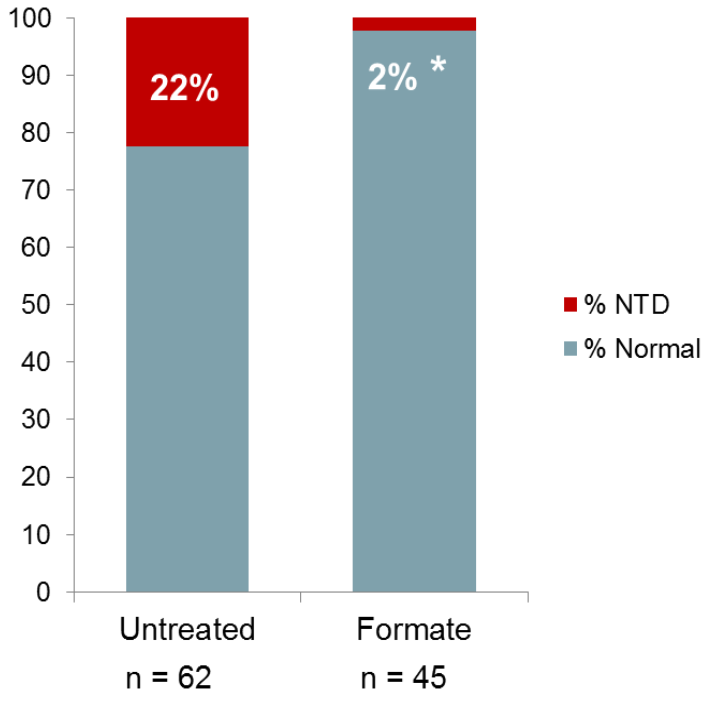

Figure 28. Effect of formate treatment on NTD incidence in $Gldc^{GT1/GT1}$ embryos.

Formate treatment reduced the incidence of NTDs in $Gldc^{GT1/GT1}$ embryos from 22% to 2%, which is a significant rescue effect (*Z-test, P = 0.007).

Formate treatment was hypothesised to have a rescue effect on NTDs by altering the proportion of folates. An alternative possibility is that excess glycine is the cause of the NTDs, and that formate treatment is able to correct this (through an unknown mechanism). To investigate this possibility, the levels of glycine in E11.5 formate-treated embryos were measured. **Figure 29** below illustrates how glycine, as observed previously, remains unchanged at a significant 4-fold increase in *Gldc*$^{GT1/GT1}$ embryos compared with wild-types. When E11.5, formate-treated embryos were tested for changes in their folate profiles, *Gldc*$^{GT1/GT1}$ embryos showed relative abundances in folate metabolites that did not differ significantly from formate-treated wild-type embryos (**Figure 30**).

The significant lowering of NTD frequency and normalisation of folate profiles with formate treatment, combined with unchanged elevation in glycine levels, strongly suggests that abnormal folate metabolism caused by disrupted supply of 1C units is responsible for the NTDs present in this model.

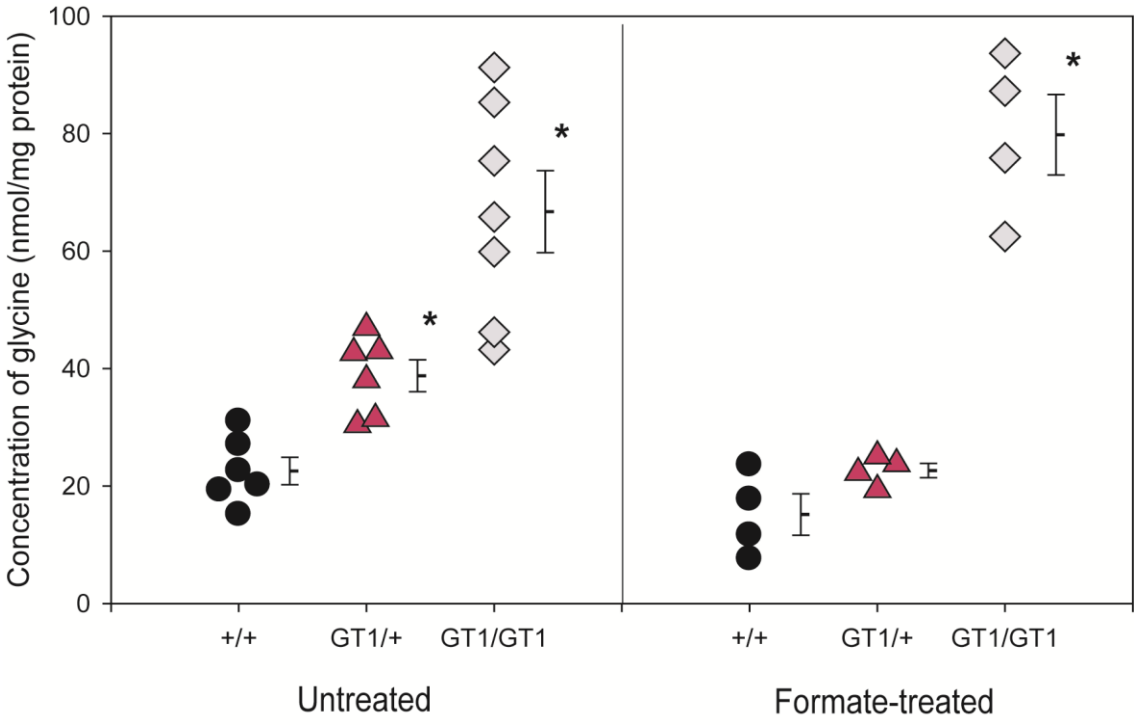

Figure 29. Glycine levels in untreated and formate-treated E11.5 *Gldc*^{GT1} embryos.

Among untreated embryos, glycine levels were significantly elevated in *Gldc*$^{GT1/+}$ (n = 6) and *Gldc*$^{GT1/GT1}$ (n = 7) compared with *Gldc*$^{+/+}$ (n = 6) embryos (graphical representation of glycine levels given in **Table 18**). In formate-treated embryos, glycine levels were also significantly increased in *Gldc*$^{GT1/GT1}$ (n = 4 per genotype) Error bars represent mean ± SEM (*ANOVA, $p<0.001$).

Figure 30. Normalisation of folates of *Gldc*^{GT1} embryos after formate treatment.

In formate-treated embryos, the abnormal folate profiles of untreated *Gldc*$^{GT1/GT1}$ embryos were normalised; there were no significant changes in levels of **(A)** DHF, **(B)** THF, **(C)** 5-methyl-THF, **(D)** 5,10-methenyl-THF, **(E)** 5,10-methylene-THF, or **(F)** 10-formyl-THF between all genotypes (n = 8 per genotype, ANOVA). Error bars represent mean ± SEM.

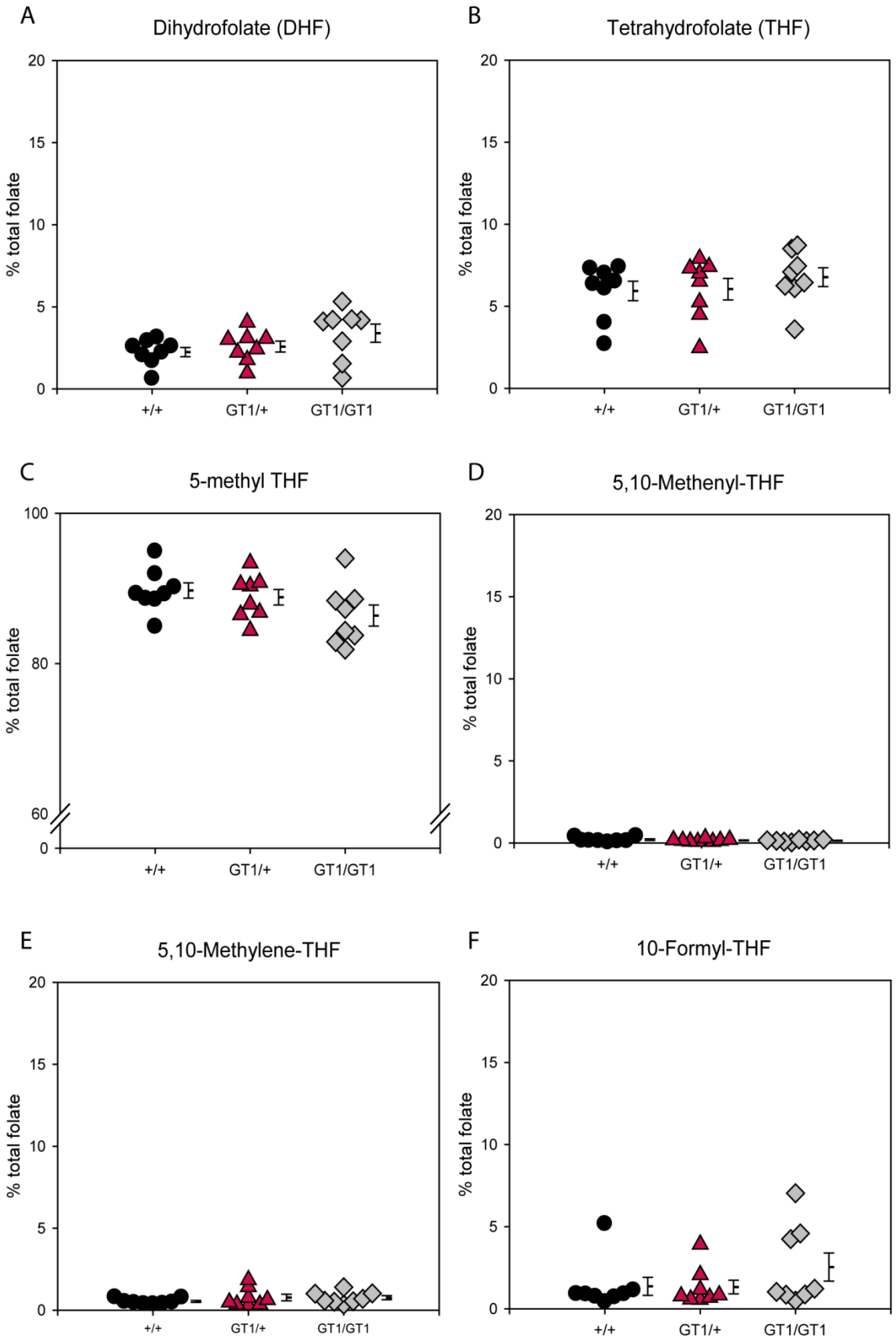

Figure 30. Normalisation of folates of *Gldc*^{GT1} embryos after formate treatment.

4.2.2.2. *Gldc*^{GT1} foetuses show signs of toxicity on prolonged formate supplementation

When mice were fed with formate-treated water until E15.5 or E18.5 (at point of embryo collection), other abnormalities were found. These were suspected as signs of formate toxicity as they have not been previously observed in untreated embryos collected at similar late-foetal stages. Prior to this, the teratological effects of prolonged formate supplementation on wild-type mice have not been studied.

The most common abnormality is non-cranial haemorrhage (unlike the cranial haemorrhage observed in E10.5 and E11.5 mutants described in **Chapter 3**) such as in the lower spine where spina bifida lesions commonly occur (**Figure 31C**), or whole-body haemorrhage with accompanying oedema reminiscent of early heart defects (**Figure 31F**). The other abnormality that has been observed is a snout deformity with the appearance of missing/underdeveloped/degenerated mandibles seen in E15.5 (**Figure 31B**) and appearing worse in E18.5 (**Figure 31E**).

The incidences of these defects are given in **Table 19** below. They appear at a combined frequency of 7.7% in wild-types, 8.3% in heterozygotes, and 33.3% in homozygotes.

Stage (E-)	Phenotype	No. with phenotype/ Total no. of foetuses		
		Gldc$^{+/+}$	*Gldc*$^{GT1/+}$	*Gldc*$^{GT1/GT1}$
15.5	Snout	0/5	0/16	2/5
(4 litters)	Haemorrhage	0/5	1/16	1/5
18.5	Snout	0/8	1/20	1/10
(7 litters)	Haemorrhage	1/8	1/20	1/10
TOTAL	**BOTH**	**1/13 (7.7%)**	**3/36 (8.3%)**	**5/15 (33.3%)**

Table 19. Incidence of toxic effects of prolonged formate supplementation in E15.5 and E18.5 *Gldc*^{GT1} foetuses.

The proportions of affected foetuses were not significantly different between *Gldc*$^{+/+}$ and *Gldc*$^{GT1/+}$ (Z-test, P = 0.600), *Gldc*$^{+/+}$ and *Gldc*$^{GT1/GT1}$ (Z-test, P = 0.236), or *Gldc*$^{GT1/+}$ and *Gldc*$^{GT1/GT1}$ (Z-test, P = 0.069).

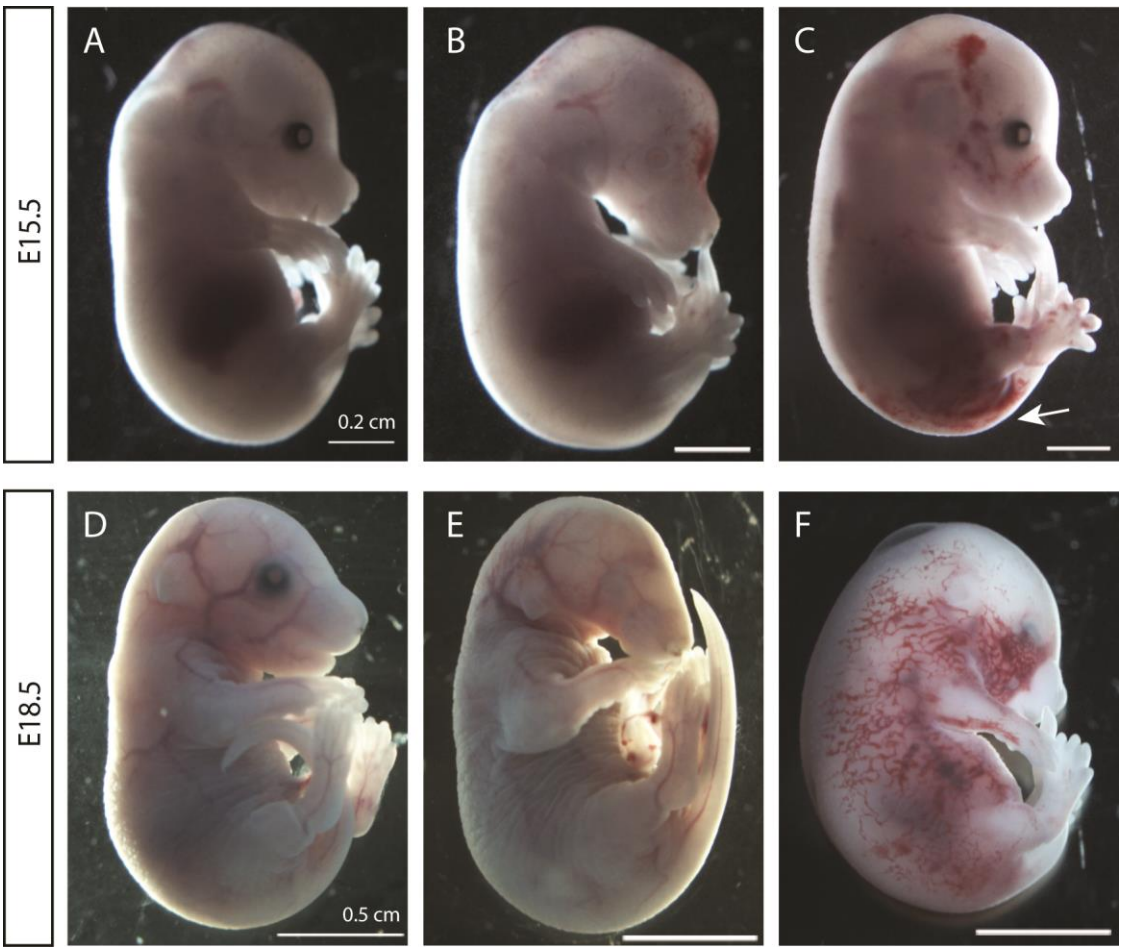

Figure 31. Signs of non-genotype specific toxicity in *Gldc*^{GT1} foetuses after prolonged formate supplementation.

Toxic effects of prolonged formate supplementation was seen in *Gldc*^{GT1} foetuses at E15.5 **(B, C)** and appear worse at E18.5 **(E, F)**, when compared to normal looking littermates **(A, D)**. In **(B)** and **(E)**, a snout deformity was observed, while in **(C)** and **(F),** haemorrhage and oedema were observed.

4.2.2.3. Folate deficiency does not exacerbate NTDs in *Gldc* mutants

The effect of folate deficiency was tested by supplementing female *Gldc*$^{GT1/+}$ mice 3 weeks prior to mating and throughout pregnancy with a folate-deficient diet with added 1% succinylsulfathiazole, an intestinal antibacterial drug which prevents the synthesis of folates by gut flora (Walzem and Clifford, 1988).

Diet-induced folate deficiency alone does not result in NTDs in rodents, but has been reported to exacerbate susceptibility to neural tube closure leading to increased incidence of NTDs in other mouse models such as *curly tail* (Burren et al., 2010), *Shmt1* (Beaudin et al., 2011) and *Splotch*^{2H} (Burren et al., 2008). Curiously, in the *Gldc*^{GT1} model folate deficiency does not increase NTD incidence (**Figure 32**). The frequency of NTDs was 17% in treated compared to 18% in untreated embryos. This may be because the limiting factor in *Gldc*^{GT1} mutants is shortage of 1C units, such that depletion in the folates themselves (i.e. the "scaffolding" molecules that carry the "functional" 1C units) did not worsen the phenotype, presumably because sufficient folate is available to carry the 1C units.

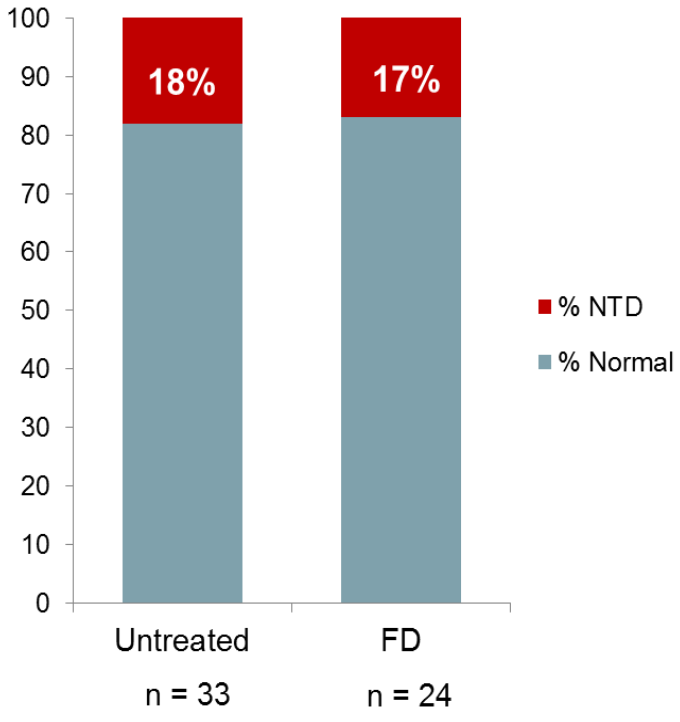

Figure 32. Effect of folate deficiency on *Gldc*$^{GT1/GT1}$ embryos.

Gldc$^{GT1/GT1}$ embryos among litters of diet-induced, folate-deficient female mice showed no significant changes in NTD incidence compared with untreated mutants (Z-test, P = 0.799).

4.2.2.4. Formate levels in *Gldc* mutant embryos

To investigate whether there are changes in circulating levels of formate between the different genotypes and/or in heterozygous mice fed with different treatments, blood from $Gldc^{GT1}$ adult mice was collected by cardiac puncture and transferred into lithium-heparin tubes. The blood was centrifuged at 3,500 rpm for 5 min to separate the plasma layer, and plasma formate was measured using gas chromatography (performed by Dr John and Margaret Brosnan, Memorial University of Newfoundland, Canada).

Levels of circulating formate did not differ between the different genotypes (**Figure 33**), suggesting that sufficient formate is generated in *Gldc*-deficient mice to maintain circulating levels. Hence, the shortage of mitochondrial-derived formate may primarily be a cell-autonomous effect, or that endogenous formate is quickly metabolised by cytosolic folate cycling when released from the mitochondria. As formate may also come from other non-mitochondrial-derived sources, this suggests that formate utilised by cytoplasmic FOCM mainly derives from the mitochondria.

The increase in formate levels of formate-treated heterozygotes confirmed that treatment administered through drinking water is efficient in delivering formate into maternal circulation. In heterozygotes with diet-induced folate deficiency, there was a significant increase in levels of circulating formate. This finding is consistent with previous studies in rats (Lamarre et al., 2012) and indicates that reducing the levels of folate molecules results in a surplus of unbound formate which is released into the circulation.

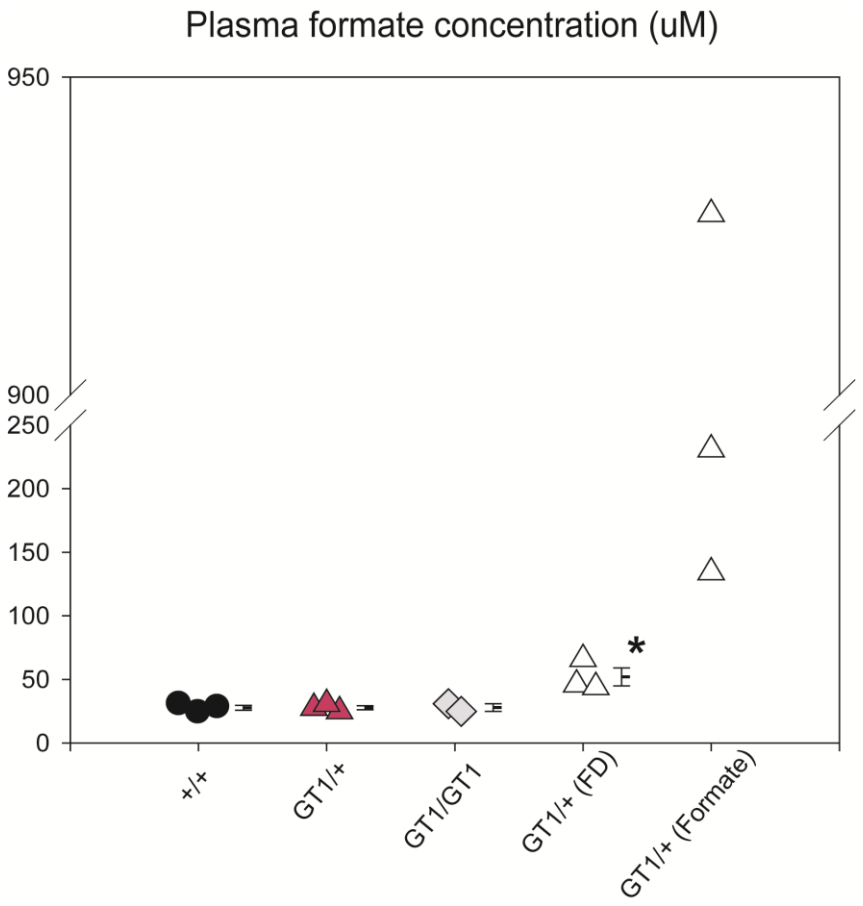

Figure 33. Plasma formate levels in untreated and formate-treated *Gldc*^{GT1} mice.

Plasma formate concentration of untreated *Gldc*^{GT1} mice did not differ significantly between the three genotypes (3 *Gldc*$^{+/+}$, 3 *Gldc*$^{GT1/+}$, and 2 *Gldc*$^{GT1/GT1}$) (ANOVA). In *Gldc*$^{GT1/+}$ mice fed with folate-deficient diet (n = 3), plasma formate levels were significantly elevated compared with untreated *Gldc*$^{GT1/+}$ mice (* t-test, P = 0.029). Plasma formate levels of formate-treated *Gldc*$^{GT1/+}$ mice (n = 3) showed a 3- to 20-fold increase compared with untreated mice. Error bars represent mean ± SEM.

4.2.3. Effect of *Gldc* deficiency on cellular proliferation, growth, and development

Downstream of folate metabolism, 1C units may enter nucleotide synthesis pathways, the methylation cycle by combining with homocysteine, and polyamine synthesis, all of which could be affected when folate cycling is disrupted. The following experiments focused mainly on cellular proliferation as an indication of disrupted nucleotide synthesis. Preliminary results from investigating the methylation cycle are also reported. The effect of altered balance of folate metabolites was further probed by introducing the *Mthfr* null mutation into *Gldc*^{GT2} mice to block the flow of 1C units into methylation.

4.2.3.1. Formate treatment normalises growth

The crown rump length (CRL) of E11.5 *Gldc*^{GT1} embryos that were treated with formate were measured and compared to untreated litters. As reported at E9.5 and E10.5 (**Chapter 3**), untreated E11.5 *Gldc*$^{GT1/GT1}$ but not *Gldc*$^{GT1/+}$ embryos showed significantly decreased CRL compared with wild-types (**Figure 34**). This difference was normalised in formate-treated homozygotes, which showed comparable CRL measurements to the wild-types. There were no significant changes in CRL measurements between untreated and treated wild-types, suggesting that formate does not affect growth when 1C units are sufficient.

The delay in growth of untreated mutants is suggestive of an overall proliferation defect which supplementation with formate was also able to correct.

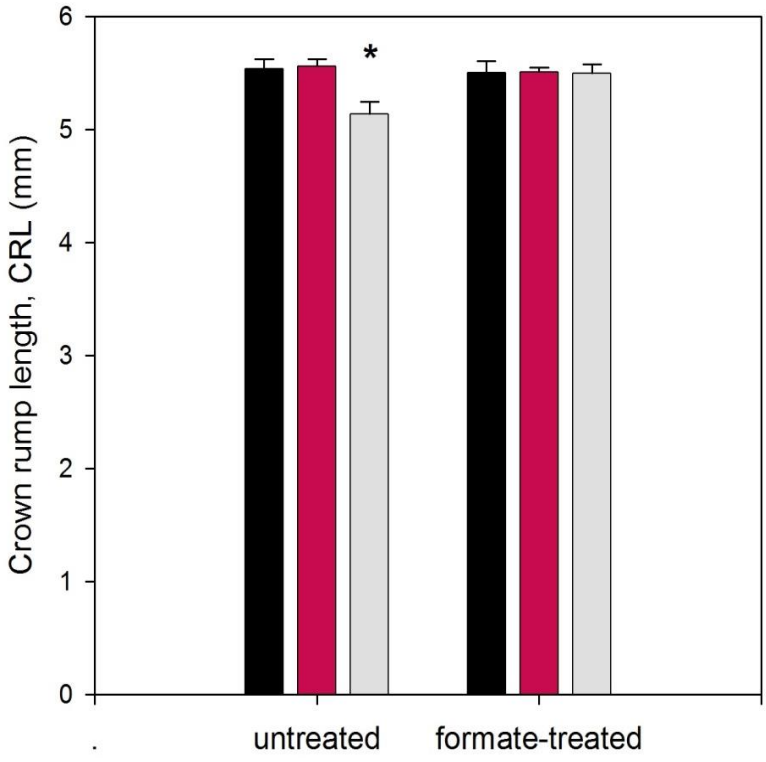

Figure 34. Effect of formate treatment on growth of *Gldc*^{GT1} embryos.

In untreated E11.5 *Gldc*^{GT1} embryos, there was a significant decrease in crown rump length, CRL of *Gldc*$^{GT1/GT1}$ embryos (n = 36) compared with *Gldc*$^{+/+}$ (n = 23) and *Gldc*$^{GT1/+}$ (n = 74). In formate-treated E11.5 embryos, no significant difference in CRL was observed between all genotypes (25 *Gldc*$^{+/+}$, 45 *Gldc*$^{GT1/+}$, and 22 *Gldc*$^{GT1/GT1}$). Error bars represent mean ± SEM (*ANOVA, $p<0.001$).

4.2.3.2. Proliferation analysis of *Gldc* mutant embryos

The rate of proliferation in the cranial neural tube of *Gldc* mutant embryos was directly assessed using immunohistochemical staining for phospho-histone H3 (PHH3) antibody, a marker of cells in late G2 and M-phase, which gives an indication of mitotic index. DAPI was also used to allow visualisation of all cell nuclei. Embryos at E9.5 (somite stage 18 to 24) were used so that embryos could be scored for presence of an open hindbrain neural tube. Older embryos risk the possibility of secondary differences in proliferation (if any were to be found) after normal closure or a defect has occurred. In addition, *Gldc* mRNA expression at E10.5 was less intense than at E9.5 (**Chapter 3**), indicating that Gldc activity may decrease slightly at some point after E9.5 and specific effects on cell proliferation may be less detectable.

The hindbrain neural tube was divided into 5 morphological regions for the proliferation analysis **(Figure 35)**: transverse sections through the neural tube just caudal to the otic vesicles were annotated as region 1 **(A1, B1)**, sections showing both otic vesicles were region 2 **(A2, B2)**, where the branchial arches were visible and the left and right sides distinct from one another was region 3 **(A3, B3)**, region 4 was where the forebrain with both optic cups were visible **(A4, B4)**, and region 5 where both optic vesicles were separated from the forebrain and the midbrain is not visible **(A5, B5)**.

Samples of positive PHH3 and DAPI staining in "region 4" of a wild-type embryo with a normal, closed neural tube and a $Gldc^{GT1/GT1}$ mutant with an open region are shown in **Figure 36**. Due to interkinetic nuclear migration, in which nuclei in polarised epithelial cells that are undergoing mitosis would migrate to the apical surface of the cell layer (Lee and Norden, 2013), PHH3-positive nuclei were mostly located at the apical surface of the neural tube **(Figure 36C, F)**. As this pattern of staining was seen in wild-type neural tubes (n = 5) and in mutants with closed (n = 3) and open (n = 4) neural tubes, interkinetic nuclear migration in *Gldc* mutants appeared to be unaffected. The stages of mitosis identified by PHH3 staining, as referenced from Li et al. (2005) and De Castro et al. (2012), is shown in **Figure 36 (G-i – G-v)**. As it is often difficult to distinguish between two or more overlapping or adjacent PHH3-stained nuclei at G2 phase (**Figure 36G-i**), G2 phase nuclei were excluded from the counts.

To account for possible variation in rate of proliferation at different axial levels of the hindbrain neural tube, four to six sections from each region of every embryo were analysed. The percentage of PHH3-positive cells as a function of the number of DAPI-stained cells in each region (sum of all four to six sections per region), i.e. mitotic index, was calculated to represent the rate of proliferation in that region of the embryo.

Figure 37A illustrates the total mitotic index of all 5 hindbrain regions in wild-types and *Gldc*^{GT1GT1} mutants (closed and open neural tubes), with the regional mitotic indices of each embryo broken down in **Figure 37B**. The total percentage of PHH3 staining was significantly lower in *Gldc*$^{GT1/GT1}$ mutants with an open neural tube compared with somite-matched wild-types, indicating defective cellular proliferation. In normal *Gldc*$^{GT1/GT1}$ mutants with closed hindbrain neural tubes, the mitotic index values are in a range between wild-type and affected mutant values. While there is variation in the mitotic indices of the different regions within the same embryo, no particular pattern of variation was observed across all embryos within and between genotypes.

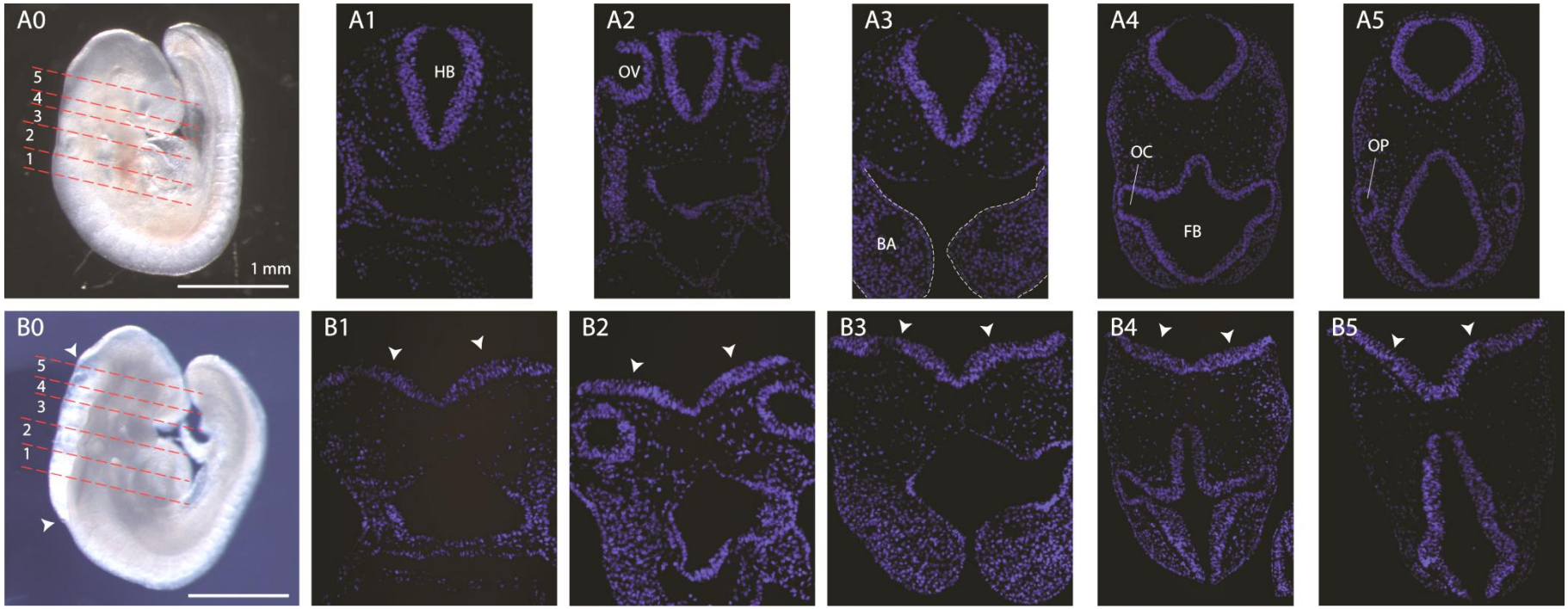

Figure 35. Defining 5 regions of the E9.5 cranial neural tube for proliferation studies.

Transverse sections through the hindbrain of an embryo with a closed neural tube **(A0)** and an NTD-affected **(B0)** (white arrowheads indicate open neural folds in B0-5), showing regions **1** to **5** (demarcated by red dotted lines) identified for proliferation analysis. A representative section from each region is shown in **A1-A5** and **B1-B5**. **Region 1** is identified as the region of the hindbrain (HB) just caudal to, but not including either of, the otic vesicles (OV), **region 2** is where both otic vesicles (OV) are visible, **region 3** where the first branchial arch (BA) is visible (outlined by white dotted lines in **A3**), **region 4** where the optic cups (OC) of the forebrain (FB) can be identified, and **region 5** where both optic vesicles (OP) are separate entities from the forebrain.

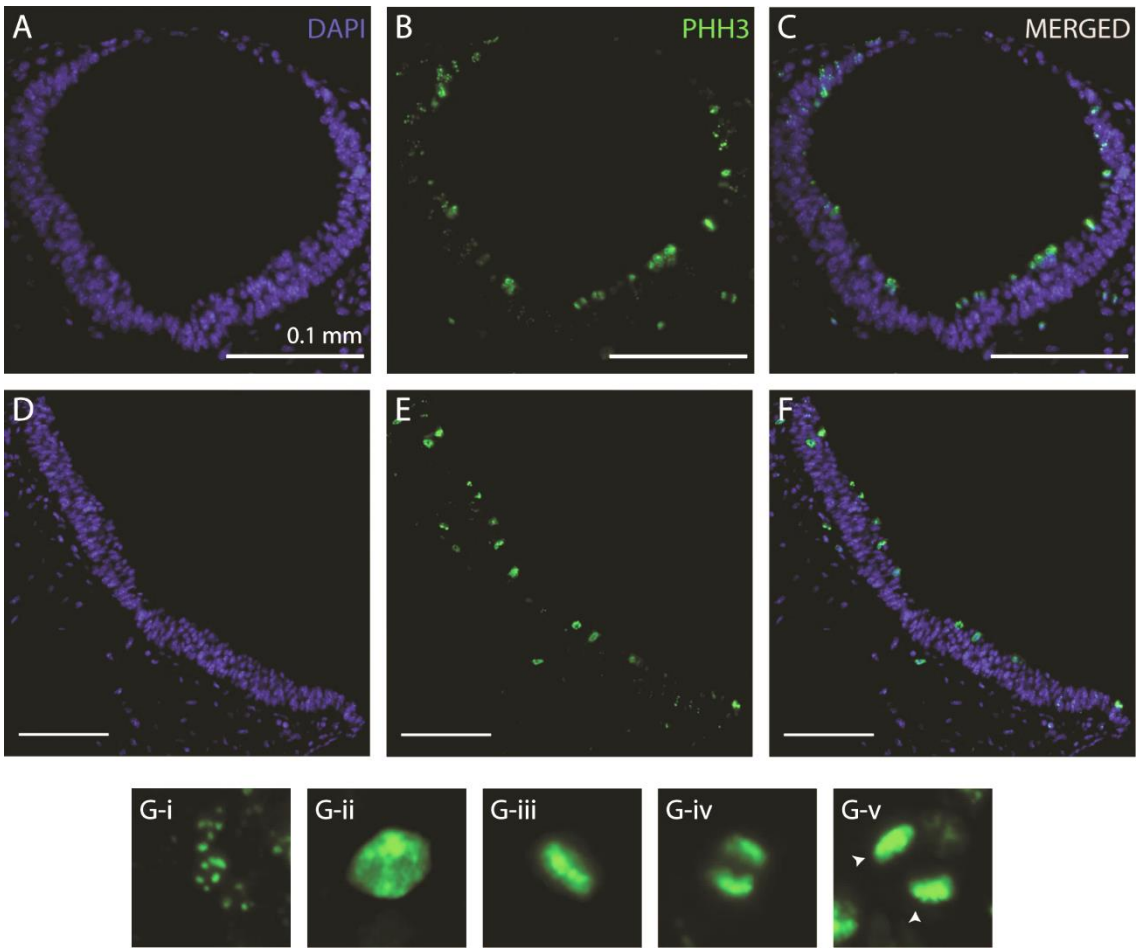

Figure 36. Positive PHH3 staining in the hindbrain of *Gldc*^{GT1} embryos.

Transverse sections of a *Gldc*$^{+/+}$ embryo with a closed cranial neural tube **(A, B, C)** and a *Gldc*$^{GT1/GT1}$ embryo with an open neural tube **(D, E, F)** were stained with DAPI nuclei stain and anti-PHH3 antibody. PHH3 staining identifies cell nuclei in G2 phase **(G-i)** and stages of mitosis: prophase **(G-ii)**, metaphase **(G-iii)**, anaphase **(G-iv)**, and telophase **(G-v)**.

Figure 37. Percentage of PHH3-labelled cells in *Gldc*^{GT1} embryos.

(A) NTD-affected *Gldc*$^{GT1/GT1}$ embryos showed an overall significantly reduced mitotic index compared with *Gldc*$^{+/+}$ embryos (*t-test, P = 0.008). In *Gldc*$^{GT1/GT1}$ embryos in which the neural tube was closed, there was a bigger spread of values compared with NTD-affected ones, and the mean value was not significantly lower than wild-type values (t-test, P = 0.200). Error bars represent mean ± SEM. When mitotic index scores are broken down by specific hindbrain regions **(B)**, little variation is seen in the the different regions of the same embryo, with no discernible pattern of change from the most caudal (1) to rostral (5) regions.

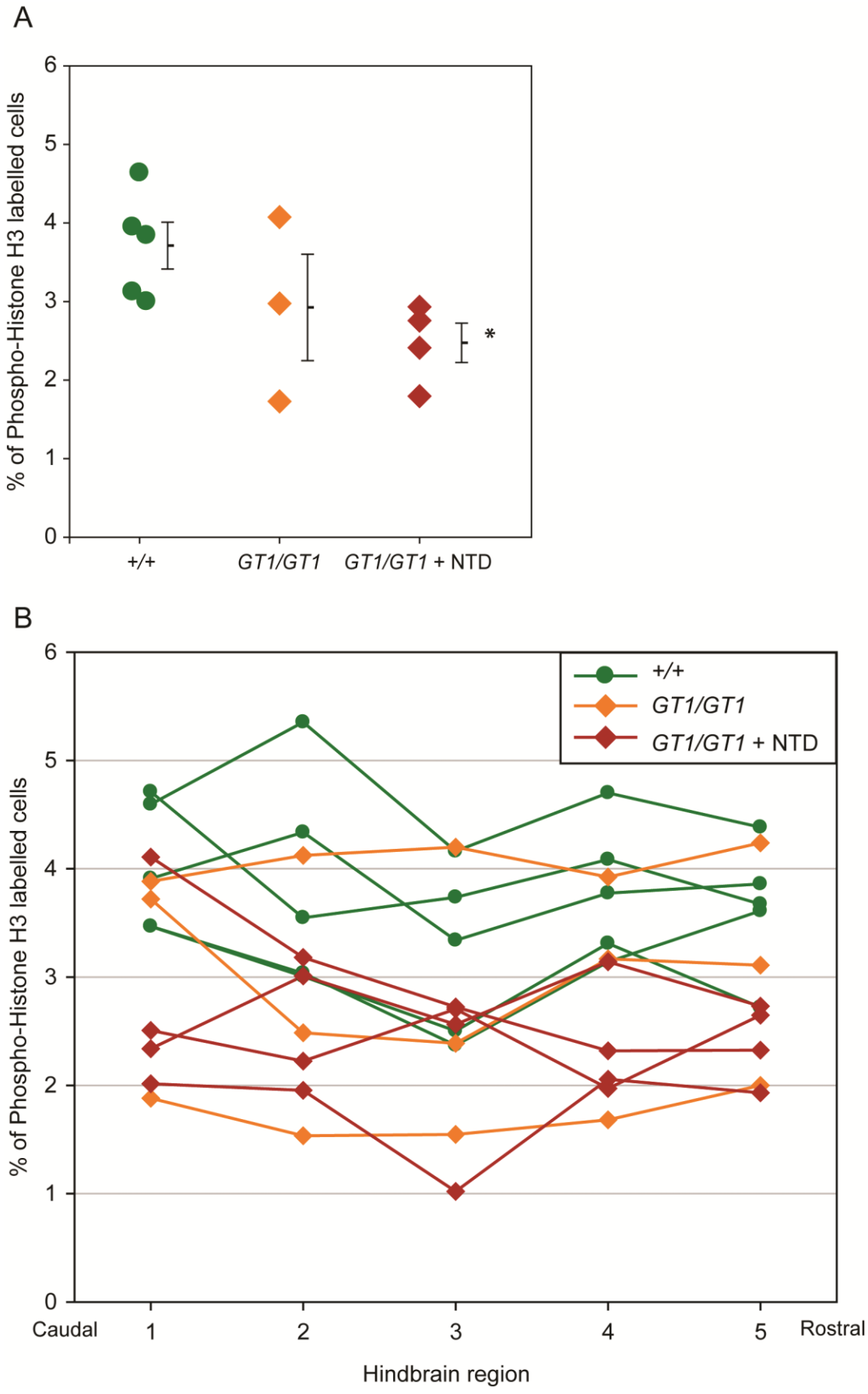

Figure 37. Percentage of PHH3 labelled cells in *Gldc*^{GT1} embryos.

4.2.3.3. Formate treatment normalises proliferation

As formate treatment was able to rescue occurrence of NTDs (**Figure 28**) and normalise folate profile (**Figure 30**) and crown rump length (**Figure 34**) of *Gldc*$^{GT1/GT1}$ embryos, the next logical step was to examine the rate of proliferation in the hindbrain neural tube of formate-treated "rescued" *Gldc*$^{GT1/GT1}$ embryos, compared with treated wild-type littermates.

From the line graph shown in **Figure 37B**, there appeared to be no pattern of variation in rate of proliferation between different regions of the hindbrain. Thus, when the same proliferation analysis was performed on E9.5 formate-treated embryos, four to six sections from region 4 and 5 were analysed. The rescued *Gldc*$^{GT1/GT1}$ embryos were found to have comparable mitotic indices to wild-type littermates (**Figure 38**), indicating that proliferation in the hindbrain neural tubes of *Gldc*$^{GT1/GT1}$ embryos was normalised by formate treatment.

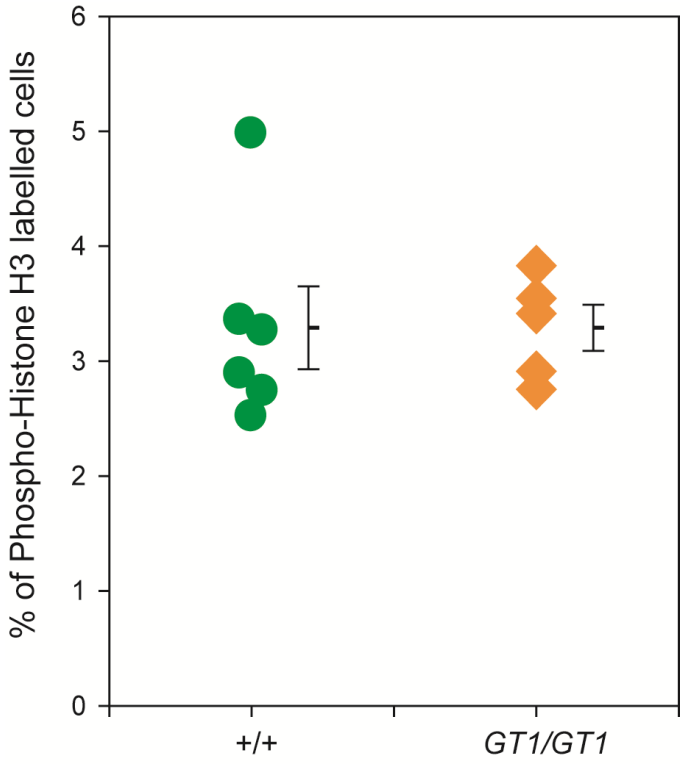

Figure 38. Percentage of PHH3 labelled cells in formate-treated *Gldc*^{GT1} embryos.

No significant difference in percentage of PHH3 staining was observed between E9.5 treated wild-types and *Gldc*^{GT1} homozygous mutants. Error bars represent mean ± SEM (t-test, P = 0.998).

4.2.3.4. SAM/SAH analysis of *Gldc* mutant embryos

A decrease in S-adenosyl methionine (SAM) combined with increase in S-adenosyl homocysteine (SAH) (thus decreasing SAM/SAH ratio) would suggest suppression of the methylation cycle, which is known to induce cranial NTDs (Dunlevy et al., 2006, Burren et al., 2008). Decreased SAM/SAH ratio has also been shown to be an effective marker of global DNA hypomethylation (Caudill et al., 2001). The levels of SAM and SAH in E11.5 *Gldc*^{GT1} whole embryos were measured by LC-MS/MS (performed by Dr K-Y Leung) to assess the efficiency of methylation in the *Gldc*^{GT1} model.

The SAM/SAH ratios of *Gldc*^{GT1} embryos showed no significant differences between all genotypes and phenotypes (**Figure 39**). This suggests that compromised methylation is unlikely to be the mechanism underlying the NTDs in *Gldc*$^{GT1/GT1}$ embryos.

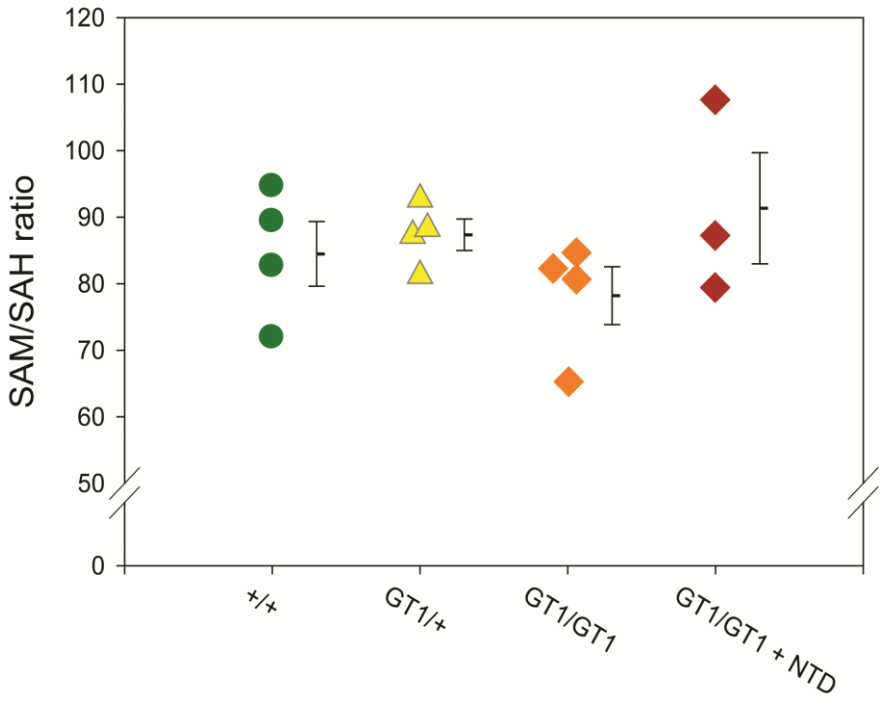

Figure 39. SAM/SAH ratios of E11.5 *Gldc*^{GT1} embryos.

No significant differences in SAM/SAH ratio were found between the different genotypes of *Gldc*^{GT1} mutant embryos, with or without NTDs. Error bars represent mean ± SEM (ANOVA).

4.2.3.5. Interaction between *Gldc* and *Mthfr* mutations

The 677C>T polymorphism in *MTHFR* is of particular interest in human NTDs due to it being the first and one of few FOCM enzyme-encoding mutations which is associated with NTDs. While the mouse knockout model of *Mthfr* did not present with NTDs, post-natal mutant tissue showed suppressed methylation (Chen et al., 2001). This presents an opportunity to test for potential gene-gene interaction between the *Mthfr* mutation (which stops conversion of 5,10-methylene-THF to 5-methyl-THF, thus preventing 1C units from entering the methylation cycle) and *Gldc* mutation (reported in this thesis to produce a shortage of mitochondrial-derived IC units, hypothesised to predominantly affect 1C supply into both nucleotide synthesis and the methylation cycle).

Given that both *MTHFR* and *GLDC* mutations may increase susceptibility to NTDs in humans, the potential for a genetic interaction was investigated. To test whether the presence of the *Mthfr* knockout allele in a $Gldc^{-GT2/GT2}$ embryo affects NTD incidence, $Mthfr^{+/-}$ mice were crossed with $Gldc^{GT2/+}$ mice to produce double heterozygous ($Gldc^{GT2/+};Mthfr^{+/-}$) mice. These were then inter-crossed to produce double homozygous mutants ($Gldc^{GT2/GT2};Mthfr^{-/-}$) in experimental litters. The results of this experiment are presented in **Table 20**.

In embryos that were wild-type for *Gldc* (i.e. $Gldc^{GT2}$ mutant allele was absent), no NTDs were present regardless of the *Mthfr* genotype. This finding corresponds with published data reporting the absence of NTDs in *Mthfr* null mice (Chen et al., 2001). When the *Mthfr* allele was absent, NTDs were present with a 43% incidence in embryos with the $Gldc^{GT2/GT2}$ genotype and 7.1% in $Gldc^{GT2/+}$, which is comparable to a $Gldc^{GT2}$ heterozygous cross as reported in **Chapter 3**. In double homozygous ($Gldc^{GT2/GT2};Mthfr^{-/-}$) embryos, the rate of NTDs appeared lower (20%) than in $Gldc^{GT2/GT2};Mthfr^{+/+}$ embryos. This result clearly suggests that having a non-functioning *Mthfr* gene in addition to defective *Gldc* does not exacerbate the phenotype. A similar pattern was observed in heterozygous $Gldc^{GT2/+}$ embryos: NTD incidence was 7.1% when *Mthfr* genotyped as wild-type ($Gldc^{GT2/+};Mthfr^{+/+}$), but were not present when *Mthfr* was absent ($Gldc^{GT2/+};Mthfr^{-/-}$).

To investigate how the *Mthfr* mutation alters the folate profile of $Gldc^{GT2}$ mutants, the proportion of folates in E11.5 whole embryos were measured by LC/MS/MS, as for $Gldc^{GT1}$ embryos (**Section 4.2.1.3**) (performed by Dr Kit-Yi Leung). The folate profiles of wild-type, individual homozygous mutant, and double homozygous mutant embryos from $Gldc^{GT2/+};Mthfr^{+/-}$ double heterozygous litters were compared (**Figure 40**).

In $Gldc^{GT2GT2};Mthfr^{+/+}$ mutants (effectively $Gldc^{GT2}$ mutant controls), there was an increase in proportion of DHF and THF, and decrease in 5-methyl-THF, when compared to the wild-

types. Although only the changes in 5-methyl-THF were significant, this pattern mimics that seen in the *Gldc*^{GT1} mutants (**Figure 27**). In *Gldc*$^{+/+}$*;Mthfr*$^{-/-}$ mutants (effectively *Mthfr* knockout controls), there was a dramatic, significant decrease in 5-methyl-THF and increase in 5,10-methylene-THF compared to wild-types, as expected from lack of Mthfr enzyme to convert 5,10-methylene-THF to 5-methyl-THF. Other significant changes include increases in THF, 5,10-methenyl THF, and 10-formyl-THF compared with wild-types, presumably as a result of the increased availability of 5,10-methylene-THF.

In *Gldc*$^{GT2/GT2}$*;Mthfr*$^{-/-}$ mutants, the changes due to the *Mthfr* mutation appear to dominate their folate profiles when compared with wild-types: a dramatic, significant decrease in 5-methyl-THF, and increases in proportion of all other folates, was observed. When compared with *Gldc*$^{GT2/GT2}$*;Mthfr*$^{+/+}$ mutants, the addition of the *Mthfr* mutation further increased the proportion of DHF and THF. Interestingly, the proportion of the 1C-carrying folates 5,10-methenyl-THF, 5,10-methylene-THF, and 10-formyl-THF in *Gldc*$^{GT2/GT2}$*;Mthfr*$^{-/-}$ mutants were significantly increased (at the cost of a severe reduction in 5-methyl-THF) compared with *Gldc*$^{GT2/GT2}$*;Mthfr*$^{+/+}$ mutants. As the *Mthfr* knockout mouse has defective methylation but does not present with NTDs, the NTDs observed in *Gldc*$^{GT2/GT2}$*;Mthfr*$^{-/-}$ double homozygotes are probably entirely caused by the *Gldc*^{GT2} mutation. The increase in their proportion of 1C-carrying folates (compared to *Gldc*$^{GT2/GT2}$*;Mthfr*$^{+/+}$ mutants) may be causing the slight decrease in NTD incidence of these mutants, though larger sample sizes would be needed to test whether this finding is statistically significant.

	No. of embryos with NTD/ Total no. of embryos (%)								
***Gldc*^{GT2} allele**	***+/+***	***+/+***	***+/+***	***GT2/+***	***GT2/+***	***GT2/+***	***GT2/GT2***	***GT2/GT2***	***GT2/GT2***
***Mthfr* allele**	***+/+***	***+/-***	***-/-***	***+/+***	***+/-***	***-/-***	***+/+***	***+/-***	***-/-***
E11.5	0/6	0/15	0/8	1/18 (5.6%)	2/71 (2.8%)	0/21	2/5 (40%)	4/17 (23.5%)	1/9 (11.1%)
E15.5	0/4	0/6	0/3	0/2	0/13	0/7	1/2 (50%)	2/5 (40%)	1/3 (33.3%)
Total	**0/10**	**0/21**	**0/11**	**1/20 (5%)**	**2/84 (2.4%)**	**0/28**	**3/7 (42.9%)**	**6/22 (27.3%)**	**2/12 (16.7%)**

Table 20. Incidence of NTDs in *Gldc*$^{GT2/+}$;*Mthfr*$^{+/-}$ double heterozygous crosses.

Figure 40. Folate profiles of *Gldc^{GT2};Mthfr$^{=}$* double mutants.

When compared with wild-types (*Gldc$^{+/+}$;Mthfr$^{+/+}$*, simplified as "+/+;+/+") (indicated *), *Gldc$^{GT2/GT2}$* mutants (*Gldc$^{GT2/GT2}$;Mthfr$^{+/+}$*, simplified as "GT2/GT2;+/+") showed significant decrease in proportion of 5-methyl-THF **(C)**, while *Mthfr$^{-/-}$* mutants (*Gldc$^{+/+}$;Mthfr$^{-/-}$*, simplified as +/+;-/-) showed significant decrease in 5-methyl-THF **(C)**, and a significant increases (*) in THF **(B)**, 5,10-methenyl-THF **(D)**, 5,10-methylene-THF **(E)**, and 10-formyl-THF **(F)**. The double homozygous mutants (*Gldc$^{GT2/GT2}$;Mthfr$^{-/-}$*, simplified as "GT2/GT2;-/-) had significantly decreased proportions of 5-methyl-THF and increase in all other folates including DHF **(A)**. When compared with GT2/GT2;+/+ mutants (**), the addition of the *Mthfr* mutant alleles in GT2/GT2;-/- mutant embryos resulted in significant decrease in 5-methyl-THF but increase in the other folates (ANOVA, $P<0.001$). Error bars represent mean ± SEM.

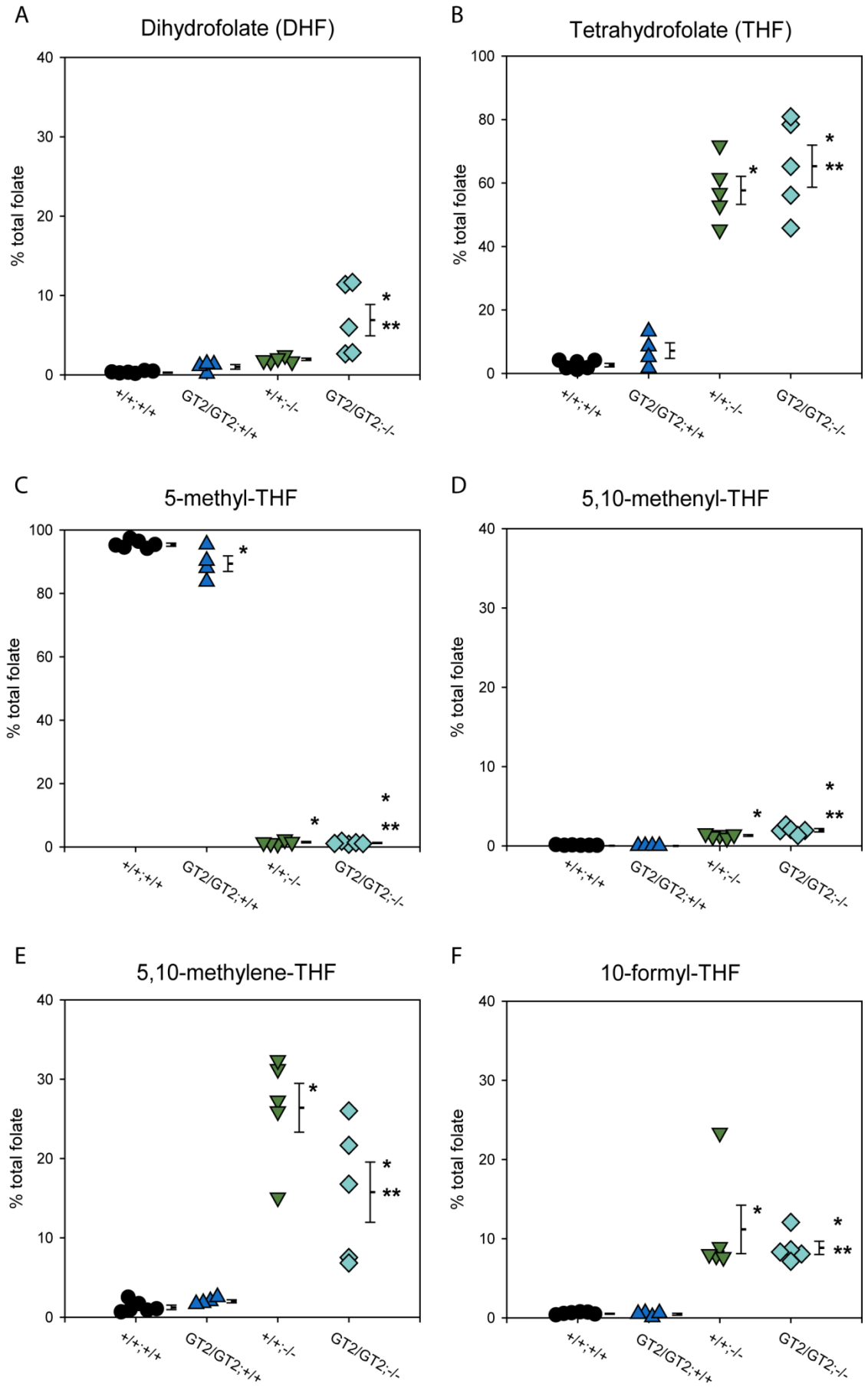

Figure 40. Folate profiles of *Gldc*^{GT2}*;Mthfr* double mutants.

4.2.3.6. Effect of anti-helminthic treatment on *Gldc*^{GT2} mutants

Due to a pinworm outbreak in the animal facility, all mice were subjected to treatment with fenbendazole in their food pellets over a 3-month period. Fenbendazole is a common, broad-spectrum, anti-helminthic drug for laboratory rodents which has been reported as safe for life-long treatment of the animals but may have tumour promoter effects (e.g. by inducing expression of specific cytochrome isoforms such as 1A1, 1A2, and 2B1) in combination with other triggers and possible myelosuppression (Villar et al., 2007). However, no immunosuppressive, reproductive, or teratologic effects from therapeutic doses of fenbendazole have been reported in rodents to date (Villar et al., 2007).

Litters from *Gldc*^{GT2} heterozygous crosses that were collected during this period (where female mice consumed fenbendazole-containing diet prior to and during pregnancy until litters were collected) were analysed separately and their incidence of NTDs is reported in **Table 21** below. There was a significant increase in the frequency of NTDs from 56.5% among 62 mutant embryos collected pre-treatment (as reported in **Chapter 3**) to 100% among 16 embryos when the dams were on fenbendazole treatment (Z-test, P = 0.002).

When the mice were taken off fenbendazole treatment and returned to their normal diet, the rate of NTDs in *Gldc*$^{GT2/GT2}$ mutants fell to an average of 84% (n = 38 mutants) (**Table 22**). While this is a reduction from the complete NTD penetrance when on fenbendazole, it remained significantly higher than the original rate from data collected prior to fenbendazole treatment (Z-test, P = 0.009). This indicates that fenbendazole may have persisting effects on *Gldc*^{GT2} dams and/or their oocytes, even after they have been taken off the treatment. To definitively assign the change in NTD rates to fenbendazole treatment, it will be necessary to test whether the NTD frequency returns to pre-treatment levels in subsequent generations of mice and then to analyse sets of treated and untreated litters in parallel.

As indicated in **Table 23**, exencephalic *Gldc*^{GT2} mutants often exhibited split face and/or truncated forebrains similar to that reported prior to fenbendazole exposure in **Chapter 3**. Craniofacial phenotypes were also observed in embryos/foetuses collected at E14.5 to E17.5 after the fenbendazole treatment period (**Figure 41**), most commonly split face with the upper jaw splayed apart at the midline and a relatively normal lower jaw (**Figure 41C', I'**). A smaller cleft was also observed in one E17.5 mutant foetus (**Figure 41H'**).

Stage (E-)	No. of litters	No. of NTDs/ Total no. of embryos (% NTD)		
		Gldc$^{+/+}$	*Gldc*$^{GT2/+}$	*Gldc*$^{GT2/GT2}$
11.5	9	0/21	2/39 (5.1%)	10/10 (100%)
15.5	2	0/2	0/8	3*/3 (100%)
17.5	2	0/8	0/8	3/3 (100%)
TOTAL	**13**	**0/31**	**2/55 (3.6%)**	**16/16 (100%)**

Table 21. Incidence of NTDs in fenbendazole-treated *Gldc*^{GT2} embryos.

* 2 exencephaly, 1 craniorachischisis

Stage (E-)	No. of litters	No. of NTDs/ Total no. of embryos (% NTD)		
		Gldc$^{+/+}$	*Gldc*$^{GT2/+}$	*Gldc*$^{GT2/GT2}$
11.5	7	0/13	2/33 (6.1%)	10/15 (67%)
14.5	4	0/7	1/24 (4.2%)	7/7 (100%)
15.5	2	0/2	0/7	6/6 (100%)
16.5	2	0/2	0/4	-
17.5	3	0/10	0/12	9*/10 (90%)
TOTAL	**18**	**0/34**	**3/80 (3.8%)**	**32/38 (84%)**

Table 22. Incidence of NTDs in *Gldc*^{GT2} embryos after fenbendazole treatment.

* 8 exencephaly, 1 craniorachischisis

Stage (E-)	No. with craniofacial defects/ No. of exencephalic mutants (%)	
	***Gldc*$^{GT2/+}$**	***Gldc*$^{GT2/GT2}$**
	During fenbendazole treatment period	
11.5	2/2 (100%)	7/10 (70%)
15.5	-	0/2
17.5	-	0/3
TOTAL	**2/2 (100%)**	**7/15 (46.7%)**
	After fenbendazole treatment period	
11.5	1/2 (50%)	5/10 (50%)
14/5	0/1	2/7 (28.6%)
15.5	-	2/6 (33.3%)
17.5	-	2/8 (25%)
TOTAL	**1/3 (33.3%)**	**11/31 (35.5%)**

Table 23. Incidence of craniofacial defects in exencephalic *Gldc*^{GT2} mutants during and after fenbendazole treatment.

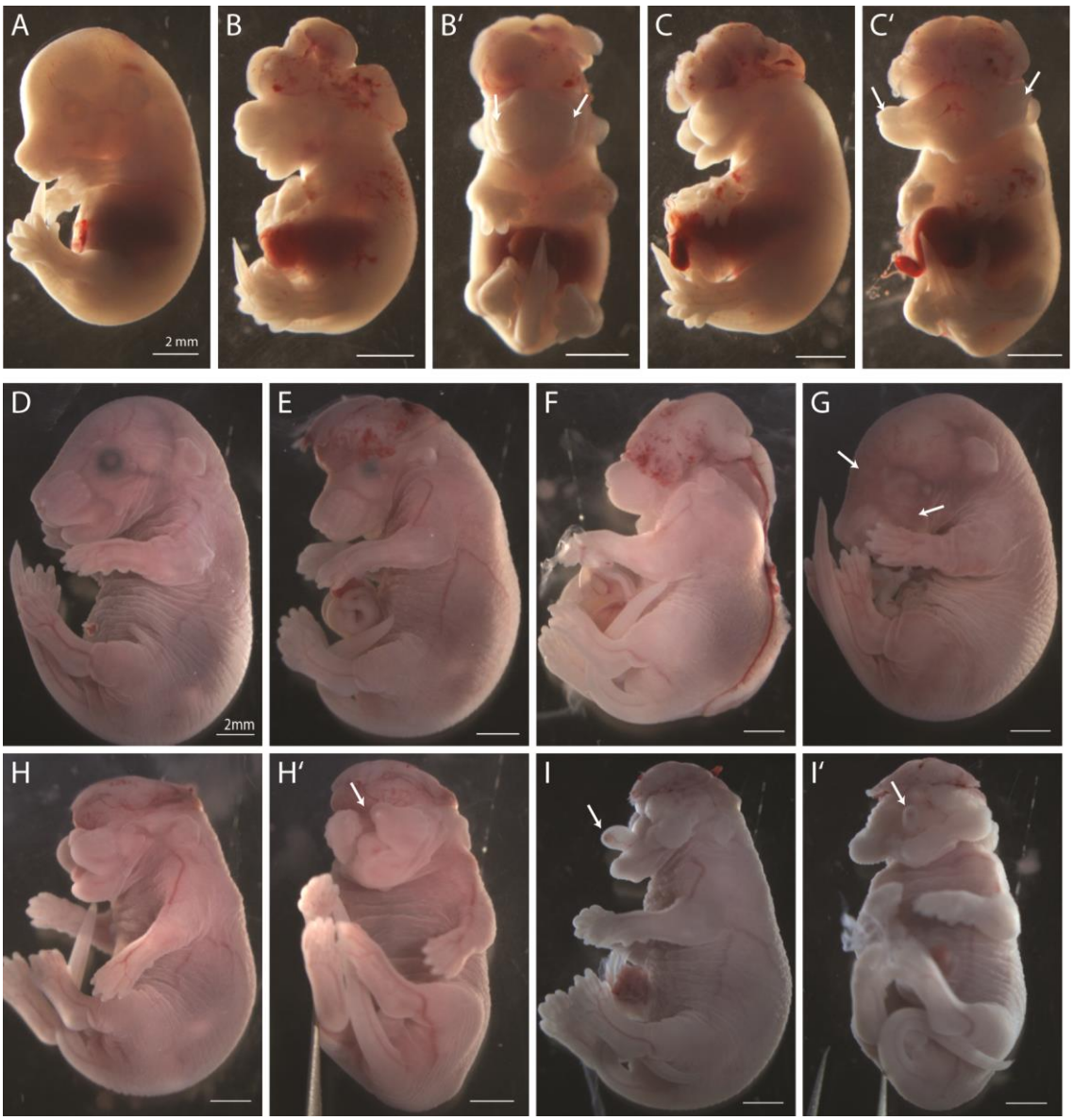

Figure 41. NTDs and craniofacial defects in E15.5 and E17.5 *Gldc*^{GT2} mutants collected after the period of fenbendazole treatment.

Wild-type *Gldc*$^{+/+}$ at E14.5 **(A)** and E17.5 **(D)** with normal head morphology. **(B, B')** E14.5 *Gldc*$^{GT2/GT2}$ mutant with exencephaly but normal face (arrows indicate normal upper jaw), and **(C, C')** exencephaly with split face (arrows indicate upper jaws splayed apart). E17.5 *Gldc*$^{GT2/GT2}$ mutant with exencephaly **(E)**, craniorachischisis **(F)**, facial haemorrhage (arrows) **(G)**, exencephaly with cleft upper jaw (arrow) **(H, H')**, and exencephaly with cleft face and proboscis (arrow) **(I, I')**.

4.3. Discussion

4.3.1. Biochemical profiles of *Gldc* deficiency

In silico predictions of hepatic folate metabolism carried out by Nijhout et al. (2006) reported that if all mitochondrial folate reaction velocities were set to zero (thus completely eliminating mitochondrial contribution), their model predicts a large reduction in activity of TYMS and AICART (i.e. in level of thymidylate and purine synthesis, respectively). In addition, MTHFD1 would favour its reverse reaction of converting 5,10-methylene-THF to 10-formyl-THF, thus causing THF levels to rise and 5-methyl-THF levels to drop. Consequently, homocysteine levels would rise due to reduced input into the methylation cycle but levels of methionine and SAM would be less affected.

Experiments in this chapter examined changes in folate metabolites resulting from elimination of GLDC both *in silico* and measured by LC/MS/MS. The data provide evidence for the importance of glycine cleavage contribution in maintaining sufficient formate pools for normal folate cycling.

However, there are several limitations to using the current *in silico* model for modelling *Gldc* deficiency during development. The model was constructed using values derived from known experimental results and cannot account for unknown factors or predict novel elements in the pathway. In addition, it was built to model hepatic FOCM in adult tissue and there are some differences between hepatic and embryonic pathways (Dr Kit-Yi Leung, personal communication). If changes in FOCM parameters (as measured experimentally) were found that did not fit with theoretical *in silico* predictions, it would be more difficult to investigate hypothetical initial conditions that might bring about a particular, abnormal change.

The protocol used for assessing folate and amino acid profiles of *Gldc*-deficient embryos in this chapter also has its limitations. E11.5 embryos were used because it is the earliest post-neurulation stage with sufficient material for reproducible measurements of single embryos. Ideally, neurulation-staged embryos at E8.5-E10.5 should be used to confirm that the abnormal folate profiles were present during neurulation. *Gldc* mRNA is restricted to specific tissues during neurulation (as shown by *in situ* studies in **Chapter 3**) and the Gldc enzyme is only localised in mitochondria. Thus, it is possible that the measured changes, from whole embryos, are of lesser magnitude as actually occurs *in vivo* in Gldc expressing cells due to dilution effects of surrounding tissue where *Gldc* is not expressed. Biochemical essays done on whole embryos would be less sensitive to changes occurring only in the mitochondrial fraction due to the presence of cytosolic content. In addition, a

recent study showed that mitochondria can maintain folate pools independent of, rather than in equilibrium with, cytosolic folates (Lawrence et al., 2014). A comparison of folate profiles between the mitochondrial and cytosolic fractions of *Gldc*-deficient embryos would be of interest to determine how the mutation influences 1C flux between mitochondria and cytosol.

Nevertheless, significant elevation of glycine levels at E11.5 indicates that glycine is not being sufficiently catabolised and thus accumulating to potentially toxic levels, and the changes in mutant embryo folate profile indicates a disturbance in their folate metabolism corresponding to a lack of 1C units which could affect FOCM outputs. Experiments with formate supplementation provide evidence that the latter biochemical perturbation (lack of 1C units) underlies the NTD phenotype in *Gldc*-deficient mutants.

4.3.2. Formate treatment and rescue

The effectiveness of formate in rescuing NTDs and normalizing folate profiles in *Gldc* homozygous mutant embryos strongly suggest that NTDs in *Gldc* mutants result from insufficient supply of 1C units for FOCM. This, combined with the observation that glycine levels were elevated in formate-treated, NTD-rescued embryos, argue against the possibility that the NTDs were a result of toxicity from elevated glycine levels.

Plasma formate levels in adult mice did not differ significantly between genotypes. It is possible that formate produced by the GCS is used in a cell-autonomous fashion and thus contribute little to circulating formate levels and/or that circulating formate is not a good indicator of cellular levels. Moreover, in terms of neural tube closure it is the cellular levels in the embryo that are crucial. Maternal formate supplementation could be protective by providing an excess of non-mitochondrial derived formate to be taken up by the cells in the embryos, as formate is rapidly transferred from maternal to foetal circulation (Hutson et al., 2013). In addition, formate levels were found to be much higher in foetal lamb plasma and amniotic fluid compared to maternal plasma, suggesting that there is higher demand for formate during developmental stages (Washburn et al., 2015).

Formate metabolism is dependent on hepatic FOCM: conversion of THF to 10-formyl-THF oxidises formate. In folate-deficient conditions, circulating formate levels are known to be elevated (Lamarre et al., 2012, Lamarre et al., 2013). This finding was replicated in *Gldc* mice fed with a folate-deficient diet which also showed increase in plasma formate levels. As folate deficiency does not exacerbate NTD incidence, the “limiting factor” precipitating the phenotype is probably 1C units rather than the folate cofactors themselves, and that

depressing the levels of folates produces excess 1C units that enter circulation. This inference also implies that treating *Gldc* mutant mice with folic acid, a non-1C unit-carrying synthetic folate, would not rescue their NTDs. Indeed, *Amt* knockout mice (also deficient in glycine cleavage) were not rescued by folic acid, but supplementation with methionine, a source of 1C units and precursor to SAM in the methylation cycle, was able to reduce their NTD rate from almost 90% to 60% (Narisawa et al., 2012). It would be of interest to test whether there is a protective effect of methionine in *Gldc*-deficient embryos.

How could a 1C shortage subsequently result in NTDs? From a biochemical perspective, the disruption in FOCM could lead to disrupted methylation or impaired nucleotide synthesis. Formate supplementation is hypothesised to act by increasing 1C unit pools. Normalisation of folate profiles was observed, but it is not yet clear how the 1C units were distributed upon entering FOCM and the level of flux into various FOCM outputs cannot yet be distinguished. However, several indirect observations were made that argue in favour of nucleotide synthesis being the affected downstream pathway of FOCM which is corrected by formate supplementation.

The finding that SAM/SAH ratio in *Gldc*-deficient mutants did not differ significantly from wild-types suggests that the methylation cycle is unperturbed by the loss of 1C units. SAM/SAH ratio alone does not completely rule out absence of a methylation defect, as any additional factors affecting levels of methionine or homocysteine could potentially distort the ratio. For example, changes in the transsulfuration pathway which is an alternative route for homocysteine catabolism (Blom, 2009), or degree of self-regulation via negative feedback loops and other enzymes such as BHMT and glycine *N*-methyltransferase to compensate for reduced 5-methyl-THF levels from the one-carbon cycle. Additional experiments such as directly measuring global DNA methylation, for example, would be needed. Other observations on the effect of formate treatment (see below) and that the presence of an *Mthfr* null mutation in *Gldc*-deficient mice does not worsen the phenotype (discussed in **Section 4.3.4**), would argue against methylation being causative.

In addition to addressing the 1C shortage and conferring phenotype rescue, formate also corrects growth delay and normalises cellular proliferation in the hindbrain neural tube of *Gldc*-deficient mutants. Proliferation defects in *Gldc* embryos could result from impaired nucleotide production which formate treatment would presumably be capable of correcting. However, as proliferation defects could simply be a marker of perturbed FOCM and as formate treatment could potentially correct all downstream FOCM pathways by correcting FOCM, whether the proliferation defect *causes* the NTDs is not satisfactorily shown.

Further studies could include, for example supplementation of *Gldc* mutants with labelled formate to directly measure the amount of labelled 1C units in nucleotides. Nucleotide supplementation has been shown to be effective in rescuing NTDs in the folic acid-resistant *curly tail* model by incorporation into embryonic DNA and stimulation of cellular proliferation (Leung et al., 2013). Thus, it would be interesting to perform supplementation of *Gldc*-deficient mice with nucleotides to attempt a rescue of proliferation but without correcting the 1C shortage (i.e. bypassing FOCM entirely). Observing a lowering of NTD incidence would provide experimental evidence to support proliferation as the causative factor.

Nucleotide treatment has, in fact, been attempted in the *Amt* model: *Amt* knockout mice were supplemented with thymidylate (dTMP) but interestingly this did not rescue their NTD phenotype (Narisawa et al., 2012). Perhaps a higher dose of dTMP or dTMP in combination with another purine or pyrimidine precursor is required to stimulate sufficient increase in proliferation. It was reported that the highest levels of rescue conferred by nucleotide treatment in the *curly tail* mouse were achieved with combined thymidine and adenine, or thymidine and guanosine monophosphate (GMP) treatment (Leung et al., 2013).

Some evidence from cancer studies also lends support to *GLDC*'s capabilities in affecting proliferation. *GLDC* retroviral knockdown in A549 cells resulted in a proliferation defect that could be rescued by sarcosine, an alternative 1C donor. However, knockdown in normal HLF cells did not cause a proliferation defect (Zhang et al., 2012).

4.3.3. Formate toxicity

Formate-treated *Gldc* embryos displayed signs of toxicity (snout defect, haemorrhage and oedema) when collected at stages E15.5 and E18.5. In other wild-type embryos (i.e. not litters from $Gldc^{GT1}$ inter-crosses) from the C57BL/6 background strain, supplementation with formate until E18.5 was also found to produce haemorrhage and oedema among 33% of foetuses, compared to no toxic signs in untreated wild-types (Sonia Sudiwala, personal communication). This implies that the haemorrhage and oedema, present in all genotypes of $Gldc^{GT1}$ embryos, were precipitated by long-term formate exposure. However, the snout phenotype only appeared in $Gldc^{GT1}$ mutants (both homozygotes and heterozygotes), and might be an uncharacterised abnormality of *Gldc* deficiency, perhaps a less severe form of the craniofacial defects observed among $Gldc^{GT2}$ foetuses. More E15.5-E18.5 formate-treated litters would need to be analysed to investigate this possibility.

The precise mechanism underlying pathology of formate toxicity in developing embryos is currently unclear. The fact that the toxic effects were only observed at late stages rather than at neurulation stages would suggest a cumulative effect in the embryos of formate-treated dams. This is supported by reports of formate being elevated in foetal lamb plasma and amniotic fluid which persisted in newborn up to 8-week-old lambs (Washburn et al., 2015). The potentially toxic effects of formate are possibly another reason why circulating formate levels appear to be at low levels in wild-type mice (and why embryos would not benefit from a maternal supply of formate when not supplemented).

Although formate can also be broken down to water and carbon dioxide by the catalase enzyme, the occurrence of formate and methanol toxicity would suggest that catalases do not play a major role in formate metabolism. In addition, the primary role of catalases is in breakdown of reactive oxygen species like hydrogen peroxide (Zamocky et al., 2008) and not formate, despite formate's ability to bind stably to catalases (Loewen et al., 2004).

Formate toxicity is commonly studied in the context of methanol poisoning, as methanol break down yields formaldehyde and subsequently formate. In vitro studies have shown that formate, given in doses of 0.5 mg/mL to 8 mg/mL, significantly affects embryo viability in a dose-dependent manner in rat but not mouse embryo culture systems (Harris et al., 2004, Hansen et al., 2005), and that it causes neuronal cell death in rat hippocampal slice cultures (Kapur et al., 2007). It is hypothesized that in methanol poisoning, formate induces toxic effects by causing acute metabolic acidosis due to insufficient levels of hepatic THF to cope with the increase in formate production (Tephly, 1991).

Despite the association of formate with toxic effects, calcium formate is used as a supplement, to supply calcium. It is possible that a "safe" dose of calcium formate would provide sufficient 1C units to ameliorate neural tube closure defects without causing toxic effects, particularly if treatment was not continued beyond neurulation stages. It will be interesting to carry out pilot experiments in mice to test whether cessation of formate supplementation after neural tube closure is complete can prevent NTDs without causing any subsequent abnormalities.

4.3.4. Interaction of the *Mthfr* mutation with *Gldc* deficiency

The action of Mthfr, which irreversibly catalyses conversion of 5,10-methylene-THF to 5-methyl-THF, can determine whether the 1C unit in 5,10-methylene-THF is irreversibly shunted towards the methylation cycle or towards nucleotide synthesis. If the methionine cycle is disrupted (for example in B12 deficiency where methionine is not synthesized) a

functioning Mthfr could cause accumulation of 5-methyl-THF and hypothetically deplete the amount of other folates entering nucleotide biosynthesis. This is known as the "methyl trap" (Beaudin and Stover, 2007).

Mthfr is the only FOCM enzyme whose action is unidirectional. Hence, when Mthfr function is disrupted, 5,10-methylene-THF accumulates but is not "trapped" and can participate in other FOCM reactions. Litters from a *Gldc*$^{GT2/+}$;*Mthfr*$^{+/-}$ double heterozygous cross revealed that NTD incidence did not increase when the *Mthfr* null mutation was introduced to *Gldc*^{GT2} mutants. The folate profiles of *Gldc*$^{GT2/GT2}$;*Mthfr*$^{-/-}$ double homozygous mutant embryos is consistent with the hypothesis that the *Mthfr* mutation, by blocking flow of 1C units into methylation, is making available more 1C units for other FOCM outputs such as nucleotide synthesis. While the numbers of compound mutant embryos generated so far are insufficient to produce statistically significant results, the gene dosage/phenotype pattern observed shows a lower rate of NTDs with increasing numbers of *Mthfr* null alleles, suggesting a possible protective effect rather than exacerbating. Metabolic tracer studies using labelled 1C units would be required to confirm the ultimate fate of the 1C units that are shunted away from methylation. This experiment indicates that the *Mthfr* mutation does not increase risk of NTDs caused by 1C unit insufficiency, and also provides additional evidence that disrupted methylation is unlikely to be the cause of NTDs in *Gldc*-deficient embryos.

This finding may have implications in human populations carrying both mutations. Variants in GCS genes that produced significantly decreased GCS activity were found in NTD patients, and the 677C>T polymorphism in *MTHFR* is an NTD risk allele in some populations. It is possible that the 677C>T polymorphism is not directly causative in populations where an association with NTDs was found, but that it acts in combination with another NTD risk factor, which is not a GCS enzyme mutation. This implies that if both a 677C>T polymorphism and a GCS gene mutation are present together, this might paradoxically confer a protective effect. These findings highlight the difficulty of interpreting data from association studies that consider only one gene at a time.

4.3.5. Effect of fenbendazole on phenotypes resulting from *Gldc* deficiency

Fenbendazole produces its anti-helminthic effect by selectively binding β-tubulin to inhibit polymerisation of microtubules, thus disrupting mitotic spindle formation and mitosis in helminths, but is reported to show little effect on mammalian microtubules (Lacey, 1990). Concerns have been raised about its potential effects on the mammalian host. It has been shown to induce mitotic arrest at metaphase in human lymphocyte cultures (Holden et al.,

1980), decrease proliferation of splenic B lymphocytes in mice (Landin et al., 2009), and exacerbate acetaminophen (an analgesic drug)-induced hepatotoxicity by prolonging suppression of hepatic glutathione (Gardner et al., 2012).

The complete penetrance of NTDs upon exposure to fenbendazole in *Gldc*$^{GT2/GT2}$ homozygous mutants but not wild-type mice indicates an interaction between fenbendazole and the *Gldc* mutation. In addition, the rate of exencephalic mutants with the split face and/or forebrain truncation phenotype rose from 9% pre-fenbendazole (reported in **Chapter 3**) to 53% (9 out of 17 total exencephalic *Gldc*$^{GT2/+}$ and *Gldc*$^{GT2/GT2}$ mutants, **Table 23**) in litters collected during the exposure period. Fenbendazole may have a non-appreciable effect on wild-type mice with robust FOCM, but produce a synergistic worsening of a phenotype that is caused by 1C depletion. This observation is in striking contrast with the folate-deficient diet treatment (**Figure 32**), which was a contemporaneous gene-environment interaction study that did not exacerbate NTDs in the *Gldc*^{GT1} model.

It should be noted that these observations were not results of a parallel controlled experiment, and thus the effects of other environmental factors cannot be completely ruled out. However, *Gldc*$^{GT2/GT2}$ mutant embryos without NTDs were successfully retrieved after the mice were returned to a normal diet, which strongly indicates that fenbendazole was responsible for the phenotype exacerbation. The incidence of exencephaly with split face and/or forebrain truncation also reduced to 35% (12 out of 34 total exencephalic *Gldc*$^{GT2/+}$ and *Gldc*$^{GT2/GT2}$ mutants, **Table 23**). The severe split face phenotype observed in several mutants collected at E14.5-E17.5 is most likely a later phenotype corresponding to progression of the split face and/or forebrain truncation observed at E10.5-E11.5, rather than a unique defect induced by fenbendazole.

5. *Gldc*^{GT1} mouse as a model for non-ketotic hyperglycinemia

5.1. Introduction

The relatively low penetrance of NTDs in the *Gldc*^{GT1} model allowed for sufficient homozygous mutants to survive to birth, weaning, and adulthood. In this chapter, post-natal characterisation of the *Gldc*^{GT1} model was carried out to assess its suitability as a model for classical NKH. Hypotheses for the pathology of NKH as well as NKH-associated brain malformations are thus reviewed below.

5.1.1. Pathology of NKH

Glycine (and D-serine) along with glutamate are co-agonists for NMDAR activation. Glycine also binds to glycinergic receptors (GlyR) to produce a postsynaptic inhibitory response. NMDAR activity has been linked to seizures in various experimental models, and antagonists of NMDAR glycine binding sites have been used as antiepileptic drugs (Lason et al., 2013). The mediator role of GABA and GlyR in cation-chloride cotransporter mechanisms have been similarly implicated in seizure activity (Blaesse et al., 2009). NMDAR signalling is involved in both cell death and cell survival, by promoting neuronal survival and antioxidant defences as well as inducing neuronal cell death via mitochondrial apoptosis in neuropathological states (Hardingham and Bading, 2003, Hardingham and Bading, 2010).

In NKH patients, it is thus reasonable to assume that the excitatory effect of glycine on NMDARs is the cause to the intractable seizures, and the inhibitory effect on GlyRs in the brain stem and spinal cord is causing the apnea, hypotonia, and hiccupping symptom (Korman et al., 2006). Sakata et al. (2001) studied the expression pattern of GCS genes in adult rat brains and noted the many overlaps in expression patterns with that of NMDAR complexes, suggesting that GCS may be regulating concentrations of glycine near NMDARs. Administration of high doses of sodium benzoate to NKH patients in order to sequester glycine is a common treatment course which generally helps ameliorate seizures. When sodium benzoate therapy was stopped in a late-onset NKH patient, her seizures recurred

(Van Hove et al., 1998). High levels of glycine have also been demonstrated to induce hyperexcitability of NMDARs in hippocampal slice cultures, resulting in neurotoxicity and consequently cell death (Newell et al., 1997). The toxic effect of high glycine could then be prevented by blocking NMDAR activation with 7-chlorokynurenic acid, a competitive glycine site antagonist (Barth et al., 2005).

There is also evidence of contributions from pathways that do not involve NMDAR or GlyR signalling in the pathology of NKH. Ichinohe et al. (2004) observed that the brain malformations in NKH patients are mainly hypoplastic in nature (such as atrophy of white matter and agenesis of the corpus callosum) and hypothesised that they may be a result of impaired proliferation and differentiation of neural progenitor cells (NPCs). They showed that *Gldc* and *Amt* mRNA and protein are highly expressed throughout the developing rat brain and in neurogenic areas of the adult rat brain, and suggested that the GCS's participation in folate metabolism, which links to cellular proliferation, may be the underlying pathway being affected.

Some *in vitro* evidence suggests that glycine may be contributing to NKH pathology via oxidative stress pathways. The addition of glycine to wild-type, rat cerebral cortex homogenates resulted in increased levels of markers of lipid peroxidation and decreased levels of glutathione (primary antioxidant in the brain) in a dose-dependent manner, indicating that glycine provokes lipid oxidative stress damage (Leipnitz et al., 2009). The same group later found that glycine suppresses activity of several mitochondrial enzymes including citrate synthase [but not other enzymes in the tricarboxylic acid (TCA) cycle], complexes I-III, II, and II-III of the electron transport chain, and creatine kinase in the rat cerebral cortex, and also suppresses Na^+,K^+-ATPase activity of synaptic plasma membranes (Busanello et al., 2010). They hypothesised that the inhibition of creatine kinase and Na^+,K^+-ATPase are a response to glycine-induced oxidative damage. These findings would seem contradictory to the contribution of glycine as one of the amino acids utilised in synthesis of the glutathione tripeptide molecule, the other major amino acids being glutamate and cysteine (Aoyama et al., 2012).

5.1.2. Expression analysis of GCS genes in rat brains

To better understand the neuropathology of NKH, an expression analysis of *Gldc*, *Amt*, and *Gcsh* mRNA and protein in adult rat brain was performed by Sakata et al. (2001), followed by a more thorough study in developing and adult rat brains by Ichinohe et al. (2004). GCS genes, especially *Gldc*, are most intensely expressed in highly proliferative and neural progenitor regions. In E15 and E18 rat brains, all three genes were highly expressed in the

neuroepithelium surrounding the lateral and fourth ventricles and the aqueduct, as well as in the external granular layer of the cerebellum. At P7 and P14 post-natal stages, intense expression of *Gldc* was found in the olfactory bulb, subventricular zone, throughout the rostral migratory stream, the dentate gyrus, and the external granular and Purkinje cell layer of the cerebellum (Ichinohe et al., 2004).

In addition, *Gldc* is co-expressed with nestin-expressing NPCs during foetal development, and then later with GLAST (an astrocyte-specific glutamate-aspartate transporter) in radial glial cells of the subventricular zone and Bergmann glia of the cerebellum of adult rat brain. It is hypothesized that the GCS genes are providing 1C units for proliferation of NPCs as well as regulate glycine concentration for proper function of NMDAR, and thus disruption in these genes results in the hypoplastic brain malformations and recurring seizures in NKH patients (Ichinohe et al., 2004).

At 7- or 8-week adult stages, GCS genes remained highly expressed in the olfactory bulb, dentate gyrus, and cerebellar Purkinje and granular cell layer. Expression was also found in glial cells of the corpus callosum and glial-like cells of all layers of the cerebral cortex, with *Gcsh* showing additional expression in neuronal layers. Examination of the spinal cord revealed abundant expression of *Amt* and *Gcsh* in grey matter (Sakata et al., 2001).

5.1.3. Treatment options

Effective treatment of NKH does not exist; measures are taken to decrease glycine levels by administration of sodium benzoate (which conjugates glycine and secretes it out) to varying degrees of success, as glycine levels tend to return to pathological levels when treatment is stopped. Treatment with strychnine, an inhibitor of GlyR, has been tested and found to be of little clinical value (von Wendt, 1979, von Wendt et al., 1980). On the other hand, treatment with NMDAR antagonists such as dextromorphan and ketamine is able to ameliorate seizures and improve EEG findings in most patients. They have also been noted to improve hypotonia and prevent apnea, which are attributed as GlyR inhibitory signs (Kure et al., 1997, Korman et al., 2006, Suzuki et al., 2010).

Anticonvulsants such as phenobarbitone and diazepam are also used alongside NMDAR antagonists for seizure control. The use of valproic acid, on the other hand, is contraindicated, as valproic acid inhibits the GCS and results in hyperglycinemia and hyperglycinuria in non-NKH, epileptic patients (Mortensen et al., 1980). With NKH patients, administration of valproic acid results in worsening of symptoms, most notably severe chorea and increased seizure activity (Hall and Ringel, 2004, Morrison et al., 2006,

Tsuyusaki et al., 2012). Korman et al. (2006) reported that immediate treatment, before the onset of symptoms, of prenatally diagnosed NKH with benzoate and ketamine was able to delay onset but cannot prevent severe long-term progression of the disease.

Treatments using precursors of 5,10-methylene-THF and providers of 1C units such as Leucovorin (i.e. 5-formyl-THF, or folinic acid), folic acid, serine, methionine, choline, and sodium formate have been tried but none proven clinically beneficial (Van Hove et al., 1998, Trijbels et al., 1974, Wijburg et al., 1988, De Groot et al., 1970, Tada et al., 1969). However, these treatments were mostly performed on single patients and thus the lack of clinically beneficial findings may simply be due to insufficient testing. Only one study found that providing 10-fold amount of methionine in addition to a serine- and glycine-free diet to one NKH patient was able to decrease plasma glycine levels, but glycine levels returned to pathological levels once treatment was stopped (De Groot et al., 1970).

5.1.4. Corpus callosum genesis and agenesis

The corpus callosum is the largest white matter tract in the brain, crossing the longitudinal fissure and connecting the left and right hemispheres. It allows for inter-hemispheric sensory and motor communication and is implicated in cognitive functions (Edwards et al., 2014).

The genesis of the corpus callosum must first be preceded by *Fgf*- and *Shh*-guided patterning of the midline and commissural plate (Smith et al., 2006a, Hayhurst et al., 2008), followed by secretion of axon guidance cues and correct specification of neurons to become callosal projection neurons (Fame et al., 2011). At E15.5 in a mouse brain, neurons arising from the cingulate cortex cross the midline and enter the contralateral cortex, "pioneering" a path for commissural neurons soon to follow (Rash and Richards, 2001). At E17, the first callosal neurons arise from layer II/III, VI, and V of the cerebral cortex and follow the path of the pioneer neurons. Guidance cues are provided by midline glial structures secreting attractive/repulsive signalling molecules (e.g. Semaphorin 3C), GABAergic and glutamatergic neuronal populations in the corpus callosum, Eph/ephrin signalling between callosal axons and midline structures, and repulsive cues between axons from the medial and lateral cerebral cortices (Niquille et al., 2009, Nishikimi et al., 2013, Edwards et al., 2014). Callosal axons that have crossed respective contralateral hemispheres form synapses with postsynaptic neurons, some of which are transient connections. Reshaping of the axons then follows, in which specific axonal connections are permanently established while excess neurons are eliminated (Innocenti and Price, 2005).

Agenesis of the corpus callosum (ACC) is a rare congenital disorder that can occur in isolation or in association with other neuropathological disorders. It arises when some of its developmental mechanisms are disrupted, and can manifest as complete absence of any callosal fibres, partial agenesis with a shorter anterior-posterior length, or hypoplasia/thinning (Edwards et al., 2014). ACC caused by disrupted axonal guidance may result in rerouting of neurons to form longitudinal bundles in the ipsilateral cortex, i.e. Probst bundles. More recently, asymmetrical connections between the frontal lobe and contralateral occipital and/or parietal lobes have also been found in partial ACC patients (Tovar-Moll et al., 2007). While ACC by itself is not a life-threatening condition, it has been associated to a number of brain abnormalities, neurological dysfunctions, and behavioural disorders, including micro and macrocephaly, epilepsy, schizophrenia, and ADHD. The majority of ACC cases are so sporadic that genetic studies are difficult and about 68% of cases have unknown causes (Schell-Apacik et al., 2008, Siffredi et al., 2013).

The occurrence of ACC has been noted in various metabolic and/or mitochondrial disorders including NKH, pyruvate dehydrogenase deficiency (Lissens et al., 2000), fumarase deficiency (Coughlin et al., 1998), and leukoencephalopathy in which a disruption in complex I, II or IV of the electron transport chain is present (Sofou et al., 2013). While a direct link between the two is unclear, occurrences of ACC in these cases are hypoplastic in nature and are likely secondary to general white matter loss.

5.1.5. The ventricular system and hydrocephalus

In higher vertebrates, as the closed neural tube starts to differentiate to distinct regions of the brain, the ventricular system begins as fluid-filled cavities known as the telencephalon, mesencephalon, and rhombencephalon. These cavities then develop into two lateral ventricles, the third ventricle, and the fourth ventricle. The cerebrospinal fluid filling the cavities are produced in the choroid plexus, predominantly in the lateral ventricles, flow through the foramen of Monroe into the third ventricle, enter the fourth ventricle via the aqueduct of Sylvius, and drain out into the subarachnoid space. The ventricular walls are covered in a layer of specialized epithelial cells known as ependymal cells. These cells have motile (9+2 configuration) cilia which contribute to the directionality of CSF flow (Fliegauf et al., 2007, Perez-Figares et al., 2001).

When the flow of CSF is disrupted, causing a build-up of fluid within the ventricular system, this results in a condition known as hydrocephalus that presents at, or shortly after, birth. Hydrocephalus is a common complication seen in other central nervous system pathologies such as NTDs, intra-ventricular and subarachnoid haemorrhages,

tumours, and infections, although the precise pathological mechanisms that precipitate it are not always known. It is also difficult to distinguish between brain damage that is causative of hydrocephalus or that occurs as a consequence of the stretching of the ventricular walls and compression of surrounding structures (McAllister, 2012).

In general, hydrocephalus is classified as being either communicating or non-communicating. Communicating hydrocephalus describes the presence of an obstruction within the ventricular system that blocks the flow of CSF, such as narrowing or closing of the aqueduct (i.e. aqueduct stenosis), or the presence of tumours within or adjacent to the ventricular wall. Non-communicating hydrocephalus refers to any impairment of flow distal to the ventricles, such as impaired absorption in the arachnoid vili, or Chiari malformations in which there is a downward displacement of the cerebellum into the foramen magna (Perez-Figares et al., 2001, Di Rocco et al., 2011). Hydrocephalus is also commonly found in cilia disorders such as primary ciliary dyskinesia (PCD) and Bardet-Biedl Syndrome (Fliegauf et al., 2007). In rare cases, it can be caused by excessive production of CSF, such as in choroid plexus papilloma (Fujimoto et al., 2004).

Hydrocephalus was first reported in one out of eight NKH patients studied by Van Hove et al. (1998), followed by a more thorough report on four patients (Van Hove et al., 2000). All four presented with absence or thinning of corpus callosum, very delayed or absent myelination, and presence of a posterior fossa cyst in their MRI scans. The cyst was not observed until onset of acute hydrocephalus, and appeared to enlarge as ventriculomegaly worsen. All cases had an acute onset between 2 to 6 months and required urgent shunting. With no evidence of impaired resorption of CSF by arachnoid vili, the report concluded that the presence of the cyst was the cause of an obstructive hydrocephalus in these patients. More cases of hydrocephalus with similar MRI findings was reported in 2009 (Yis et al., 2009) and in 2012 (Manel et al., 2012).

Parallels were drawn to the Dandy-Walker malformation, in which the cerebellar vermis is hypoplastic and cysts form in the fourth ventricle, subsequently resulting in hydrocephalus and enlargement of the posterior fossa (Treble-Barna et al., 2014, Basson and Wingate, 2013). The origin of the cyst, however, is not known. The occurrence of hydrocephalus in NKH patients is considered rare, with only 5 reported cases out of 62 patients reviewed by Hoover-Fong et al. (2004). It is generally associated with poor prognosis. Dobyns (1989) mentioned findings of ventricular enlargement in 5 out of 15 NKH patients that had been reported up until then. Flusser et al. (2005) also reported mild enlargement of ventricles accompanied by increased frontal subarachnoid fluid in atypical NKH patients which they diagnosed as external benign hydrocephalus. There was no follow-up data for patient outcome in either report.

5.2. Results

5.2.1. Mendelian ratios of post-natal *Gldc*^{GT1} and *Gldc*^{GT2} mutant pups

Heterozygous matings of *Gldc*$^{GT1/+}$ mice were performed and pregnant mice were left to litter down as described in **Chapter 3**. The litter information and Mendelian ratios of post-natal mice as genotyped at 10 days of age (P10) are summarized in **Table 24** below.

At P10, fewer numbers of *Gldc*$^{GT1/GT1}$ pups was observed than would be expected from Mendelian ratios (15 instead of 21), although this difference does not reach statistical significance (Z-test, P = 0.347). These litters were sacrificed at 5 weeks of age for collection of brain samples. Out of the 15 *Gldc*$^{GT1/GT1}$ mutant pups reported above, 6 mice (40%) developed acute hydrocephalus at varying ages between 10 days and 5 weeks.

	Gldc$^{+/+}$	*Gldc*$^{GT1/+}$	*Gldc*$^{GT1/GT1}$	Total
No. of pups at P10	20	49	15	84
Expected no. of pups (1:2:1)	21	42	21	84

Table 24. Ratio of genotypes of P10 *Gldc*^{GT1} mice from 15 litters.
Figures did not account for 2 pups (*Gldc*$^{+/+}$ and *Gldc*$^{GT1/GT1}$) found dead at P1, and 1 pup of unknown genotype.

Likewise, seven litters of *Gldc*$^{GT2/+}$ heterozygous crosses were similarly left to litter down and surviving pups were ear-clipped and genotyped at about P10. Litter information and Mendelian ratios are summarized in **Table 25** below. At P10, unlike with *Gldc*$^{GT1/GT1}$ pups, no surviving *Gldc*$^{GT2/GT2}$ pups was observed compared to the expected 11. This difference is significant (Z-test, P=0.001).

	Gldc$^{+/+}$	*Gldc*$^{GT2/+}$	*Gldc*$^{GT2/GT2}$	Total
No. of pups at P10	15	29	0	44
Expected no. of pups (1:2:1)	11	22	11	44

Table 25. Ratio of genotypes of P10 *Gldc*^{GT2} mice from 7 litters.

5.2.2. Survival studies and hydrocephalus incidence

As some *Gldc*$^{GT1/GT1}$ homozygous mutants were able to live past 6 weeks and found to be viable, homozygous matings were set up in order to expedite generation of mutants to study their survival rates and incidence of hydrocephalus. Several wild-type and heterozygous *Gldc*^{GT1} mice at similar date of births (within the same week) as the mutants were also followed up as age-matched environmental controls.

The survival curve of *Gldc*^{GT1} mice is shown in **Figure 42**. While all wild-type and heterozygous mutants survived to the end of the study (1 year from start of study), only 58% of homozygous mutants survived to adulthood (6 weeks) and 45% past 16 weeks onto a year. About 22% of the mutants developed hydrocephalus at any age between 3 and 13 weeks, with majority occurring between 5 and 7 weeks. The cause of the pre-natal deaths not attributed to hydrocephalus is not known; some of those pups were simply found dead in their cages without any obvious physical malformations or illnesses.

Hydrocephalic mice were recognizable by a characteristic dome-shaped head (**Figure 43A**) and had to be culled within 48 hours as the onset and deterioration of health was very rapid. Their craniums were noticeably enlarged (**Figure 43B**) and their skulls more brittle. Opening of the skulls revealed evident swelling of the brain and haemorrhage (**Figure 43C**). Histological examination of the brain revealed severely enlarged ventricles with obvious thinning of the cortex and distorted hippocampus (**Figure 43D, E**).

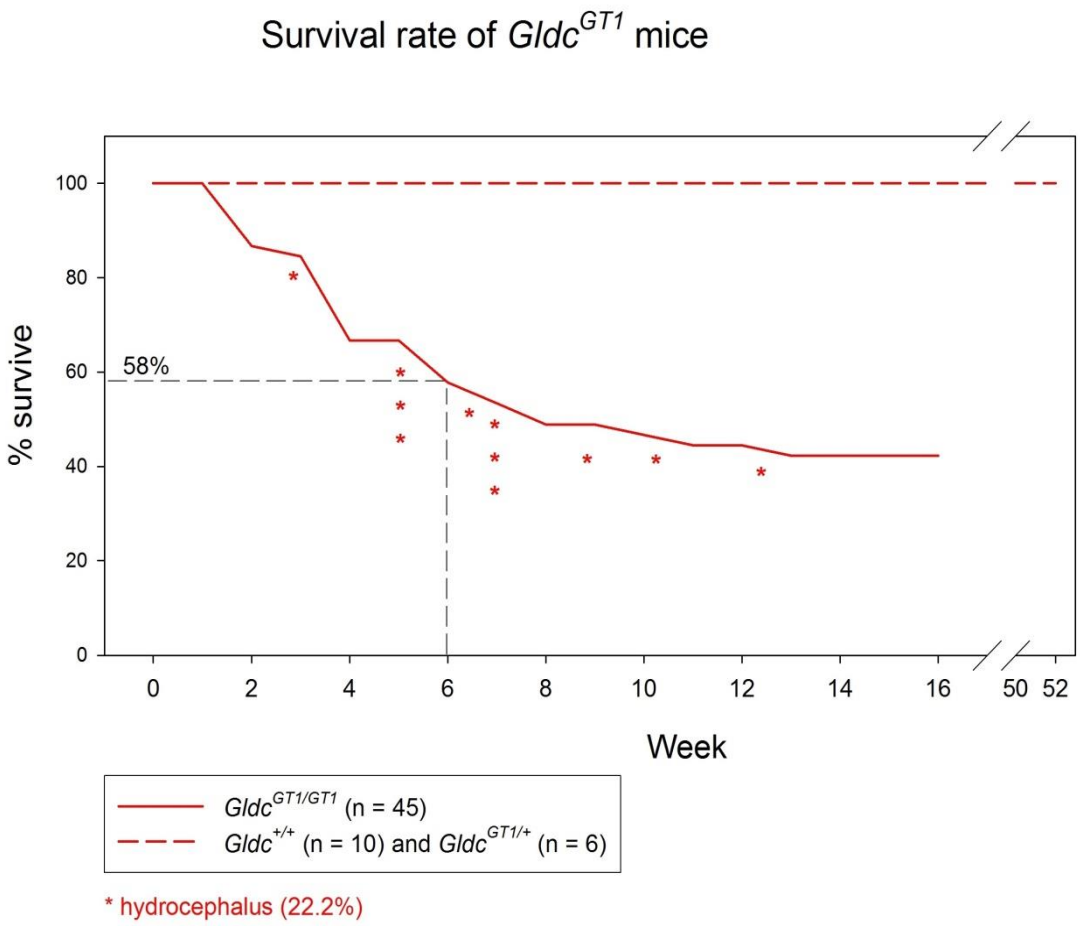

Figure 42. Survival curve of *Gldc^{GT1}* mice.

Only 58% of *Gldc$^{GT1/GT1}$* mice survived to 6 weeks of age, while no *Gldc$^{+/+}$* or *Gldc$^{GT1/+}$* displayed any early lethality. About 22% of *Gldc$^{GT1/GT1}$* mice developed acute hydrocephalus with varied ages of onset as indicated with (*).

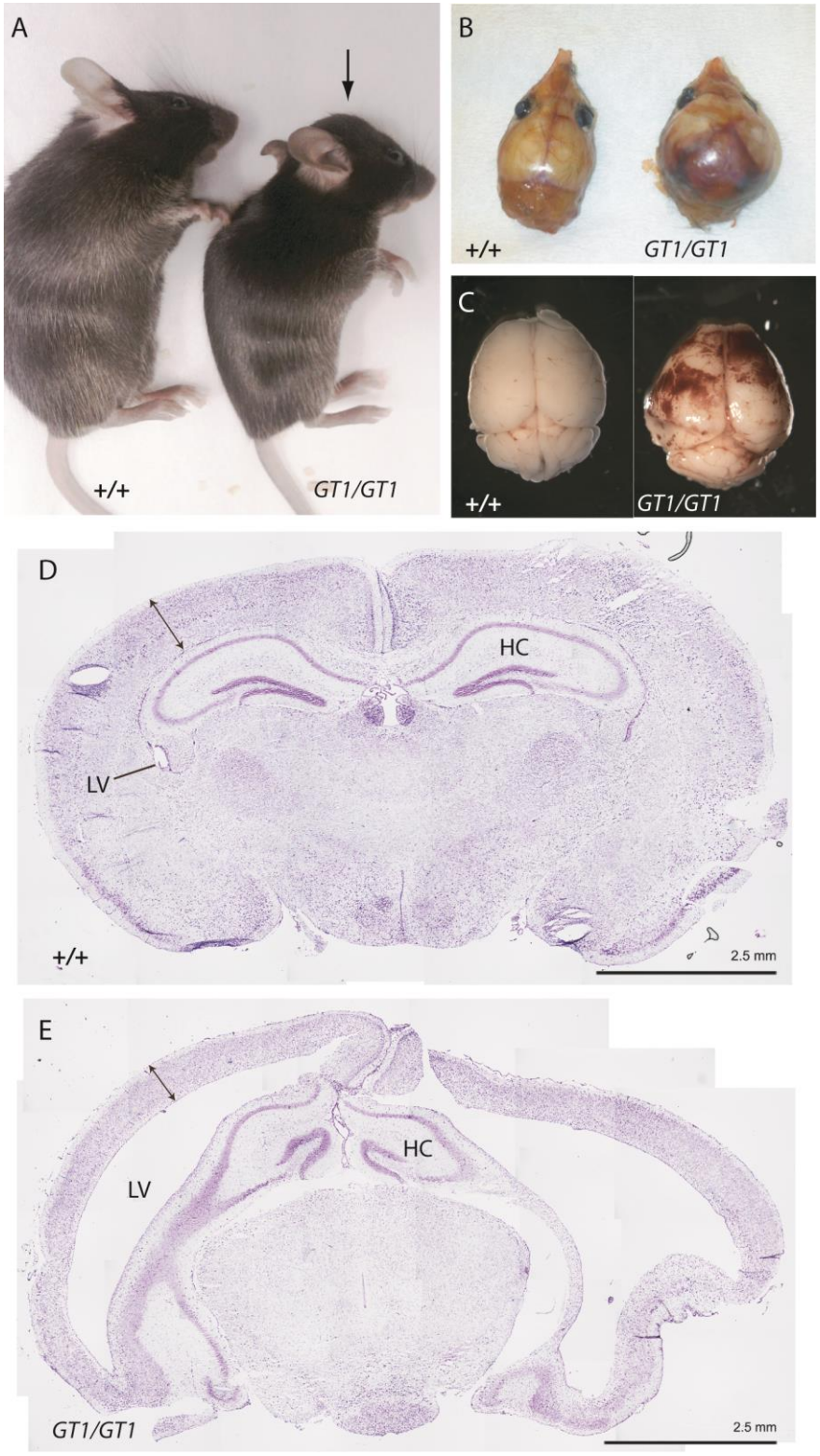

Figure 43. Hydrocephalus in *Gldc*$^{GT1/GT1}$ mice.

Gldc$^{GT1/GT1}$ mice with hydrocephalus, showing **(A)** dome-shaped head (arrow), **(B)** enlarged cranium, and **(C)** swelling and haemorrhage of the brain. Coronal sections through **(D)** wild-type and **(E)** hydrocephalic mutant brains revealed grossly enlarged lateral ventricles (LV), thinning of the neocortex (double-sided arrows), and a distorted hippocampus (HC) in the mutant brain. Sections were stained with cresyl violet.

As gender differences in NKH patients have been implicated (Hoover-Fong et al., 2004), the mutants used in the survival studies were sexed and the hydrocephalus and survival rates between the two genders are summarised in **Table 26** below. A higher percentage of males (65%, 13 out of 20 males) were able to survive to adulthood compared to females (33%, 7 out of 21 females), although this difference is not significant (Z-test, P = 0.082). Strikingly, all 10 hydrocephalic mice were female (Z-test, P < 0.001). The hydrocephalus phenotype is not exclusive to female *Gldc* mutants as male mutants not used for the survival study have been found with hydrocephalus.

	Hydrocephalic deaths	Non-hydrocephalic deaths before 6 weeks	Survive to 6 weeks	Total
Male	0	7 (35%)	13 (65%)	20
Female	10 (47%)	4 (19%)	7 (33%)	21
Unknown	0	4*	0	4

Table 26. Number of hydrocephalus, non-hydrocephalic deaths before 6 weeks, and survivors up to 6 weeks in *Gldc*$^{GT1/GT1}$ mice.

5.2.3. Elevated glycine in plasma and urine of *Gldc* mutant mice

The biochemical hallmark of NKH is elevation of glycine in body fluids, thus concentration of glycine (and other amino acids) in the plasma and urine of *Gldc* mutant mice was determined using ion-exchange chromatography and displayed in **Table 27** and **Table 28,** respectively (measured by Helen Prunty and Dr Simon Heales, Great Ormond Street Hospital for Children NHS Foundation Trust). Concentrations in the urine samples were normalised to creatinine levels as determined by LC/MS/MS (measured by Dr Kit-Yi Leung).

Similar to the changes found in E11.5 *Gldc* mutant embryos (**Chapter 4**), there was a significant increase in glycine levels in both the plasma and urine of *Gldc*$^{GT1/GT1}$ compared to *Gldc*$^{+/+}$ mice. Other amino acids of interest due to their role as 1C donors to FOCM are serine and threonine. Interestingly, threonine levels were decreased in both *Gldc*$^{GT1/+}$ and *Gldc*$^{GT1/GT1}$ plasma and urine, while serine levels were decreased in only the plasma of *Gldc*$^{GT1/+}$ and urine of *Gldc*$^{GT1/GT1}$ mice. In addition to those changes, *Gldc*$^{GT1/GT1}$ mice also showed elevation of aspartic acid and 3-histidine levels in their plasma, and decreased levels of leucine and isoleucine in urine.

Amino acid	Concentration in plasma (μmol/L)		
	Gldc$^{+/+}$ (n=3)	*Gldc*$^{GT1/+}$ (n=3)	*Gldc*$^{GT1/GT1}$ (n=3)
Alanine (ALA)	514.7 ± 40.4	472.7 ± 36.7	542.7 ± 35.9
Asparagine (ASN)	74 ± 6.4	62 ± 3.1	71.3 ± 2.9
Aspartic acid (ASP)	12 ± 0	15.3 ± 2.4	**21.3 ± 1.3***
Citrulline (CIT)	78 ± 13.6	71.3 ± 2.4	73.3 ± 4.8
Glutamine (GLN)	526.7 ± 67.1	526.7 ± 50.8	529.3 ± 48.2
L-glutamate (GLT)	36.7 ± 1.8	60.7 ± 15.9	35.3 ± 2.4
Glycine (GLY)	238.7 ± 12.7	283.3 ± 17.5	**884.7 ± 109.6***
Histidine (HIS)	68 ± 7.0	63.3 ± 1.8	52 ± 5.3
3-Histidine (3-HIS)	1.3 ± 0.7	3.3 ± 0.7	**4.7 ± 0.7***
Leucine (LEU)	208.7 ± 16.7	169.3 ± 26.1	154 ± 7.0
Isoleucine (ILEU)	107.3 ± 6.6	92.7 ± 9.3	78.7 ± 9.3
Lysine (LYS)	388.7 ± 23.7	334 ± 32.5	293.3 ± 29.1
Methionine (MET)	78.7 ± 5.2	63.3 ± 6.6	70 ± 5.3
Ornithine (ORN)	100.7 ± 7.1	123.3 ± 33.6	78 ± 12.0
Phenylalanine (PHE)	72.7 ± 5.3	63.3 ± 5.2	64.7 ± 1.8
Serine (SER)	154 ± 3.5	**127.3 ± 4.8****	147.3 ± 5.2
Taurine (TAU)	546.7 ± 123.1	472 ± 17.5	384.7 ± 57.8
Threonine (THR)	218 ± 6.4	**155.3 ± 7.1****	**172.7 ± 4.8****
Tryptophan (TRY)	110 ± 11.7	82 ± 15.1	77.3 ± 20.7
Tyrosine (TYR)	107.3 ± 14.5	92 ± 16.0	100.7 ± 5.8
Valine (VAL)	245.3 ± 14.8	209.3 ± 31.8	191.3 ± 7.9

Table 27. Concentration of amino acids in *Gldc* mice plasma.

Significant increases are indicated with (*) while decreases are indicated with (**), as compared to *Gldc*$^{+/+}$ (ANOVA, $p<0.05$).

Amino acid	Concentration in urine (µmol/ µmol creatinine)		
	Gldc$^{+/+}$ (n=3)	*Gldc*$^{GT1/+}$ (n=3)	*Gldc*$^{GT1/GT1}$ (n=3)
Alanine (ALA)	2.25 ± 0.94	1.43 ± 0.38	0.74 ± 0.14
Arginine (ARG)	1.10 ± 0.62	0.67 ± 0.12	0.48 ± 0.14
Asparagine (ASN)	0.87 ± 0.06	1.13 ± 0.31	0.77 ± 0.27
Aspartic acid (ASP)	3.11 ± 1.58	1.24 ± 0.33	1.19 ± 0.30
Citrulline (CIT)	0.51 ± 0.05	0.23 ± 0.14	0.21 ± 0.06
Cysteine (CYS)	0.31 ± 0.12	0.45 ± 0.11	0.40 ± 0.06
Glutamine (GLN)	2.47 ± 0.27	2.98 ± 0.85	1.27 ± 0.09
L-glutamate (GLT)	1.34 ± 0.98	0.56 ± 0.14	0.47 ± 0.15
Glycine (GLY)	3.58 ± 0.67	3.79 ± 0.30	**5.34 ± 0.32***
Homocysteine (HCYS)	2.75 ± 1.05	1.82 ± 0.32	1.14 ± 0.12
Histidine (HIS)	0.51 ± 0.05	0.37 ± 0.14	0.16 ± 0.02
1-Histidine (1-HIS)	0.61 ± 0.06	0.71 ± 0.07	0.55 ± 0.06
3-Histidine (3-HIS)	0.47 ± 0.004	0.55 ± 0.04	0.34 ± 0.04
Leucine (LEU)	1.21 ± 0.47	0.829 ± 0.14	**0.42 ± 0.09****
Isoleucine (ILEU)	0.25 ± 0.06	0.17 ± 0.04	**0.04 ± 0.02****
Lysine (LYS)	5.43 ± 3.05	2.72 ± 0.43	2.01 ± 0.50
Methionine (MET)	3.26 ± 0.88	1.86 ± 0.50	1.11 ± 0.24
Ornithine (ORN)	0.36 ± 0.16	0.24 ± 0.03	0.22 ± 0.01
Phenethylamine (PEA)	7.84 ± 0.46	6.44 ± 2.07	4.75 ± 0.61
Phenylalanine (PHE)	0.85 ± 0.39	0.67 ± 0.11	0.44 ± 0.03
Serine (SER)	1.14 ± 0.32	0.59 ± 0.16	**0.33 ± 0.05****
Taurine (TAU)	13.0 ± 4.90	5.78 ± 1.96	9.47 ± 1.13
Threonine (THR)	2.28 ± 0.18	**0.82 ± 0.22****	**0.82 ± 0.09****
Tyrosine (TYR)	0.74 ± 0.19	0.67 ± 0.21	0.31 ± 0.04
Valine (VAL)	0.77 ± 0.21	0.45 ± 0.14	0.22 ± 0.04

Table 28. Concentrations of amino acids in *Gldc* mice urine.

Significant increases are indicated with (*) while decreases are indicated with (**), as compared to *Gldc*$^{+/+}$ (ANOVA, $p<0.05$).

5.2.4. Late-foetal ventriculomegaly in *Gldc* mutant mice

To determine if the hydrocephalus phenotype was congenital and has a pre-natal onset, E18.5 $Gldc^{GT1}$ foetuses were collected. An illustration of the ventricular system of an E18.5 mouse brain is provided in **Figure 44**, where the position of the brain ventricles relative to one another is shown. Coronal sections were made through non-exencephalic brains (n = 5 of $Gldc^{+/+}$ and n = 12 of $Gldc^{GT1/GT1}$) in **Figure 45**, **Figure 46**, and **Figure 47**.

Out of the 12 $Gldc^{GT1/GT1}$ mutants histologically examined, 6 showed obvious dilation of their lateral and third ventricles (**Figure 45**), hereon in referred to as "affected" mutants. Examination of the aqueduct (**Figure 46**) revealed stenosis in these affected mutants, in which the narrowest regions of their aqueducts were closed. The subcommissural organ (SCO) located on the roof of the aqueduct was completely obliterated. In the wild-types and normal, unaffected mutants, the aqueduct retains a small opening throughout with the SCO clearly visible. The pineal gland, a small structure located superior to the SCO, was also missing in affected mutants. Further posterior to this stenosis (i.e. pass the point of obstruction), the aqueduct and fourth ventricle of affected mutants were not dilated and remained comparable in size to wild-type and normal mutants (**Figure 47**). Other structures such as the choroid plexus and corpus callosum appeared comparable between all groups.

The presence of an obstruction in the ventricular system of *Gldc* mutants from E18.5 indicates that the hydrocephalus is congenital and non-communicating. Owing to the comparably normal fourth ventricle and aqueduct at regions past the obstruction, the cause of the dilated lateral and third ventricles can be attributed to aqueduct stenosis.

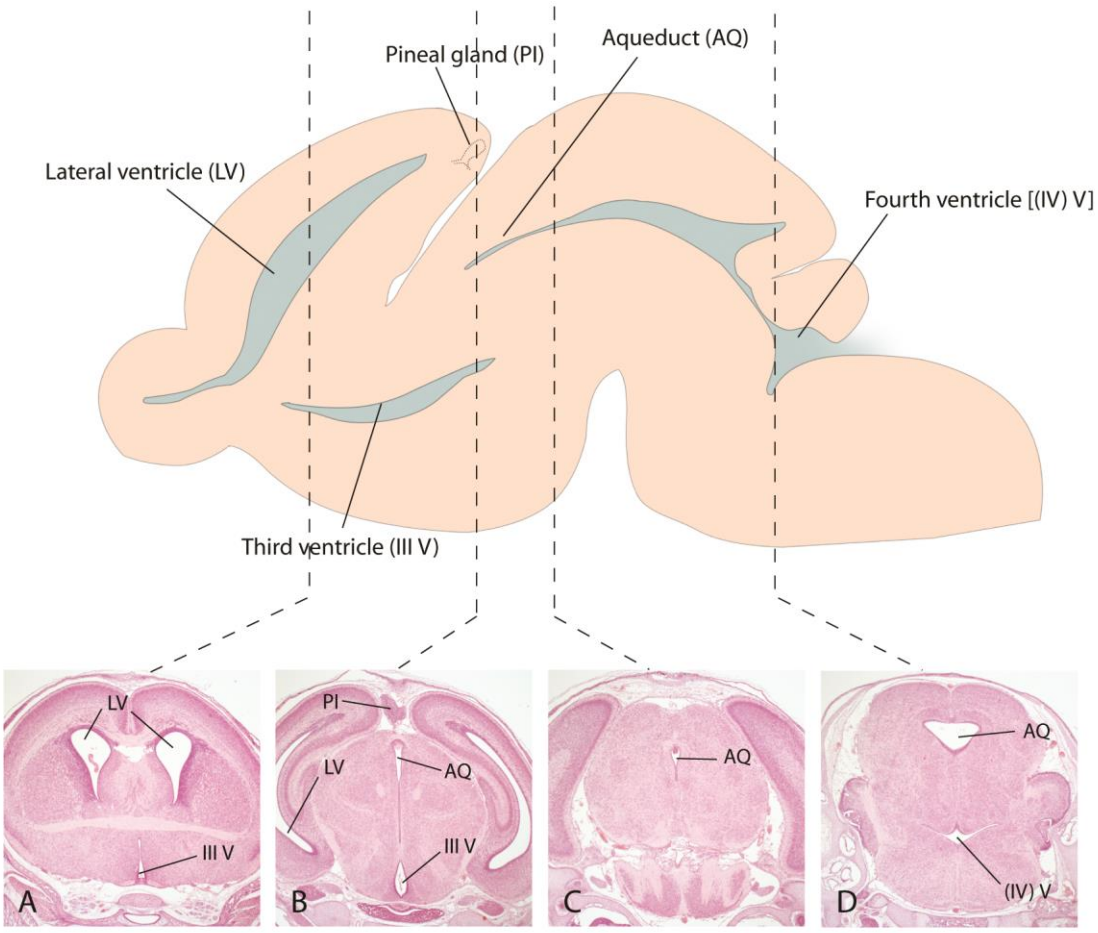

Figure 44. The ventricular system in an E18.5 mouse brain.

Diagram of a sagittal view of an E18.5 mouse brain. (A-D) Representative, H&E-stained, coronal sections progressing in an anterior-posterior manner with their estimated positions indicated (in dotted lines) in the diagram above. The diagram was drawn with references from coronal sections of wild-type *Gldc* mice, the Allen Developing Mouse Brain Atlas (available from: http://developingmouse.brain-map.org) and Fliegauf et al. (2007).

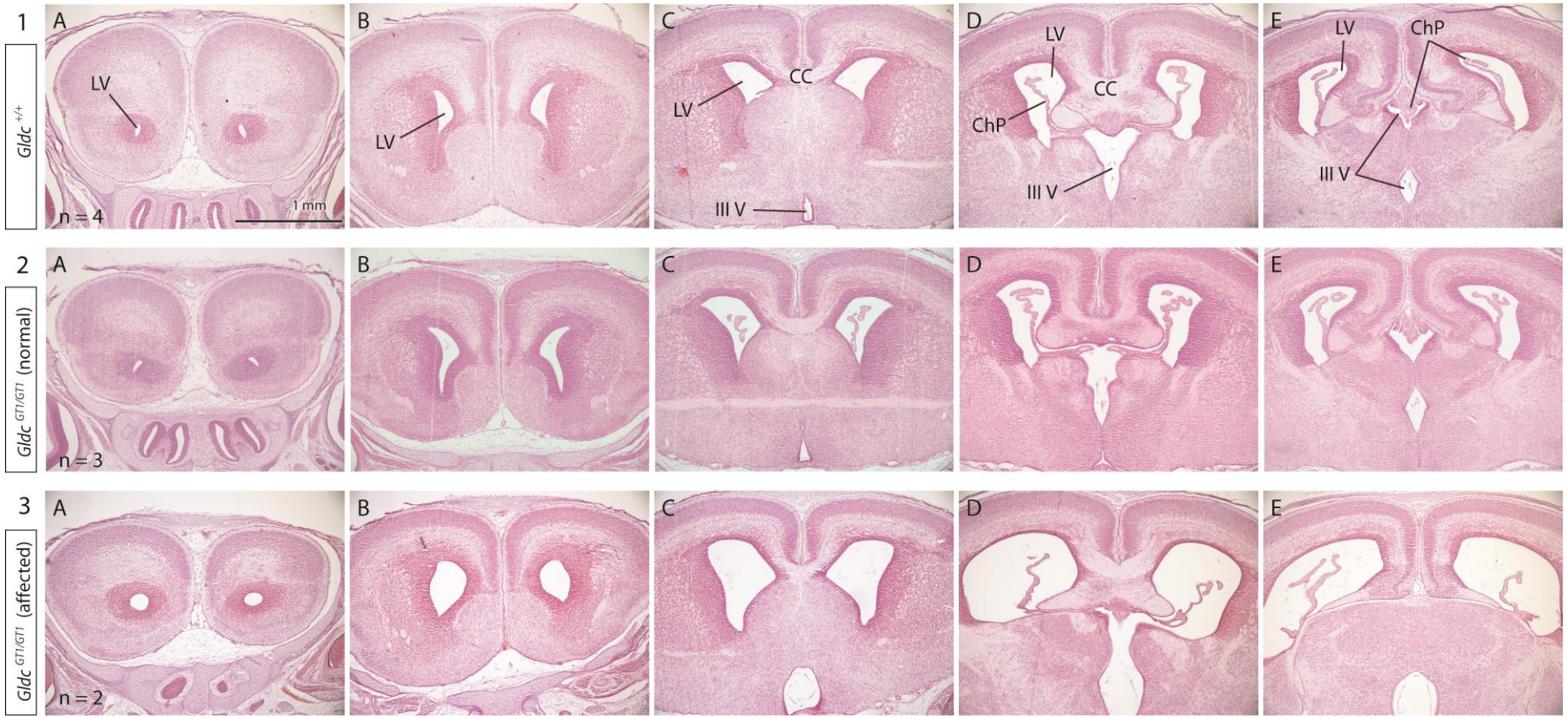

Figure 45. E18.5 *Gldc*$^{GT1/GT1}$ brains show dilation of lateral and third ventricles.

Coronal sections of (row **1A-E**) *Gldc*$^{+/+}$, (row **2A-E**) normal *Gldc*$^{GT1/+}$, and (row **3A-E**) affected *Gldc*$^{GT1/GT1}$ brains at E18.5, progressing in anterior-posterior sequence. Affected *Gldc*$^{GT1/GT1}$ mutant brains **(3A-E)** revealed consistent dilation of the lateral (LV) and third ventricles (III V) through all the sections, compared to unaffected mutants and wild-type controls. Other abbreviations: corpus callosum (CC), choroid plexus (ChP). Sections were stained with H&E.

Figure 46. Aqueduct stenosis and obliteration of the subcommissural organ in E18.5 *Gldc*$^{GT1/GT1}$ brains.

Coronal sections of *Gldc*$^{+/+}$ (column **1A-4A**), normal *Gldc*$^{GT1/+}$ (column **1B-4B**), and affected *Gldc*$^{GT1/GT1}$ (column **1C-4C**) brains at E18.5 through the aqueduct region. In affected *Gldc*$^{GT1/GT1}$ mutant brains with dilated ventricles **(1C-4C)**, the aqueduct (AQ) is closed and the subcommissural organ (SCO) is absent (shown with arrows), compared to wild-types and normal, unaffected mutants. The pineal gland (PI), shown in sections **(2A, 3A)** in the wild-type and **(1B, 2B)** in the normal mutant, is absent in the affected mutant **(1C-3C)**.

The left-most row **(1-4)** indicates the area (dotted box) that is being shown in the close-ups on the right, progressing in an anterior-posterior fashion from 1 to 4.

Scale bars: 2 mm for 1-4; 0.2 mm for all A-C close-ups. Sections were stained with H&E.

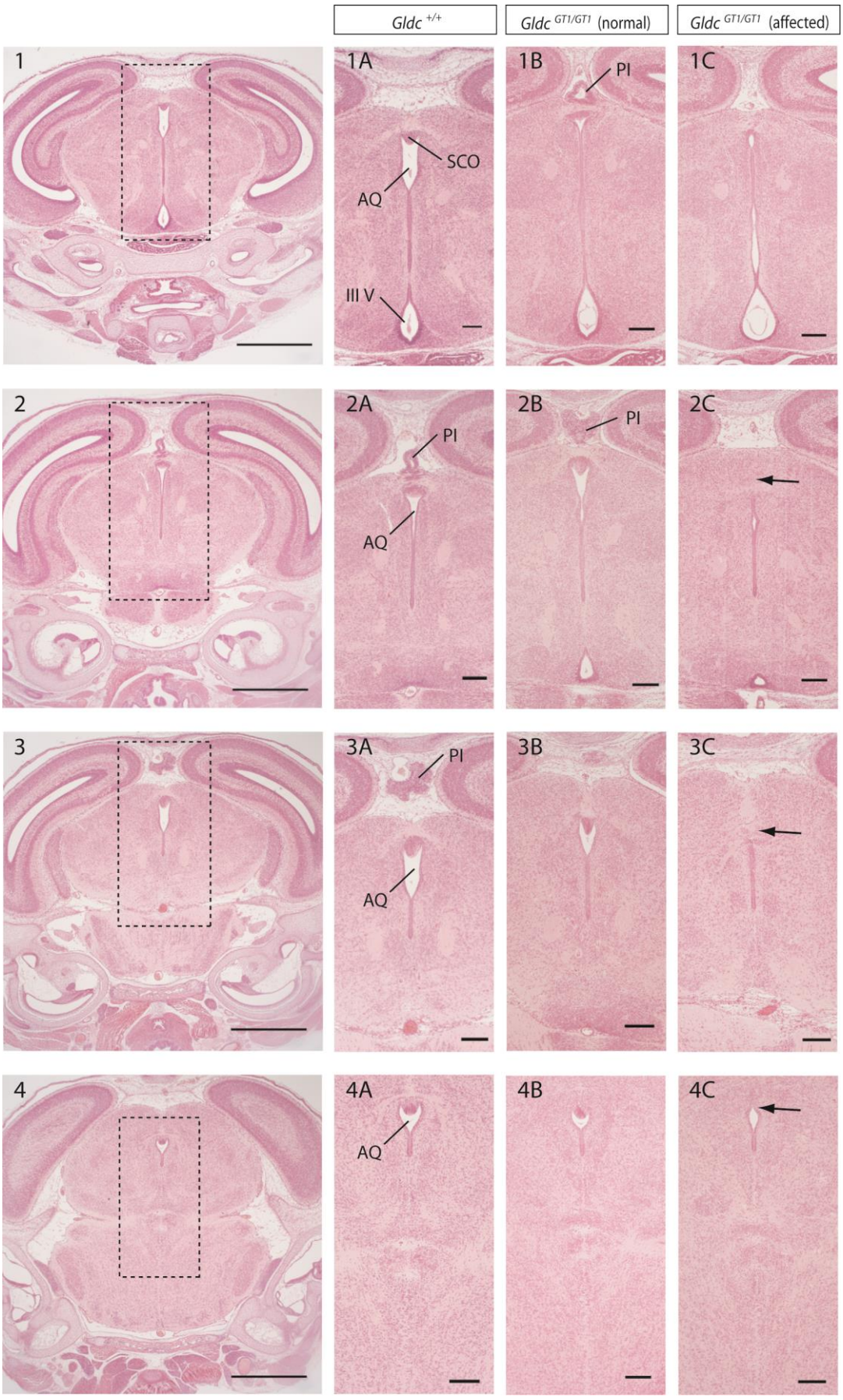

Figure 46. Aqueduct stenosis and obliteration of the subcommissural organ in E18.5 *Gldc*$^{GT1/GT1}$ brains.

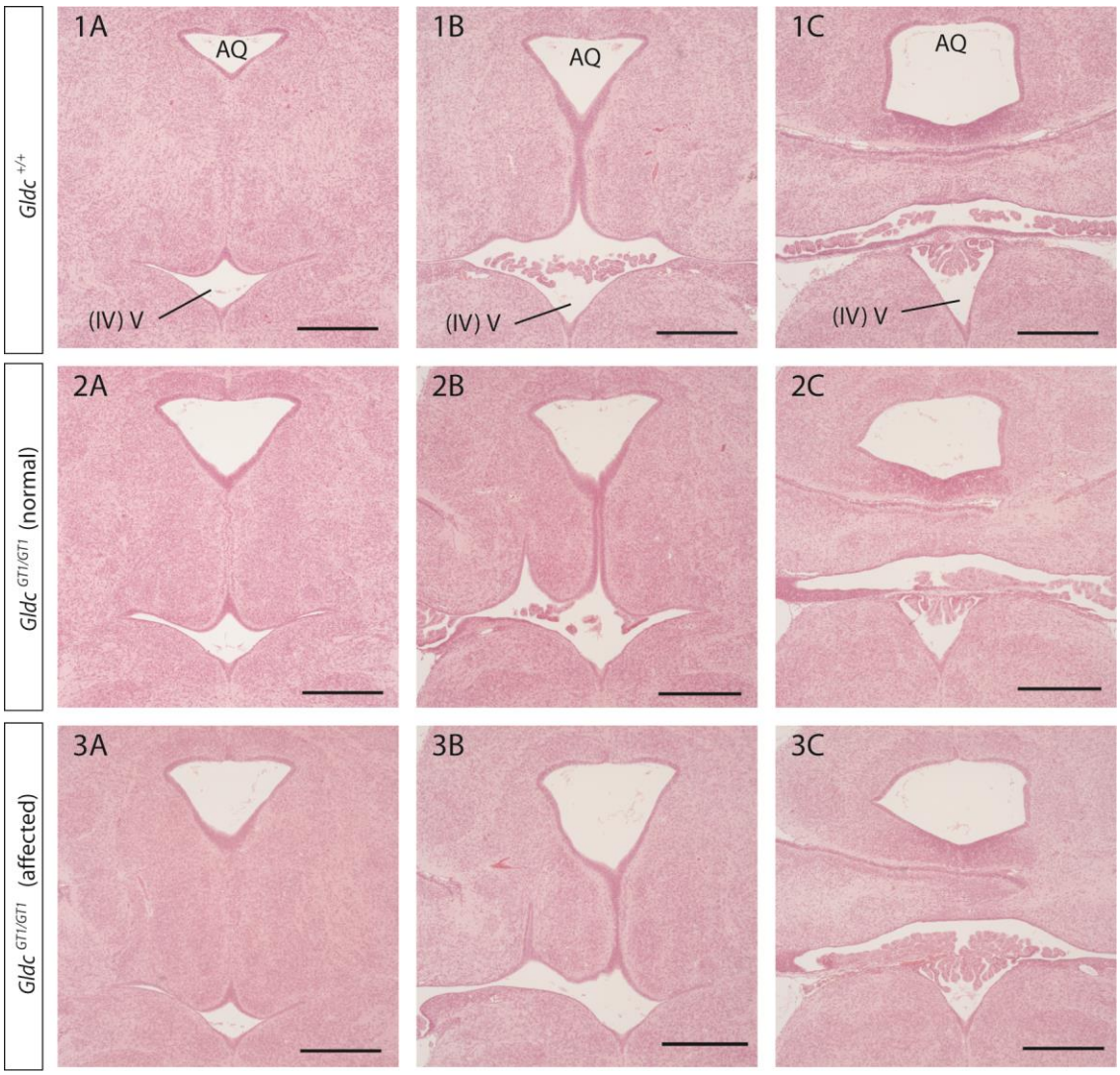

Figure 47. Sections of E18.5 *Gldc^{GT1}* brains showing normal fourth ventricles.

Coronal sections of *Gldc$^{+/+}$* (row **1A-1C**), normal *Gldc$^{GT1/+}$* (row **2A-2C**), and affected *Gldc$^{GT1/GT1}$* (row **3A-3C**) brains at E18.5 through the aqueduct (AQ) and fourth ventricle [(IV) V] in anterior-posterior sequence, showing no observable difference in size of the ventricles between all groups.

Scale bars: 0.5 mm. Sections were stained with H&E.

5.2.5. Analysis of the corpus callosum

At E18.5, no obvious thinning or absence of the corpus callosum was detected in *Gldc*$^{GT1/GT1}$ mutants via examination of coronal sections (as described in the previous section). 5-week old brains were collected and examined to further confirm this finding, as any hypoplasia or partial agenesis would presumably be more obvious at post-natal stages. The brains were bisected to reveal a sagittal view of the corpus callosum and stained whole and *en bloc* with gold chloride to visualize the commissures. Measurements of the anterior-posterior length of the corpus callosum were then made.

No difference in the anterior-posterior length of the corpus callosum was found between genotypes (**Figure 48**). In two *Gldc*$^{GT1/GT1}$ brains with hydrocephalus, the corpus callosum cannot be identified due to the severely enlarged ventricles. As the anterior and hippocampal commissures were still present (albeit slightly deformed) in these brains, the corpus callosum was more likely obliterated by the hydrocephalus rather than missing due to genuine agenesis during development.

5.2.6. Analysis of the cerebellum

Several gold chloride-stained, 5-week old brains of *Gldc*^{GT1} mice that were used in the corpus callosum analysis also had their cerebellums photographed for preliminary examination of the cerebellum (**Figure 49**). The cerebellar vermis of hydrocephalic mutants appeared mildly compressed along the anterior-posterior axis. No Dandy-Walker (DW)-like malformation resembling that seen in NKH patients, or severe loss of volume and/or foliation as seen in the DW mouse model (Blank et al., 2011), was observed.

Vermis folia were identified with reference to Blank et al. (2011) and Sgaier et al. (2007) as anatomical guides for labelling the folia of the mouse cerebellum, specifically comparing wild-type mice to mice with cerebellar foliation defects. Further validation of the anatomical labelling of wild-type cerebellum was carried out by referring to the Allen Mouse Brain Atlas (available from: http://mouse.brain-map.org). In *Gldc*^{GT1} samples, the wild-types, heterozygotes, and non-hydrocephalic homozygotes (n = 2, each) all showed comparable amount of foliation (marked in Roman numerals II to X). In hydrocephalic mutant brains (n = 2), one folium anterior to the primary fissure is missing due to the loss of a fissure between folia II/III. Thus, a subtle foliation defect may be present alongside the hydrocephalus, but a more careful examination of histologically prepared sections is required before a conclusion can be drawn.

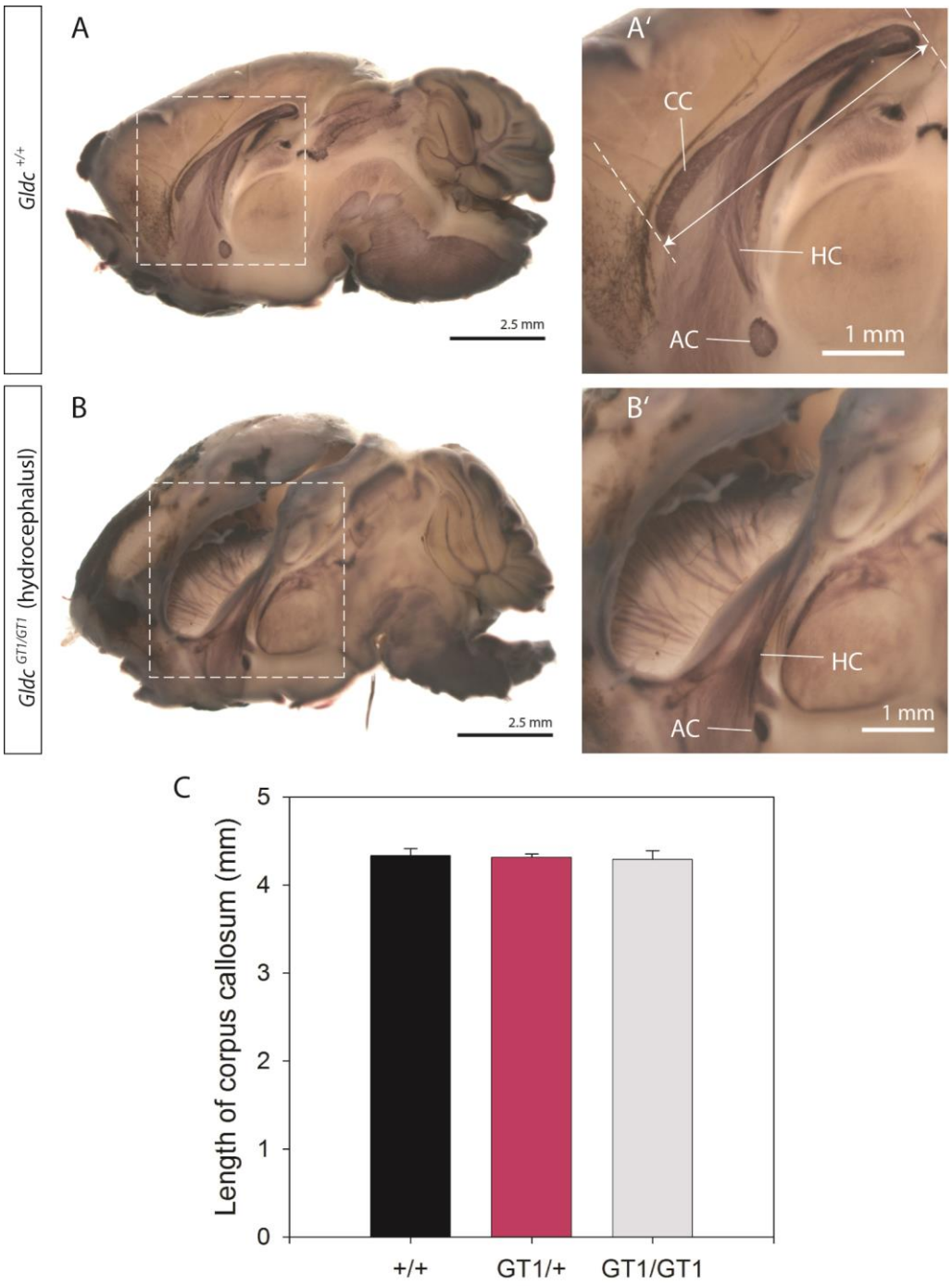

Figure 48. Corpus callosum analysis.

(A) Normal *Gldc*$^{+/+}$ and **(B)** hydrocephalic *Gldc*$^{GT1/GT1}$ 5-week bisected brains, with boxed areas shown at higher magnification in **(A')** and **(B')**, respectively. **(A')** indicates how the anterior-posterior lengths of the corpus callosum (CC) of non-hydrocephalic brains were measured (double-sided arrow). **(C)** No difference in anterior-posterior lengths of the corpus callosum was found between all genotypes (n = 5, each). The corpus callosum cannot be identified in the hydrocephalic *Gldc*$^{GT1/GT1}$ mutants (n = 2). The brains were stained *en bloc* with gold chloride solution.

Other abbreviations: hippocampal commissure (HC), anterior commissure (AC).

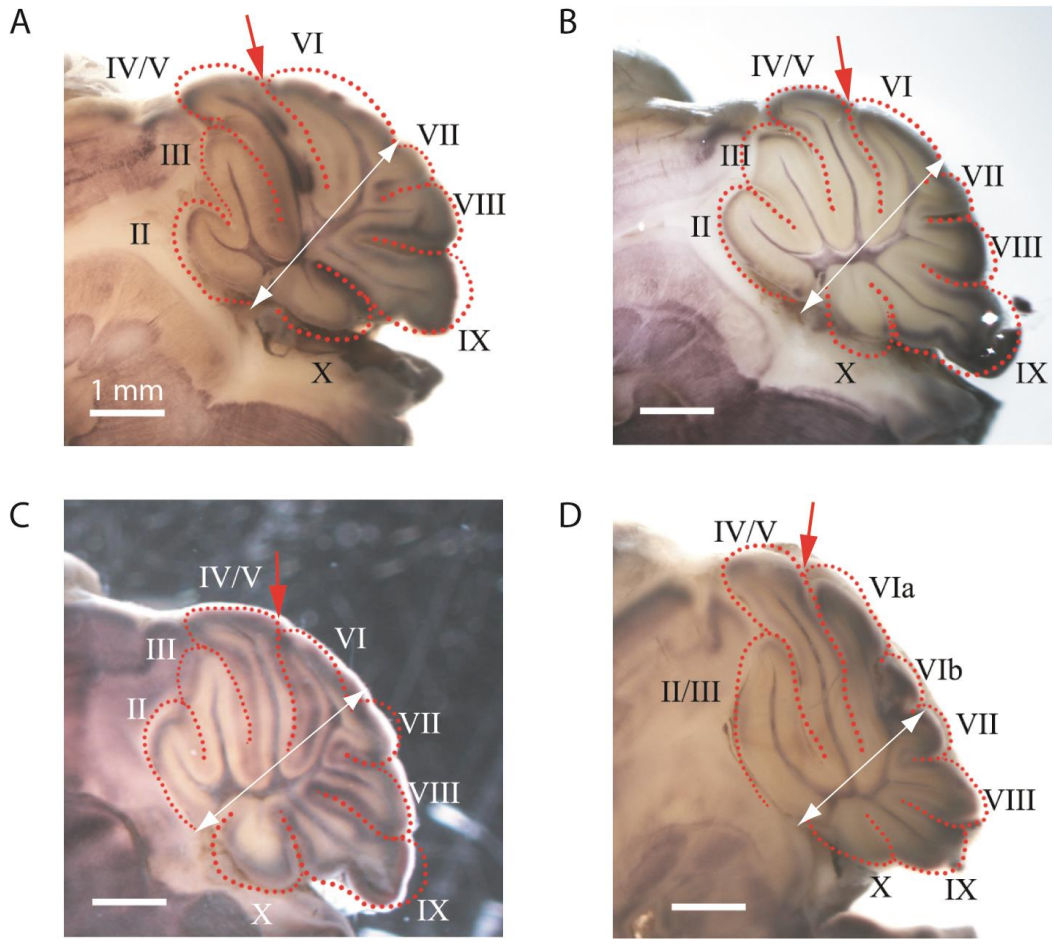

Figure 49. Preliminary cerebellar folia analysis.

Cerebellar size and foliation (traced out in dotted red lines) was comparable between **(A)** *Gldc*$^{+/+}$, **(B)** *Gldc*$^{GT1/+}$ and **(C)** non-hydrocephalic *Gldc*$^{GT1/GT1}$ 5-week brains. **(D)** Hydrocephalic *Gldc*$^{GT1/GT1}$ brains appeared compressed along the anterior-posterior axis (compare double-sided white arrows) and were missing one folia anterior to the primary fissure (red arrows). Roman numerals represent folia II to X of the cerebellar vermis. Sample size, n = 2 for each comparison group.

5.3. Discussion

5.3.1. *Gldc* mutant mice exhibit characteristic features of NKH

The *Gldc*^{GT1} mutant mice exhibit several features that are hallmarks of human NKH: they have significantly elevated levels of glycine in their plasma and urine, virtually no hepatic Gldc enzymatic activity (as shown in **Chapter 3**), occurrence of early, post-natal deaths amongst pre-weaning mutant pups, and about 20% incidence of hydrocephalus. These findings make the *Gldc* mutant mouse a suitable model for studying the pathology of *classical* NKH and would be valuable for testing treatment options. This is unlike the *Amt* knockout mouse, in which NTDs are almost fully penetrant (Narisawa et al., 2012), and the low/high-GCS transgenic lines with higher levels of residual Gldc enzymatic activity and phenotypes that more closely resemble atypical NKH (Oda et al., 2007, Kojima-ishii et al., 2008).

There are several possibilities that may account for the occurrence of early post-natal lethality in *Gldc* mutants that were not caused by hydrocephalus. Although the post-natal Mendelian ratios from heterozygous crosses do not reflect significant loss of mutants, the number of mutants born were nonetheless fewer than would be expected. This could partly be attributed to being born with anencephaly and eaten shortly after birth by the mother. The relatively normal appearance of the dead pups (within a few days of age) occasionally found in the cages would suggest that other mechanisms are at play to cause early lethality. Occurrence of respiratory distress and epileptic seizures, the major causes of death amongst neonates with NKH, was possibly present but missed in these pups. Neither phenotype has so far been observed in surviving pups or in adult mutant mice, although this does not rule out possible aberrant EEG readings and the occurrence of very mild seizures that go unnoticed.

A common brain imaging finding in NKH patients that does not appear to be present in *Gldc* mutant mice is agenesis or dysgenesis of the corpus callosum. It is likely that the corpus callosum defects seen in NKH patients are secondary to a mechanism that is causing a more generalized loss of white matter and myelination, neither of which were particularly obvious in the brains of *Gldc* mutant mice as observed at 5 weeks of age.

Due to the similarities in corpus callosum development between mice and humans, mice models have been used extensively to study ACC. Several genes associated to human ACC syndromes are also found with a corresponding callosal phenotype in the mouse [listed in Edwards et al. (2014)], for example *MKS3* in Meckel-Gruber syndrome patients with the

rat *Wpk* mutation (Smith et al., 2006b), and *HESX1*/*Hesx1* mutation in septo-optic dysplasia (Dattani et al., 1998).

In hydrocephalic *Gldc* mutants, the relatively normal staining of the hippocampal and anterior commissures suggest that the obliteration of the corpus callosum in those brains were likely secondary to the grossly enlarged ventricles, and not due to a real agenesis of the corpus callosum resulting from a defect in the interhemispheric crossing of commissural neurons. In addition, all E18.5 mutants with enlarged ventricles did not show any overt corpus callosum agenesis.

The ventricular dilation seen in some *Gldc* mutants at late-foetal stages is suggestive of a chronic pathology underlying their hydrocephalus, and that it begun at developmental stages. The various causes of hydrocephalus in other mice models, as well as hypotheses of the likely cause in this particular model, are discussed in following sections.

5.3.2. Pathogenesis of hydrocephalus

In more recent years, some findings have challenged the classical separation of obstructive and non-obstructive causes of hydrocephalus. Finding obstructions that block the flow of CSF is by no means the end to explaining the pathology of hydrocephalus, as it simply begs the question of how the obstruction arose in the first place. It has also been suggested that the obstructions are not the cause of CSF accumulation in the ventricles, but rather a consequence of the dilating ventricles pushing on, and causing further narrowing of, the narrowest regions in the CSF pathway (i.e. the aqueduct), which then causes the dilation to worsen. For example, aqueduct stenosis has been argued as being a consequence (rather than cause) of hydrocephalus (Williams, 1973), though several studies have observed this defect preceding the onset of ventricular enlargement (Takeuchi and Takeuchi, 1986, Somera and Jones, 2004).

Several hypotheses have been formulated to address this issue, for example disruption in the ependymal monolayer lining the ventricles. Loss of integrity of ependymal cells, especially in the aqueduct regions, is frequently reported in hydrocephalus mouse models. It has been reported to occur through a variety of pathways such as cell polarity, cell-cell junctional complex assembly, proliferation, differentiation, and maturation of ependymal cells, and proliferation and migration of other NPCs, as summarized in **Table 29** and by Huh et al. (2009). Ependymal disruptions have also been shown in human foetuses with communicating hydrocephalus in which the aqueduct is not obstructed (Dominguez-Pinos et al., 2005). Perturbations in the ependymal cell lineage leading to ependymal denudation

have been shown to occur before the onset of hydrocephalus in mice models, suggesting that the loss of ependymal integrity is not secondary to the stretching of walls of the dilating ventricles but rather is contributing to the cause.

Alterations in the subcommissural organ (SCO) are another frequently reported histological finding in hydrocephalus, often accompanying ependymal disruptions and aqueduct stenosis. The SCO is a secretory gland consisting of hypendymal cells underlying a layer of ependymal cells, located at the roof of the narrowest region of the aqueduct and and posterior to the pineal gland. The SCO is thought to play a role in CSF circulation and absorption, but its involvement in the pathology of hydrocephalus is unclear (Perez-Figares et al., 2001). Underdeveloped and displaced SCO caused by X-irradiation of pregnant rats was hypothesized to cause the aqueduct stenosis and subsequent hydrocephalus in their litters, due to reduced amount of SCO secretion to keep the aqueduct open (Takeuchi and Takeuchi, 1986). Hypotrophic SCO with normal ependymal lining of the aqueduct has been reported in hydrocephalic human foetuses (Castaneyra-Perdomo et al., 1994). A comprehensive review of hydrocephalic mice mutants with an SCO phenotype is provided by Huh et al. (2009).

There is also evidence of suboptimal proliferation of neural progenitor cells (NPCs) in hydrocephalus mouse models (**Table 29**). This finding is often present in combination with other defects such as aqueduct stenosis in the *Wrp-Nestin*^{Cre} mouse (Kim et al., 2012), disrupted ependymal lining in the *hyh* mouse (Jimenez et al., 2009), and defective cilia in the *myc-Klf4* mouse (Qin et al., 2011). It has also been reported independent of other hydrocephalus-associated phenotypes, e.g. in *Pak4-Nestin*^{Cre} (Tian et al., 2011) and *Bbs1-Pdgfrα*^{Cre} (Carter et al., 2012) mice. While a causative relationship has not been established, it is clear that suboptimal proliferation is involved in the pathogenicity of some of these cases of hydrocephalus, especially in mice with communicating hydrocephalus where no obstruction can be found.

Owen-Lynch et al. (2003) demonstrated that the CSF of hydrocephalic Texas (H-Tx) rat brains had an inhibitory effect on proliferation of NPCs *in vitro,* which suggests that the contents of the CSF itself plays a role in brain development. Interestingly, the same team observed low levels of 10-formyl-THF in the CSF of H-Tx rat brains, and that supplementation with THF and 5-formyl-THF was able to decrease the incidence of hydrocephalus in these rats but supplementation with folic acid increased the incidence (Cains et al., 2009). This finding may be of relevance to the *Gldc* mutant mouse which is also demonstrated to have an altered folate profile.

Gene	Protein description	Obstruction	Phenotype	Reference
Aspp2	Apoptosis-stimulating protein of p53	N.R.	NPC proliferation defect	(Sottocornola et al., 2010)
Bbs1	Bardet-Biedl Syndrome protein	N.R.	NPC proliferation defect, abnormal ependymal cilia	(Davis et al., 2007)
Bbs1-Pdgfrα^{Cre}	Bardet-Biedl Syndrome protein	N.F.	NPC proliferation defect, abnormal ependymal cilia	(Carter et al., 2012)
Cdc42-Nestin^{Cre}	GTP-binding protein	Aqueduct	Tight junction assembly defect, ependymal denudation	(Peng et al., 2013)
Dlg5	Epithelial cell structure maintenance	Aqueduct	Tight junction assembly defect, no aqueduct lumen	(Nechiporuk et al., 2007)
Dnaic1	Dynein, axonemal, intermediate chain	Aqueduct	No ependymal cilia	(Ostrowski et al., 2010)
FoxJ1	Forkhead transcription factor	N.R.	Radial glia differentiation defect, abnormal ependymal cilia	(Jacquet et al., 2009)
Lgl1	Maintenance of cell polarity	N.R.	NPC proliferation and differentiation defect, ependymal over-proliferation	(Klezovitch et al., 2004)
Lhx9	Pineal homeobox	N.R.	Pineal gland hypoplasia	(Yamazaki et al., 2014)
Msi1	RNA-binding	Aqueduct	NPC proliferation defect, abnormal SCO, ependymal denudation	(Sakakibara et al., 2002)
Myo9a	Myosin class IX	Aqueduct	Tight junction assembly defect, ependymal maturation defect	(Abouhamed et al., 2009)
N-WASP-Nestin^{Cre}	Actin nucleation regulator	Aqueduct	Tight junction assembly defect, ependymal maturation defect	(Jain et al., 2014)

Gene	Protein description	Obstruction	Phenotype	Reference
Pak4-Nestin^{Cre}	p21-activated kinase	N.R.	NPC proliferation defect, adherens junction assembly defect	(Tian et al., 2011)
Rnd3	Rho family GTPase	Aqueduct	Notch signalling defect, ependymal over-proliferation	(Lin et al., 2013)
Wrp-Nestin^{Cre}	WAVE-associated Rac GTPase-activating protein	Aqueduct	NPC migration defect, astrogliosis	(Kim et al., 2012)

Table 29. Hydrocephalic mouse mutants with NPC proliferation and/or ependymal defects.

Mutants listed in a review of SCO agenesis by Huh et al. (2009) were not included in this table.

Abbreviations: neural progenitor cell (NPC), none reported (N.R.), none found (N.F.).

Oreskovic and Klarica (2011) proposed a new model for CSF hydrodynamics in which pathologies that change the osmolality of the CSF, interstitial fluid, and/or blood may disrupt the osmotic and hydrostatic pressure between the three fluids, thus resulting in net movement of water across the brain parenchyma into the ventricles. This implies that any pathology that causes a sustained elevation in solutes, thus increasing the osmolality of the CSF, may be the cause of increased movement of water into the ventricles.

5.3.3. Hydrocephalus in *Gldc*-deficient mice

As demonstrated in the results, aqueduct stenosis is present in $Gldc^{GT1}$ mutant mice with dilated ventricles. In addition to the narrowing of the aqueduct, the SCO and pineal gland appear to be absent. This model is thus a non-communicating hydrocephalus model, but the question remains as to what caused the aqueduct to narrow, and whether this is causative of the ventricular enlargement.

There appears to be no obvious denudation of the ependymal layer infiltrating the aqueduct lumen, and the fact that the ventricles are obviously dilated by E18.5 would suggest that lack of ependymal cilia, which only reaches maturity at a post-natal age, is not the cause. The defect in formation of the SCO is a striking clue for explaining the narrowing of the aqueduct. As *Gldc* mRNA and protein is expressed in radial glial cells (Ichinohe et al., 2004) from which ependymal cells are derived (Spassky et al., 2005), this would suggest that suboptimal proliferation of radial glia could lead to a defect in formation of glia-derived structures such as the SCO. This is further supported by the finding that $Gldc^{GT1/GT1}$ embryos showed a defect in proliferation at neurulation stages (**Chapter 4**).

The presence of SCO-spondin, the first detectable glycoprotein to be secreted by the SCO, can be detected from E14.5 (Goncalves-Mendes et al., 2003), although the morphological development of the SCO organ itself would have begun earlier, shortly after neural tube closure, at the diencephalon-mesencephalic boundary of an E11.5 mouse embryo. The formation of the pineal primordium begins at E14.5 in the mouse and by E16.5, the pineal gland and the region of the mesencephalic vesicle that is to be the future aqueduct as well as the SCO structure is clearly recognisable (Kaufman, 1992), while pineal genes such as *Crx* and *NeuroD1* can be detected from E17.5 in rat embryos (Munoz et al., 2007).

The absence of the SCO could be causing the narrowing of the aqueduct (in regions where the SCO should be present), either due to lack of secretory signals helping to regulate aqueduct narrowing, or simply lack of the SCO structure itself physically keeping the aqueduct open. In addition, work carried out by another member of the lab, Maria-Chiara

Autuori, revealed that ventricle size in *Gldc*$^{GT1/+}$;*Gldc*$^{GT2/+}$ compound heterozygotes at E16.5 were still comparable to wild-types. The lack of secretory signals from the SCO, which is needed for pineal gland development, could also explain the absence of the pineal gland in hydrocephalic mutants.

If this SCO agenesis hypothesis is correct, defects in formation of the SCO and pineal gland should be present prior to the formation of the aqueduct, and may be predictive of a hydrocephalus phenotype later. E14.5-16.5 are suitable stages to observe for defects in the development of the aqueduct, and if they are present prior to onset of ventricular enlargement. However, if initial defects in SCO development are what precipitate the aqueduct stenosis, abnormalities (such as defective proliferation or differentiation of neural precursors of the radial glia lineage) may already be present from as early as E11.5. Such findings have precedence in the *hyh* mutant mouse and the H-Tx rat models. In the *hyh* mutant on a C57BL/10J background, ependymal denudations and delayed SCO-spondin expression precedes the onset of hydrocephalus, but does not result in prenatal aqueduct stenosis (Jimenez et al., 2001), while in the H-Tx model, reduced SCO-spondin expression precedes aqueduct stenosis which precedes hydrocephalus (Somera and Jones, 2004).

The osmotic pressure hypothesis is another attractive mechanism for explaining the hydrocephalus in *Gldc* mutant mice, in which highly elevated levels of glycine in body fluids are present. However, if osmotic pressure alone is responsible for causing the hydrocephalus, the aqueduct and fourth ventricle would presumably be dilated as well. In addition to that, glycine would presumably continue to build up in the CSF of these mutant mice as they age, which would suggest that all mutants, sooner or later, would show ventricular dilation and develop hydrocephalus, and this does not appear to be the case. However, this possibility has not been ruled out and it is also possible that it could contribute to worsening of the ventricular dilation.

In NKH patients with hydrocephalus that is severe and requires shunting, the presence of a posterior fossa cyst and a DW-like malformation is often present as well. Hydrocephalus (as well as aqueduct stenosis) is a frequently reported complication of patients with DW malformation (Spennato et al., 2011). Mutations in *ZIC1* and *ZIC4* are implicated in DW malformation, which has a characteristic hypoplasia of the cerebellar vermis (Grinberg et al., 2004). Cerebellar hypoplasia is often attributed to a defect in the rapid growth of the cerebellum that is driven by proliferation of granule cell progenitors in the external granular layer (EGL), mostly coordinated by the Purkinje neuron layer (Basson and Wingate, 2013). The *Zic1;Zic4* double knockout mouse presents with brain malformations that resemble the DW phenotype and have reduced *Shh*-derived proliferation of the EGL

(Blank et al., 2011). However, hydrocephalus has not been reported in this mouse model, unlike with DW patients.

The mildly compressed cerebellum in hydrocephalic *Gldc* mutant brains could arguably be a consequence of the grossly dilated lateral ventricles pushing out at, and distorting, surrounding structures. However, it is unlikely to lead to the observed loss of one anterior folium in the vermis. As *Gldc* mRNA is reportedly present in the Purkinje layer and EGL of adult mice (Ichinohe et al., 2004), a reduction or loss of *Gldc* expression in the mutant may lead to subtle proliferation defects in progenitor populations (not unlike the *Zic1;Zic4* model) during cerebellar development.

6. General Discussion

The physiological significance of the glycine cleavage system (GCS) in breaking down glycine has been recognised since the 1960s, as a consequence of efforts to determine the enzyme defect responsible for non-ketotic hyperglycinemia (NKH) (Gerritsen et al., 1965, Ando et al., 1968, Tada et al., 1969). The discovery of its importance in folate one-carbon metabolism (FOCM) came about relatively recently owing to improved appreciation of mitochondrial FOCM reactions (Pike et al., 2010, Tibbetts and Appling, 2010), along with their association with neural tube defects (NTDs) (Narisawa et al., 2012).

The *Gldc*^{GT1} and *Gldc*^{GT2} mouse models presented in this thesis will allow in-depth exploration of the role of the GCS in embryonic brain development *in vivo* and the pathogenesis of two distinct disease phenotypes: the rare metabolic disorder, NKH, and the common congenital malformation, NTD. The incidence of hydrocephalus in the *Gldc*^{GT1} model also provides an opportunity to study this common but aetiologically complex neonatal condition. The findings in this thesis are summarised in this chapter and hypotheses regarding other unexplored disease mechanisms are also discussed.

6.1. Phenotypic spectrum of *Gldc* deficiency

6.1.1. Effect of background strain on disease severity in *Gldc*-deficient mice

During the generation of *Gldc*-deficient mice, a background strain effect was noticed. The *Gldc*^{GT1} allele caused high resorption rates in homozygous mutants on the 129/Sv background, but transferring them to a C57BL/6 background strain by inter-crossing and repeated back-crossing was able to drastically improve survival of the mutants. This indicates the presence of genetic modifiers in either backgrounds that can alter disease severity, and which may also contribute to the partial penetrance of the NTD phenotype. Genetic modifiers have previously been recognised to significantly alter phenotype incidence in other NTD mouse models including *Splotch*^{2H} (Fleming and Copp, 2000) and *curly tail* (De Castro et al., 2012). Alternatively, it is possible that the 129/Sv background is more sensitive to defects in folate metabolism at earlier stages of development, as severe insufficiency of folate uptake is known to result in early embryonic lethality.

The incidence of hydrocephalus and late-foetal ventricular dilation in *Gldc*^{GT1} mutants was found to be higher than the prevalence of hydrocephalus reported in NKH patients. Similarly, hydrocephalus in primary ciliary dyskinesia (PCD) is much more common in PCD mouse models than human patients. In these models, strain differences were also found to have an impact on incidence of hydrocephalus. PCD models on a C57BL/6 background developed severe, chronic hydrocephalus with gliosis and ependymal disruptions and die within a few weeks, while those on a 129 or mixed background do not develop any gross hydrocephalus (Lee, 2013). Thus, it is possible that a genetic modifier in the C57BL/6 background also exacerbates the hydrocephalus in *Gldc* mice.

The effect of background strains on NTDs and hydrocephalus caused by the *Gldc* mutation can be tested by backcrossing *Gldc*^{GT1} or *Gldc*^{GT2} into other background strains.

6.1.2. Partial penetrance of NTDs in *Gldc* mutant mice and comparison with the spectrum of NKH severity

In **Chapter 3**, attempts were made to explain the partial penetrance of NTDs in *Gldc* mutant embryos. There is precedent from NKH case reports on levels of mRNA and/or GCS activity showing an effect on severity of the disease manifestation, made obvious by comparing between neonatal/classical forms and the late-onset/atypical forms of NKH.

Kure et al. (1997) reported levels of GCS activity that were less than 1% in all 26 neonatal NKH patients and 2–5% in all 4 late-onset cases. They subsequently reported 2 patients presenting with a typical neonatal onset but who later showed dramatic improvements (i.e. transient NKH) and had compound heterozygous *GLDC* mutations conferring 5.5–7.5% residual GCS activities (Kure et al., 2004). Flusser et al. (2005) made a similar observation in analysis of *GLDC* mRNA levels from lymphoblastic cell lines of NKH patients: atypical, mild cases showed 4-6% residual levels and had much better clinical outcomes than is reported of the classical form of the disease. The highest level of residual GCS activity found in an NKH diagnosis (32%) to date was reported by Korman et al. (2004), who described 3 patients with novel, homozygous *GLDC* mutations and persistent biochemical features of NKH, but had transient neonatal or no symptoms followed by a normal outcome.

Several attempts have been made to explain the spectrum of severity in NKH, particularly in the mild forms caused by AMT mutations. Okamura-Ikeda et al. (2010) elucidated the crystal structure of AMT and found that the mutations in NKH patients that altered the THF binding site of AMT conferred severe reduction (80%) in enzyme activity. They

suggested grouping AMT mutations to three different sites on the AMT enzyme (folate binding site, catalytic site, and N-terminal domain) that affect its overall activity to varying degrees, thus resulting in varying disease severity. In addition, mutant AMT protein from mild, undiagnosed NKH patients (who were originally screened in search of inherited autism genes) was found to be poorly soluble compared with wild-type protein, suggesting that a temperature-sensitive stability defect rather than a complete catalytic failure may explain their mild presentation (Yu et al., 2013).

This explanation is plausible for the variable severity of NKH caused by different mutations in human patients but cannot account for the partial penetrance of NTDs observed in the models which all carry the same mutation. However, it does provide an example of how slight changes in GCS enzymatic activity, particularly in the lower ranges, can have drastically different outcomes in disease severity.

6.2. Abnormal FOCM in *Gldc* deficiency

6.2.1. Potential mechanisms for abnormal FOCM to result in NTDs

Sub-optimal FOCM can be viewed as either a problem of impaired folate status due to insufficient dietary supply or impaired absorption, or impaired utilisation of folate in the cells due to a genetic abnormality in the metabolic cycle itself (Beaudin and Stover, 2009). The exact mechanism or pathways by which a defect in FOCM leads to failure of neural tube closure, however, is not clear.

Very severe folate deficiency is incompatible with life and subtle impairments in FOCM can result in significant changes in folate and homocysteine levels, but most NTD-affected pregnancies do not show maternal folate-deficient status. It is generally assumed that increased folate intake (e.g. by folic acid supplementation) helps to overcome a dietary insufficiency or a problem in folate metabolism. Studies in the *Cited2* mouse have shown that folic acid supplementation can rescue the NTDs of a genetic model with no evidence of an initial FOCM impairment (Barbera et al., 2002), suggesting that folic acid can also produce a protective effect where the primary defect is not FOCM-related.

The ways in which impaired FOCM can potentially affect neural tube closure include decreased *de novo* purine and/or pyrimidine synthesis leading to decreased proliferation or increased uracil misincorporation, and disruptions in the methylation cycle leading to global hypomethylation and homocysteine toxicity (**Figure 50**). The challenge lies in

determining causation, as more than one of these defects may be present at once and may simply indicate a disturbance in folate metabolism.

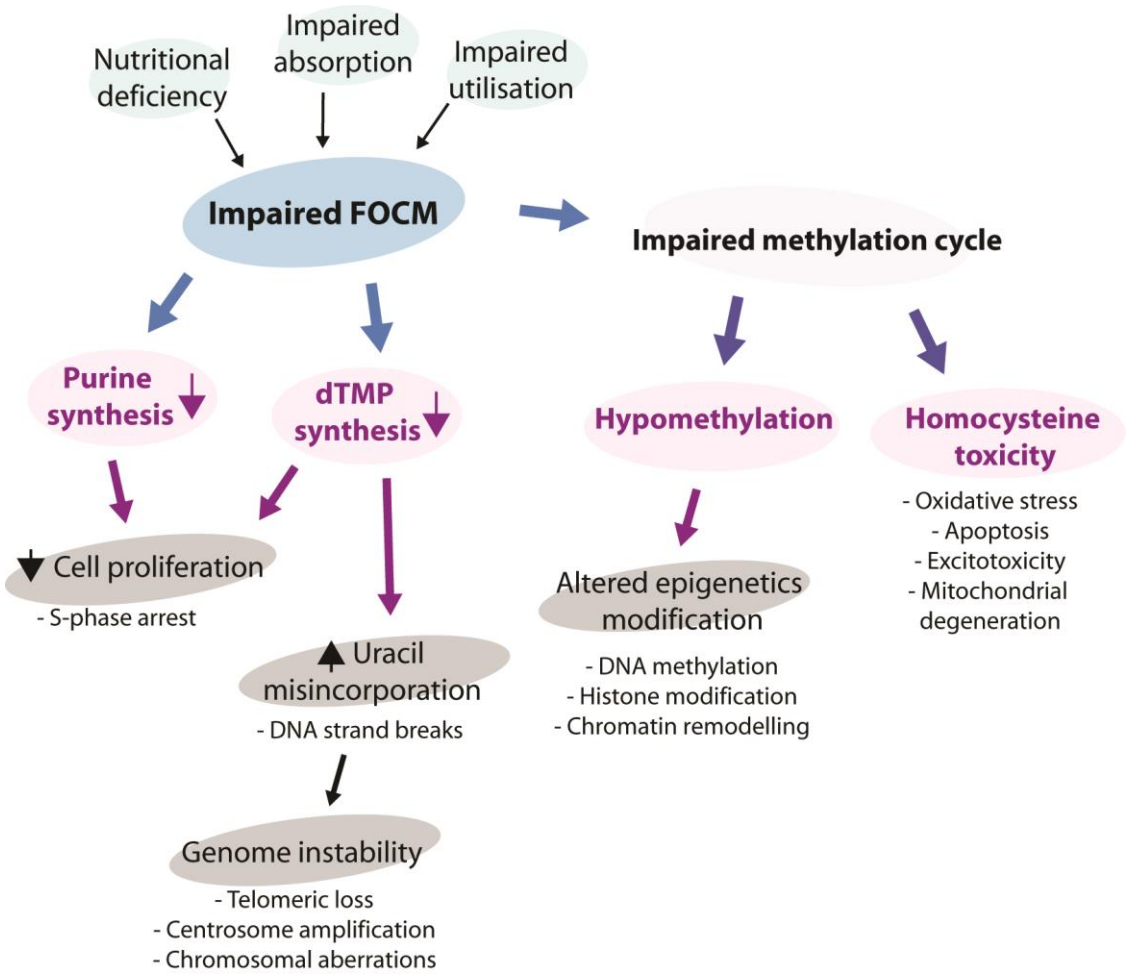

Figure 50. Schematic representation of possible mechanisms through which impaired FOCM may lead to NTDs (description in text).

6.2.1.1. Effect of FOCM on proliferation

Folate deficiency is commonly associated with conditions such as megaloblastic anaemia and immunosuppression caused by low blood cell count. Arrest at mitotic S-phase followed by apoptosis of the blood cells was often observed, which were reversible by folic acid or nucleoside treatment (Koury et al., 2000, Courtemanche et al., 2004). This suggests that folate deficiency can indeed result in a folic acid-responsive defect in cell proliferation.

During neurulation, there is a high demand for rapid cellular proliferation for the neural tube to expand, elongate and elevate. NTD mouse models of genes involved in cell cycle,

proliferation, differentiation, and apoptosis (see **Chapter 1**) suggest that imbalance in proliferation and apoptosis has a role in NTD pathology, especially in the cranial neural tube (Copp, 2005).

Treatment with nucleotides (thymidine in combination with adenine or GMP) of the folic acid-resistant *curly tail* mouse was able to significantly rescue spina bifida by correcting the hindgut proliferation defect in this model (Leung et al., 2013). In several FOCM mouse models showing embryonic lethality such as *Mthfd1* (Christensen et al., 2005, MacFarlane et al., 2009), *Mthfd1S* (Christensen et al., 2013), and *Mthfd2* (Patel et al., 2003), observations from *in vitro* studies of fibroblasts generated from all their null stem cells were consistent with a defect in purine synthesis. Insufficient purine synthesis was thus hypothesised to be the cause of their embryonic lethality. The embryonic lethality in *Mthfs*-nulls was also suspected to result from defective purine synthesis, as MTHFS was shown to associate with the purinosome complex (Field et al., 2011).

6.2.1.2. Increased genome instability

Another way in which reduced thymidylate synthesis may affect neural tube closure is increased misincorporation of uracil into DNA during cell replication, which increases the chances of DNA strand breaks and lead to increased genome instability. Folate deficiency resulting in decreased thymidylate pools and increased uracil misincorporation is a common finding in cancer (Blount et al., 1997, Goulian et al., 1980).

Direct experimental evidence linking FOCM defects, increased uracil misincorporation and NTDs is so far lacking. However, evidence of genomic instability such as telomeric loss, centrosome amplification, and chromosomal abnormalities has been reported in NTD mice models. Mice deficient for telomerase RNA component (TERC) showed significant telomere loss and chromosomal instability (Herrera et al., 1999). They exhibited NTDs that increased in incidence with every generation, with increased neuroepithelial apoptosis, and hematopoietic defects. However, this finding did not extend to *TERC* variants and human NTDs (Benz et al., 2004). Mouse embryonic fibroblasts generated from *Gadd45a*$^{-/-}$ and *Trp53*$^{-/-}$-null embryos (both of which have low incidence of exencephaly) displayed chromosomal aberrations, aneuploidy, and abnormal amplification of centrosomes (Hollander et al., 1999). Strikingly, when the *Gadd45a* mutant was crossed to the *Brca1* mutant, all *Brca1*$^{\Delta 11/\Delta 11}$;*Gadd45a*$^{-/-}$ double homozygous mutants exhibited exencephaly with significantly increased apoptosis *in vivo* and decreased proliferation *in vitro*, and centrosome amplification (Wang et al., 2004).

6.2.1.3. Abnormal FOCM and hypomethylation

The methylation cycle is intimately linked to the one-carbon cycle, and folate deficiency is commonly reported with hypomethylation, alongside uracil misincorporation, in cancers (Ghoshal et al., 2006, Wang et al., 2014b, McGlynn et al., 2013, James et al., 2003). Suppression of methylation processes can have consequences for epigenetic regulation at a local or genome-wide scale. Several lines of evidence point towards defective methylation or other alterations in the epigenome resulting in NTDs (Greene et al., 2011, Blom, 2009).

Neural tube closure has been shown to be sensitive to perturbations in the methylation cycle, as treatment of mouse embryos in culture with an inhibitor of SAM production was able to induce exencephaly without causing generalised developmental retardation (Dunlevy et al., 2006). Inactivation of DNA methyltransferases Dnmt3a and Dnmt3b completely prevented *de novo* methylation in ES cells. *Dnmt3a*$^{-/-}$ null mice were normal at birth but died by 4 weeks, while *Dnmt3b*$^{-/-}$ null embryos exhibited NTDs and were embryonically lethal. *Dnmt3a*$^{-/-}$*;Dnmt3b*$^{-/-}$ double homozygotes showed significant loss of methylation, were severely developmentally delayed and died before E11.5 (Okano et al., 1999). Mouse models with perturbation in other epigenetic mechanisms that also exhibited NTDs include hypomorphs or loss of acetyltransferase activity of the histone acetylation gene, *Gcn5* (Bu et al., 2007, Lin et al., 2008), mutants of chromatin remodelling proteins such as BRG1 and Brd2 (Bultman et al., 2000, Gyuris et al., 2009), and mutants for histone demethylase encoding-gene, *Fbxl10* (Fukuda et al., 2011).

In human NTD cases, Wang et al. (2010) showed that methylation of long interspersed nucleotide element-1 (LINE-1), which may be indicative of global DNA methylation, was significantly decreased in DNA from NTD-aborted foetuses. They also showed that folate deficiency was able to induce LINE-1 hypomethylation in mouse ES cells (Chang et al., 2013). However, late gestation supplementation with folic acid (beyond 12 weeks) was found to be associated with *reduced* methylation of LINE-1 elements (Haggarty et al., 2013).

6.2.1.4. Homocysteine toxicity

A common consequence of perturbing FOCM and methylation is a decrease in homocysteine remethylation, resulting in a build-up of homocysteine to toxic levels. For example, both the *MTHFR* 677C>T polymorphism in humans and *Mthfr* mutation in mice

resulted in hyperhomocysteinemia (Jacques et al., 1996, Frosst et al., 1995, Chen et al., 2001).

The pathology of homocysteine toxicity in cardiovascular diseases is commonly attributed to its activation of the coagulation system or by inducing oxidative stress, causing damage to endothelial tissue (Glushchenko and Jacobsen, 2007, Li et al., 2006). Homocysteine toxicity has also been hypothesised to act by inducing apoptosis (Kruman et al., 2000) and by over-activating NMDARs resulting in excitotoxicity (as it is an agonist of the glutamate binding site) (Lipton et al., 1997, Ho et al., 2002). Hyperhomocysteinemia has been shown to result in cytoplasmic swelling and mitochondrial degeneration in the cerebral vasculature of folate-deficient rats (Kim et al., 2002). However, there is not yet any direct evidence of homocysteine toxicity resulting in NTDs. Treatment of mouse and rat embryos in culture with homocysteine resulted in generalised toxicity but did not induce NTDs, suggesting that increased levels of homocysteine in NTD pregnancies may serve as a marker of perturbed FOCM but is not causative of the NTD (Greene et al., 2003, Vanaerts et al., 1994).

6.2.2. Proposed mechanism underlying NTDs in *Gldc*-deficient mutant embryos

Taking into consideration the various possible mechanisms by which abnormal FOCM could result in NTDs and the experimental findings in this thesis, the most likely mechanism for *Gldc* deficiency to result in NTDs is summarised in **Figure 51**. Impaired glycine cleavage due to *Gldc* deficiency results in decreased production of mitochondrial-derived 1C units. This causes a decrease in 1C units entering cytosolic FOCM reactions and thus suppresses purine and thymidylate synthesis. Consequently, there is a decrease in cellular proliferation in tissues which express *Gldc*, i.e. the neuroepithelium, which results in failure of neural tube closure.

Outstanding questions include whether decreased nucleotide synthesis alone is sufficient to cause the phenotype, if uracil misincorporation is increased as a result of *Gldc* deficiency, whether apoptosis is abnormal in the neural tube of *Gldc*-deficient mice, and how a decrease in proliferation of neuroepithelial cells lead to failure of neural tube closure.

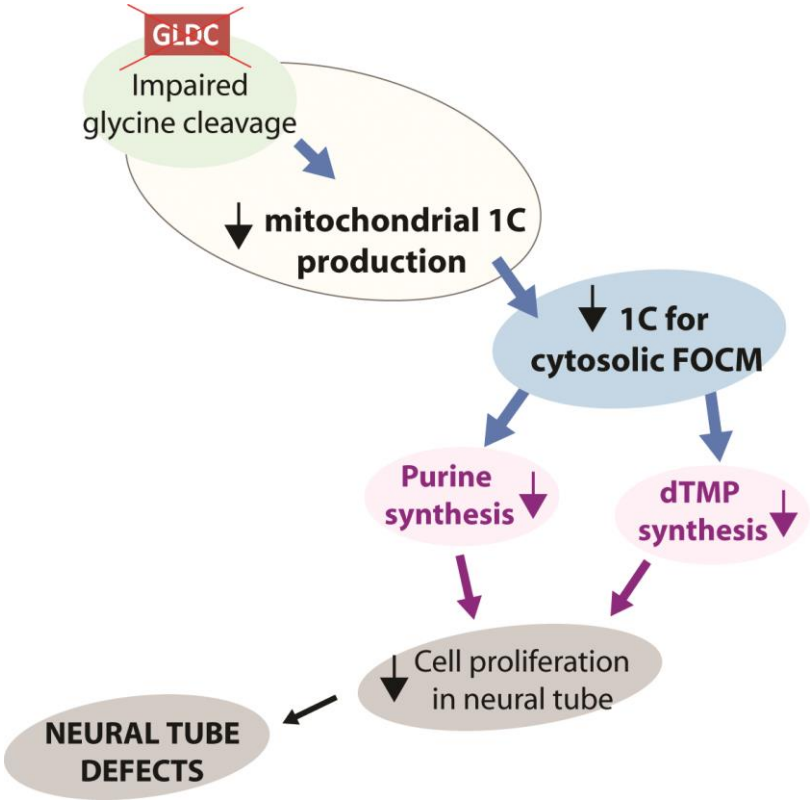

Figure 51. Proposed mechanism for *Gldc* deficiency to result in NTDs.

6.2.3. Does a deficit of one-carbon units contribute to NKH-related phenotypes?

The pathogenesis of NKH is mostly attributed to excess glycine as a result of impaired GCS activity. This thesis presents evidence for foetal malformation (i.e. NTDs) that can be caused by GCS-derived abnormalities in FOCM. It has been hypothesised that some of the brain malformations in NKH may be due to abnormal FOCM rather than an effect of excess glycine, as GCS components were found to be highly expressed in developing neuroepithelium and post-natal neural progenitor niches such as the dentate gyrus (Ichinohe et al., 2004). In fact, another FOCM enzyme, *Shmt1*, has also been implicated in neurogenesis in the mouse. *Shmt1* was found to be present in the dentate gyrus and heterozygosity for a null mutation in *Shmt1* results in impaired dTMP synthesis and affects hippocampal neurogenesis (Abarinov et al., 2013).

Abnormalities in FOCM due to GCS deficiency have not been directly investigated in the context of NKH, possibly due to the lack of a suitable GCS mouse model previously. Treatment of NKH patients with 1C donors showed little success (Van Hove et al., 1998), which suggests that either 1C insufficiency is not a major contribution to the pathology of NKH unlike in the NTDs in *Gldc*-deficient mice, or that intervention that far into the disease progression was too late. It is also possible that this treatment route was not tested

sufficiently, as very few patients were treated, there was no matched control group, and the selection of dosage was not based on measured biochemical outcomes. If abnormal FOCM can account for some of the foetal brain malformations, an ideal strategy would be to correct FOCM at appropriate developmental stages before the malformations occur. This would be of particular relevance to the hydrocephalus phenotype in *Gldc*^{GT1} mutants, which occurs in NKH and which is shown in this thesis to stem from malformations present at late-foetal stages (see **Figure 52** for diagrammatic summary of the possible mechanisms that can give rise to hydrocephalus in *Gldc*-deficient mice).

A straightforward way of testing this hypothesis is to supplement *Gldc*^{GT1} mutants with formate beyond neurulation stages and investigate whether there are changes in post-natal occurrence of hydrocephalus. However, formate was shown to produce toxicity upon prolonged supplementation (**Chapter 4**). The 7,500 mg/kg/day dose used in **Chapter 4** was based on previously published results in *Mthfd1L* null embryos (Momb et al., 2013). The *Mthfd1L* nulls displayed a severe phenotype of 100% NTD penetrance and embryonic lethality that was partially rescued by the 7,500 mg/kg/day dose of formate. A 5,000 mg/kg/day dose showed a lesser degree of rescue, suggesting a dose-dependent effect.

As the phenotype and NTD incidence of *Gldc*$^{GT1/GT1}$ homozygous embryos are not as severe as *Mthfd1L* nulls and could be completely rescued by formate, it might be possible to determine a lower dose of formate which can confer the same level of rescue but does not result in toxicity. Alternatively, formate treatment could be stopped at a stage where the subcommissural organ (SCO) is visible and the aqueduct appreciably narrows (approximately E16.5). Foetuses could then be examined at E18.5 for signs of ventricular enlargement. As formate has been shown to be present in the milk of lactating sheep and in newborn lamb plasma (Washburn et al., 2015), it would be possible to stop formate supplementation at E15.5-E16.5 (i.e. to allow for embryonic development of SCO, pineal gland, and aqueduct) and resume treatment after birth. This might prevent excessive accumulation of formate while formate remains in post-natal *Gldc*^{GT1} mutant plasma long enough to have an effect on incidence of hydrocephalus.

Hydrocephalus in NKH frequently present with a posterior fossa cyst and a cerebellar defect resembling Dandy-Walker (DW) malformation (Van Hove et al., 2000). Williams (1973) suggested that aqueduct stenosis resulting *from* (rather than being causative of) enlargement of the lateral ventricles can lead to a flattening of the tentorium, which may displace the cerebellum downwards, a hypothesis that could link aqueduct stenosis to a cerebellar displacement phenotype. The fourth ventricle appears normal in *Gldc* mutant mice and the DW malformation involves an upward displacement of the tentorium and severe hypoplasia of the vermis. Therefore, it is possible that different morphogenetic

processes are involved in the development of hydrocephalus in NKH patients and in the *Gldc* model, in which no severe abnormalities of the cerebellum is observed. It would be interesting to determine whether aqueduct stenosis is present in hydrocephalic NKH patients.

In DW malformation where hydrocephalus is also frequently reported, it has been suggested that the superior vermis may herniate into the quadrigeminal cistern, resulting in compression and thus stenosis of the aqueduct (Spennato et al., 2011, Cinalli et al., 2011). This gives a potential mechanism for a cerebellar defect to result in aqueduct stenosis. However in the *Gldc* mouse model, no severe, gross deformities in the cerebellum were observed. While a defect in cerebellar foliation may be present, it does not seem likely that this could produce the amount of compression that would result in aqueduct stenosis, as overall cerebellar size did not appear grossly abnormal.

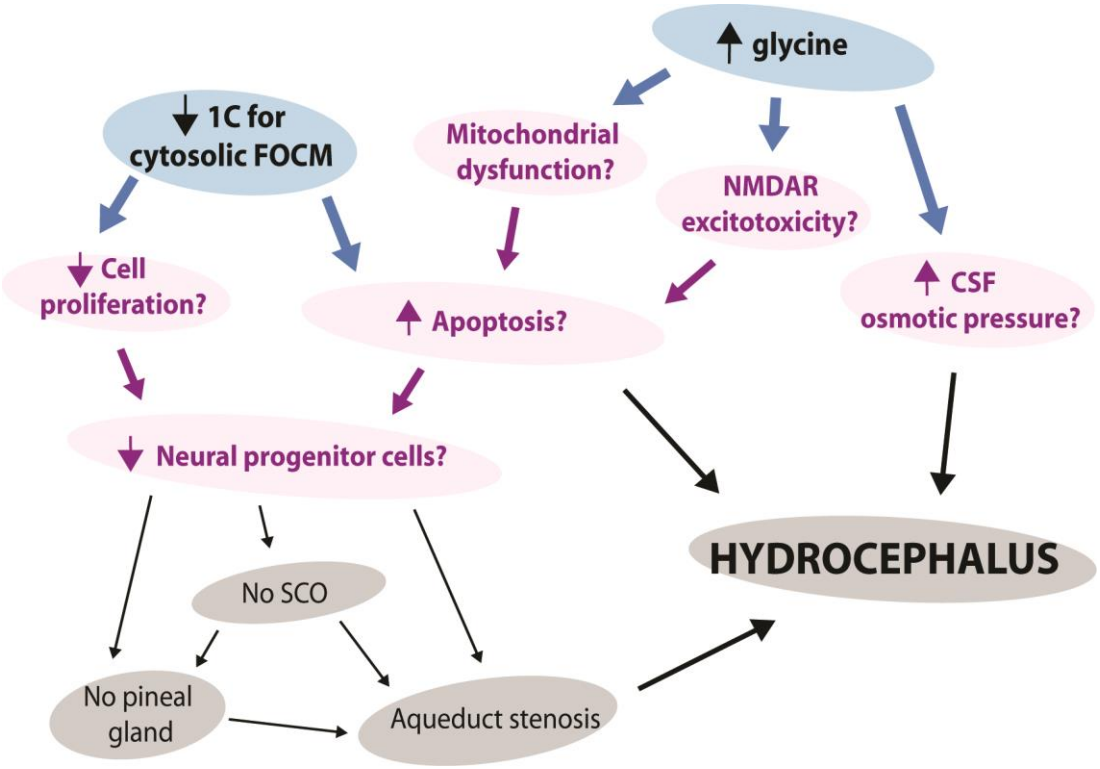

Figure 52. Summary of possible mechanisms that could lead to hydrocephalus in *Gldc*-deficient mice.

The two main metabolic disturbances caused by *Gldc* deficiency are reduced supply of mitochondrial 1C units resulting in abnormal FOCM, and elevation of glycine (blue). A number of possible mechanisms may follow (magenta), leading to the late-foetal malformations and post-natal occurrence of hydrocephalus (grey).

6.3. Glycine toxicity in *Gldc* deficiency

While NTDs in *Gldc*-deficient mice are most likely due to 1C insufficiency, it should be noted that tissue glycine levels at E11.5 are significantly elevated, and remain elevated in adult plasma and urine. The potential toxic effects of glycine in this model have not been extensively assessed. There is a possibility that glycine is involved in late-foetal and post-natal phenotypes due to the persistent exposure of *Gldc*-deficient tissue to elevated glycine. Korman et al. (2006) found that cord blood plasma glycine levels in a patient with atypical NKH were within the reference range but CSF glycine was very high at birth, which suggested that the placental circulation was able to prevent build-up of glycine in the foetal circulation, but the developing foetal brain would have been exposed to high levels of glycine through development. Thus, *Gldc*-deficient mice could mimic the conditions present in NKH during prenatal stages.

The effects of high glycine have been reported on several occasions and speculated to cause much of the pathology of NKH. The two main hypotheses for mechanism of glycine toxicity is over-activation of NMDARs and mitochondrial toxicity, both of which have been introduced in **Chapter 5**. This section draws from further studies not performed in the context of NKH, and briefly discusses how *Gldc*-deficient mice may be used to probe these possibilities.

6.3.1. Over-activation of NMDARs in NKH-related phenotypes

During central nervous system development, NMDAR activation (coupled with GlyR inhibition) in neuronal and glial precursor populations contributes to neuronal migration, cell survival and cell fate and may influence morphogenetic events (Nguyen et al., 2001). However, the effect of high glycine on NMDARs leading to neuronal survival or death are complicated by the downstream effects of NMDAR signalling, which can be both survival and death promoting (also known as the "NMDAR paradox"). Synaptic NMDAR signalling can activate neuroprotective pathways by suppressing apoptosis and/or reducing peroxide levels (i.e. boosting antioxidant capabilities) and promoting neuronal survival, while extrasynaptic NMDAR signalling could, inversely, favour pro-apoptotic pathways. Synaptic NMDARs contain both the GluN2A and GluN2B subunits, while extrasynaptic NMDARs are GluN2A-enriched (Hardingham and Bading, 2010).

NMDAR/GlyR signalling provides a second possible mechanism (other than FOCM) through which proliferation and/or apoptosis in the brain may be affected by the loss of

glycine cleavage. Staining for mitotic and apoptotic markers can be performed to assess the level of proliferation and apoptosis in, for example, the developing hippocampus or dentate gyrus region of *Gldc*-deficient late-foetal and/or post-natal brains. Assessment of the neural progenitor subtypes affected could be performed by staining with neuronal (e.g. NeuN) or glial (e.g. glial fibrillary acidic protein, GFAP) markers and correlating them with sites of *Gldc* expression.

Just as the FOCM-driven hypothesis in the previous section can be tested by rescue experiments with sodium formate, so can the effects of glycine toxicity be tested by supplementation with sodium benzoate. As benzoate is commonly given to NKH patients for sequestering glycine, it would be interesting to attempt to correct the elevated glycine in *Gldc*-deficient mice and determine whether amelioration of any phenotypes occur (e.g. early post-natal survival and hydrocephalus rates). It is more likely that both abnormal FOCM and high glycine contribute to the phenotypes, thus a rescue experiment using both formate and benzoate could also be attempted. It would also be interesting to test whether sequestering glycine would have any effect on the NTD phenotype. It should be noted that the cellular abnormalities caused by GCS deficiency will not necessarily be entirely corrected, so enzyme replacement or gene therapy may be required.

6.3.2. Possibility of mitochondrial dysfunction in *Gldc* deficiency

The clinical presentation of NKH bears striking resemblance to that of mitochondrial disorders with an underlying metabolic defect. For example, autosomal recessive fumarase deficiency (Coughlin et al., 1998) and X-linked pyruvate dehydrogenase deficiency (Brown et al., 1994) are disorders affecting the tricarboxylic acid (TCA) cycle (and thus energy metabolism) with a clinical presentation that resembles NKH: severe neurological impairment, corpus callosum defects and white matter atrophy, ventricular dilation, DW malformation, hypotonia, lethargy, seizures, and feeding difficulties, but with the additional presence of lactic acidosis which does not occur in NKH.

Mitochondrial dysfunctions are commonly reported in patients with organic acidurias, either as a primary effect due to a mutation in nuclear genes encoding components of the TCA cycle or oxidative phosphorylation (OXPHOS), or secondarily through inhibition of mitochondrial function by endogenous metabolites that accumulate in organic acidurias (Wajner and Goodman, 2011). This includes methylmalonic and proprionic acidemia, i.e. *ketotic* hyperglycinemia, in which there was a decrease in amount of OXPHOS complexes and ATP production, 50% reduction in mitochondrial DNA, and abnormal mitochondrial ultrastructures (Schwab et al., 2006).

Experiments performed in rat cerebral cortex homogenates suggest that high glycine can induce oxidative stress damage and result in mitochondrial energy dysfunction (Busanello et al., 2010, Leipnitz et al., 2009). Taken together, this suggests that accumulation of glycine to toxic levels could potentially lead to secondary mitochondrial dysfunction, which may contribute to the pathology of NKH. In addition, mitochondrial FOCM was recently found to be required for NADPH production which is important for reductive reactions and redox defence. Knockdown of both cytoplasmic MTHFD1 and mitochondrial MTHFD2 in HEK293T cells resulted in reduced redox defence, increased reactive oxygen species, and impaired resistance to oxidative stress. Thus, a loss of Gldc activity could disrupt mitochondrial FOCM and potentially alter redox balance (Fan et al., 2014).

In future experiments, the possibility of a mitochondrial dysfunction in *Gldc*-deficient mice could be probed in a number of ways. Decreases or increases in mitochondrial number, abundance and activities of OXPHOS and/or TCA cycle enzymes as well as changes in mitochondrial distribution and morphology might indicate presence of mitochondrial dysfunction. Measurement of oxygen consumption rates and respiratory control ratio would provide good functional indication regardless of the specific mitochondrial component affected (Brand and Nicholls, 2011). In addition, altered levels of glutathione, lipid peroxidation, and reactive oxygen species (i.e. various measures of oxidative stress) as well as caspase activation and apoptosis may serve as signs of mitochondrial dysfunction (Sas et al., 2007).

6.3.3. Alternative pathways for glycine catabolism

When considering the potential toxic effects of glycine, it is worth briefly considering other pathways of glycine catabolism that do not involve the GCS and their contributions to regulating overall glycine levels in the body. As described in **Chapter 4**, glycine can be utilised in the synthesis of serine through SHMT. Glycine is also consumed in a reaction catalysed by the glycine *N*-methyltransferase enzyme which converts SAM to SAH and generates sarcosine (Ogawa et al., 1998). The primary role of this reaction appears to be for the regulation of SAM/SAH ratio, as the production of sarcosine does not appear to serve any other significant metabolic function (Luka et al., 2009). However, sarcosine can act as a potential 1C donor.

In addition, other pathways for glycine catabolism have also been reported, such as through formation of glyoxylate and formate, conversion to pyruvate through serine, and the succinate-glycine cycle (Nakada et al., 1955). Conversion to pyruvate as a pathway for glycine (and serine) catabolism did not occur at significant levels in rat liver (Nakada et al.,

1955) or cancer cells (Fan et al., 2014). The succinate-glycine cycle was discovered to be involved in the synthesis of pyrrole rings and subsequently porphyrin in heme (Shemin et al., 1955), but does not appear to utilise significant amounts of glycine. Glycine is also used in synthesis of creatine (Brosnan et al., 2009) and the antioxidant glutathione (Wang et al., 2014a, Aoyama et al., 2012), conjugation of bile (Maekawa et al., 2014), and conjugation of benzoic acid (Kristensen et al., 2009). However, the significance of these alternative pathways is not clear, and the GCS remains the most important pathway for glycine catabolism in vertebrates (Yoshida and Kikuchi, 1972, Yoshida and Kikuchi, 1973, Wang et al., 2013).

References

ABARINOV, E. V., BEAUDIN, A. E., FIELD, M. S., PERRY, C. A., ALLEN, R. H., STABLER, S. P. & STOVER, P. J. 2013. Disruption of shmt1 impairs hippocampal neurogenesis and mnemonic function in mice. *J Nutr,* 143**,** 1028-35.

ABOUHAMED, M., GROBE, K., SAN, I. V., THELEN, S., HONNERT, U., BALDA, M. S., MATTER, K. & BAHLER, M. 2009. Myosin IXa regulates epithelial differentiation and its deficiency results in hydrocephalus. *Mol Biol Cell,* 20**,** 5074-85.

ACKERMAN, L. L. & MENEZES, A. H. 2003. Spinal congenital dermal sinuses: a 30-year experience. *Pediatrics,* 112**,** 641-7.

AKHTAR, M., CALDER, M. R., CORINA, D. L. & WRIGHT, J. N. 1982. Mechanistic studies on C-19 demethylation in oestrogen biosynthesis. *Biochem J,* 201**,** 569-80.

ALIEFENDIOGLU, D., TANA ASLAN, A., COSKUN, T., DURSUN, A., CAKMAK, F. N. & KESIMER, M. 2003. Transient nonketotic hyperglycinemia: two case reports and literature review. *Pediatr Neurol,* 28**,** 151-5.

ALLACHE, R., LACHANCE, S., GUYOT, M. C., DE MARCO, P., MERELLO, E., JUSTICE, M. J., CAPRA, V. & KIBAR, Z. 2014. Novel mutations in Lrp6 orthologs in mouse and human neural tube defects affect a highly dosage-sensitive Wnt non-canonical planar cell polarity pathway. *Hum Mol Genet,* 23**,** 1687-99.

AMELIO, I., CUTRUZZOLA, F., ANTONOV, A., AGOSTINI, M. & MELINO, G. 2014. Serine and glycine metabolism in cancer. *Trends Biochem Sci,* 39**,** 191-198.

ANDERSON, D. D., QUINTERO, C. M. & STOVER, P. J. 2011. Identification of a de novo thymidylate biosynthesis pathway in mammalian mitochondria. *Proc Natl Acad Sci U S A,* 108**,** 15163-8.

ANDERSON, D. D. & STOVER, P. J. 2009. SHMT1 and SHMT2 are functionally redundant in nuclear de novo thymidylate biosynthesis. *PLoS One,* 4**,** e5839.

ANDO, T., NYHAN, W. L., CONNOR, J. D., RASMUSSEN, K., DONNELL, G., BARNES, N., COTTOM, D. & HULL, D. 1972. The oxidation of glycine and propionic acid in propionic acidemia with ketotic hyperglycinemia. *Pediatr Res,* 6**,** 576-83.

ANDO, T., NYHAN, W. L., GERRITSEN, T., GONG, L., HEINER, D. C. & BRAY, P. F. 1968. Metabolism of glycine in the nonketotic form of hyperglycinemia. *Pediatr Res,* 2**,** 254-63.

ANDONIADOU, C. L. & MARTINEZ-BARBERA, J. P. 2013. Developmental mechanisms directing early anterior forebrain specification in vertebrates. *Cell Mol Life Sci,* 70**,** 3739-52.

AOYAMA, K., WATABE, M. & NAKAKI, T. 2012. Modulation of neuronal glutathione synthesis by EAAC1 and its interacting protein GTRAP3-18. *Amino Acids,* 42**,** 163-9.

AOYAMA, Y. & MOTOKAWA, Y. 1981. L-Threonine dehydrogenase of chicken liver. Purification, characterization, and physiological significance. *J Biol Chem,* 256**,** 12367-73.

APPLEGARTH, D. A. & TOONE, J. R. 2001. Nonketotic hyperglycinemia (glycine encephalopathy): laboratory diagnosis. *Mol Genet Metab,* 74**,** 139-46.

APPLEGARTH, D. A., TOONE, J. R. & LOWRY, R. B. 2000. Incidence of inborn errors of metabolism in British Columbia, 1969-1996. *Pediatrics,* 105**,** e10.

ARAKAWA, T., YOSHIDA, T., KONNO, T. & HONDA, Y. 1972. Defect of incorporation of glycine-1- 14 C into urinary uric acid in formiminotransferase deficiency syndrome. *Tohoku J Exp Med,* 106**,** 213-8.

BARBERA, J. P., RODRIGUEZ, T. A., GREENE, N. D., WENINGER, W. J., SIMEONE, A., COPP, A. J., BEDDINGTON, R. S. & DUNWOODIE, S. 2002. Folic acid prevents exencephaly in Cited2 deficient mice. *Hum Mol Genet,* 11**,** 283-93.

BARTH, A., NGUYEN, L. B., BARTH, L. & NEWELL, D. W. 2005. Glycine-induced neurotoxicity in organotypic hippocampal slice cultures. *Exp Brain Res,* 161**,** 351-7.

BASSON, M. A. & WINGATE, R. J. 2013. Congenital hypoplasia of the cerebellum: developmental causes and behavioral consequences. *Front Neuroanat,* 7**,** 29.

BAUMGARTNER, R., ANDO, T. & NYHAN, W. L. 1969. Nonketotic hyperglycinemia. *J Pediatr,* 75**,** 1022-30.
BEAUDIN, A. E., ABARINOV, E. V., MALYSHEVA, O., PERRY, C. A., CAUDILL, M. & STOVER, P. J. 2012. Dietary folate, but not choline, modifies neural tube defect risk in Shmt1 knockout mice. *Am J Clin Nutr,* 95**,** 109-14.
BEAUDIN, A. E., ABARINOV, E. V., NODEN, D. M., PERRY, C. A., CHU, S., STABLER, S. P., ALLEN, R. H. & STOVER, P. J. 2011. Shmt1 and de novo thymidylate biosynthesis underlie folate-responsive neural tube defects in mice. *Am J Clin Nutr,* 93**,** 789-98.
BEAUDIN, A. E. & STOVER, P. J. 2007. Folate-mediated one-carbon metabolism and neural tube defects: balancing genome synthesis and gene expression. *Birth Defects Res C Embryo Today,* 81**,** 183-203.
BEAUDIN, A. E. & STOVER, P. J. 2009. Insights into metabolic mechanisms underlying folate-responsive neural tube defects: a minireview. *Birth Defects Res A Clin Mol Teratol,* 85**,** 274-84.
BENZ, L. P., SWIFT, F. E., GRAHAM, F. L., ENTERLINE, D. S., MELVIN, E. C., HAMMOCK, P., GILBERT, J. R., SPEER, M. C., BASSUK, A. G., KESSLER, J. A. & GEORGE, T. M. 2004. TERC is not a major gene in human neural tube defects. *Birth Defects Res A Clin Mol Teratol,* 70**,** 531-3.
BLAESSE, P., AIRAKSINEN, M. S., RIVERA, C. & KAILA, K. 2009. Cation-chloride cotransporters and neuronal function. *Neuron,* 61**,** 820-38.
BLANK, M. C., GRINBERG, I., ARYEE, E., LALIBERTE, C., CHIZHIKOV, V. V., HENKELMAN, R. M. & MILLEN, K. J. 2011. Multiple developmental programs are altered by loss of Zic1 and Zic4 to cause Dandy-Walker malformation cerebellar pathogenesis. *Development,* 138**,** 1207-16.
BLENCOWE, H., COUSENS, S., MODELL, B. & LAWN, J. 2010. Folic acid to reduce neonatal mortality from neural tube disorders. *Int J Epidemiol,* 39 Suppl 1**,** i110-21.
BLOM, H. J. 2009. Folic acid, methylation and neural tube closure in humans. *Birth Defects Res A Clin Mol Teratol,* 85**,** 295-302.
BLOM, H. J., SHAW, G. M., DEN HEIJER, M. & FINNELL, R. H. 2006. Neural tube defects and folate: case far from closed. *Nat Rev Neurosci,* 7**,** 724-31.
BLOUNT, B. C., MACK, M. M., WEHR, C. M., MACGREGOR, J. T., HIATT, R. A., WANG, G., WICKRAMASINGHE, S. N., EVERSON, R. B. & AMES, B. N. 1997. Folate deficiency causes uracil misincorporation into human DNA and chromosome breakage: implications for cancer and neuronal damage. *Proc Natl Acad Sci U S A,* 94**,** 3290-5.
BOHNSACK, B. L. & HIRSCHI, K. K. 2004. Red light, green light: signals that control endothelial cell proliferation during embryonic vascular development. *Cell Cycle,* 3**,** 1506-11.
BOLUSANI, S., YOUNG, B. A., COLE, N. A., TIBBETTS, A. S., MOMB, J., BRYANT, J. D., SOLMONSON, A. & APPLING, D. R. 2011. Mammalian MTHFD2L encodes a mitochondrial methylenetetrahydrofolate dehydrogenase isozyme expressed in adult tissues. *J Biol Chem,* 286**,** 5166-74.
BONEH, A., KORMAN, S. H., SATO, K., KANNO, J., MATSUBARA, Y., LERER, I., BEN-NERIAH, Z. & KURE, S. 2005. A single nucleotide substitution that abolishes the initiator methionine codon of the GLDC gene is prevalent among patients with glycine encephalopathy in Jerusalem. *J Hum Genet,* 50**,** 230-4.
BOTTO, L. D., LISI, A., ROBERT-GNANSIA, E., ERICKSON, J. D., VOLLSET, S. E., MASTROIACOVO, P., BOTTING, B., COCCHI, G., DE VIGAN, C., DE WALLE, H., FEIJOO, M., IRGENS, L. M., MCDONNELL, B., MERLOB, P., RITVANEN, A., SCARANO, G., SIFFEL, C., METNEKI, J., STOLL, C., SMITHELLS, R. & GOUJARD, J. 2005. International retrospective cohort study of neural tube defects in relation to folic acid recommendations: are the recommendations working? *BMJ,* 330**,** 571.
BOTTO, L. D. & YANG, Q. 2000. 5,10-Methylenetetrahydrofolate reductase gene variants and congenital anomalies: a HuGE review. *Am J Epidemiol,* 151**,** 862-77.
BOWER, C. & STANLEY, F. J. 1989. Dietary folate as a risk factor for neural-tube defects: evidence from a case-control study in Western Australia. *Med J Aust,* 150**,** 613-9.

BOYLES, A. L., HAMMOCK, P. & SPEER, M. C. 2005. Candidate gene analysis in human neural tube defects. *Am J Med Genet C Semin Med Genet,* 135C**,** 9-23.

BRAND, M. D. & NICHOLLS, D. G. 2011. Assessing mitochondrial dysfunction in cells. *Biochem J,* 435**,** 297-312.

BRODY, L. C., CONLEY, M., COX, C., KIRKE, P. N., MCKEEVER, M. P., MILLS, J. L., MOLLOY, A. M., O'LEARY, V. B., PARLE-MCDERMOTT, A., SCOTT, J. M. & SWANSON, D. A. 2002. A polymorphism, R653Q, in the trifunctional enzyme methylenetetrahydrofolate dehydrogenase/methenyltetrahydrofolate cyclohydrolase/formyltetrahydrofolate synthetase is a maternal genetic risk factor for neural tube defects: report of the Birth Defects Research Group. *Am J Hum Genet,* 71**,** 1207-15.

BROOK, F. A., SHUM, A. S., VAN STRAATEN, H. W. & COPP, A. J. 1991. Curvature of the caudal region is responsible for failure of neural tube closure in the curly tail (ct) mouse embryo. *Development,* 113**,** 671-8.

BROSNAN, J. T., WIJEKOON, E. P., WARFORD-WOOLGAR, L., TROTTIER, N. L., BROSNAN, M. E., BRUNTON, J. A. & BERTOLO, R. F. 2009. Creatine synthesis is a major metabolic process in neonatal piglets and has important implications for amino acid metabolism and methyl balance. *J Nutr,* 139**,** 1292-7.

BROUNS, M. R., DE CASTRO, S. C., TERWINDT-ROUWENHORST, E. A., MASSA, V., HEKKING, J. W., HIRST, C. S., SAVERY, D., MUNTS, C., PARTRIDGE, D., LAMERS, W., KOHLER, E., VAN STRAATEN, H. W., COPP, A. J. & GREENE, N. D. 2011. Over-expression of Grhl2 causes spina bifida in the Axial defects mutant mouse. *Hum Mol Genet,* 20**,** 1536-46.

BROUNS, M. R., MATHESON, S. F., HU, K. Q., DELALLE, I., CAVINESS, V. S., SILVER, J., BRONSON, R. T. & SETTLEMAN, J. 2000. The adhesion signaling molecule p190 RhoGAP is required for morphogenetic processes in neural development. *Development,* 127**,** 4891-903.

BROUWER, I. A., VAN DUSSELDORP, M., WEST, C. E., MEYBOOM, S., THOMAS, C. M., DURAN, M., VAN HET HOF, K. H., ESKES, T. K., HAUTVAST, J. G. & STEEGERS-THEUNISSEN, R. P. 1999. Dietary folate from vegetables and citrus fruit decreases plasma homocysteine concentrations in humans in a dietary controlled trial. *J Nutr,* 129**,** 1135-9.

BROWN, G. K., OTERO, L. J., LEGRIS, M. & BROWN, R. M. 1994. Pyruvate dehydrogenase deficiency. *J Med Genet,* 31**,** 875-9.

BU, P., EVRARD, Y. A., LOZANO, G. & DENT, S. Y. 2007. Loss of Gcn5 acetyltransferase activity leads to neural tube closure defects and exencephaly in mouse embryos. *Mol Cell Biol,* 27**,** 3405-16.

BULTMAN, S., GEBUHR, T., YEE, D., LA MANTIA, C., NICHOLSON, J., GILLIAM, A., RANDAZZO, F., METZGER, D., CHAMBON, P., CRABTREE, G. & MAGNUSON, T. 2000. A Brg1 null mutation in the mouse reveals functional differences among mammalian SWI/SNF complexes. *Mol Cell,* 6**,** 1287-95.

BURREN, K. A., SAVERY, D., MASSA, V., KOK, R. M., SCOTT, J. M., BLOM, H. J., COPP, A. J. & GREENE, N. D. 2008. Gene-environment interactions in the causation of neural tube defects: folate deficiency increases susceptibility conferred by loss of Pax3 function. *Hum Mol Genet,* 17**,** 3675-85.

BURREN, K. A., SCOTT, J. M., COPP, A. J. & GREENE, N. D. 2010. The genetic background of the curly tail strain confers susceptibility to folate-deficiency-induced exencephaly. *Birth Defects Res A Clin Mol Teratol,* 88**,** 76-83.

BUSANELLO, E. N., MOURA, A. P., VIEGAS, C. M., ZANATTA, A., DA COSTA FERREIRA, G., SCHUCK, P. F. & WAJNER, M. 2010. Neurochemical evidence that glycine induces bioenergetical dysfunction. *Neurochem Int,* 56**,** 948-54.

BUSBY, A., ABRAMSKY, L., DOLK, H., ARMSTRONG, B., ADDOR, M. C., ANNEREN, G., ARMSTRONG, N., BAGUETTE, A., BARISIC, I., BERGHOLD, A., BIANCA, S., BRAZ, P., CALZOLARI, E., CHRISTIANSEN, M., COCCHI, G., DALTVEIT, A. K., DE WALLE, H., EDWARDS, G., GATT, M., GENER, B., GILLEROT, Y., GJERGJA, R., GOUJARD, J., HAEUSLER, M., LATOS-BIELENSKA, A., MCDONNELL, R., NEVILLE, A., OLARS, B., PORTILLO, I., RITVANEN, A., ROBERT-GNANSIA, E., ROSCH, C., SCARANO, G. &

STEINBICKER, V. 2005. Preventing neural tube defects in Europe: a missed opportunity. *Reprod Toxicol,* 20**,** 393-402.
CAINS, S., SHEPHERD, A., NABIUNI, M., OWEN-LYNCH, P. J. & MIYAN, J. 2009. Addressing a folate imbalance in fetal cerebrospinal fluid can decrease the incidence of congenital hydrocephalus. *J Neuropathol Exp Neurol,* 68**,** 404-16.
CARMICHAEL, S. L., RASMUSSEN, S. A. & SHAW, G. M. 2010. Prepregnancy obesity: a complex risk factor for selected birth defects. *Birth Defects Res A Clin Mol Teratol,* 88**,** 804-10.
CARTER, C. S., VOGEL, T. W., ZHANG, Q., SEO, S., SWIDERSKI, R. E., MONINGER, T. O., CASSELL, M. D., THEDENS, D. R., KEPPLER-NOREUIL, K. M., NOPOULOS, P., NISHIMURA, D. Y., SEARBY, C. C., BUGGE, K. & SHEFFIELD, V. C. 2012. Abnormal development of NG2+PDGFR-alpha+ neural progenitor cells leads to neonatal hydrocephalus in a ciliopathy mouse model. *Nat Med,* 18**,** 1797-804.
CARTER, T. C., PANGILINAN, F., TROENDLE, J. F., MOLLOY, A. M., VANDERMEER, J., MITCHELL, A., KIRKE, P. N., CONLEY, M. R., SHANE, B., SCOTT, J. M., BRODY, L. C. & MILLS, J. L. 2011. Evaluation of 64 candidate single nucleotide polymorphisms as risk factors for neural tube defects in a large Irish study population. *Am J Med Genet A,* 155A**,** 14-21.
CASERO, R. A., JR. & MARTON, L. J. 2007. Targeting polyamine metabolism and function in cancer and other hyperproliferative diseases. *Nat Rev Drug Discov,* 6**,** 373-90.
CASTANEYRA-PERDOMO, A., MEYER, G., CARMONA-CALERO, E., BANUELOS-PINEDA, J., MENDEZ-MEDINA, R., ORMAZABAL-RAMOS, C. & FERRES-TORRES, R. 1994. Alterations of the subcommissural organ in the hydrocephalic human fetal brain. *Brain Res Dev Brain Res,* 79**,** 316-20.
CAUDILL, M. A., WANG, J. C., MELNYK, S., POGRIBNY, I. P., JERNIGAN, S., COLLINS, M. D., SANTOS-GUZMAN, J., SWENDSEID, M. E., COGGER, E. A. & JAMES, S. J. 2001. Intracellular S-adenosylhomocysteine concentrations predict global DNA hypomethylation in tissues of methyl-deficient cystathionine beta-synthase heterozygous mice. *J Nutr,* 131**,** 2811-8.
CEDERBAUM, A. I. & QURESHI, A. 1982. Role of catalase and hydroxyl radicals in the oxidation of methanol by rat liver microsomes. *Biochem Pharmacol,* 31**,** 329-35.
CHALFIE, M. 1995. Green fluorescent protein. *Photochem Photobiol,* 62**,** 651-6.
CHANARIN, I., MACGIBBON, B. M., O'SULLIVAN, W. J. & MOLLIN, D. L. 1959. Folic-acid deficiency in pregnancy. The pathogenesis of megaloblastic anaemia of pregnancy. *Lancet,* 2**,** 634-9.
CHANG, S., WANG, L., GUAN, Y., SHANGGUAN, S., DU, Q., WANG, Y., ZHANG, T. & ZHANG, Y. 2013. Long interspersed nucleotide element-1 hypomethylation in folate-deficient mouse embryonic stem cells. *J Cell Biochem,* 114**,** 1549-58.
CHEN, X., WATKINS, R., DELOT, E., RELIENE, R., SCHIESTL, R. H., BURGOYNE, P. S. & ARNOLD, A. P. 2008. Sex difference in neural tube defects in p53-null mice is caused by differences in the complement of X not Y genes. *Dev Neurobiol,* 68**,** 265-73.
CHEN, Z., KARAPLIS, A. C., ACKERMAN, S. L., POGRIBNY, I. P., MELNYK, S., LUSSIER-CACAN, S., CHEN, M. F., PAI, A., JOHN, S. W., SMITH, R. S., BOTTIGLIERI, T., BAGLEY, P., SELHUB, J., RUDNICKI, M. A., JAMES, S. J. & ROZEN, R. 2001. Mice deficient in methylenetetrahydrofolate reductase exhibit hyperhomocysteinemia and decreased methylation capacity, with neuropathology and aortic lipid deposition. *Hum Mol Genet,* 10**,** 433-43.
CHRISTENSEN, K. E., DAHHOU, M., KRAMER, M. S. & ROZEN, R. 2014. The MTHFD1 1958G>A variant is associated with elevated C-reactive protein and body mass index in Canadian women from a premature birth cohort. *Mol Genet Metab,* 111**,** 390-2.
CHRISTENSEN, K. E., DENG, L., LEUNG, K. Y., ARNING, E., BOTTIGLIERI, T., MALYSHEVA, O. V., CAUDILL, M. A., KRUPENKO, N. I., GREENE, N. D., JEROME-MAJEWSKA, L., MACKENZIE, R. E. & ROZEN, R. 2013. A novel mouse model for genetic variation in

10-formyltetrahydrofolate synthetase exhibits disturbed purine synthesis with impacts on pregnancy and embryonic development. *Hum Mol Genet,* 22**,** 3705-19.
CHRISTENSEN, K. E., MIKAEL, L. G., LEUNG, K. Y., LEVESQUE, N., DENG, L., WU, Q., MALYSHEVA, O. V., BEST, A., CAUDILL, M. A., GREENE, N. D. & ROZEN, R. 2015. High folic acid consumption leads to pseudo-MTHFR deficiency, altered lipid metabolism, and liver injury in mice. *Am J Clin Nutr,* 101**,** 646-58.
CHRISTENSEN, K. E., PATEL, H., KUZMANOV, U., MEJIA, N. R. & MACKENZIE, R. E. 2005. Disruption of the mthfd1 gene reveals a monofunctional 10-formyltetrahydrofolate synthetase in mammalian mitochondria. *J Biol Chem,* 280**,** 7597-602.
CINALLI, G., SPENNATO, P., NASTRO, A., ALIBERTI, F., TRISCHITTA, V., RUGGIERO, C., MIRONE, G. & CIANCIULLI, E. 2011. Hydrocephalus in aqueductal stenosis. *Childs Nerv Syst,* 27**,** 1621-42.
COCKROFT, D. L., BROOK, F. A. & COPP, A. J. 1992. Inositol deficiency increases the susceptibility to neural tube defects of genetically predisposed (curly tail) mouse embryos in vitro. *Teratology,* 45**,** 223-32.
COERDT, W., MILLER, K., HOLZGREVE, W., RAUSKOLB, R., SCHWINGER, E. & REHDER, H. 1997. Neural tube defects in chromosomally normal and abnormal human embryos. *Ultrasound Obstet Gynecol,* 10**,** 410-5.
COGRAM, P., HYNES, A., DUNLEVY, L. P., GREENE, N. D. & COPP, A. J. 2004. Specific isoforms of protein kinase C are essential for prevention of folate-resistant neural tube defects by inositol. *Hum Mol Genet,* 13**,** 7-14.
COGRAM, P., TESH, S., TESH, J., WADE, A., ALLAN, G., GREENE, N. D. & COPP, A. J. 2002. D-chiro-inositol is more effective than myo-inositol in preventing folate-resistant mouse neural tube defects. *Hum Reprod,* 17**,** 2451-8.
COOPER, A. F., YU, K. P., BRUECKNER, M., BRAILEY, L. L., JOHNSON, L., MCGRATH, J. M. & BALE, A. E. 2005. Cardiac and CNS defects in a mouse with targeted disruption of suppressor of fused. *Development,* 132**,** 4407-17.
COPP, A., COGRAM, P., FLEMING, A., GERRELLI, D., HENDERSON, D., HYNES, A., KOLATSI-JOANNOU, M., MURDOCH, J. & YBOT-GONZALEZ, P. 2000. Neurulation and neural tube closure defects. *Methods Mol Biol,* 136**,** 135-60.
COPP, A. J. 2005. Neurulation in the cranial region--normal and abnormal. *J Anat,* 207**,** 623-35.
COPP, A. J., ADZICK, N. S., CHITTY, L. S., FLETCHER, J. M., HOLMBECK, G. N. & SHAW, G. M. 2015. Spina bifida. *Nature Reviews Disease Primers*.
COPP, A. J. & GREENE, N. D. 2010 Genetics and development of neural tube defects. *J Pathol,* 220**,** 217-30.
COPP, A. J. & GREENE, N. D. 2013. Neural tube defects--disorders of neurulation and related embryonic processes. *Wiley Interdiscip Rev Dev Biol,* 2**,** 213-27.
COPP, A. J., GREENE, N. D. & MURDOCH, J. N. 2003. The genetic basis of mammalian neurulation. *Nat Rev Genet,* 4**,** 784-93.
COPP, A. J., STANIER, P. & GREENE, N. D. 2013. Neural tube defects: recent advances, unsolved questions, and controversies. *Lancet Neurol,* 12**,** 799-810.
CORNEL, M. C. & ERICKSON, J. D. 1997. Comparison of national policies on periconceptional use of folic acid to prevent spina bifida and anencephaly (SBA). *Teratology,* 55**,** 134-7.
CORREA, A., GILBOA, S. M., BESSER, L. M., BOTTO, L. D., MOORE, C. A., HOBBS, C. A., CLEVES, M. A., RIEHLE-COLARUSSO, T. J., WALLER, D. K. & REECE, E. A. 2008. Diabetes mellitus and birth defects. *Am J Obstet Gynecol,* 199**,** 237 e1-9.
COUGHLIN, E. M., CHRISTENSEN, E., KUNZ, P. L., KRISHNAMOORTHY, K. S., WALKER, V., DENNIS, N. R., CHALMERS, R. A., ELPELEG, O. N., WHELAN, D., POLLITT, R. J., RAMESH, V., MANDELL, R. & SHIH, V. E. 1998. Molecular analysis and prenatal diagnosis of human fumarase deficiency. *Mol Genet Metab,* 63**,** 254-62.
COURTEMANCHE, C., ELSON-SCHWAB, I., MASHIYAMA, S. T., KERRY, N. & AMES, B. N. 2004. Folate deficiency inhibits the proliferation of primary human CD8+ T lymphocytes in vitro. *J Immunol,* 173**,** 3186-92.

CRAIG, S. A. 2004. Betaine in human nutrition. *Am J Clin Nutr,* 80**,** 539-49.
CREUZET, S. E., MARTINEZ, S. & LE DOUARIN, N. M. 2006. The cephalic neural crest exerts a critical effect on forebrain and midbrain development. *Proc Natl Acad Sci U S A,* 103**,** 14033-8.
CRIDER, K. S., BAILEY, L. B. & BERRY, R. J. 2011. Folic acid food fortification-its history, effect, concerns, and future directions. *Nutrients,* 3**,** 370-84.
CROES, K., CASTEELS, M., DE HOFFMANN, E., MANNAERTS, G. P. & VAN VELDHOVEN, P. P. 1996. alpha-Oxidation of 3-methyl-substituted fatty acids in rat liver. Production of formic acid instead of CO2, cofactor requirements, subcellular localization and formation of a 2-hydroxy-3-methylacyl-CoA intermediate. *Eur J Biochem,* 240**,** 674-83.
CURTIN, J. A., QUINT, E., TSIPOURI, V., ARKELL, R. M., CATTANACH, B., COPP, A. J., HENDERSON, D. J., SPURR, N., STANIER, P., FISHER, E. M., NOLAN, P. M., STEEL, K. P., BROWN, S. D., GRAY, I. C. & MURDOCH, J. N. 2003. Mutation of Celsr1 disrupts planar polarity of inner ear hair cells and causes severe neural tube defects in the mouse. *Curr Biol,* 13**,** 1129-33.
CZEIZEL, A. E. & DUDAS, I. 1992. Prevention of the first occurrence of neural-tube defects by periconceptional vitamin supplementation. *N Engl J Med,* 327**,** 1832-5.
DALY, L. E., KIRKE, P. N., MOLLOY, A., WEIR, D. G. & SCOTT, J. M. 1995. Folate levels and neural tube defects. Implications for prevention. *JAMA,* 274**,** 1698-702.
DATTANI, M. T., MARTINEZ-BARBERA, J. P., THOMAS, P. Q., BRICKMAN, J. M., GUPTA, R., MARTENSSON, I. L., TORESSON, H., FOX, M., WALES, J. K., HINDMARSH, P. C., KRAUSS, S., BEDDINGTON, R. S. & ROBINSON, I. C. 1998. Mutations in the homeobox gene HESX1/Hesx1 associated with septo-optic dysplasia in human and mouse. *Nat Genet,* 19**,** 125-33.
DAVIDSON, C. M., NORTHRUP, H., KING, T. M., FLETCHER, J. M., TOWNSEND, I., TYERMAN, G. H. & AU, K. S. 2008. Genes in glucose metabolism and association with spina bifida. *Reprod Sci,* 15**,** 51-8.
DAVIS, R. E., SWIDERSKI, R. E., RAHMOUNI, K., NISHIMURA, D. Y., MULLINS, R. F., AGASSANDIAN, K., PHILP, A. R., SEARBY, C. C., ANDREWS, M. P., THOMPSON, S., BERRY, C. J., THEDENS, D. R., YANG, B., WEISS, R. M., CASSELL, M. D., STONE, E. M. & SHEFFIELD, V. C. 2007. A knockin mouse model of the Bardet-Biedl syndrome 1 M390R mutation has cilia defects, ventriculomegaly, retinopathy, and obesity. *Proc Natl Acad Sci U S A,* 104**,** 19422-7.
DE CASTRO, S. C., MALHAS, A., LEUNG, K. Y., GUSTAVSSON, P., VAUX, D. J., COPP, A. J. & GREENE, N. D. 2012. Lamin b1 polymorphism influences morphology of the nuclear envelope, cell cycle progression, and risk of neural tube defects in mice. *PLoS Genet,* 8**,** e1003059.
DE GROOT, C. J., TROELSTRA, J. A. & HOMMES, F. A. 1970. Nonketotic hyperglycinemia: an in vitro study of the glycine-serine conversion in liver of three patients and the effect of dietary methionine. *Pediatr Res,* 4**,** 238-43.
DE WALS, P., TAIROU, F., VAN ALLEN, M. I., UH, S. H., LOWRY, R. B., SIBBALD, B., EVANS, J. A., VAN DEN HOF, M. C., ZIMMER, P., CROWLEY, M., FERNANDEZ, B., LEE, N. S. & NIYONSENGA, T. 2007. Reduction in neural-tube defects after folic acid fortification in Canada. *N Engl J Med,* 357**,** 135-42.
DEAK, K. L., SIEGEL, D. G., GEORGE, T. M., GREGORY, S., ASHLEY-KOCH, A. & SPEER, M. C. 2008. Further evidence for a maternal genetic effect and a sex-influenced effect contributing to risk for human neural tube defects. *Birth Defects Res A Clin Mol Teratol,* 82**,** 662-9.
DEBELJAK, N., FINK, M. & ROZMAN, D. 2003. Many facets of mammalian lanosterol 14alpha-demethylase from the evolutionarily conserved cytochrome P450 family CYP51. *Arch Biochem Biophys,* 409**,** 159-71.
DENG, L., ELMORE, C. L., LAWRANCE, A. K., MATTHEWS, R. G. & ROZEN, R. 2008. Methionine synthase reductase deficiency results in adverse reproductive outcomes and congenital heart defects in mice. *Mol Genet Metab,* 94**,** 336-42.

DETRAIT, E. R., GEORGE, T. M., ETCHEVERS, H. C., GILBERT, J. R., VEKEMANS, M. & SPEER, M. C. 2005. Human neural tube defects: developmental biology, epidemiology, and genetics. *Neurotoxicol Teratol,* 27**,** 515-24.

DI PIETRO, E., SIROIS, J., TREMBLAY, M. L. & MACKENZIE, R. E. 2002. Mitochondrial NAD-dependent methylenetetrahydrofolate dehydrogenase-methenyltetrahydrofolate cyclohydrolase is essential for embryonic development. *Mol Cell Biol,* 22**,** 4158-66.

DI ROCCO, C., FRASSANITO, P., MASSIMI, L. & PERAIO, S. 2011. Hydrocephalus and Chiari type I malformation. *Childs Nerv Syst,* 27**,** 1653-64.

DINOPOULOS, A., MATSUBARA, Y. & KURE, S. 2005. Atypical variants of nonketotic hyperglycinemia. *Mol Genet Metab,* 86**,** 61-9.

DOBYNS, W. B. 1989. Agenesis of the corpus callosum and gyral malformations are frequent manifestations of nonketotic hyperglycinemia. *Neurology,* 39**,** 817-20.

DOMINGUEZ-PINOS, M. D., PAEZ, P., JIMENEZ, A. J., WEIL, B., ARRAEZ, M. A., PEREZ-FIGARES, J. M. & RODRIGUEZ, E. M. 2005. Ependymal denudation and alterations of the subventricular zone occur in human fetuses with a moderate communicating hydrocephalus. *J Neuropathol Exp Neurol,* 64**,** 595-604.

DROLET, B. A. & BOUDREAU, C. 2004. When good is not good enough: the predictive value of cutaneous lesions of the lumbosacral region for occult spinal dysraphism. *Arch Dermatol,* 140**,** 1153-5.

DUNLEVY, L. P., BURREN, K. A., MILLS, K., CHITTY, L. S., COPP, A. J. & GREENE, N. D. 2006. Integrity of the methylation cycle is essential for mammalian neural tube closure. *Birth Defects Res A Clin Mol Teratol,* 76**,** 544-52.

DUNLEVY, L. P., CHITTY, L. S., BURREN, K. A., DOUDNEY, K., STOJILKOVIC-MIKIC, T., STANIER, P., SCOTT, R., COPP, A. J. & GREENE, N. D. 2007. Abnormal folate metabolism in foetuses affected by neural tube defects. *Brain,* 130**,** 1043-9.

ECHELARD, Y., EPSTEIN, D. J., ST-JACQUES, B., SHEN, L., MOHLER, J., MCMAHON, J. A. & MCMAHON, A. P. 1993. Sonic hedgehog, a member of a family of putative signaling molecules, is implicated in the regulation of CNS polarity. *Cell,* 75**,** 1417-30.

EDWARDS, M. J. 1986. Hyperthermia as a teratogen: a review of experimental studies and their clinical significance. *Teratog Carcinog Mutagen,* 6**,** 563-82.

EDWARDS, T. J., SHERR, E. H., BARKOVICH, A. J. & RICHARDS, L. J. 2014. Clinical, genetic and imaging findings identify new causes for corpus callosum development syndromes. *Brain,* 137**,** 1579-613.

EGGENSCHWILER, J. T., ESPINOZA, E. & ANDERSON, K. V. 2001. Rab23 is an essential negative regulator of the mouse Sonic hedgehog signalling pathway. *Nature,* 412**,** 194-8.

EHLERS, K., STURJE, H., MERKER, H. J. & NAU, H. 1992. Valproic acid-induced spina bifida: a mouse model. *Teratology,* 45**,** 145-54.

ELMORE, C. L., WU, X., LECLERC, D., WATSON, E. D., BOTTIGLIERI, T., KRUPENKO, N. I., KRUPENKO, S. A., CROSS, J. C., ROZEN, R., GRAVEL, R. A. & MATTHEWS, R. G. 2007. Metabolic derangement of methionine and folate metabolism in mice deficient in methionine synthase reductase. *Mol Genet Metab,* 91**,** 85-97.

ELWOOD, J. M. 1983. Can vitamins prevent neural tube defects? *Can Med Assoc J,* 129**,** 1088-92.

EPSTEIN, D. J., VEKEMANS, M. & GROS, P. 1991. Splotch (Sp2H), a mutation affecting development of the mouse neural tube, shows a deletion within the paired homeodomain of Pax-3. *Cell,* 67**,** 767-74.

ETHERIDGE, S. L., RAY, S., LI, S., HAMBLET, N. S., LIJAM, N., TSANG, M., GREER, J., KARDOS, N., WANG, J., SUSSMAN, D. J., CHEN, P. & WYNSHAW-BORIS, A. 2008. Murine dishevelled 3 functions in redundant pathways with dishevelled 1 and 2 in normal cardiac outflow tract, cochlea, and neural tube development. *PLoS Genet,* 4**,** e1000259.

EVANS, M. J. & KAUFMAN, M. H. 1981. Establishment in culture of pluripotential cells from mouse embryos. *Nature,* 292**,** 154-6.

FAME, R. M., MACDONALD, J. L. & MACKLIS, J. D. 2011. Development, specification, and diversity of callosal projection neurons. *Trends Neurosci,* 34**,** 41-50.

FAN, J., YE, J., KAMPHORST, J. J., SHLOMI, T., THOMPSON, C. B. & RABINOWITZ, J. D. 2014. Quantitative flux analysis reveals folate-dependent NADPH production. *Nature,* 510**,** 298-302.

FIELD, M. S., ANDERSON, D. D. & STOVER, P. J. 2011. Mthfs is an Essential Gene in Mice and a Component of the Purinosome. *Front Genet,* 2**,** 36.

FINE, E. L., HORAL, M., CHANG, T. I., FORTIN, G. & LOEKEN, M. R. 1999. Evidence that elevated glucose causes altered gene expression, apoptosis, and neural tube defects in a mouse model of diabetic pregnancy. *Diabetes,* 48**,** 2454-62.

FINNELL, R. H., BENNETT, G. D., KARRAS, S. B. & MOHL, V. K. 1988. Common hierarchies of susceptibility to the induction of neural tube defects in mouse embryos by valproic acid and its 4-propyl-4-pentenoic acid metabolite. *Teratology,* 38**,** 313-20.

FINNELL, R. H., MOON, S. P., ABBOTT, L. C., GOLDEN, J. A. & CHERNOFF, G. F. 1986. Strain differences in heat-induced neural tube defects in mice. *Teratology,* 33**,** 247-52.

FLEMING, A. & COPP, A. J. 1998. Embryonic folate metabolism and mouse neural tube defects. *Science,* 280**,** 2107-9.

FLEMING, A. & COPP, A. J. 2000. A genetic risk factor for mouse neural tube defects: defining the embryonic basis. *Hum Mol Genet,* 9**,** 575-81.

FLETCHER, J. M., BYE, A. M., NAYANAR, V. & WILCKEN, B. 1995. Non-ketotic hyperglycinaemia presenting as pachygyria. *J Inherit Metab Dis,* 18**,** 665-8.

FLIEGAUF, M., BENZING, T. & OMRAN, H. 2007. When cilia go bad: cilia defects and ciliopathies. *Nat Rev Mol Cell Biol,* 8**,** 880-93.

FLUSSER, H., KORMAN, S. H., SATO, K., MATSUBARA, Y., GALIL, A. & KURE, S. 2005. Mild glycine encephalopathy (NKH) in a large kindred due to a silent exonic GLDC splice mutation. *Neurology,* 64**,** 1426-30.

FROSST, P., BLOM, H. J., MILOS, R., GOYETTE, P., SHEPPARD, C. A., MATTHEWS, R. G., BOERS, G. J., DEN HEIJER, M., KLUIJTMANS, L. A., VAN DEN HEUVEL, L. P. & ET AL. 1995. A candidate genetic risk factor for vascular disease: a common mutation in methylenetetrahydrofolate reductase. *Nat Genet,* 10**,** 111-3.

FUJIMOTO, Y., MATSUSHITA, H., PLESE, J. P. & MARINO, R., JR. 2004. Hydrocephalus due to diffuse villous hyperplasia of the choroid plexus. Case report and review of the literature. *Pediatr Neurosurg,* 40**,** 32-6.

FUJIWARA, K. & MOTOKAWA, Y. 1983. Mechanism of the glycine cleavage reaction. Steady state kinetic studies of the P-protein-catalyzed reaction. *J Biol Chem,* 258**,** 8156-62.

FUJIWARA, K., OKAMURA-IKEDA, K. & MOTOKAWA, Y. 1984. Mechanism of the glycine cleavage reaction. Further characterization of the intermediate attached to H-protein and of the reaction catalyzed by T-protein. *J Biol Chem,* 259**,** 10664-8.

FUKUDA, T., TOKUNAGA, A., SAKAMOTO, R. & YOSHIDA, N. 2011. Fbxl10/Kdm2b deficiency accelerates neural progenitor cell death and leads to exencephaly. *Mol Cell Neurosci,* 46**,** 614-24.

GARDNER, C. R., MISHIN, V., LASKIN, J. D. & LASKIN, D. L. 2012. Exacerbation of acetaminophen hepatotoxicity by the anthelmentic drug fenbendazole. *Toxicol Sci,* 125**,** 607-12.

GARROW, T. A., BRENNER, A. A., WHITEHEAD, V. M., CHEN, X. N., DUNCAN, R. G., KORENBERG, J. R. & SHANE, B. 1993. Cloning of human cDNAs encoding mitochondrial and cytosolic serine hydroxymethyltransferases and chromosomal localization. *J Biol Chem,* 268**,** 11910-6.

GATENBY, P. B. & LILLIE, E. W. 1960. Clinical analysis of 100 cases of severe megaloblastic anaemia of pregnancy. *Br Med J,* 2**,** 1111-4.

GEELEN, J. A. & LANGMAN, J. 1979. Ultrastructural observations on closure of the neural tube in the mouse. *Anat Embryol (Berl),* 156**,** 73-88.

GELINEAU-VAN WAES, J., HELLER, S., BAUER, L. K., WILBERDING, J., MADDOX, J. R., ALEMAN, F., ROSENQUIST, T. H. & FINNELL, R. H. 2008. Embryonic development in the reduced folate carrier knockout mouse is modulated by maternal folate supplementation. *Birth Defects Res A Clin Mol Teratol,* 82**,** 494-507.

GELINEAU-VAN WAES, J., RAINEY, M. A., MADDOX, J. R., VOSS, K. A., SACHS, A. J., GARDNER, N. M., WILBERDING, J. D. & RILEY, R. T. 2012. Increased sphingoid base-1-

phosphates and failure of neural tube closure after exposure to fumonisin or FTY720. *Birth Defects Res A Clin Mol Teratol,* 94**,** 790-803.
GELINEAU-VAN WAES, J., STARR, L., MADDOX, J., ALEMAN, F., VOSS, K. A., WILBERDING, J. & RILEY, R. T. 2005. Maternal fumonisin exposure and risk for neural tube defects: mechanisms in an in vivo mouse model. *Birth Defects Res A Clin Mol Teratol,* 73**,** 487-97.
GERRITSEN, T., KAVEGGIA, E. & WAISMAN, H. A. 1965. A new type of idiopathic hyperglycinemia with hypo-oxaluria. *Pediatrics,* 36**,** 882-91.
GHOSHAL, K., LI, X., DATTA, J., BAI, S., POGRIBNY, I., POGRIBNY, M., HUANG, Y., YOUNG, D. & JACOB, S. T. 2006. A folate- and methyl-deficient diet alters the expression of DNA methyltransferases and methyl CpG binding proteins involved in epigenetic gene silencing in livers of F344 rats. *J Nutr,* 136**,** 1522-7.
GLUSHCHENKO, A. V. & JACOBSEN, D. W. 2007. Molecular targeting of proteins by L-homocysteine: mechanistic implications for vascular disease. *Antioxid Redox Signal,* 9**,** 1883-98.
GOLDEN, J. A. & CHERNOFF, G. F. 1993. Intermittent pattern of neural tube closure in two strains of mice. *Teratology,* 47**,** 73-80.
GOLDEN, J. A. & CHERNOFF, G. F. 1995. Multiple sites of anterior neural tube closure in humans: evidence from anterior neural tube defects (anencephaly). *Pediatrics,* 95**,** 506-10.
GONCALVES-MENDES, N., SIMON-CHAZOTTES, D., CREVEAUX, I., MEINIEL, A., GUENET, J. L. & MEINIEL, R. 2003. Mouse SCO-spondin, a gene of the thrombospondin type 1 repeat (TSR) superfamily expressed in the brain. *Gene,* 312**,** 263-70.
GOODRICH, L. V., MILENKOVIC, L., HIGGINS, K. M. & SCOTT, M. P. 1997. Altered neural cell fates and medulloblastoma in mouse patched mutants. *Science,* 277**,** 1109-13.
GOULIAN, M., BLEILE, B. & TSENG, B. Y. 1980. Methotrexate-induced misincorporation of uracil into DNA. *Proc Natl Acad Sci U S A,* 77**,** 1956-60.
GREENE, N. D. & COPP, A. J. 1997. Inositol prevents folate-resistant neural tube defects in the mouse. *Nat Med,* 3**,** 60-6.
GREENE, N. D. & COPP, A. J. 2009. Development of the vertebrate central nervous system: formation of the neural tube. *Prenat Diagn,* 29**,** 303-11.
GREENE, N. D. & COPP, A. J. 2014. Neural tube defects. *Annu Rev Neurosci,* 37**,** 221-42.
GREENE, N. D., DUNLEVY, L. E. & COPP, A. J. 2003. Homocysteine is embryotoxic but does not cause neural tube defects in mouse embryos. *Anat Embryol (Berl),* 206**,** 185-91.
GREENE, N. D., STANIER, P. & COPP, A. J. 2009. Genetics of human neural tube defects. *Hum Mol Genet,* 18**,** R113-29.
GREENE, N. D., STANIER, P. & MOORE, G. E. 2011. The emerging role of epigenetic mechanisms in the aetiology of neural tube defects. *Epigenetics,* 6.
GRINBERG, I., NORTHRUP, H., ARDINGER, H., PRASAD, C., DOBYNS, W. B. & MILLEN, K. J. 2004. Heterozygous deletion of the linked genes ZIC1 and ZIC4 is involved in Dandy-Walker malformation. *Nat Genet,* 36**,** 1053-5.
GROENEN, P. M., PEER, P. G., WEVERS, R. A., SWINKELS, D. W., FRANKE, B., MARIMAN, E. C. & STEEGERS-THEUNISSEN, R. P. 2003. Maternal myo-inositol, glucose, and zinc status is associated with the risk of offspring with spina bifida. *Am J Obstet Gynecol,* 189**,** 1713-9.
GUGGISBERG, D., HADJ-RABIA, S., VINEY, C., BODEMER, C., BRUNELLE, F., ZERAH, M., PIERRE-KAHN, A., DE PROST, Y. & HAMEL-TEILLAC, D. 2004. Skin markers of occult spinal dysraphism in children: a review of 54 cases. *Arch Dermatol,* 140**,** 1109-15.
GUNTHER, T., STRUWE, M., AGUZZI, A. & SCHUGHART, K. 1994. Open brain, a new mouse mutant with severe neural tube defects, shows altered gene expression patterns in the developing spinal cord. *Development,* 120**,** 3119-30.
GURNIAK, C. B., PERLAS, E. & WITKE, W. 2005. The actin depolymerizing factor n-cofilin is essential for neural tube morphogenesis and neural crest cell migration. *Dev Biol,* 278**,** 231-41.

GUSTAVSSON, P., GREENE, N. D., LAD, D., PAUWS, E., DE CASTRO, S. C., STANIER, P. & COPP, A. J. 2007. Increased expression of Grainyhead-like-3 rescues spina bifida in a folate-resistant mouse model. *Hum Mol Genet,* 16**,** 2640-6.

GYURIS, A., DONOVAN, D. J., SEYMOUR, K. A., LOVASCO, L. A., SMILOWITZ, N. R., HALPERIN, A. L., KLYSIK, J. E. & FREIMAN, R. N. 2009. The chromatin-targeting protein Brd2 is required for neural tube closure and embryogenesis. *Biochim Biophys Acta,* 1789**,** 413-21.

HAGGARTY, P., HOAD, G., CAMPBELL, D. M., HORGAN, G. W., PIYATHILAKE, C. & MCNEILL, G. 2013. Folate in pregnancy and imprinted gene and repeat element methylation in the offspring. *Am J Clin Nutr,* 97**,** 94-9.

HALL, D. A. & RINGEL, S. P. 2004. Adult nonketotic hyperglycinemia (NKH) crisis presenting as severe chorea and encephalopathy. *Mov Disord,* 19**,** 485-6.

HAMBLET, N. S., LIJAM, N., RUIZ-LOZANO, P., WANG, J., YANG, Y., LUO, Z., MEI, L., CHIEN, K. R., SUSSMAN, D. J. & WYNSHAW-BORIS, A. 2002. Dishevelled 2 is essential for cardiac outflow tract development, somite segmentation and neural tube closure. *Development,* 129**,** 5827-38.

HAMOSH, A. & VAN HOVE, J. 2003. Concerns regarding transience and heterozygosity in neonatal hyperglycenemia. *Ann Neurol,* 53**,** 685; author reply 685-6.

HAN, Q., ROBINSON, H. & LI, J. 2012. Biochemical identification and crystal structure of kynurenine formamidase from Drosophila melanogaster. *Biochem J,* 446**,** 253-60.

HANSEN, J. M., CONTRERAS, K. M. & HARRIS, C. 2005. Methanol, formaldehyde, and sodium formate exposure in rat and mouse conceptuses: a potential role of the visceral yolk sac in embryotoxicity. *Birth Defects Res A Clin Mol Teratol,* 73**,** 72-82.

HARDINGHAM, G. E. & BADING, H. 2003. The Yin and Yang of NMDA receptor signalling. *Trends Neurosci,* 26**,** 81-9.

HARDINGHAM, G. E. & BADING, H. 2010. Synaptic versus extrasynaptic NMDA receptor signalling: implications for neurodegenerative disorders. *Nat Rev Neurosci,* 11**,** 682-96.

HARRINGTON, M. J., HONG, E. & BREWSTER, R. 2009. Comparative analysis of neurulation: first impressions do not count. *Mol Reprod Dev,* 76**,** 954-65.

HARRIS, C., DIXON, M. & HANSEN, J. M. 2004. Glutathione depletion modulates methanol, formaldehyde and formate toxicity in cultured rat conceptuses. *Cell Biol Toxicol,* 20**,** 133-45.

HARRIS, M. J. & JURILOFF, D. M. 2007. Mouse mutants with neural tube closure defects and their role in understanding human neural tube defects. *Birth Defects Res A Clin Mol Teratol,* 79**,** 187-210.

HARRIS, M. J. & JURILOFF, D. M. 2010. An update to the list of mouse mutants with neural tube closure defects and advances toward a complete genetic perspective of neural tube closure. *Birth Defects Res A Clin Mol Teratol,* 88**,** 653-69.

HAYHURST, M., GORE, B. B., TESSIER-LAVIGNE, M. & MCCONNELL, S. K. 2008. Ongoing sonic hedgehog signaling is required for dorsal midline formation in the developing forebrain. *Dev Neurobiol,* 68**,** 83-100.

HEID, M. K., BILLS, N. D., HINRICHS, S. H. & CLIFFORD, A. J. 1992. Folate deficiency alone does not produce neural tube defects in mice. *J Nutr,* 122**,** 888-94.

HENDRICKS, K. A., NUNO, O. M., SUAREZ, L. & LARSEN, R. 2001. Effects of hyperinsulinemia and obesity on risk of neural tube defects among Mexican Americans. *Epidemiology,* 12**,** 630-5.

HENNEBERGER, C., BARD, L., KING, C., JENNINGS, A. & RUSAKOV, D. A. 2013. NMDA receptor activation: two targets for two co-agonists. *Neurochem Res,* 38**,** 1156-62.

HENNERMANN, J. B., BERGER, J. M., GRIEBEN, U., SCHARER, G. & VAN HOVE, J. L. 2012. Prediction of long-term outcome in glycine encephalopathy: a clinical survey. *J Inherit Metab Dis,* 35**,** 253-61.

HERBERT, S. P. & STAINIER, D. Y. 2011. Molecular control of endothelial cell behaviour during blood vessel morphogenesis. *Nat Rev Mol Cell Biol,* 12**,** 551-64.

HERNANDEZ-DIAZ, S., WERLER, M. M., WALKER, A. M. & MITCHELL, A. A. 2001. Neural tube defects in relation to use of folic acid antagonists during pregnancy. *Am J Epidemiol,* 153**,** 961-8.

HERRERA, E., SAMPER, E. & BLASCO, M. A. 1999. Telomere shortening in mTR-/- embryos is associated with failure to close the neural tube. *EMBO J,* 18**,** 1172-81.

HERTRAMPF, E. & CORTES, F. 2004. Folic acid fortification of wheat flour: Chile. *Nutr Rev,* 62**,** S44-8; discussion S49.

HESEKER, H. B., MASON, J. B., SELHUB, J., ROSENBERG, I. H. & JACQUES, P. F. 2009. Not all cases of neural-tube defect can be prevented by increasing the intake of folic acid. *Br J Nutr,* 102**,** 173-80.

HIBBARD, B. M. 1964. The Role of Folic Acid in Pregnancy; with Particular Reference to Anaemia, Abruption and Abortion. *J Obstet Gynaecol Br Commonw,* 71**,** 529-42.

HIBBARD, B. M. & HIBBARD, E. D. 1963. Aetiological Factors in Abruptio Placentae. *Br Med J,* 2**,** 1430-6.

HIBBARD, E. D. & SMITHELLS, R. 1965. Folic acid metabolism and human embryopathy. *Lancet,* 285**,** 1.

HILDEBRAND, J. D. & SORIANO, P. 1999. Shroom, a PDZ domain-containing actin-binding protein, is required for neural tube morphogenesis in mice. *Cell,* 99**,** 485-97.

HIRAGA, K. & KIKUCHI, G. 1980. The mitochondrial glycine cleavage system. Purification and properties of glycine decarboxylase from chicken liver mitochondria. *J Biol Chem,* 255**,** 11664-70.

HIRAGA, K., KOCHI, H., HAYASAKA, K., KIKUCHI, G. & NYHAN, W. L. 1981. Defective glycine cleavage system in nonketotic hyperglycinemia. Occurrence of a less active glycine decarboxylase and an abnormal aminomethyl carrier protein. *J Clin Invest,* 68**,** 525-34.

HO, P. I., ORTIZ, D., ROGERS, E. & SHEA, T. B. 2002. Multiple aspects of homocysteine neurotoxicity: glutamate excitotoxicity, kinase hyperactivation and DNA damage. *J Neurosci Res,* 70**,** 694-702.

HOFFMANN, L., BRAUERS, G., GEHRMANN, T., HAUSSINGER, D., MAYATEPEK, E., SCHLIESS, F. & SCHWAHN, B. C. 2013. Osmotic regulation of hepatic betaine metabolism. *Am J Physiol Gastrointest Liver Physiol,* 304**,** G835-46.

HOL, F. A., VAN DER PUT, N. M., GEURDS, M. P., HEIL, S. G., TRIJBELS, F. J., HAMEL, B. C., MARIMAN, E. C. & BLOM, H. J. 1998. Molecular genetic analysis of the gene encoding the trifunctional enzyme MTHFD (methylenetetrahydrofolate-dehydrogenase, methenyltetrahydrofolate-cyclohydrolase, formyltetrahydrofolate synthetase) in patients with neural tube defects. *Clin Genet,* 53**,** 119-25.

HOLDEN, H. E., CRIDER, P. A. & WAHRENBERG, M. G. 1980. Mitotic arrest by benzimidazole analogs in human lymphocyte cultures. *Environ Mutagen,* 2**,** 67-73.

HOLLANDER, M. C., SHEIKH, M. S., BULAVIN, D. V., LUNDGREN, K., AUGERI-HENMUELLER, L., SHEHEE, R., MOLINARO, T. A., KIM, K. E., TOLOSA, E., ASHWELL, J. D., ROSENBERG, M. P., ZHAN, Q., FERNANDEZ-SALGUERO, P. M., MORGAN, W. F., DENG, C. X. & FORNACE, A. J., JR. 1999. Genomic instability in Gadd45a-deficient mice. *Nat Genet,* 23**,** 176-84.

HONEIN, M. A., PAULOZZI, L. J., MATHEWS, T. J., ERICKSON, J. D. & WONG, L. Y. 2001. Impact of folic acid fortification of the US food supply on the occurrence of neural tube defects. *JAMA,* 285**,** 2981-6.

HOOVER-FONG, J. E., SHAH, S., VAN HOVE, J. L., APPLEGARTH, D., TOONE, J. & HAMOSH, A. 2004. Natural history of nonketotic hyperglycinemia in 65 patients. *Neurology,* 63**,** 1847-53.

HUH, M. S., TODD, M. A. & PICKETTS, D. J. 2009. SCO-ping out the mechanisms underlying the etiology of hydrocephalus. *Physiology (Bethesda),* 24**,** 117-26.

HUTSON, J. R., LUBETSKY, A., EICHHORST, J., HACKMON, R., KOREN, G. & KAPUR, B. M. 2013. Adverse placental effect of formic acid on hCG secretion is mitigated by folic acid. *Alcohol Alcohol,* 48**,** 283-7.

ICHINOHE, A., KURE, S., MIKAWA, S., UEKI, T., KOJIMA, K., FUJIWARA, K., IINUMA, K., MATSUBARA, Y. & SATO, K. 2004. Glycine cleavage system in neurogenic regions. *Eur J Neurosci,* 19**,** 2365-70.

IKEDA, A., IKEDA, S., GRIDLEY, T., NISHINA, P. M. & NAGGERT, J. K. 2001. Neural tube defects and neuroepithelial cell death in Tulp3 knockout mice. *Hum Mol Genet,* 10**,** 1325-34.

INNOCENTI, G. M. & PRICE, D. J. 2005. Exuberance in the development of cortical networks. *Nat Rev Neurosci,* 6**,** 955-65.

ISHIBASHI, M., ANG, S. L., SHIOTA, K., NAKANISHI, S., KAGEYAMA, R. & GUILLEMOT, F. 1995. Targeted disruption of mammalian hairy and Enhancer of split homolog-1 (HES-1) leads to up-regulation of neural helix-loop-helix factors, premature neurogenesis, and severe neural tube defects. *Genes Dev,* 9**,** 3136-48.

JACKSON, I. J. & ABBOTT, C. M. 2000. *Mouse Genetics and Transgenics: A Practical Approach*, Oxford University Press.

JACQUES, P. F., BOSTOM, A. G., WILLIAMS, R. R., ELLISON, R. C., ECKFELDT, J. H., ROSENBERG, I. H., SELHUB, J. & ROZEN, R. 1996. Relation between folate status, a common mutation in methylenetetrahydrofolate reductase, and plasma homocysteine concentrations. *Circulation,* 93**,** 7-9.

JACQUET, B. V., SALINAS-MONDRAGON, R., LIANG, H., THERIT, B., BUIE, J. D., DYKSTRA, M., CAMPBELL, K., OSTROWSKI, L. E., BRODY, S. L. & GHASHGHAEI, H. T. 2009. FoxJ1-dependent gene expression is required for differentiation of radial glia into ependymal cells and a subset of astrocytes in the postnatal brain. *Development,* 136**,** 4021-31.

JAIN, M., NILSSON, R., SHARMA, S., MADHUSUDHAN, N., KITAMI, T., SOUZA, A. L., KAFRI, R., KIRSCHNER, M. W., CLISH, C. B. & MOOTHA, V. K. 2012. Metabolite profiling identifies a key role for glycine in rapid cancer cell proliferation. *Science,* 336**,** 1040-4.

JAIN, N., LIM, L. W., TAN, W. T., GEORGE, B., MAKEYEV, E. & THANABALU, T. 2014. Conditional N-WASP knockout in mouse brain implicates actin cytoskeleton regulation in hydrocephalus pathology. *Exp Neurol,* 254**,** 29-40.

JAMES, S. J., POGRIBNY, I. P., POGRIBNA, M., MILLER, B. J., JERNIGAN, S. & MELNYK, S. 2003. Mechanisms of DNA damage, DNA hypomethylation, and tumor progression in the folate/methyl-deficient rat model of hepatocarcinogenesis. *J Nutr,* 133**,** 3740S-3747S.

JIMENEZ, A. J., GARCIA-VERDUGO, J. M., GONZALEZ, C. A., BATIZ, L. F., RODRIGUEZ-PEREZ, L. M., PAEZ, P., SORIANO-NAVARRO, M., ROALES-BUJAN, R., RIVERA, P., RODRIGUEZ, S., RODRIGUEZ, E. M. & PEREZ-FIGARES, J. M. 2009. Disruption of the neurogenic niche in the subventricular zone of postnatal hydrocephalic hyh mice. *J Neuropathol Exp Neurol,* 68**,** 1006-20.

JIMENEZ, A. J., TOME, M., PAEZ, P., WAGNER, C., RODRIGUEZ, S., FERNANDEZ-LLEBREZ, P., RODRIGUEZ, E. M. & PEREZ-FIGARES, J. M. 2001. A programmed ependymal denudation precedes congenital hydrocephalus in the hyh mutant mouse. *J Neuropathol Exp Neurol,* 60**,** 1105-19.

JOHNSON, J. W. & ASCHER, P. 1987. Glycine potentiates the NMDA response in cultured mouse brain neurons. *Nature,* 325**,** 529-31.

JOVANOVIC-PETERSON, L. & PETERSON, C. M. 1993. Abnormal metabolism and the risk for birth defects with emphasis on diabetes. *Ann N Y Acad Sci,* 678**,** 228-43.

JOYNER, A. L. 2000. *Gene Targeting: A Practical Approach*, Oxford University Press.

JURILOFF, D. M. & HARRIS, M. J. 2012a. A consideration of the evidence that genetic defects in planar cell polarity contribute to the etiology of human neural tube defects. *Birth Defects Res A Clin Mol Teratol,* 94**,** 824-40.

JURILOFF, D. M. & HARRIS, M. J. 2012b. Hypothesis: the female excess in cranial neural tube defects reflects an epigenetic drag of the inactivating X chromosome on the molecular mechanisms of neural fold elevation. *Birth Defects Res A Clin Mol Teratol,* 94**,** 849-55.

JURILOFF, D. M., HARRIS, M. J., TOM, C. & MACDONALD, K. B. 1991. Normal mouse strains differ in the site of initiation of closure of the cranial neural tube. *Teratology,* 44**,** 225-33.

KAAJA, E., KAAJA, R. & HIILESMAA, V. 2003. Major malformations in offspring of women with epilepsy. *Neurology,* 60**,** 575-9.

KALTER, H. & WARKANY, J. 1959. Experimental production of congenital maiformations in mammals by metabolic procedure. *Physiol Rev,* 39**,** 69-115.

KANNO, J., HUTCHIN, T., KAMADA, F., NARISAWA, A., AOKI, Y., MATSUBARA, Y. & KURE, S. 2007. Genomic deletion within GLDC is a major cause of non-ketotic hyperglycinaemia. *J Med Genet,* 44**,** e69.

KAPUR, B. M., VANDENBROUCKE, A. C., ADAMCHIK, Y., LEHOTAY, D. C. & CARLEN, P. L. 2007. Formic acid, a novel metabolite of chronic ethanol abuse, causes neurotoxicity, which is prevented by folic acid. *Alcohol Clin Exp Res,* 31**,** 2114-20.

KAUFMAN, M. H. 1992. *The Atlas of Mouse Development*, Academic Press.

KELLER, R. 2002. Shaping the vertebrate body plan by polarized embryonic cell movements. *Science,* 298**,** 1950-4.

KELLER, R., DAVIDSON, L., EDLUND, A., ELUL, T., EZIN, M., SHOOK, D. & SKOGLUND, P. 2000. Mechanisms of convergence and extension by cell intercalation. *Philos Trans R Soc Lond B Biol Sci,* 355**,** 897-922.

KENNEDY, D., CHITAYAT, D., WINSOR, E. J., SILVER, M. & TOI, A. 1998. Prenatally diagnosed neural tube defects: ultrasound, chromosome, and autopsy or postnatal findings in 212 cases. *Am J Med Genet,* 77**,** 317-21.

KIBAR, Z., TORBAN, E., MCDEARMID, J. R., REYNOLDS, A., BERGHOUT, J., MATHIEU, M., KIRILLOVA, I., DE MARCO, P., MERELLO, E., HAYES, J. M., WALLINGFORD, J. B., DRAPEAU, P., CAPRA, V. & GROS, P. 2007. Mutations in VANGL1 associated with neural-tube defects. *N Engl J Med,* 356**,** 1432-7.

KIKUCHI, G., MOTOKAWA, Y., YOSHIDA, T. & HIRAGA, K. 2008. Glycine cleavage system: reaction mechanism, physiological significance, and hyperglycinemia. *Proc Jpn Acad Ser B Phys Biol Sci,* 84**,** 246-63.

KIM, I. H., CARLSON, B. R., HEINDEL, C. C., KIM, H. & SODERLING, S. H. 2012. Disruption of wave-associated Rac GTPase-activating protein (Wrp) leads to abnormal adult neural progenitor migration associated with hydrocephalus. *J Biol Chem,* 287**,** 39263-74.

KIM, J. M., LEE, H. & CHANG, N. 2002. Hyperhomocysteinemia due to short-term folate deprivation is related to electron microscopic changes in the rat brain. *J Nutr,* 132**,** 3418-21.

KIRKE, P. N., MOLLOY, A. M., DALY, L. E., BURKE, H., WEIR, D. G. & SCOTT, J. M. 1993. Maternal plasma folate and vitamin B12 are independent risk factors for neural tube defects. *Q J Med,* 86**,** 703-8.

KLEZOVITCH, O., FERNANDEZ, T. E., TAPSCOTT, S. J. & VASIOUKHIN, V. 2004. Loss of cell polarity causes severe brain dysplasia in Lgl1 knockout mice. *Genes Dev,* 18**,** 559-71.

KNOX, A. J., GRAHAM, C., BLESKAN, J., BRODSKY, G. & PATTERSON, D. 2009. Mutations in the Chinese hamster ovary cell GART gene of de novo purine synthesis. *Gene,* 429**,** 23-30.

KNOX, E. G. 1974. Twins and neural tube defects. *Br J Prev Soc Med,* 28**,** 73-80.

KOJIMA-ISHII, K., KURE, S., ICHINOHE, A., SHINKA, T., NARISAWA, A., KOMATSUZAKI, S., KANNO, J., KAMADA, F., AOKI, Y., YOKOYAMA, H., ODA, M., SUGAWARA, T., MIZOI, K., NAKAHARA, D. & MATSUBARA, Y. 2008. Model mice for mild-form glycine encephalopathy: behavioral and biochemical characterizations and efficacy of antagonists for the glycine binding site of N-methyl D-aspartate receptor. *Pediatr Res,* 64**,** 228-33.

KORMAN, S. H., BONEH, A., ICHINOHE, A., KOJIMA, K., SATO, K., ERGAZ, Z., GOMORI, J. M., GUTMAN, A. & KURE, S. 2004. Persistent NKH with transient or absent symptoms and a homozygous GLDC mutation. *Ann Neurol,* 56**,** 139-43.

KORMAN, S. H., WEXLER, I. D., GUTMAN, A., ROLLAND, M. O., KANNO, J. & KURE, S. 2006. Treatment from birth of nonketotic hyperglycinemia due to a novel GLDC mutation. *Ann Neurol,* 59**,** 411-5.

KOURY, M. J., PRICE, J. O. & HICKS, G. G. 2000. Apoptosis in megaloblastic anemia occurs during DNA synthesis by a p53-independent, nucleoside-reversible mechanism. *Blood,* 96**,** 3249-55.

KRISTENSEN, N. B., NORGAARD, J. V., WAMBERG, S., ENGBAEK, M., FERNANDEZ, J. A., ZACHO, H. D. & POULSEN, H. D. 2009. Absorption and metabolism of benzoic acid in growing pigs. *J Anim Sci,* 87**,** 2815-22.

KRUMAN, II, CULMSEE, C., CHAN, S. L., KRUMAN, Y., GUO, Z., PENIX, L. & MATTSON, M. P. 2000. Homocysteine elicits a DNA damage response in neurons that promotes apoptosis and hypersensitivity to excitotoxicity. *J Neurosci,* 20**,** 6920-6.

KUHNERT, F., CAMPAGNOLO, L., XIONG, J. W., LEMONS, D., FITCH, M. J., ZOU, Z., KIOSSES, W. B., GARDNER, H. & STUHLMANN, H. 2005. Dosage-dependent requirement for mouse Vezf1 in vascular system development. *Dev Biol,* 283**,** 140-56.

KUIDA, K., HAYDAR, T. F., KUAN, C. Y., GU, Y., TAYA, C., KARASUYAMA, H., SU, M. S., RAKIC, P. & FLAVELL, R. A. 1998 Reduced apoptosis and cytochrome c-mediated caspase activation in mice lacking caspase 9. *Cell,* 94**,** 325-37.

KURE, S., ICHINOHE, A., KOJIMA, K., SATO, K., KIZAKI, Z., INOUE, F., YAMANAKA, C. & MATSUBARA, Y. 2004. Mild variant of nonketotic hyperglycinemia with typical neonatal presentations: mutational and in vitro expression analyses in two patients. *J Pediatr,* 144**,** 827-9.

KURE, S., KATO, K., DINOPOULOS, A., GAIL, C., DEGRAUW, T. J., CHRISTODOULOU, J., BZDUCH, V., KALMANCHEY, R., FEKETE, G., TROJOVSKY, A., PLECKO, B., BRENINGSTALL, G., TOHYAMA, J., AOKI, Y. & MATSUBARA, Y. 2006a. Comprehensive mutation analysis of GLDC, AMT, and GCSH in nonketotic hyperglycinemia. *Hum Mutat,* 27**,** 343-52.

KURE, S., KOJIMA, K., ICHINOHE, A., MAEDA, T., KALMANCHEY, R., FEKETE, G., BERG, S. Z., FILIANO, J., AOKI, Y., SUZUKI, Y., IZUMI, T. & MATSUBARA, Y. 2002. Heterozygous GLDC and GCSH gene mutations in transient neonatal hyperglycinemia. *Ann Neurol,* 52**,** 643-6.

KURE, S., KORMAN, S. H., KANNO, J., NARISAWA, A., KUBOTA, M., TAKAYANAGI, T., TAKAYANAGI, M., SAITO, T., MATSUI, A., KAMADA, F., AOKI, Y., OHURA, T. & MATSUBARA, Y. 2006b. Rapid diagnosis of glycine encephalopathy by 13C-glycine breath test. *Ann Neurol,* 59**,** 862-7.

KURE, S., KOYATA, H., KUME, A., ISHIGURO, Y. & HIRAGA, K. 1991. The glycine cleavage system. The coupled expression of the glycine decarboxylase gene and the H-protein gene in the chicken. *J Biol Chem,* 266**,** 3330-4.

KURE, S., MANDEL, H., ROLLAND, M. O., SAKATA, Y., SHINKA, T., DRUGAN, A., BONEH, A., TADA, K., MATSUBARA, Y. & NARISAWA, K. 1998. A missense mutation (His42Arg) in the T-protein gene from a large Israeli-Arab kindred with nonketotic hyperglycinemia. *Hum Genet,* 102**,** 430-4.

KURE, S., TADA, K. & NARISAWA, K. 1997. Nonketotic hyperglycinemia: biochemical, molecular, and neurological aspects. *Jpn J Hum Genet,* 42**,** 13-22.

KURE, S., TAKAYANAGI, M., NARISAWA, K., TADA, K. & LEISTI, J. 1992. Identification of a common mutation in Finnish patients with nonketotic hyperglycinemia. *J Clin Invest,* 90**,** 160-4.

LABUSCHAGNE, C. F., VAN DEN BROEK, N. J., MACKAY, G. M., VOUSDEN, K. H. & MADDOCKS, O. D. 2014. Serine, but not glycine, supports one-carbon metabolism and proliferation of cancer cells. *Cell Rep,* 7**,** 1248-58.

LACEY, E. 1990. Mode of action of benzimidazoles. *Parasitol Today,* 6**,** 112-5.

LAGUTIN, O. V., ZHU, C. C., KOBAYASHI, D., TOPCZEWSKI, J., SHIMAMURA, K., PUELLES, L., RUSSELL, H. R., MCKINNON, P. J., SOLNICA-KREZEL, L. & OLIVER, G. 2003. Six3 repression of Wnt signaling in the anterior neuroectoderm is essential for vertebrate forebrain development. *Genes Dev,* 17**,** 368-79.

LAKKIS, M. M., GOLDEN, J. A., O'SHEA, K. S. & EPSTEIN, J. A. 1999. Neurofibromin deficiency in mice causes exencephaly and is a modifier for Splotch neural tube defects. *Dev Biol,* 212**,** 80-92.

LAMARRE, S. G., MACMILLAN, L., MORROW, G. P., RANDELL, E., PONGNOPPARAT, T., BROSNAN, M. E. & BROSNAN, J. T. 2014. An isotope-dilution, GC-MS assay for formate and its application to human and animal metabolism. *Amino Acids,* 46**,** 1885-91.

LAMARRE, S. G., MOLLOY, A. M., REINKE, S. N., SYKES, B. D., BROSNAN, M. E. & BROSNAN, J. T. 2012. Formate can differentiate between hyperhomocysteinemia due to impaired remethylation and impaired transsulfuration. *Am J Physiol Endocrinol Metab,* 302**,** E61-7.

LAMARRE, S. G., MORROW, G., MACMILLAN, L., BROSNAN, M. E. & BROSNAN, J. T. 2013. Formate: an essential metabolite, a biomarker, or more? *Clin Chem Lab Med,* 51**,** 571-8.

LAMERS, Y., WILLIAMSON, J., GILBERT, L. R., STACPOOLE, P. W. & GREGORY, J. F., 3RD 2007. Glycine turnover and decarboxylation rate quantified in healthy men and women using primed, constant infusions of [1,2-(13)C2]glycine and [(2)H3]leucine. *J Nutr,* 137**,** 2647-52.

LANDIN, A. M., FRASCA, D., ZAIAS, J., VAN DER PUT, E., RILEY, R. L., ALTMAN, N. H. & BLOMBERG, B. B. 2009. Effects of fenbendazole on the murine humoral immune system. *J Am Assoc Lab Anim Sci,* 48**,** 251-7.

LARDELLI, M., WILLIAMS, R., MITSIADIS, T. & LENDAHL, U. 1996. Expression of the Notch 3 intracellular domain in mouse central nervous system progenitor cells is lethal and leads to disturbed neural tube development. *Mech Dev,* 59**,** 177-90.

LASON, W., CHLEBICKA, M. & REJDAK, K. 2013. Research advances in basic mechanisms of seizures and antiepileptic drug action. *Pharmacol Rep,* 65**,** 787-801.

LAVADO, A., LAGUTIN, O. V. & OLIVER, G. 2008. Six3 inactivation causes progressive caudalization and aberrant patterning of the mammalian diencephalon. *Development,* 135**,** 441-50.

LAWRENCE, J. M., PETITTI, D. B., WATKINS, M. & UMEKUBO, M. A. 1999. Trends in serum folate after food fortification. *Lancet,* 354**,** 915-6.

LAWRENCE, S. A., HACKETT, J. C. & MORAN, R. G. 2011. Tetrahydrofolate recognition by the mitochondrial folate transporter. *J Biol Chem,* 286**,** 31480-9.

LAWRENCE, S. A., TITUS, S. A., FERGUSON, J., HEINEMAN, A. L., TAYLOR, S. M. & MORAN, R. G. 2014. Mammalian mitochondrial and cytosolic folylpolyglutamate synthetase maintain the subcellular compartmentalization of folates. *J Biol Chem,* 289**,** 29386-96.

LE DOUARIN, N. M., BRITO, J. M. & CREUZET, S. 2007. Role of the neural crest in face and brain development. *Brain Res Rev,* 55**,** 237-47.

LEE, H. O. & NORDEN, C. 2013. Mechanisms controlling arrangements and movements of nuclei in pseudostratified epithelia. *Trends Cell Biol,* 23**,** 141-50.

LEE, L. 2013. Riding the wave of ependymal cilia: genetic susceptibility to hydrocephalus in primary ciliary dyskinesia. *J Neurosci Res,* 91**,** 1117-32.

LEI, Y., ZHU, H., DUHON, C., YANG, W., ROSS, M. E., SHAW, G. M. & FINNELL, R. H. 2013. Mutations in planar cell polarity gene SCRIB are associated with spina bifida. *PLoS One,* 8**,** e69262.

LEI, Y. P., ZHANG, T., LI, H., WU, B. L., JIN, L. & WANG, H. Y. 2010. VANGL2 mutations in human cranial neural-tube defects. *N Engl J Med,* 362**,** 2232-5.

LEIPNITZ, G., SOLANO, A. F., SEMINOTTI, B., AMARAL, A. U., FERNANDES, C. G., BESKOW, A. P., DUTRA FILHO, C. S. & WAJNER, M. 2009. Glycine provokes lipid oxidative damage and reduces the antioxidant defenses in brain cortex of young rats. *Cell Mol Neurobiol,* 29**,** 253-61.

LEPESHEVA, G. I. & WATERMAN, M. R. 2007. Sterol 14alpha-demethylase cytochrome P450 (CYP51), a P450 in all biological kingdoms. *Biochim Biophys Acta,* 1770**,** 467-77.

LEUNG, K. Y., DE CASTRO, S. C., SAVERY, D., COPP, A. J. & GREENE, N. D. 2013. Nucleotide precursors prevent folic acid-resistant neural tube defects in the mouse. *Brain,* 136**,** 2836-41.

LEVINE, A. J. & BRIVANLOU, A. H. 2007. Proposal of a model of mammalian neural induction. *Dev Biol,* 308**,** 247-56.

LEW, S. M. & KOTHBAUER, K. F. 2007. Tethered cord syndrome: an updated review. *Pediatr Neurosurg,* 43**,** 236-48.

LI, D. W., YANG, Q., CHEN, J. T., ZHOU, H., LIU, R. M. & HUANG, X. T. 2005. Dynamic distribution of Ser-10 phosphorylated histone H3 in cytoplasm of MCF-7 and CHO cells during mitosis. *Cell Res,* 15**,** 120-6.

LI, M., CHEN, J., LI, Y. S., FENG, Y. B., GU, X. & SHI, C. Z. 2006. Folic acid reduces adhesion molecules VCAM-1 expession in aortic of rats with hyperhomocysteinemia. *Int J Cardiol,* 106**,** 285-8.

LIN, W., ZHANG, Z., SRAJER, G., CHEN, Y. C., HUANG, M., PHAN, H. M. & DENT, S. Y. 2008. Proper expression of the Gcn5 histone acetyltransferase is required for neural tube closure in mouse embryos. *Dev Dyn,* 237**,** 928-40.

LIN, X., LIU, B., YANG, X., YUE, X., DIAO, L., WANG, J. & CHANG, J. 2013. Genetic deletion of Rnd3 results in aqueductal stenosis leading to hydrocephalus through up-regulation of Notch signaling. *Proc Natl Acad Sci U S A,* 110**,** 8236-41.

LIPTON, S. A., KIM, W. K., CHOI, Y. B., KUMAR, S., D'EMILIA, D. M., RAYUDU, P. V., ARNELLE, D. R. & STAMLER, J. S. 1997. Neurotoxicity associated with dual actions of homocysteine at the N-methyl-D-aspartate receptor. *Proc Natl Acad Sci U S A,* 94**,** 5923-8.

LISSENS, W., DE MEIRLEIR, L., SENECA, S., LIEBAERS, I., BROWN, G. K., BROWN, R. M., ITO, M., NAITO, E., KURODA, Y., KERR, D. S., WEXLER, I. D., PATEL, M. S., ROBINSON, B. H. & SEYDA, A. 2000. Mutations in the X-linked pyruvate dehydrogenase (E1) alpha subunit gene (PDHA1) in patients with a pyruvate dehydrogenase complex deficiency. *Hum Mutat,* 15**,** 209-19.

LIU, T. C., KIM, H., ARIZMENDI, C., KITANO, A. & PATEL, M. S. 1993. Identification of two missense mutations in a dihydrolipoamide dehydrogenase-deficient patient. *Proc Natl Acad Sci U S A,* 90**,** 5186-90.

LOCASALE, J. W. 2013. Serine, glycine and one-carbon units: cancer metabolism in full circle. *Nat Rev Cancer,* 13**,** 572-83.

LOEKEN, M. R. 2005. Current perspectives on the causes of neural tube defects resulting from diabetic pregnancy. *Am J Med Genet C Semin Med Genet,* 135C**,** 77-87.

LOEWEN, P. C., CARPENA, X., ROVIRA, C., IVANCICH, A., PEREZ-LUQUE, R., HAAS, R., ODENBREIT, S., NICHOLLS, P. & FITA, I. 2004. Structure of Helicobacter pylori catalase, with and without formic acid bound, at 1.6 A resolution. *Biochemistry,* 43**,** 3089-103.

LOWRY, M., HALL, D. E. & BROSNAN, J. T. 1985a. Hydroxyproline metabolism by the rat kidney: distribution of renal enzymes of hydroxyproline catabolism and renal conversion of hydroxyproline to glycine and serine. *Metabolism,* 34**,** 955-61.

LOWRY, M., HALL, D. E. & BROSNAN, J. T. 1985b. Metabolism of glycine- and hydroxyproline-containing peptides by the isolated perfused rat kidney. *Biochem J,* 229**,** 545-9.

LUKA, Z., MUDD, S. H. & WAGNER, C. 2009. Glycine N-methyltransferase and regulation of S-adenosylmethionine levels. *J Biol Chem,* 284**,** 22507-11.

LUPO, P. J., CANFIELD, M. A., CHAPA, C., LU, W., AGOPIAN, A. J., MITCHELL, L. E., SHAW, G. M., WALLER, D. K., OLSHAN, A. F., FINNELL, R. H. & ZHU, H. 2012. Diabetes and obesity-related genes and the risk of neural tube defects in the national birth defects prevention study. *Am J Epidemiol,* 176**,** 1101-9.

MACDONALD, K. B., JURILOFF, D. M. & HARRIS, M. J. 1989. Developmental study of neural tube closure in a mouse stock with a high incidence of exencephaly. *Teratology,* 39**,** 195-213.

MACFARLANE, A. J., LIU, X., PERRY, C. A., FLODBY, P., ALLEN, R. H., STABLER, S. P. & STOVER, P. J. 2008. Cytoplasmic serine hydroxymethyltransferase regulates the

metabolic partitioning of methylenetetrahydrofolate but is not essential in mice. *J Biol Chem,* 283**,** 25846-53.

MACFARLANE, A. J., PERRY, C. A., GIRNARY, H. H., GAO, D., ALLEN, R. H., STABLER, S. P., SHANE, B. & STOVER, P. J. 2009. Mthfd1 is an essential gene in mice and alters biomarkers of impaired one-carbon metabolism. *J Biol Chem,* 284**,** 1533-9.

MAEKAWA, M., SHIMADA, M., IIDA, T., GOTO, J. & MANO, N. 2014. Tandem mass spectrometric characterization of bile acids and steroid conjugates based on low-energy collision-induced dissociation. *Steroids,* 80**,** 80-91.

MANEL, L., HOUNEIDA, Z. B., HABIB, A., DEJLA, B. & CHEKIB, K. 2012. A rare inborn error of metabolism associated with a Dandy-Walker malformation. *Acta Neurol Belg,* 112**,** 425-6.

MARTINEZ-FRIAS, M. L. 1994. Epidemiological analysis of outcomes of pregnancy in diabetic mothers: identification of the most characteristic and most frequent congenital anomalies. *Am J Med Genet,* 51**,** 108-13.

MARTINEZ-FRIAS, M. L., URIOSTE, M., BERMEJO, E., SANCHIS, A. & RODRIGUEZ-PINILLA, E. 1996. Epidemiological analysis of multi-site closure failure of neural tube in humans. *Am J Med Genet,* 66**,** 64-8.

MARTINIOVA, L., FIELD, M. S., FINKELSTEIN, J. L., PERRY, C. A. & STOVER, P. J. 2015. Maternal dietary uridine causes, and deoxyuridine prevents, neural tube closure defects in a mouse model of folate-responsive neural tube defects. *Am J Clin Nutr,* 101**,** 860-9.

MASSA, V., SAVERY, D., YBOT-GONZALEZ, P., FERRARO, E., RONGVAUX, A., CECCONI, F., FLAVELL, R., GREENE, N. D. & COPP, A. J. 2009 Apoptosis is not required for mammalian neural tube closure. *Proc Natl Acad Sci U S A,* 106**,** 8233-8.

MATHERLY, L. H. & HOU, Z. 2008. Structure and function of the reduced folate carrier a paradigm of a major facilitator superfamily mammalian nutrient transporter. *Vitam Horm,* 79**,** 145-84.

MCALLISTER, J. P., 2ND 2012. Pathophysiology of congenital and neonatal hydrocephalus. *Semin Fetal Neonatal Med,* 17**,** 285-94.

MCCARTHY, E. A., TITUS, S. A., TAYLOR, S. M., JACKSON-COOK, C. & MORAN, R. G. 2004. A mutation inactivating the mitochondrial inner membrane folate transporter creates a glycine requirement for survival of chinese hamster cells. *J Biol Chem,* 279**,** 33829-36.

MCGLYNN, A. P., WASSON, G. R., O'REILLY, S. L., MCNULTY, H., DOWNES, C. S., CHANG, C. K., HOEY, L., MOLLOY, A. M., WARD, M., STRAIN, J. J., MCKERR, G., WEIR, D. G. & SCOTT, J. M. 2013. Low colonocyte folate is associated with uracil misincorporation and global DNA hypomethylation in human colorectum. *J Nutr,* 143**,** 27-33.

MENEGOLA, E., DI RENZO, F., BROCCIA, M. L., PRUDENZIATI, M., MINUCCI, S., MASSA, V. & GIAVINI, E. 2005. Inhibition of histone deacetylase activity on specific embryonic tissues as a new mechanism for teratogenicity. *Birth Defects Res B Dev Reprod Toxicol,* 74**,** 392-8.

MENZIES, A. S., ASZODI, A., WILLIAMS, S. E., PFEIFER, A., WEHMAN, A. M., GOH, K. L., MASON, C. A., FASSLER, R. & GERTLER, F. B. 2004. Mena and vasodilator-stimulated phosphoprotein are required for multiple actin-dependent processes that shape the vertebrate nervous system. *J Neurosci,* 24**,** 8029-38.

MERELLO, E., MASCELLI, S., RASO, A., PIATELLI, G., CONSALES, A., CAMA, A., KIBAR, Z., CAPRA, V. & MARCO, P. D. 2015. Expanding the mutational spectrum associated to neural tube defects: literature revision and description of novel VANGL1 mutations. *Birth Defects Res A Clin Mol Teratol,* 103**,** 51-61.

MILLS, J. L., MCPARTLIN, J. M., KIRKE, P. N., LEE, Y. J., CONLEY, M. R., WEIR, D. G. & SCOTT, J. M. 1995. Homocysteine metabolism in pregnancies complicated by neural-tube defects. *Lancet,* 345**,** 149-51.

MILUNSKY, A., JICK, H., JICK, S. S., BRUELL, C. L., MACLAUGHLIN, D. S., ROTHMAN, K. J. & WILLETT, W. 1989. Multivitamin/folic acid supplementation in early pregnancy reduces the prevalence of neural tube defects. *JAMA,* 262**,** 2847-52.

MILUNSKY, A., MORRIS, J. S., JICK, H., ROTHMAN, K. J., ULCICKAS, M., JICK, S. S., SHOUKIMAS, P. & WILLETT, W. 1992. Maternal zinc and fetal neural tube defects. *Teratology,* 46**,** 341-8.

MISSMER, S. A., SUAREZ, L., FELKNER, M., WANG, E., MERRILL, A. H., JR., ROTHMAN, K. J. & HENDRICKS, K. A. 2006. Exposure to fumonisins and the occurrence of neural tube defects along the Texas-Mexico border. *Environ Health Perspect,* 114**,** 237-41.

MITCHELL, L. E. 2005. Epidemiology of neural tube defects. *Am J Med Genet C Semin Med Genet,* 135C**,** 88-94.

MOLLOY, A. M., BRODY, L. C., MILLS, J. L., SCOTT, J. M. & KIRKE, P. N. 2009a. The search for genetic polymorphisms in the homocysteine/folate pathway that contribute to the etiology of human neural tube defects. *Birth Defects Res A Clin Mol Teratol,* 85**,** 285-94.

MOLLOY, A. M., KIRKE, P. N., TROENDLE, J. F., BURKE, H., SUTTON, M., BRODY, L. C., SCOTT, J. M. & MILLS, J. L. 2009b. Maternal vitamin B12 status and risk of neural tube defects in a population with high neural tube defect prevalence and no folic Acid fortification. *Pediatrics,* 123**,** 917-23.

MOLLOY, A. M., MILLS, J. L., KIRKE, P. N., RAMSBOTTOM, D., MCPARTLIN, J. M., BURKE, H., CONLEY, M., WHITEHEAD, A. S., WEIR, D. G. & SCOTT, J. M. 1998. Low blood folates in NTD pregnancies are only partly explained by thermolabile 5,10-methylenetetrahydrofolate reductase: low folate status alone may be the critical factor. *Am J Med Genet,* 78**,** 155-9.

MOMB, J., LEWANDOWSKI, J. P., BRYANT, J. D., FITCH, R., SURMAN, D. R., VOKES, S. A. & APPLING, D. R. 2013. Deletion of Mthfd1l causes embryonic lethality and neural tube and craniofacial defects in mice. *Proc Natl Acad Sci U S A,* 110**,** 549-54.

MORETTI, M. E., BAR-OZ, B., FRIED, S. & KOREN, G. 2005. Maternal hyperthermia and the risk for neural tube defects in offspring: systematic review and meta-analysis. *Epidemiology,* 16**,** 216-9.

MORRISON, P. F., SANKAR, R. & SHIELDS, W. D. 2006. Valproate-induced chorea and encephalopathy in atypical nonketotic hyperglycinemia. *Pediatr Neurol,* 35**,** 356-8.

MORRISS-KAY, G. M. 1981. Growth and development of pattern in the cranial neural epithelium of rat embryos during neurulation. *J Embryol Exp Morphol,* 65 Suppl**,** 225-41.

MORTENSEN, P. B., KOLVRAA, S. & CHRISTENSEN, E. 1980. Inhibition of the glycine cleavage system: hyperglycinemia and hyperglycinuria caused by valproic acid. *Epilepsia,* 21**,** 563-9.

MOSLEY, B. S., CLEVES, M. A., SIEGA-RIZ, A. M., SHAW, G. M., CANFIELD, M. A., WALLER, D. K., WERLER, M. M. & HOBBS, C. A. 2009. Neural tube defects and maternal folate intake among pregnancies conceived after folic acid fortification in the United States. *Am J Epidemiol,* 169**,** 9-17.

MRC 1991. Prevention of neural tube defects: results of the Medical Research Council Vitamin Study. MRC Vitamin Study Research Group. *Lancet,* 338**,** 131-7.

MULINARE, J., CORDERO, J. F., ERICKSON, J. D. & BERRY, R. J. 1988. Periconceptional use of multivitamins and the occurrence of neural tube defects. *JAMA,* 260**,** 3141-5.

MUNOZ, E. M., BAILEY, M. J., RATH, M. F., SHI, Q., MORIN, F., COON, S. L., MOLLER, M. & KLEIN, D. C. 2007. NeuroD1: developmental expression and regulated genes in the rodent pineal gland. *J Neurochem,* 102**,** 887-99.

MURDOCH, J. N. & COPP, A. J. 2010. The relationship between sonic Hedgehog signaling, cilia, and neural tube defects. *Birth Defects Res A Clin Mol Teratol,* 88**,** 633-52.

MURDOCH, J. N., DOUDNEY, K., PATERNOTTE, C., COPP, A. J. & STANIER, P. 2001a. Severe neural tube defects in the loop-tail mouse result from mutation of Lpp1, a novel gene involved in floor plate specification. *Hum Mol Genet,* 10**,** 2593-601.

MURDOCH, J. N., HENDERSON, D. J., DOUDNEY, K., GASTON-MASSUET, C., PHILLIPS, H. M., PATERNOTTE, C., ARKELL, R., STANIER, P. & COPP, A. J. 2003. Disruption of scribble (Scrb1) causes severe neural tube defects in the circletail mouse. *Hum Mol Genet,* 12**,** 87-98.

MURDOCH, J. N., RACHEL, R. A., SHAH, S., BEERMANN, F., STANIER, P., MASON, C. A. & COPP, A. J. 2001b. Circletail, a new mouse mutant with severe neural tube defects: chromosomal localization and interaction with the loop-tail mutation. *Genomics,* 78**,** 55-63.

NAKADA, H. I., FRIEDMANN, B. & WEINHOUSE, S. 1955. Pathways of glycine catabolism in rat liver. *J Biol Chem,* 216**,** 583-92.

NAKATSU, T., UWABE, C. & SHIOTA, K. 2000. Neural tube closure in humans initiates at multiple sites: evidence from human embryos and implications for the pathogenesis of neural tube defects. *Anat Embryol (Berl),* 201**,** 455-66.

NARISAWA, A., KOMATSUZAKI, S., KIKUCHI, A., NIIHORI, T., AOKI, Y., FUJIWARA, K., TANEMURA, M., HATA, A., SUZUKI, Y., RELTON, C. L., GRINHAM, J., LEUNG, K. Y., PARTRIDGE, D., ROBINSON, A., STONE, V., GUSTAVSSON, P., STANIER, P., COPP, A. J., GREENE, N. D., TOMINAGA, T., MATSUBARA, Y. & KURE, S. 2012. Mutations in genes encoding the glycine cleavage system predispose to neural tube defects in mice and humans. *Hum Mol Genet,* 21**,** 1496-503.

NECHIPORUK, T., FERNANDEZ, T. E. & VASIOUKHIN, V. 2007. Failure of epithelial tube maintenance causes hydrocephalus and renal cysts in Dlg5-/- mice. *Dev Cell,* 13**,** 338-50.

NEWELL, D. W., BARTH, A., RICCIARDI, T. N. & MALOUF, A. T. 1997. Glycine causes increased excitability and neurotoxicity by activation of NMDA receptors in the hippocampus. *Exp Neurol,* 145**,** 235-44.

NGUYEN, L., RIGO, J. M., ROCHER, V., BELACHEW, S., MALGRANGE, B., ROGISTER, B., LEPRINCE, P. & MOONEN, G. 2001. Neurotransmitters as early signals for central nervous system development. *Cell Tissue Res,* 305**,** 187-202.

NIJHOUT, H. F., REED, M. C., BUDU, P. & ULRICH, C. M. 2004. A mathematical model of the folate cycle: new insights into folate homeostasis. *J Biol Chem,* 279**,** 55008-16.

NIJHOUT, H. F., REED, M. C., LAM, S. L., SHANE, B., GREGORY, J. F., 3RD & ULRICH, C. M. 2006. In silico experimentation with a model of hepatic mitochondrial folate metabolism. *Theor Biol Med Model,* 3**,** 40.

NIQUILLE, M., GAREL, S., MANN, F., HORNUNG, J. P., OTSMANE, B., CHEVALLEY, S., PARRAS, C., GUILLEMOT, F., GASPAR, P., YANAGAWA, Y. & LEBRAND, C. 2009. Transient neuronal populations are required to guide callosal axons: a role for semaphorin 3C. *PLoS Biol,* 7**,** e1000230.

NISHIKIMI, M., OISHI, K. & NAKAJIMA, K. 2013. Axon guidance mechanisms for establishment of callosal connections. *Neural Plast,* 2013**,** 149060.

O'RAHILLY, R. & MULLER, F. 1994. Neurulation in the normal human embryo. *Ciba Found Symp,* 181**,** 70-82; discussion 82-9.

O'RAHILLY, R. & MULLER, F. 2002. The two sites of fusion of the neural folds and the two neuropores in the human embryo. *Teratology,* 65**,** 162-70.

OAKLEY, G. P., JR., ADAMS, M. J., JR. & JAMES, L. M. 1983. Vitamins and neural tube defects. *Lancet,* 2**,** 798-9.

ODA, M., KURE, S., SUGAWARA, T., YAMAGUCHI, S., KOJIMA, K., SHINKA, T., SATO, K., NARISAWA, A., AOKI, Y., MATSUBARA, Y., OMAE, T., MIZOI, K. & KINOUCHI, H. 2007. Direct correlation between ischemic injury and extracellular glycine concentration in mice with genetically altered activities of the glycine cleavage multienzyme system. *Stroke,* 38**,** 2157-64.

OGAWA, H., GOMI, T., TAKUSAGAWA, F. & FUJIOKA, M. 1998. Structure, function and physiological role of glycine N-methyltransferase. *Int J Biochem Cell Biol,* 30**,** 13-26.

OKAMURA-IKEDA, K., FUJIWARA, K. & MOTOKAWA, Y. 1987. Mechanism of the glycine cleavage reaction. Properties of the reverse reaction catalyzed by T-protein. *J Biol Chem,* 262**,** 6746-9.

OKAMURA-IKEDA, K., HOSAKA, H., MAITA, N., FUJIWARA, K., YOSHIZAWA, A. C., NAKAGAWA, A. & TANIGUCHI, H. 2010. Crystal structure of aminomethyltransferase in complex with dihydrolipoyl-H-protein of the glycine cleavage system: implications for recognition of lipoyl protein substrate, disease-related mutations, and reaction mechanism. *J Biol Chem,* 285**,** 18684-92.

OKANO, M., BELL, D. W., HABER, D. A. & LI, E. 1999. DNA methyltransferases Dnmt3a and Dnmt3b are essential for de novo methylation and mammalian development. *Cell,* 99**,** 247-57.

ORESKOVIC, D. & KLARICA, M. 2011. Development of hydrocephalus and classical hypothesis of cerebrospinal fluid hydrodynamics: facts and illusions. *Prog Neurobiol,* 94**,** 238-58.

OSTROWSKI, L. E., YIN, W., ROGERS, T. D., BUSALACCHI, K. B., CHUA, M., O'NEAL, W. K. & GRUBB, B. R. 2010. Conditional deletion of dnaic1 in a murine model of primary ciliary dyskinesia causes chronic rhinosinusitis. *Am J Respir Cell Mol Biol,* 43**,** 55-63.

OWEN-LYNCH, P. J., DRAPER, C. E., MASHAYEKHI, F., BANNISTER, C. M. & MIYAN, J. A. 2003. Defective cell cycle control underlies abnormal cortical development in the hydrocephalic Texas rat. *Brain,* 126**,** 623-31.

PAI, Y. J., LEUNG, K. Y., SAVERY, D., HUTCHIN, T., PRUNTY, H., HEALES, S., BROSNAN, M. E., BROSNAN, J. T., COPP, A. J. & GREENE, N. D. 2015. Glycine decarboxylase deficiency causes neural tube defects and features of non-ketotic hyperglycinemia in mice. *Nat Commun,* 6**,** 6388.

PANG, D., ZOVICKIAN, J. & MOES, G. S. 2011. Retained medullary cord in humans: late arrest of secondary neurulation. *Neurosurgery,* 68**,** 1500-19; discussion 1519.

PANGILINAN, F., MOLLOY, A. M., MILLS, J. L., TROENDLE, J. F., PARLE-MCDERMOTT, A., SIGNORE, C., O'LEARY, V. B., CHINES, P., SEAY, J. M., GEILER-SAMEROTTE, K., MITCHELL, A., VANDERMEER, J. E., KREBS, K. M., SANCHEZ, A., CORNMAN-HOMONOFF, J., STONE, N., CONLEY, M., KIRKE, P. N., SHANE, B., SCOTT, J. M. & BRODY, L. C. 2012. Evaluation of common genetic variants in 82 candidate genes as risk factors for neural tube defects. *BMC Med Genet,* 13**,** 62.

PARLE-MCDERMOTT, A., KIRKE, P. N., MILLS, J. L., MOLLOY, A. M., COX, C., O'LEARY, V. B., PANGILINAN, F., CONLEY, M., CLEARY, L., BRODY, L. C. & SCOTT, J. M. 2006. Confirmation of the R653Q polymorphism of the trifunctional C1-synthase enzyme as a maternal risk for neural tube defects in the Irish population. *Eur J Hum Genet,* 14**,** 768-72.

PARLE-MCDERMOTT, A., PANGILINAN, F., O'BRIEN, K. K., MILLS, J. L., MAGEE, A. M., TROENDLE, J., SUTTON, M., SCOTT, J. M., KIRKE, P. N., MOLLOY, A. M. & BRODY, L. C. 2009. A common variant in MTHFD1L is associated with neural tube defects and mRNA splicing efficiency. *Hum Mutat,* 30**,** 1650-6.

PATEL, H., PIETRO, E. D. & MACKENZIE, R. E. 2003. Mammalian fibroblasts lacking mitochondrial NAD+-dependent methylenetetrahydrofolate dehydrogenase-cyclohydrolase are glycine auxotrophs. *J Biol Chem,* 278**,** 19436-41.

PATTERSON, V. L., DAMRAU, C., PAUDYAL, A., REEVE, B., GRIMES, D. T., STEWART, M. E., WILLIAMS, D. J., SIGGERS, P., GREENFIELD, A. & MURDOCH, J. N. 2009. Mouse hitchhiker mutants have spina bifida, dorso-ventral patterning defects and polydactyly: identification of Tulp3 as a novel negative regulator of the Sonic hedgehog pathway. *Hum Mol Genet,* 18**,** 1719-39.

PEGG, A. E. 2009. Mammalian polyamine metabolism and function. *IUBMB Life,* 61**,** 880-94.

PENG, X., LIN, Q., LIU, Y., JIN, Y., DRUSO, J. E., ANTONYAK, M. A., GUAN, J. L. & CERIONE, R. A. 2013. Inactivation of Cdc42 in embryonic brain results in hydrocephalus with ependymal cell defects in mice. *Protein Cell,* 4**,** 231-42.

PEREZ-FIGARES, J. M., JIMENEZ, A. J. & RODRIGUEZ, E. M. 2001. Subcommissural organ, cerebrospinal fluid circulation, and hydrocephalus. *Microsc Res Tech,* 52**,** 591-607.

PIEDRAHITA, J. A., OETAMA, B., BENNETT, G. D., VAN WAES, J., KAMEN, B. A., RICHARDSON, J., LACEY, S. W., ANDERSON, R. G. & FINNELL, R. H. 1999. Mice lacking the folic acid-binding protein Folbp1 are defective in early embryonic development. *Nat Genet,* 23**,** 228-32.

PIKE, S. T., RAJENDRA, R., ARTZT, K. & APPLING, D. R. 2010. Mitochondrial C1-tetrahydrofolate synthase (MTHFD1L) supports the flow of mitochondrial one-carbon units into the methyl cycle in embryos. *J Biol Chem,* 285**,** 4612-20.

POSSEMATO, R., MARKS, K. M., SHAUL, Y. D., PACOLD, M. E., KIM, D., BIRSOY, K., SETHUMADHAVAN, S., WOO, H. K., JANG, H. G., JHA, A. K., CHEN, W. W., BARRETT,

F. G., STRANSKY, N., TSUN, Z. Y., COWLEY, G. S., BARRETINA, J., KALAANY, N. Y., HSU, P. P., OTTINA, K., CHAN, A. M., YUAN, B., GARRAWAY, L. A., ROOT, D. E., MINO-KENUDSON, M., BRACHTEL, E. F., DRIGGERS, E. M. & SABATINI, D. M. 2011. Functional genomics reveal that the serine synthesis pathway is essential in breast cancer. *Nature,* 476**,** 346-50.

POULOS, A., SHARP, P., SINGH, H., JOHNSON, D. W., CAREY, W. F. & EASTON, C. 1993. Formic acid is a product of the alpha-oxidation of fatty acids by human skin fibroblasts: deficiency of formic acid production in peroxisome-deficient fibroblasts. *Biochem J,* 292 (Pt 2)**,** 457-61.

PRESS, G. A., BARSHOP, B. A., HAAS, R. H., NYHAN, W. L., GLASS, R. F. & HESSELINK, J. R. 1989. Abnormalities of the brain in nonketotic hyperglycinemia: MR manifestations. *AJNR Am J Neuroradiol,* 10**,** 315-21.

PRUDOVA, A., MARTINOV, M. V., VITVITSKY, V. M., ATAULLAKHANOV, F. I. & BANERJEE, R. 2005. Analysis of pathological defects in methionine metabolism using a simple mathematical model. *Biochim Biophys Acta,* 1741**,** 331-8.

PYRGAKI, C., TRAINOR, P., HADJANTONAKIS, A. K. & NISWANDER, L. 2010. Dynamic imaging of mammalian neural tube closure. *Dev Biol,* 344**,** 941-7.

QIN, S., LIU, M., NIU, W. & ZHANG, C. L. 2011. Dysregulation of Kruppel-like factor 4 during brain development leads to hydrocephalus in mice. *Proc Natl Acad Sci U S A,* 108**,** 21117-21.

QIU, A., JANSEN, M., SAKARIS, A., MIN, S. H., CHATTOPADHYAY, S., TSAI, E., SANDOVAL, C., ZHAO, R., AKABAS, M. H. & GOLDMAN, I. D. 2006. Identification of an intestinal folate transporter and the molecular basis for hereditary folate malabsorption. *Cell,* 127**,** 917-28.

RASH, B. G. & RICHARDS, L. J. 2001. A role for cingulate pioneering axons in the development of the corpus callosum. *J Comp Neurol,* 434**,** 147-57.

RAY, J. G., WYATT, P. R., THOMPSON, M. D., VERMEULEN, M. J., MEIER, C., WONG, P. Y., FARRELL, S. A. & COLE, D. E. 2007. Vitamin B12 and the risk of neural tube defects in a folic-acid-fortified population. *Epidemiology,* 18**,** 362-6.

REECE, E. A. 2012. Diabetes-induced birth defects: what do we know? What can we do? *Curr Diab Rep,* 12**,** 24-32.

REED, M. C., NIJHOUT, H. F., NEUHOUSER, M. L., GREGORY, J. F., 3RD, SHANE, B., JAMES, S. J., BOYNTON, A. & ULRICH, C. M. 2006. A mathematical model gives insights into nutritional and genetic aspects of folate-mediated one-carbon metabolism. *J Nutr,* 136**,** 2653-61.

REED, M. C., NIJHOUT, H. F., SPARKS, R. & ULRICH, C. M. 2004. A mathematical model of the methionine cycle. *J Theor Biol,* 226**,** 33-43.

ROBERT, E. & GUIBAUD, P. 1982. Maternal valproic acid and congenital neural tube defects. *Lancet,* 2**,** 937.

ROBINSON, A., ESCUIN, S., DOUDNEY, K., VEKEMANS, M., STEVENSON, R. E., GREENE, N. D., COPP, A. J. & STANIER, P. 2012. Mutations in the planar cell polarity genes CELSR1 and SCRIB are associated with the severe neural tube defect craniorachischisis. *Hum Mutat,* 33**,** 440-7.

ROSE, M. L., MADREN, J., BUNZENDAHL, H. & THURMAN, R. G. 1999. Dietary glycine inhibits the growth of B16 melanoma tumors in mice. *Carcinogenesis,* 20**,** 793-8.

ROSENTHAL, J., CASAS, J., TAREN, D., ALVERSON, C. J., FLORES, A. & FRIAS, J. 2014. Neural tube defects in Latin America and the impact of fortification: a literature review. *Public Health Nutr,* 17**,** 537-50.

ROSS, J. F., CHAUDHURI, P. K. & RATNAM, M. 1994. Differential regulation of folate receptor isoforms in normal and malignant tissues in vivo and in established cell lines. Physiologic and clinical implications. *Cancer,* 73**,** 2432-43.

RULAND, J., DUNCAN, G. S., ELIA, A., DEL BARCO BARRANTES, I., NGUYEN, L., PLYTE, S., MILLAR, D. G., BOUCHARD, D., WAKEHAM, A., OHASHI, P. S. & MAK, T. W. 2001. Bcl10 is a positive regulator of antigen receptor-induced activation of NF-kappaB and neural tube closure. *Cell,* 104**,** 33-42.

RUSSELL, L. B., HUNSICKER, P. R., CACHEIRO, N. L., BANGHAM, J. W., RUSSELL, W. L. & SHELBY, M. D. 1989. Chlorambucil effectively induces deletion mutations in mouse germ cells. *Proc Natl Acad Sci U S A,* 86**,** 3704-8.

RUSSELL, W. L., KELLY, E. M., HUNSICKER, P. R., BANGHAM, J. W., MADDUX, S. C. & PHIPPS, E. L. 1979. Specific-locus test shows ethylnitrosourea to be the most potent mutagen in the mouse. *Proc Natl Acad Sci U S A,* 76**,** 5818-9.

SADLER, T. W., MERRILL, A. H., STEVENS, V. L., SULLARDS, M. C., WANG, E. & WANG, P. 2002. Prevention of fumonisin B1-induced neural tube defects by folic acid. *Teratology,* 66**,** 169-76.

SAKAKIBARA, S., NAKAMURA, Y., YOSHIDA, T., SHIBATA, S., KOIKE, M., TAKANO, H., UEDA, S., UCHIYAMA, Y., NODA, T. & OKANO, H. 2002. RNA-binding protein Musashi family: roles for CNS stem cells and a subpopulation of ependymal cells revealed by targeted disruption and antisense ablation. *Proc Natl Acad Sci U S A,* 99**,** 15194-9.

SAKATA, Y., OWADA, Y., SATO, K., KOJIMA, K., HISANAGA, K., SHINKA, T., SUZUKI, Y., AOKI, Y., SATOH, J., KONDO, H., MATSUBARA, Y. & KURE, S. 2001. Structure and expression of the glycine cleavage system in rat central nervous system. *Brain Res Mol Brain Res,* 94**,** 119-30.

SALOJIN, K. V., CABRERA, R. M., SUN, W., CHANG, W. C., LIN, C., DUNCAN, L., PLATT, K. A., READ, R., VOGEL, P., LIU, Q., FINNELL, R. H. & ORAVECZ, T. 2011. A mouse model of hereditary folate malabsorption: deletion of the PCFT gene leads to systemic folate deficiency. *Blood,* 117**,** 4895-904.

SANTAGATI, F. & RIJLI, F. M. 2003. Cranial neural crest and the building of the vertebrate head. *Nat Rev Neurosci,* 4**,** 806-18.

SAS, K., ROBOTKA, H., TOLDI, J. & VECSEI, L. 2007. Mitochondria, metabolic disturbances, oxidative stress and the kynurenine system, with focus on neurodegenerative disorders. *J Neurol Sci,* 257**,** 221-39.

SATO, K., YOSHIDA, S., FUJIWARA, K., TADA, K. & TOHYAMA, M. 1991. Glycine cleavage system in astrocytes. *Brain Res,* 567**,** 64-70.

SAUKA-SPENGLER, T. & BRONNER-FRASER, M. 2008. A gene regulatory network orchestrates neural crest formation. *Nat Rev Mol Cell Biol,* 9**,** 557-68.

SAYED, A. R., BOURNE, D., PATTINSON, R., NIXON, J. & HENDERSON, B. 2008. Decline in the prevalence of neural tube defects following folic acid fortification and its cost-benefit in South Africa. *Birth Defects Res A Clin Mol Teratol,* 82**,** 211-6.

SCHELL-APACIK, C. C., WAGNER, K., BIHLER, M., ERTL-WAGNER, B., HEINRICH, U., KLOPOCKI, E., KALSCHEUER, V. M., MUENKE, M. & VON VOSS, H. 2008. Agenesis and dysgenesis of the corpus callosum: clinical, genetic and neuroimaging findings in a series of 41 patients. *Am J Med Genet A,* 146A**,** 2501-11.

SCHOENWOLF, G. C. 1984. Histological and ultrastructural studies of secondary neurulation in mouse embryos. *Am J Anat,* 169**,** 361-76.

SCHORAH, C. J., WILD, J., HARTLEY, R., SHEPPARD, S. & SMITHELLS, R. W. 1983. The effect of periconceptional supplementation on blood vitamin concentrations in women at recurrence risk for neural tube defect. *Br J Nutr,* 49**,** 203-11.

SCHWAB, M. A., SAUER, S. W., OKUN, J. G., NIJTMANS, L. G., RODENBURG, R. J., VAN DEN HEUVEL, L. P., DROSE, S., BRANDT, U., HOFFMANN, G. F., TER LAAK, H., KOLKER, S. & SMEITINK, J. A. 2006. Secondary mitochondrial dysfunction in propionic aciduria: a pathogenic role for endogenous mitochondrial toxins. *Biochem J,* 398**,** 107-12.

SCHWAHN, B. C., LARYEA, M. D., CHEN, Z., MELNYK, S., POGRIBNY, I., GARROW, T., JAMES, S. J. & ROZEN, R. 2004. Betaine rescue of an animal model with methylenetetrahydrofolate reductase deficiency. *Biochem J,* 382**,** 831-40.

SCHWARCZ, R., BRUNO, J. P., MUCHOWSKI, P. J. & WU, H. Q. 2012. Kynurenines in the mammalian brain: when physiology meets pathology. *Nat Rev Neurosci,* 13**,** 465-77.

SELLER, M. J. 1995. Further evidence for an intermittent pattern of neural tube closure in humans. *J Med Genet,* 32**,** 205-7.

SELLER, M. J. & NEVIN, N. C. 1984. Periconceptional vitamin supplementation and the prevention of neural tube defects in south-east England and Northern Ireland. *J Med Genet,* 21**,** 325-30.

SEPULVEDA, W., CORRAL, E., AYALA, C., BE, C., GUTIERREZ, J. & VASQUEZ, P. 2004. Chromosomal abnormalities in fetuses with open neural tube defects: prenatal identification with ultrasound. *Ultrasound Obstet Gynecol,* 23**,** 352-6.

SGAIER, S. K., LAO, Z., VILLANUEVA, M. P., BERENSHTEYN, F., STEPHEN, D., TURNBULL, R. K. & JOYNER, A. L. 2007. Genetic subdivision of the tectum and cerebellum into functionally related regions based on differential sensitivity to engrailed proteins. *Development,* 134**,** 2325-35.

SHAFIZADEH, T. B. & HALSTED, C. H. 2007. gamma-Glutamyl hydrolase, not glutamate carboxypeptidase II, hydrolyzes dietary folate in rat small intestine. *J Nutr,* 137**,** 1149-53.

SHEMIN, D., RUSSELL, C. S. & ABRAMSKY, T. 1955. The succinate-glycine cycle. I. The mechanism of pyrrole synthesis. *J Biol Chem,* 215**,** 613-26.

SHEPPARD, S., NEVIN, N. C., SELLER, M. J., WILD, J., SMITHELLS, R. W., READ, A. P., HARRIS, R., FIELDING, D. W. & SCHORAH, C. J. 1989. Neural tube defect recurrence after 'partial' vitamin supplementation. *J Med Genet,* 26**,** 326-9.

SHIELDS, D. C., KIRKE, P. N., MILLS, J. L., RAMSBOTTOM, D., MOLLOY, A. M., BURKE, H., WEIR, D. G., SCOTT, J. M. & WHITEHEAD, A. S. 1999. The "thermolabile" variant of methylenetetrahydrofolate reductase and neural tube defects: An evaluation of genetic risk and the relative importance of the genotypes of the embryo and the mother. *Am J Hum Genet,* 64**,** 1045-55.

SIFFREDI, V., ANDERSON, V., LEVENTER, R. J. & SPENCER-SMITH, M. M. 2013. Neuropsychological profile of agenesis of the corpus callosum: a systematic review. *Dev Neuropsychol,* 38**,** 36-57.

SILVER, L. M. 1995. *Mouse Genetics: Concepts and Applications*, Oxford University Press.

SIU, M. T., WILEY, M. J. & WELLS, P. G. 2013. Methanol teratogenicity in mutant mice with deficient catalase activity and transgenic mice expressing human catalase. *Reprod Toxicol,* 36**,** 33-9.

SKARNES, W. C., AUERBACH, B. A. & JOYNER, A. L. 1992. A gene trap approach in mouse embryonic stem cells: the lacZ reported is activated by splicing, reflects endogenous gene expression, and is mutagenic in mice. *Genes Dev,* 6**,** 903-18.

SMITH, K. M., OHKUBO, Y., MARAGNOLI, M. E., RASIN, M. R., SCHWARTZ, M. L., SESTAN, N. & VACCARINO, F. M. 2006a. Midline radial glia translocation and corpus callosum formation require FGF signaling. *Nat Neurosci,* 9**,** 787-97.

SMITH, U. M., CONSUGAR, M., TEE, L. J., MCKEE, B. M., MAINA, E. N., WHELAN, S., MORGAN, N. V., GORANSON, E., GISSEN, P., LILLIQUIST, S., ALIGIANIS, I. A., WARD, C. J., PASHA, S., PUNYASHTHITI, R., MALIK SHARIF, S., BATMAN, P. A., BENNETT, C. P., WOODS, C. G., MCKEOWN, C., BUCOURT, M., MILLER, C. A., COX, P., ALGAZALI, L., TREMBATH, R. C., TORRES, V. E., ATTIE-BITACH, T., KELLY, D. A., MAHER, E. R., GATTONE, V. H., 2ND, HARRIS, P. C. & JOHNSON, C. A. 2006b. The transmembrane protein meckelin (MKS3) is mutated in Meckel-Gruber syndrome and the wpk rat. *Nat Genet,* 38**,** 191-6.

SMITHELLS, R. W., ANKERS, C., CARVER, M. E., LENNON, D., SCHORAH, C. J. & SHEPPARD, S. 1977. Maternal nutrition in early pregnancy. *Br J Nutr,* 38**,** 497-506.

SMITHELLS, R. W., NEVIN, N. C., SELLER, M. J., SHEPPARD, S., HARRIS, R., READ, A. P., FIELDING, D. W., WALKER, S., SCHORAH, C. J. & WILD, J. 1983. Further experience of vitamin supplementation for prevention of neural tube defect recurrences. *Lancet,* 1**,** 1027-31.

SMITHELLS, R. W., SHEPPARD, S. & SCHORAH, C. J. 1976. Vitamin dificiencies and neural tube defects. *Arch Dis Child,* 51**,** 944-50.

SMITHELLS, R. W., SHEPPARD, S., SCHORAH, C. J., SELLER, M. J., NEVIN, N. C., HARRIS, R., READ, A. P. & FIELDING, D. W. 1980. Possible prevention of neural-tube defects by periconceptional vitamin supplementation. *Lancet,* 1**,** 339-40.

SMITHELLS, R. W., SHEPPARD, S., SCHORAH, C. J., SELLER, M. J., NEVIN, N. C., HARRIS, R., READ, A. P. & FIELDING, D. W. 1981. Apparent prevention of neural tube defects by periconceptional vitamin supplementation. *Arch Dis Child,* 56**,** 911-8.

SMITHELLS, R. W., SHEPPARD, S., WILD, J. & SCHORAH, C. J. 1989. Prevention of neural tube defect recurrences in Yorkshire: final report. *Lancet,* 2**,** 498-9.

SMITHERMAN, M., LEE, K., SWANGER, J., KAPUR, R. & CLURMAN, B. E. 2000. Characterization and targeted disruption of murine Nup50, a p27(Kip1)-interacting component of the nuclear pore complex. *Mol Cell Biol,* 20**,** 5631-42.

SMITHIES, O., GREGG, R. G., BOGGS, S. S., KORALEWSKI, M. A. & KUCHERLAPATI, R. S. 1985. Insertion of DNA sequences into the human chromosomal beta-globin locus by homologous recombination. *Nature,* 317**,** 230-4.

SNELL, K., NATSUMEDA, Y. & WEBER, G. 1987. The modulation of serine metabolism in hepatoma 3924A during different phases of cellular proliferation in culture. *Biochem J,* 245**,** 609-12.

SOFOU, K., STENERYD, K., WIKLUND, L. M., TULINIUS, M. & DARIN, N. 2013. MRI of the brain in childhood-onset mitochondrial disorders with central nervous system involvement. *Mitochondrion,* 13**,** 364-71.

SOMERA, K. C. & JONES, H. C. 2004. Reduced subcommissural organ glycoprotein immunoreactivity precedes aqueduct closure and ventricular dilatation in H-Tx rat hydrocephalus. *Cell Tissue Res,* 315**,** 361-73.

SOTTOCORNOLA, R., ROYER, C., VIVES, V., TORDELLA, L., ZHONG, S., WANG, Y., RATNAYAKA, I., SHIPMAN, M., CHEUNG, A., GASTON-MASSUET, C., FERRETTI, P., MOLNAR, Z. & LU, X. 2010. ASPP2 binds Par-3 and controls the polarity and proliferation of neural progenitors during CNS development. *Dev Cell,* 19**,** 126-37.

SPASSKY, N., MERKLE, F. T., FLAMES, N., TRAMONTIN, A. D., GARCIA-VERDUGO, J. M. & ALVAREZ-BUYLLA, A. 2005. Adult ependymal cells are postmitotic and are derived from radial glial cells during embryogenesis. *J Neurosci,* 25**,** 10-8.

SPENNATO, P., MIRONE, G., NASTRO, A., BUONOCORE, M. C., RUGGIERO, C., TRISCHITTA, V., ALIBERTI, F. & CINALLI, G. 2011. Hydrocephalus in Dandy-Walker malformation. *Childs Nerv Syst,* 27**,** 1665-81.

SPIEGELSTEIN, O., MITCHELL, L. E., MERRIWEATHER, M. Y., WICKER, N. J., ZHANG, Q., LAMMER, E. J. & FINNELL, R. H. 2004. Embryonic development of folate binding protein-1 (Folbp1) knockout mice: Effects of the chemical form, dose, and timing of maternal folate supplementation. *Dev Dyn,* 231**,** 221-31.

STEEGERS-THEUNISSEN, R. P., BOERS, G. H., TRIJBELS, F. J., FINKELSTEIN, J. D., BLOM, H. J., THOMAS, C. M., BORM, G. F., WOUTERS, M. G. & ESKES, T. K. 1994. Maternal hyperhomocysteinemia: a risk factor for neural-tube defects? *Metabolism,* 43**,** 1475-80.

STEVENS, V. L. & TANG, J. 1997. Fumonisin B1-induced sphingolipid depletion inhibits vitamin uptake via the glycosylphosphatidylinositol-anchored folate receptor. *J Biol Chem,* 272**,** 18020-5.

STOVER, P. J. 2004. Physiology of folate and vitamin B12 in health and disease. *Nutr Rev,* 62**,** S3-12; discussion S13.

STUMPO, D. J., BOCK, C. B., TUTTLE, J. S. & BLACKSHEAR, P. J. 1995. MARCKS deficiency in mice leads to abnormal brain development and perinatal death. *Proc Natl Acad Sci U S A,* 92**,** 944-8.

SUAREZ, L., HENDRICKS, K., FELKNER, M. & GUNTER, E. 2003. Maternal serum B12 levels and risk for neural tube defects in a Texas-Mexico border population. *Ann Epidemiol,* 13**,** 81-8.

SUZUKI, Y., KURE, S., OOTA, M., HINO, H. & FUKUDA, M. 2010. Nonketotic hyperglycinemia: proposal of a diagnostic and treatment strategy. *Pediatr Neurol,* 43**,** 221-4.

SWANSON, D. A., LIU, M. L., BAKER, P. J., GARRETT, L., STITZEL, M., WU, J., HARRIS, M., BANERJEE, R., SHANE, B. & BRODY, L. C. 2001. Targeted disruption of the methionine synthase gene in mice. *Mol Cell Biol,* 21**,** 1058-65.

TADA, K. & ARAKAWA, T. 1970. Hyperglycinemia and propionate carboxylation. *Tohoku J Exp Med,* 102**,** 313-4.

TADA, K., NARISAWA, K., YOSHIDA, T., KONNO, T. & YOKOYAMA, Y. 1969. Hyperglycinemia: a defect in glycine cleavage reaction. *Tohoku J Exp Med,* 98**,** 289-96.

TAKEUCHI, I. K. & TAKEUCHI, Y. K. 1986. Congenital hydrocephalus following X-irradiation of pregnant rats on an early gestational day. *Neurobehav Toxicol Teratol,* 8**,** 143-50.

TAKEUCHI, T., YAMAZAKI, Y., KATOH-FUKUI, Y., TSUCHIYA, R., KONDO, S., MOTOYAMA, J. & HIGASHINAKAGAWA, T. 1995. Gene trap capture of a novel mouse gene, jumonji, required for neural tube formation. *Genes Dev,* 9**,** 1211-22.

TEDESCHI, P. M., MARKERT, E. K., GOUNDER, M., LIN, H., DVORZHINSKI, D., DOLFI, S. C., CHAN, L. L., QIU, J., DIPAOLA, R. S., HIRSHFIELD, K. M., BOROS, L. G., BERTINO, J. R., OLTVAI, Z. N. & VAZQUEZ, A. 2013. Contribution of serine, folate and glycine metabolism to the ATP, NADPH and purine requirements of cancer cells. *Cell Death Dis,* 4**,** e877.

TEPHLY, T. R. 1991. The toxicity of methanol. *Life Sci,* 48**,** 1031-41.

THOMAS, K. R. & CAPECCHI, M. R. 1987. Site-directed mutagenesis by gene targeting in mouse embryo-derived stem cells. *Cell,* 51**,** 503-12.

TIAN, Y., LEI, L. & MINDEN, A. 2011. A key role for Pak4 in proliferation and differentiation of neural progenitor cells. *Dev Biol,* 353**,** 206-16.

TIBBETTS, A. S. & APPLING, D. R. 2010. Compartmentalization of Mammalian folate-mediated one-carbon metabolism. *Annu Rev Nutr,* 30**,** 57-81.

TING, S. B., WILANOWSKI, T., AUDEN, A., HALL, M., VOSS, A. K., THOMAS, T., PAREKH, V., CUNNINGHAM, J. M. & JANE, S. M. 2003. Inositol- and folate-resistant neural tube defects in mice lacking the epithelial-specific factor Grhl-3. *Nat Med,* 9**,** 1513-9.

TITUS, S. A. & MORAN, R. G. 2000. Retrovirally mediated complementation of the glyB phenotype. Cloning of a human gene encoding the carrier for entry of folates into mitochondria. *J Biol Chem,* 275**,** 36811-7.

TORTORI-DONATI, P., ROSSI, A. & CAMA, A. 2000. Spinal dysraphism: a review of neuroradiological features with embryological correlations and proposal for a new classification. *Neuroradiology,* 42**,** 471-91.

TOVAR-MOLL, F., MOLL, J., DE OLIVEIRA-SOUZA, R., BRAMATI, I., ANDREIUOLO, P. A. & LENT, R. 2007. Neuroplasticity in human callosal dysgenesis: a diffusion tensor imaging study. *Cereb Cortex,* 17**,** 531-41.

TREBLE-BARNA, A., KULESZ, P. A., DENNIS, M. & FLETCHER, J. M. 2014. Covert orienting in three etiologies of congenital hydrocephalus: the effect of midbrain and posterior fossa dysmorphology. *J Int Neuropsychol Soc,* 20**,** 268-77.

TRESSEL, T., THOMPSON, R., ZIESKE, L. R., MENENDEZ, M. I. & DAVIS, L. 1986. Interaction between L-threonine dehydrogenase and aminoacetone synthetase and mechanism of aminoacetone production. *J Biol Chem,* 261**,** 16428-37.

TRIJBELS, J. M., MONNENS, L. A., VAN DER ZEE, S. P., VRENKEN, J. A., SENGERS, R. C. & SCHRETLEN, E. D. 1974. A patient with nonketotic hyperglycinemia: biochemical findings and therapeutic approaches. *Pediatr Res,* 8**,** 598-605.

TSUYUSAKI, Y., SHIMBO, H., WADA, T., IAI, M., TSUJI, M., YAMASHITA, S., AIDA, N., KURE, S. & OSAKA, H. 2012. Paradoxical increase in seizure frequency with valproate in nonketotic hyperglycinemia. *Brain Dev,* 34**,** 72-5.

VAN ALLEN, M. I., KALOUSEK, D. K., CHERNOFF, G. F., JURILOFF, D., HARRIS, M., MCGILLIVRAY, B. C., YONG, S. L., LANGLOIS, S., MACLEOD, P. M., CHITAYAT, D. & ET AL. 1993. Evidence for multi-site closure of the neural tube in humans. *Am J Med Genet,* 47**,** 723-43.

VAN DER LINDEN, I. J., HEIL, S. G., KOUWENBERG, I. C., DEN HEIJER, M. & BLOM, H. J. 2007. The methylenetetrahydrofolate dehydrogenase (MTHFD1) 1958G>A variant is not associated with spina bifida risk in the Dutch population. *Clin Genet,* 72**,** 599-600.

VAN DER PUT, N. M., STEEGERS-THEUNISSEN, R. P., FROSST, P., TRIJBELS, F. J., ESKES, T. K., VAN DEN HEUVEL, L. P., MARIMAN, E. C., DEN HEYER, M., ROZEN, R. & BLOM, H. J. 1995. Mutated methylenetetrahydrofolate reductase as a risk factor for spina bifida. *Lancet,* 346**,** 1070-1.

VAN HOVE, J. L., KISHNANI, P. S., DEMAEREL, P., KAHLER, S. G., MILLER, C., JAEKEN, J. & RUTLEDGE, S. L. 2000. Acute hydrocephalus in nonketotic hyperglycemia. *Neurology,* 54**,** 754-6.

VAN HOVE, J. L., LAZEYRAS, F., ZEISEL, S. H., BOTTIGLIERI, T., HYLAND, K., CHARLES, H. C., GRAY, L., JAEKEN, J. & KAHLER, S. G. 1998. One-methyl group metabolism in non-ketotic hyperglycinaemia: mildly elevated cerebrospinal fluid homocysteine levels. *J Inherit Metab Dis,* 21**,** 799-811.

VAN STRAATEN, H. W. & COPP, A. J. 2001. Curly tail: a 50-year history of the mouse spina bifida model. *Anat Embryol (Berl),* 203**,** 225-37.

VANAERTS, L. A., BLOM, H. J., DEABREU, R. A., TRIJBELS, F. J., ESKES, T. K., COPIUS PEEREBOOM-STEGEMAN, J. H. & NOORDHOEK, J. 1994. Prevention of neural tube defects by and toxicity of L-homocysteine in cultured postimplantation rat embryos. *Teratology,* 50**,** 348-60.

VAZQUEZ, A., MARKERT, E. K. & OLTVAI, Z. N. 2011. Serine biosynthesis with one carbon catabolism and the glycine cleavage system represents a novel pathway for ATP generation. *PLoS One,* 6**,** e25881.

VERHOEVEN, N. M. & JAKOBS, C. 2001. Human metabolism of phytanic acid and pristanic acid. *Prog Lipid Res,* 40**,** 453-66.

VILLAR, D., CRAY, C., ZAIAS, J. & ALTMAN, N. H. 2007. Biologic effects of fenbendazole in rats and mice: a review. *J Am Assoc Lab Anim Sci,* 46**,** 8-15.

VIOLA, A., CHABROL, B., NICOLI, F., CONFORT-GOUNY, S., VIOUT, P. & COZZONE, P. J. 2002. Magnetic resonance spectroscopy study of glycine pathways in nonketotic hyperglycinemia. *Pediatr Res,* 52**,** 292-300.

VISENTIN, M., DIOP-BOVE, N., ZHAO, R. & GOLDMAN, I. D. 2014. The intestinal absorption of folates. *Annu Rev Physiol,* 76**,** 251-74.

VON WENDT, L. 1979. Experimental hyperglycinaemia--an evaluation of the efficacy of strychnine therapy in nonketotic hyperglycinaemia. *J Ment Defic Res,* 23**,** 195-205.

VON WENDT, L., HIRVASNIEMI, A. & SIMILA, S. 1979. Nonketotic hyperglycinemia. A genetic study of 13 Finnish families. *Clin Genet,* 15**,** 411-7.

VON WENDT, L., SIMILA, S., SAUKKONEN, A. L. & KOIVISTO, M. 1980. Failure of strychnine treatment during the neonatal period in three Finnish children with nonketotic hyperglycinemia. *Pediatrics,* 65**,** 1166-9.

WAHLSTEN, D., COLBOURNE, F. & PLEUS, R. 2003. A robust, efficient and flexible method for staining myelinated axons in blocks of brain tissue. *J Neurosci Methods,* 123**,** 207-14.

WAJNER, M. & GOODMAN, S. I. 2011. Disruption of mitochondrial homeostasis in organic acidurias: insights from human and animal studies. *J Bioenerg Biomembr,* 43**,** 31-8.

WALD, N. J. & POLANI, P. E. 1984. Neural-tube defects and vitamins: the need for a randomized clinical trial. *Br J Obstet Gynaecol,* 91**,** 516-23.

WALKUP, A. S. & APPLING, D. R. 2005. Enzymatic characterization of human mitochondrial C1-tetrahydrofolate synthase. *Arch Biochem Biophys,* 442**,** 196-205.

WALZEM, R. L. & CLIFFORD, A. J. 1988. Folate deficiency in rats fed diets containing free amino acids or intact proteins. *J Nutr,* 118**,** 1089-96.

WANG, J., ALEXANDER, P. & MCKNIGHT, S. L. 2011. Metabolic specialization of mouse embryonic stem cells. *Cold Spring Harb Symp Quant Biol,* 76**,** 183-93.

WANG, J., HAMBLET, N. S., MARK, S., DICKINSON, M. E., BRINKMAN, B. C., SEGIL, N., FRASER, S. E., CHEN, P., WALLINGFORD, J. B. & WYNSHAW-BORIS, A. 2006. Dishevelled genes mediate a conserved mammalian PCP pathway to regulate convergent extension during neurulation. *Development,* 133**,** 1767-78.

WANG, L., WANG, F., GUAN, J., LE, J., WU, L., ZOU, J., ZHAO, H., PEI, L., ZHENG, X. & ZHANG, T. 2010. Relation between hypomethylation of long interspersed nucleotide elements and risk of neural tube defects. *Am J Clin Nutr,* 91**,** 1359-67.

WANG, W., WU, Z., DAI, Z., YANG, Y., WANG, J. & WU, G. 2013. Glycine metabolism in animals and humans: implications for nutrition and health. *Amino Acids,* 45**,** 463-77.

WANG, W., WU, Z., LIN, G., HU, S., WANG, B., DAI, Z. & WU, G. 2014a. Glycine stimulates protein synthesis and inhibits oxidative stress in pig small intestinal epithelial cells. *J Nutr,* 144**,** 1540-8.

WANG, X., WANG, R. H., LI, W., XU, X., HOLLANDER, M. C., FORNACE, A. J., JR. & DENG, C. X. 2004. Genetic interactions between Brca1 and Gadd45a in centrosome duplication, genetic stability, and neural tube closure. *J Biol Chem,* 279**,** 29606-14.

WANG, Y., XU, S., CAO, Y., XIE, Z., LAI, C., JI, X. & BI, J. 2014b. Folate deficiency exacerbates apoptosis by inducing hypomethylation and resultant overexpression of DR4 together with altering DNMTs in Alzheimer's disease. *Int J Clin Exp Med,* 7**,** 1945-57.

WASHBURN, S. E., CAUDILL, M. A., MALYSHEVA, O., MACFARLANE, A. J., BEHAN, N. A., HARNETT, B., MACMILLAN, L., PONGNOPPARAT, T., BROSNAN, J. T. & BROSNAN, M. E. 2015. Formate metabolism in the fetal and neonatal sheep. *Am J Physiol Endocrinol Metab***,** ajpendo 00046 2015.

WATKINS, M. L., RASMUSSEN, S. A., HONEIN, M. A., BOTTO, L. D. & MOORE, C. A. 2003. Maternal obesity and risk for birth defects. *Pediatrics,* 111**,** 1152-8.

WERLER, M. M., AHRENS, K. A., BOSCO, J. L., MITCHELL, A. A., ANDERKA, M. T., GILBOA, S. M. & HOLMES, L. B. 2011. Use of antiepileptic medications in pregnancy in relation to risks of birth defects. *Ann Epidemiol,* 21**,** 842-50.

WIJBURG, F. A., DE GROOT, C. J., SCHUTGENS, R. B., BARTH, P. G. & TADA, K. 1988. Clinical effects of serine medication in non-ketotic hyperglycinaemia due to deficiency of P-protein of the glycine cleavage complex. *J Inherit Metab Dis,* 11 Suppl 2**,** 218-20.

WILLIAMS, B. 1973. Is aqueduct stenosis a result of hydrocephalus? *Brain,* 96**,** 399-412.

WLODARCZYK, B., SPIEGELSTEIN, O., GELINEAU-VAN WAES, J., VORCE, R. L., LU, X., LE, C. X. & FINNELL, R. H. 2001. Arsenic-induced congenital malformations in genetically susceptible folate binding protein-2 knockout mice. *Toxicol Appl Pharmacol,* 177**,** 238-46.

WLODARCZYK, B. J., PALACIOS, A. M., GEORGE, T. M. & FINNELL, R. H. 2012. Antiepileptic drugs and pregnancy outcomes. *Am J Med Genet A,* 158A**,** 2071-90.

WLODARCZYK, B. J., TANG, L. S., TRIPLETT, A., ALEMAN, F. & FINNELL, R. H. 2006. Spontaneous neural tube defects in splotch mice supplemented with selected micronutrients. *Toxicol Appl Pharmacol,* 213**,** 55-63.

WYSZYNSKI, D. F. 2006. Maternal exposure to selected environmental factors and risk for neural tube defects in the offspring. *In:* WYSZYNSKI, D. F. (ed.) *Neural Tube Defects: From Origin to Treatment.* Oxford: Oxford University Press.

XU, W., BARIBAULT, H. & ADAMSON, E. D. 1998. Vinculin knockout results in heart and brain defects during embryonic development. *Development,* 125**,** 327-37.

YAMAZAKI, F., MOLLER, M., FU, C., CLOKIE, S. J., ZYKOVICH, A., COON, S. L., KLEIN, D. C. & RATH, M. F. 2014. The Lhx9 homeobox gene controls pineal gland development and prevents postnatal hydrocephalus. *Brain Struct Funct*.

YANG, P., LI, X., XU, C., ECKERT, R. L., REECE, E. A., ZIELKE, H. R. & WANG, F. 2013. Maternal hyperglycemia activates an ASK1-FoxO3a-caspase 8 pathway that leads to embryonic neural tube defects. *Sci Signal,* 6**,** ra74.

YBOT-GONZALEZ, P., COGRAM, P., GERRELLI, D. & COPP, A. J. 2002. Sonic hedgehog and the molecular regulation of mouse neural tube closure. *Development,* 129**,** 2507-17.

YBOT-GONZALEZ, P. & COPP, A. J. 1999. Bending of the neural plate during mouse spinal neurulation is independent of actin microfilaments. *Dev Dyn,* 215**,** 273-83.

YBOT-GONZALEZ, P., GASTON-MASSUET, C., GIRDLER, G., KLINGENSMITH, J., ARKELL, R., GREENE, N. D. & COPP, A. J. 2007a. Neural plate morphogenesis during mouse neurulation is regulated by antagonism of Bmp signalling. *Development,* 134**,** 3203-11.

YBOT-GONZALEZ, P., SAVERY, D., GERRELLI, D., SIGNORE, M., MITCHELL, C. E., FAUX, C. H., GREENE, N. D. & COPP, A. J. 2007b. Convergent extension, planar-cell-polarity signalling and initiation of mouse neural tube closure. *Development,* 134**,** 789-99.

YIS, U., KURUL, S. H. & DIRIK, E. 2009. Nonketotic hyperglycinemia and acquired hydrocephalus. *Pediatr Neurol,* 40**,** 138-40.

YOSHIDA, H., KONG, Y. Y., YOSHIDA, R., ELIA, A. J., HAKEM, A., HAKEM, R., PENNINGER, J. M. & MAK, T. W. 1998. Apaf1 is required for mitochondrial pathways of apoptosis and brain development. *Cell,* 94**,** 739-50.

YOSHIDA, T. & KIKUCHI, G. 1972. Comparative study on major pathways of glycine and serine catabolism in vertebrate livers. *J Biochem,* 72**,** 1503-16.

YOSHIDA, T. & KIKUCHI, G. 1973. Majors pathways of serine and glycine catabolism in various organs of the rat and cock. *J Biochem,* 73**,** 1013-22.

YU, T. W., CHAHROUR, M. H., COULTER, M. E., JIRALERSPONG, S., OKAMURA-IKEDA, K., ATAMAN, B., SCHMITZ-ABE, K., HARMIN, D. A., ADLI, M., MALIK, A. N., D'GAMA, A. M., LIM, E. T., SANDERS, S. J., MOCHIDA, G. H., PARTLOW, J. N., SUNU, C. M., FELIE, J. M., RODRIGUEZ, J., NASIR, R. H., WARE, J., JOSEPH, R. M., HILL, R. S., KWAN, B. Y., AL-SAFFAR, M., MUKADDES, N. M., HASHMI, A., BALKHY, S., GASCON, G. G., HISAMA, F. M., LECLAIR, E., PODURI, A., ONER, O., AL-SAAD, S., AL-AWADI, S. A., BASTAKI, L., BEN-OMRAN, T., TEEBI, A. S., AL-GAZALI, L., EAPEN, V., STEVENS, C. R., RAPPAPORT, L., GABRIEL, S. B., MARKIANOS, K., STATE, M. W., GREENBERG, M. E., TANIGUCHI, H., BRAVERMAN, N. E., MORROW, E. M. & WALSH, C. A. 2013. Using whole-exome sequencing to identify inherited causes of autism. *Neuron,* 77**,** 259-73.

ZAMOCKY, M., FURTMULLER, P. G. & OBINGER, C. 2008. Evolution of catalases from bacteria to humans. *Antioxid Redox Signal,* 10**,** 1527-48.

ZHANG, W. C., SHYH-CHANG, N., YANG, H., RAI, A., UMASHANKAR, S., MA, S., SOH, B. S., SUN, L. L., TAI, B. C., NGA, M. E., BHAKOO, K. K., JAYAPAL, S. R., NICHANE, M., YU, Q., AHMED, D. A., TAN, C., SING, W. P., TAM, J., THIRUGANANAM, A., NOGHABI, M. S., PANG, Y. H., ANG, H. S., MITCHELL, W., ROBSON, P., KALDIS, P., SOO, R. A., SWARUP, S., LIM, E. H. & LIM, B. 2012. Glycine decarboxylase activity drives non-small cell lung cancer tumor-initiating cells and tumorigenesis. *Cell,* 148**,** 259-72.

ZHAO, A., TSECHANSKY, M., ELLINGTON, A. D. & MARCOTTE, E. M. 2014. Revisiting and revising the purinosome. *Mol Biosyst,* 10**,** 369-74.

ZHAO, R., DIOP-BOVE, N., VISENTIN, M. & GOLDMAN, I. D. 2011. Mechanisms of membrane transport of folates into cells and across epithelia. *Annu Rev Nutr,* 31**,** 177-201.

ZHAO, R., MATHERLY, L. H. & GOLDMAN, I. D. 2009. Membrane transporters and folate homeostasis: intestinal absorption and transport into systemic compartments and tissues. *Expert Rev Mol Med,* 11**,** e4.

ZHAO, R., MIN, S. H., QIU, A., SAKARIS, A., GOLDBERG, G. L., SANDOVAL, C., MALATACK, J. J., ROSENBLATT, D. S. & GOLDMAN, I. D. 2007. The spectrum of mutations in the PCFT gene, coding for an intestinal folate transporter, that are the basis for hereditary folate malabsorption. *Blood,* 110**,** 1147-52.

ZHAO, R., RUSSELL, R. G., WANG, Y., LIU, L., GAO, F., KNEITZ, B., EDELMANN, W. & GOLDMAN, I. D. 2001. Rescue of embryonic lethality in reduced folate carrier-deficient mice by maternal folic acid supplementation reveals early neonatal failure of hematopoietic organs. *J Biol Chem,* 276**,** 10224-8.

Appendix: *Gldc*^{GT1} gene-trap sequence

The *Gldc*^{GT1} gene-trap construct was sequenced from 2 kb fragments that were amplified using Long-Range PCR (see **Chapter 2**, **Section 2.1.4**). The site of gene-trap insertion and all Frt, F3, loxP, and lox5171 sites were confirmed (see **Chapter 3**, **Section 3.2.2.1**) and annotated below:

AGCACTTATGCTAACTAGATAATGTTAAACATTTGTGGAGCGCCTCCTGT	*Gldc* intron 2-3
GGGCACTTTTGAAAAGTGCTTTTTGTGTATTATTTATTTAGTCCTCATTA	
CAGTCT**GTGAACGGAGTCCCTCTCTCTCCC**CCCTCTGCCGTTTGTTTTAG	**F2 primer**
AGATAAGGGTCTCAATTGTGTTGCCCAGGCTGGTCATGTTCATGGACTCC	
AATGCTTCTCTAATCTTCCCTTCCCAGATACCTGGGACTCTAGGCCCACAT	
GACCATTGCACAGCTATTAACCCCTTTAAAAGAAAGAAACCGTGGTATAC	
AGAGGCTCTTTAACTTGCCAGGGTCTTAGCCCGTGACCTTTGGATGGGAGC	
AGAATGCAAACTCAGGCCATCTGACTCCATTGCCAACCCCCACTCCCCACC	
CCCCAATGATGACATTGCTGTTTTCATGGTGTCCCAGGCAAAGCAGAGAA	
CTCCTGTCCTGGCTCTTCTAAGGTGCACAAGCCAGTCATCCTTTTGTCTTG	
TGCAAACTGCCCCTTTGGGAATGAGACACCACAGTGAGGCTAAGTGTGGA	
GTTCTCAGGCCCACCAC//TGAAAGACCCCCGCTGACGGGTAGTCAATCAC	// insertion site
TCAGAGGAGACCCTCCCAAGGAACAGCGAGACCACAAGTCGGATGCAACT	Vector sequence
GCAAGAGGGTTTATTGGATACACGGGTACCCGG	
(missing sequences)	
TACAGGTGGGGTCTTTCATTCCCCCCTTTTTCTGGAGACTAAATAAAATCT	
TTTATTTTATCGATTCAAGCCACTATGCGCACAGCTGGTCGAGCCCGGGCC	
CTCGAGAATTC**GAAGTTCCTATTCCGAAGTTCCTATTCTCTAGAAAGT**	**Frt**
ATAGGAACTTCAGCAGATCCTTATTTGTCATATTGTAAGTGCTTTCTCTA	
ATCACTTTCTTTCATGGCAAGCAGGGTATGGATCTGCT**GAAGTTCCTATT**	**F3**
CCGAAGTTCCTATTCTTCAAATAGTATAGGAACTTCGTTGCTAGAAGC	
GGTTTTCGGGAGAATACGACTCACTATAGGGCGAATTG**ATAACTTCGTA**	**loxP**
TAGCATACATTATACGAAGTTATCCAAGCTTCACCATCGACCCGAATTG	
CCAAGCATCACCATCGACCC**ATAACTTCGTATAGTACACATTATACGAA**	**lox5171**
GTTATCGAATTCCTACGTACTAGATTCCATGTAAATTTGTAGCCAGCTTC	
CTTCTGATTTTCAATGTTTCTTCCAAAGGTGCAGTCTCCAAAGAGATTAC	
GAATGCCTTGGAAACCTGGGGTGCCTTGGGTCAGGACATCAACTTGGACA	
TTCCTAGTTTTCAAATGAGTGATGATATTGACGATATAAAATGGGAAAAA	
ACTTCAGACAAGAAAAAGATTGCACAATTCAGAAAAGAGAAAGAGACTTT	

CAAGGAAAAAGATACATATAAGCTATTTAAAAATGGAACTCTGATAATTA	
AGCATCTGAAGACCGATGATCAGGATATCTACAAGGTATCAATATATGAT	
ACAAAAGGAAAAAATGTGTTGG	
(missing sequences)	
ACATCTATCTCATCATTGGCATATGTGGAGGAGGCAGCCTCTTGATGGTC	
TTTGTGGCACTGCTCGTTTTCTATATCACCAAAAGGAAAAAACAGAGGAG	
TCGGAGAAATGATGAGGAGCTGGAGACAAGAGCCCACAGAGTAGCTACGG	
ATCCCATTGAACAAGATGGATTGCACGCAGGTTCTCCGGCCGCTTGGGTGG	*Neo* sequence
AGAGGCTATTCGGCTATGACTGGGCACAACAGACAATCGGCTGCTCTGAT	
GCCGCCGTGTTCCGGCTGTCAGCGCAGGGGCGCCCGGTTCTTTTTGTCAAG	
ACCGACCTGTCCGGTGCCCTGAATGAACTGCAGGACGAGGCAGCGCGGCTA	
TCGTGGCTGGCCACGACGGGCGTTCCTTGCGCAG**CTGTGCTCGACGTTGT**	**F3 primer**
CACTGAAGCGGGAAGGGACTGGCTGCTATTGGGCGAAGTGCCGGGGCAGG	
ACCTCCTGTCATCTCACCTTGCTCCTGCCGAGAAAGTATCCATCATGGCTG	
ATGCAATGCGGCGGCTGCATACGCTTGATCCGGCTACCTGCCCATTCGACC	
ACCAAGCGAAACATCGCATCGAGCGAGCACGTACTCGGATGGAAGCCGGT	
CTTGTCGATCAGGATGATCTGGACGAAGAGCATCAGGGGCTCGCGCCAGC	
CGAACTGTTCGCCAGGCTCAAGGCGCGCATGCCCGACGGCGAGGATCTCGT	
CGTGACCCATGGCGATGCCTGCTTGCCGAATATCATGGTGGAAAATGGCC	
GCTTTTCTGGATTCATCGACTGTGGCCGGCTGGGTGTGGCGGACCGCTATC	
AGGACATAGCGTTGGCTACCCGTGATATTGCTGAAGAGCTTGGCGGCGAA	
TGGGCTGACCGCTTCCTCGTGCTTTACGGTATCGCCGCTCCCGATTCGCAG	
CGCATCGCCTTCTATCGCCTTCTTG**ACGAGTTCTTCTGAGGGGATC**AATT	**R2 primer**
CTCTAGAGCTCGCTGATCAGCCTCGACTGTGCCTTCTAGTTGCCAGCCATC	
TGTTGTTTGCCCCTCCCCCGTGCCTTCCTTGACCCTGGAAGGTGCCACTCC	
CACTGTCCTTTCCTAATAAAATGAGGAA**ATTGCATCGCATTGTCTGAG**T	**LR-F1**
AGGTGTCATTCTATTCTGGGGGGTGGGGTGGGGCAGGACAGCAAGGGGGA	
GGATTGGGAAGACAATAGCAGGCATGCTGGGGATGCGGTGGGCTCTATGG	
CTTCTGAGGCGGAAAGAACCAGCTGGGGCTCGATCCTCTAGAGTCGACCTC	
GAGTACCACCACACTGGGATCCG**ATAACTTCGTATAATGTATGCTATAC**	**loxP**
GAAGTTATCCAAGCATCACCATCGACCCTCTAGTCCAGATCTCACCATCG	
ACCC**ATAACTTCGTATAATGTGTACTATACGAAGTTAT**TCTAGACTCT	**lox5171**
TCCGCTTCCTCGCTCCACCGCGGCTTCGATACCGTCACGA**GAAGTTCCTAT**	**Frt**
ACTTTCTAGAGAATAGGAACTTCGGAATAGGAACTTCGTTAAC**GAAGT**	**F3**
TCCTATACTATTTGAAGAATAGGAACTTCGGAATAGGAACTTCAGCAA	
CGGATCCGGCCGGCGCCTAGAGAAGGAGTGAGGGCTGGATAAAGGGAGGA	
TCGAGGCGGGGTCGAACGAGGAGGTTCAAGGGGGAGAGACGGGGCGGATG	

GAGGAAGAGGAGGCGGAGGCTTAGGGTGTACAAAGGGCTTGACCCAGGGA	
GGGGGGTCAAAAGCCAAGGCTTCCCAGGTCACGATGTAGGGGACCTGGTC	
TGGGTGTCCATGCGGGCCAGGTGAAAAGACCTTGATCTTAACCTGGGTGA	
TGAGGTCTCGGTTAAAGGTGCCGTCTCGCGGCCATCCGACGTTAAAGGTT	
GGCCATTCTGCA**GAGCAGAAGGTAACCCAACG**TCTCTTCTTGACATCTAC	**LR-R1 primer**
CGACTGGTTGTGAGCGATCCGCTCGACATCTTTCCAGTGACCTAAGGTCAA	
ACTTAAGGGAGTGGTAACAGTCTGGCCCTAATTTTCAGACAAATACAGAA	
ACACAGTCAGACAGAGACAACACAGAACGATGCTGCAGCGCTGCAGCAGA	
CAAGACGCGCGGCTTCGGTTCCAAACCGAAAGCAAAAATTCAGACGGAGG	
CGGGAACTGTTTTAGGTTCTCGTCTCCTACCAGAACCACATATCCTGACGG	
GGTCGGATTCCACATCGACTCCCTTCCTCAGGTCGGGCCACAAAAACGGCC	
CCCAAAGTCCCTGGGACGTCTCCCAGGGTTGCGGCCGGGTGTTCAGAACTC	
GTCAGTTCCACCACGGGTCCGCCAGATACAGAGCTAGTTAGCTAACTAGT	
ACCGACGCAGGCGCATAAAATCAGTCATAGACACTAGACAATCGGACAGA	
CACAGATAAGTTGCTGGCCAGCTTGCCTCCCGGTGGTGGGTCGGTGGTCCC	
TGGGCAGGGGTCTCCCGATCCCGGACGAGCCCCCAAATGAAAGACCCCCGC	
TGACGGGTAGTCAATCACTCAGAGGAGACCCTCCCAAGGAACAGCGAGAC	
CACAAGTCGGATGCAACTGCAAGA	
(missing sequences)	
CAGGTTGAAGGAAGTTGTTATGGAGGCCCAGTGCTTGCTTGGGTGAGAAA	*Gldc* intron 2-3
CAACCCCTTCCTGACAAACCTGGAGGATGCTGATGCAGGCAGGGACCAGCA	
AGTAAAGGACGGAGCCTAAGGGTTCCATCAGTCTGGAAAGAGTCTT**CCTC**	**R3 primer**
TCCAACCCTTCAGAAAGTGAAAAATAATATTATTTATTTATTTATTTAT	
TTATTCACATTCCTAATGCTGCCCCCCCCCCATCGCCCCAGAAAAATACTT	
TTATCGGTCTCTCAGTAAGTTATTACTCAAGAGAAACAAGCAATACCTCT	